Lymph node germinal centres and B cell responses in triple negative breast cancer

Alberts, Ellie

Awarding institution:
King's College London

Lymph node germinal centres and B cell responses in triple negative breast cancer

Submitted for the degree of Doctor of Philosophy
at
King's College London

Elena Alberts

24th March 2023

Statement of originality

I confirm that the work presented in this thesis is my own or, where it has been indicated, carried out in collaboration. Where published or unpublished work has been used, it has been referenced and acknowledged in the text. The work presented here is original and has not been submitted towards the award of another degree at this, or another university.

Elena Alberts

28th March 2023

Thesis word count: 53,109

Abstract

Triple negative breast cancers (TNBCs) are a morphologically and molecularly heterogeneous group of breast cancers, defined by the absence of estrogen receptor (ER), progesterone receptor and human epidermal growth factor receptor (HER2). Characterised by an aggressive phenotype, high prevalence in younger women and those of African American ethnicity, TNBC represents a significant unmet medical need despite therapeutic advances. These developments in targeted therapies have harnessed the immunogenic nature of TNBCs and subsequent approval in combination with chemotherapy in the adjuvant and metastatic setting. As such, assessment of stromal tumour-infiltrating lymphocytes (sTILs) within TNBCs has shown greater predictive value over classical staging parameters in response to chemotherapy and immunotherapy. Critically, the presence of cancerous cells within the sentinel lymph nodes and the number of metastatic lymph nodes are essential assessment parameters for routine pathological diagnoses. Our group have previously shown the additive prognostic value of immune responses within the tumour-adjacent lymph nodes, in particular germinal centre formation, and their subsequent association with sTIL density, the incidence of tertiary lymphoid structures at the primary tumour and longer distant-metastasis free survival. This thesis therefore aimed to explore the temporal, cellular and spatial immune composition of lymph nodes and the lymph node-tumour crosstalk, utilising several imaging, molecular and *in vivo* modalities.

We harnessed transcriptional analyses of microarray data from TNBC primary tumours and assessed the prognostic

Immunophenotyping a pilot study of lymph nodes from two patients with opposing disease trajectories and sTIL scores at the primary tumour revealed a reduction in PD1+T cell populations potentially influencing germinal centre responses, and upregulation of immunosuppressive subsets with distinct spatial properties within the lymph node. A wider exploration of molecular data of these subsets defined a subgroup of immunologically cold TNBCs with increased plasma cell infiltration; low sTILs, high plasma (IThP), exhibiting features of the luminal androgen receptor subtype and shorter time to distant metastasis. The spatial orientation and infiltration of plasma cells within the tumour and lymph node were subsequently validated within an independent cohort of high-risk low sTILs TNBC patients.

I further utilised four distinct mouse models of TNBC with a range of metastatic abilities, to study for the first time, the temporal characteristics of germinal centre development in response to nearby tumour growth. This revealed differences in the kinetic features of the germinal centre B cell response within the tumour draining lymph nodes, and the phenotype of memory B and plasma cell subsets generated in response to the developing tumour.

To elucidate potential mechanisms that may be impacting germinal centre formation and plasma cell production in lymph nodes, I subsequently focussed on the IGF1 pathway. This revealed that overexpression of IGF1 promoted tumour growth *in vitro* and *in vivo*, dampened germinal centre responses and promoted an IgM+ plasma cell phenotype. Overall, this thesis provides new insights into the molecular features of a subgroup of immunologically cold TNBCs. I provide preliminary evidence of the relationship between germinal centre B cell responses in lymph nodes and tumours, which ultimately may influence an inferior disease trajectory for these high-risk TNBC patients.

Acknowledgements

I would like to thank my supervisors Dr Anita Grigoriadis and Professor Sophia Karagiannis for their invaluable guidance and support throughout this project. I am particularly grateful for all the wonderful opportunities and experiences I have had under their supervision. I would also like to thank the MRC Doctoral Training Partnership (MRC-DTP) at King's College London for providing the funding for my 4-year PhD studentship.

I am also immensely grateful for the support from the King's Health Partners Biobank, Dr Cheryl Gillet and Dr Fangfang Liu for their assistance in sample selection. I would like to recognise the work and support of Dr Thomas Hardiman whose previous PhD project provided the foundations of this thesis. I further would like to thank all the members of the Cancer Bioinformatics group, and the Karagiannis laboratory for their technical assistance and support with many of the experiments and analyses. In particular, I would like to acknowledge Victoire Boulat and Isobelle Wall for their contribution to many of the experiments, and Mengyuan Li and Matthew Hung for analytical support. Finally, I would like to thank Dr Jelmar Quist and Radhika Kataria for their continued encouragement throughout the last 4 years. Much of this work was also performed in collaboration with Dr. Dinis Calado, whose knowledge and expertise were invaluable and integral to this project.

Finally, I would like to thank my friends and my family for their unwavering support, patience and encouragement throughout this process. Throughout my time at King's College London, I have made some lifelong friendships within the MRC DTP programme, without which this experience would not have been the same.

Table of contents

List of figures

List of tables

Abbreviations

AI	Aromatase inhibitor
AR	Androgen receptor
B-LG	Bovine β-lactoglobulin
BCR	B cell receptor
BL1	Basal-like 1
BL2	Basal-like 2
BLIA	Basal-like immune activated
BLIS	Basal-like immune suppressed
Breg	Regulatory B cell
CAF	Cancer-associated fibroblast
CCL	C-C motif chemokine ligand
CCR	C-C motif chemokine receptor
CD	Cluster of differentiation
cf-LN	Cancer-free lymph node
CI	Confidence interval
CMV	Cytomegalovirus
cn	Cellular neighbourhood
CNA	Copy Number Alteration
COX-2	Cyclo-oxygenase-2
CSR	Class switch recombination
CTCF	Connective tissue growth factor
CTLA-4	Cytotoxic T-lymphocyte-associated antigen 4
CXCL	C-X-C motif chemokine ligand
CXCR	C-X-C motif chemokine receptor
d-LN	Draining lymph node
DAMP	Damage associated molecular pattern
DCIS	Ductal carcinoma in situ
DDR	DNA damage response
DN	Double negative
DZ	Dark zone
ECM	Extracelluar matrix
EF1A	Eukaryotic translation elongation factor 1 α1
EGFP	Enhanced green fluorescent protein
EMT	Epithelial-mesenchymal transition
ER	Estrogen receptor
FDC	Follicular dendritic cell
FO	Follicular
GC	Germinal centre
GEMM	Genetically engineered mouse model
HBV	Hepatitis B virus
HCC	Hepatocellular carcinoma
HER2	Human epidermal growth factor receptor 2

HIGM2	Hyper-IgM syndrome
HR	Hormon receptors
HR	Hazard ratio
HRD	Homologous recombination deficiency
hThP	High sTILs high plasma
hTIP	High sTILs low plasma
ICOS	Inducible T-cell costimulator
IHC	Immunohistochemistry
IL	Interleukin
IM	Immunomudulatory
IMC	Imaging mass cytometry
in-LN	Involved lymph node
ISH	*In situ* hybridisation *or Immune-stromal-histological*
LAG-3	Lymphocyte-activation gene 3
LAR	Luminal androgen receptor
LCIS	Lobular carcinoma in situ
LN	Lymph node
lThP	Low sTILs high plasma
lTIP	Low sTILs low plasma
LTR	Long terminal repeat
LZ	Light zone
M	Mesenchymal
MES	Mesenchymal
MFI	Median fluorescence intensity
MHC	Major histocompability complex
MMP-1	Matrix metalloproteinase-1
MMTV	Mouse mammary tumour virus
MSL1	Mesenchymal stem-like
MT	Metallothionein
MZ	Marginal zone
NACT	Neoadjuvant chemotherapy
nd-LN	Non-draining lymph node
NHEJ	Non-homologous end joining
NK	Natural killer
PAM50	Prediction Analysis of Microarray 50
PAMP	Pattern-associated molecular pattern
pCR	Pathological complete response
PD-1	Programmed death ligand 1
PD-L1	Programmed death-ligand 1
PR	Progesterone receptor
PyMT	Polyoma middle T
ROI	Region of interest
RT	Room temperature
SARMs	Selective AR modulators
sc	Spatial context or single cell
scRNA-seq	Single-cell RNA-sequencing
SERD	Selective estrogen receptor degrades
SHM	Somatic hypermutation
SLE	System lupus etythematosus

SSB	Single stranded breaks
sTIL	Stromal tumour infiltrating lymphocyte
SV40	Simian virus 40 late
T1	Transitional 1
TAA	Tumour associated antigen
TAM	Tumour associated macrophage
TAN	Tumour associated neutrophil
TCR	T cell receptor
td-LN	Tumour draining lymph node
Tfh	T follicular helper
Tfr	T follicular regulatory
Th	T helper
TIGIT	T-cell immunoreceptor with Ig and ITIM domains
TIL	Tumour infiltrating lymphocyte
TIL-B	Tumour infiltrating B cell
TIL-T	Tumour infiltrating T cell
TIM3	T-cell immunoglobulin and mucin-domain containing 3
TLR	Toll-like receptor
TLS	Tertiary lymphoid structures
TME	Tumour microenvrionment
TNBC	Triple Negative Breast Cancer
TNM	Tumour, Node, Metastasis
Treg	Regulatory T cell
TSA	Tumour specific antigen
WAP	Whey acid protein
WSI	Whole slide images

Academic outputs

Publications

- Alberts *et al*., 2021, Immune Crosstalk Between Lymph Nodes and Breast Carcinomas, With a Focus on B cells, Frontiers in Molecular Biosciences, 8

Contributing author to:

- Li M, Quintana A, Alberts E *et al*., 2023, B cells in Breast Pathology, Cancers, 15 (5)

- Wall *et al*., 2022, Leveraging the Dynamic Immune Environment Triad in Patients with Breast Cancer: Tumour, Lymph Node and Peripheral Blood. Cancers, 14 (8)

- Harris *et al*., 2021, Tumour-Infiltrating B Lymphocyte Profiling Identifies IgG-Biased, Clonally Expanded Prognostic Phenotypes in Triple-Negative Breast Cancer. Cancer Research, 81(16)

Abstracts

Elements of this thesis were presented in poster format at:

- EMBO Workshop on Germinal centres and immune niches, 5th- 8th September 2022
- ESMO Breast Cancer, 3rd-5th May 2022
- B cell UK, British Society for Immunology, 26th April 2022

COVID-19 impact statement

During 2020/21, as a result of the COVID-19 global pandemic, research at King's College London was interrupted. In addition to the disruption this caused to laboratory and analytical work, it prevented the acquisition of samples in the following chapters:

Chapter 3: Characterisation of molecular features and B cell populations in human TNBC tumours and axillary LNs

Chapter 5: Molecular features of TNBC and their association with germinal centres and plasma cell responses

There was further a delay to starting *in vivo* work due to access restrictions during the pandemic. This meant that there was interruption to beginning the work in the following chapters:

Chapter 4: Profiling GCs and B cell responses in mammary gland tumours and lymph nodes of *in vivo* TNBC mouse models

Chapter 5: Molecular features of TNBC and their association with germinal centres and plasma cell responses

Chapter 1:

Introduction

1.1 Breast cancer

Breast cancer is the leading cause of death among women, accounting for around 30% of all cancers diagnosed annually (Azamjah et al., 2019). On rare occasion, breast cancer can affect the male population, which attributes to only 1% of these cases. It presents as a morphologically heterogeneous disease, classified as ductal carcinoma *in situ* (DCIS), invasive lobular or ductal carcinoma, or inflammatory breast cancer (Azamjah et al., 2019; Nounou et al., 2015). Within breast cancer, DCIS is considered a preinvasive lesion, appearing as abnormal cells within the milk ducts of the breast. Lobular carcinoma *in situ* (LCIS) is the manifestation of malignant cells within the milk glands (lobules). Both invasive ductal and lobular carcinomas arise when cancerous cells break free from the duct or lobule from which they originated and enter nearby tissue. Secondary breast cancer, also known as metastatic breast cancer, is when cancerous cells migrate to peripheral organs, primarily the lymph nodes (LNs) (defined as regional metastasis), or spread further throughout the lymphatic and circulatory systems to distant sites, most commonly to the lungs, bones, liver, skin, and brain (referred to as distant metastasis) (Redig and McAllister, 2013). The five-year survival rate for patients with primary breast cancer is 91%, however, this is substantially lower in patients with both regional metastasis (~65%), and distant metastasis (~11%) (“Cancer Statistics Review, 1975-2015).

1.1.1 Histological classification

Histological examination of the tissue is used to assess the morphological features of breast cancer to determine the grade, stage and advise treatment regime. Utilising cellular arrangement, nuclear grade (how abnormal the cells look compared to healthy cells), and mitotic count (cell division rate), tumours are histologically graded between 1 and 3. Low grade (1) exhibit the slowest growth rate, whilst high grade (3) present as highly proliferative, poorly differentiated tumours and are associated with the most detrimental overall disease trajectory (Rakha et al., 2010). Whilst these grading scores offer some understanding of the characteristics of these tumours, the morphologically heterogeneous nature of breast cancer carcinomas requires precision-based techniques to identify robust prognostic markers.

1.1.2 Clinical staging

Other clinical parameters used to evaluate the features of the tumour include Tumour, Node, Metastasis (TNM) staging. Frequently used in pan-cancer diagnoses, this accounts for the tumour size (T), the level of nodal involvement (N), and metastatic spread to distant organs (M). Tumour sizes are graded from Tx (cannot be assessed) to T4 (the tumour has spread to the chest wall and/or the skin). LN status is evaluated either during surgery (pathological staging) or after undergoing X-rays and CT scans (clinical staging) (Barrett et al., 2009). Broadly, both stages range from pNx or cNx (the LNs cannot be assessed) to pN3 and cN3, where cancerous cells are found in one or more LNs above the collarbone. Metastasis can also be determined pathologically or clinically. M0 describes no evidence of metastasis, whereas cM1 (clinical) is diagnosed when evidence of tumour cells is recorded by physical evaluation or scans, and pM1 (pathological) defines a tumour measuring more than 0.2mm in size detected, often by biopsy (Barrett et al., 2009; Nelson et al., 2016).

1.1.3 Immunohistochemical classification

Breast cancer can further be categorised based on the immunohistochemical expression of the human epidermal growth factor receptor 2 (HER2) and hormone receptors (HR); estrogen receptor (ER) and progesterone receptor (PR) (Zaha, 2014). The majority of cases are classed as ER+ (~65% of all cases), followed by HER2+ (~20%), with the minority accounting for those with a triple-negative phenotype (TNBC;~15%) (Onitilo et al., 2009). Classification using IHC methods has led to the development of targeted therapies and paved the way for clinical advancements in oncology treatment. Anti-estrogen therapies including tamoxifen, aromatase inhibitors (AI) and selective estrogen receptor degraders (SERDs) are now common practice for the treatment of ER+ cancers and have significantly improved patient overall survival. Further, the recognition of hormone-targeted treatments also led to the development of anti-HER2+ mediated therapies, including trastuzumab (Herceptin) (Cameron et al. 2017). Prior to this treatment, patients with metastatic HER2+ disease had a high rate of disease recurrence, mortality and were limited to standard chemotherapy regimens. Since, multiple agents have been developed to target HER2+ breast cancers, extending time to progression and improving overall survival rates (Wang et al, 2019).

Typically, HER2 scoring is a binary process, and patients are diagnosed as either HER2+ or HER2-. Immunohistochemistry (IHC) scores of 3+ are considered HER2+, 2+ are classed as borderline, whilst anything below this threshold (1+ or 0+) is defined as HER2-. Borderline patients require an additional *in situ* hybridisation (ISH) test, which measures gene amplification. The DESTINY-Breast-4 trial in 2022 introduced a new therapeutic strategy for ‘HER-low breast cancer’ which represents borderline HER2 expression and is currently not treatable with traditional HER2-targeting therapies. This study showed that a novel next-generation antibody-drug conjugate (ADC) named trastuzumab deruxtecan (T-DXd) elicited a robust response in patients with HER2-low metastatic breast cancer, significantly improving

survival compared to those that received chemotherapy alone. Among 494 participants, the risk of disease progression and death was reduced by approximately 50% compared to 36% respectively (Eiger et al., 2021). As such, current developments are in the pipeline to improve the sensitivity of assays to detect and measure low levels of HER2, which will enable further stratification for patients that may benefit from these new therapies (Modi et al,2022).

1.1.4 Molecular subtyping

Whilst IHC scoring has been the mainstay of breast cancer stratification, the development of the PAM50 (Prediction Analysis of Microarray 50) gene signature identified 50 differentially expressed genes that could categorise breast cancer tumours into Luminal A, Luminal B, Basal-like, HER2-enriched and normal-like (Parker et al., 2009; Perou et al., 2000). Whilst ER+PR+ cancers typically present with a luminal A and luminal B phenotype, HER2+ are encompassed within the HER-enriched category. Tumours with luminal A phenotypes typically have improved breast cancer-specific survival and distant disease-free survival, presenting with low-grade, differentiated tumours that respond well to endocrine therapy. In contrast, basal-like breast tumours are typically the most aggressive, defined by an upregulation of cytokeratin 14 and 17, normally found in the basal cell layer of the mammary duct (Dai et al., 2017).

1.2 Triple Negative Breast Cancer

Triple Negative Breast Cancer (TNBC) also known as HR-HER2-, accounts for 10-15% of all breast cancers and is predominantly basal-like within the PAM50 classifications (Rao et al., 2013). It is a highly proliferative subtype, often of high histological grade and occurs more frequently in women under 50 years of age. It amounts to around 200,000 cases diagnosed worldwide each year and is more prevalent in those of an African American or Hispanic ethnicity (Foulkes et al., 2010). TNBC classically exhibits more aggressive characteristics and a high prevalence of both regional and distant metastasis (Al-Mahmood et al., 2018; Rao et al., 2013). Key driver mutations within TNBC occur within tumour-suppressor genes including *TP53*, *RB1*, *PTEN* and to a lesser extent the PI3K/AKT pathway. These mutations are often as a result of Copy Number Alterations (CNAs) of genomic regions in pathways affecting PI3K signaling, ERBB2 signaling and extracellular matrix (ECM) interactions (Shah et al., 2012).

1.2.1 TNBC subtypes

In 2011, Lehmann *et al*., sampled 587 TNBC tumours, demonstrating that gene expression analyses could identify 6 groups within this subtype: basal-like 1 (BL1), basal-like 2 (BL2), mesenchymal (M), mesenchymal stem-like (MSL1), immunomodulatory (IM) and luminal androgen receptor (LAR). Here, it was shown that BL1 and BL2 subtypes were enriched for cell cycle and DNA damage response genes, whereas M and MSL had a higher incidence of epithelial-mesenchymal transition (EMT) and responded well to NVP-BEZ235 inhibitors that target the PI3K/mTOR pathway. LAR subtypes exhibited a decreased relapse-free survival and were characterised by high levels of androgen receptor signalling, with LAR cell lines responsive to androgen receptor (AR) antagonists (Lehmann et al., 2011). Other studies have identified intrinsic TNBC subtypes with extensive overlap namely LAR, mesenchymal (MES), Basal-like immune suppressed (BLIS) and Basal-like immune activated (BLIA). DNA profiling

revealed subtype-specific gene amplification and differences in overall prognoses, with the BLIS TNBC tumours exhibiting the most detrimental disease trajectory (Burstein et al., 2015). Furthermore, other studies using decision tree-based analyses of core genes including *ST8SIA1*, *EXO2, NEK2, C8ORF46* and *MMS22L* identified 6 subtypes that were non-synonymous with other breast cancer classifications (Quist et al., 2019).

1.2.2 Treatment for TNBC patients

Whilst patients exhibiting HR and HER2 expression benefit from anti-hormone therapies, the standard treatment regime for TNBC is primarily surgery, radiation therapy and chemotherapy. Patients with germline *BRCA* gene mutations are eligible for alternative treatments that target cellular DNA damage pathways. Furthermore, TNBC accounts for 70% of breast tumours arising from *BRCA1* mutation carriers and 16-23% from *BRCA2* mutation carriers (Mahfoudh et al., 2019). These genes are responsible for the maintenance of homologous recombination, one of the processes involved in the repair of DNA double stranded breaks. Tumours with homologous recombination deficiency (HRD) are subsequently candidates for poly (ADP-ribose) polymerase (PARP) targeted therapy. PARP is required for the repair of single stranded breaks (SSB); therefore, inhibition of this process will subsequently lead to the development of double stranded breaks. In healthy cells, homologous recombination can restore this damage, however malignant cells with *BRCA* mutations are unable to utilize HRD and will ultimately undergo cell death by apoptosis (Singh et al., 2021).

TNBC has also become a candidate for immunotherapies within the oncology field due to its immunogenic properties. Immunotherapies are monoclonal antibodies that target immune checkpoint axes within the tumour microenvironment (TME). Infiltrating immune cells with an exhausted phenotype commonly express high levels of checkpoint markers, including

programmed death ligand 1 (PD-1), cytotoxic T-lymphocyte-associated antigen 4 (CTLA-4), lymphocyte-activation gene 3 (LAG-3) and inducible T-cell costimulator (ICOS), induced by elevated levels of their ligands on malignant cells. Studies including the KEYNOTE-522, IMpassion131, and KEYNOTE-355 trials have harnessed the use of immunotherapies including atezolizumab and pembrolizumab that target the programmed death ligand 1 (PD-L1)/PD-1 axis, in combination with chemotherapy for patients with advanced TNBC (Cortes et al., 2020; Miles et al., 2021; Schmid et al., 2020). Promising significant increases in pathological complete responses (pCR) has led to the FDA approval for both atezolizumab and pembrolizumab in combination with neoadjuvant chemotherapy for both early-stage high risk and locally advanced or metastatic TNBC. However, more than half of TNBCs express insufficient levels of PD-L1 required to be eligible for immunotherapy, therefore additional work is needed to elucidate the benefit of immune checkpoint targeting treatment for these patients (Mittendorf et al., 2014).

1.3 Immune cell development and maturation

The immune system can be crudely split into the innate or adaptive, with minor crossover between the origin of some subsets of cells. All leukocytic cells originate from a common hematopoietic progenitor within the bone marrow, and then differentiate into either a myeloid progenitor cell (innate immune system) or lymphocytic progenitor cell (adaptive immune system).

1.3.1 The innate immune system

The innate immune system, present in all multicellular organisms, is evolutionarily older than the adaptive immune system and provides the first line of defense against invading pathogens. Comprised of physical barriers including the skin and mucosal membranes, the innate immune system also encompasses a multitude of cell types (Chaplin, 2010). Phagocytic cells including monocytes, macrophages, neutrophils and dendritic cells engulf foreign microorganisms and present antigenic peptides via major histocompatibility complexes (MHC) to complementary T cell receptors (TCRs) on T cells (Chaplin, 2010). Natural killer (NK) cells bridge the innate and adaptive immune responses, engaging with other immune subsets to exacerbate and suppress their function through activating and inhibitory receptors, respectively (Rosales and Uribe-Querol, 2017). Although primarily acting as an aid to the adaptive arm, innate cells can also elicit powerful reactive oxidative bursts to promote cytotoxic activity against invading pathogens (Vivier et al., 2008).

1.3.2 T cell development

As a key player within the adaptive immune response, T cell development has been heavily studied. Originating in the bone marrow, T cell progenitors exit and are recruited to the thymus via the P-selectin/PSGL-1 axis and a CCL21, CCL25 and CCL19 gradient (Kozai et al., 2017). Here, developing T cells are presented with antigenic peptides and undergo both positive and negative selection. This ensures sufficient binding of TCR to foreign MHC complexes, while hindering the development of autoreactive cells. T cells that survive both selection processes develop as double positive cells (DP) which express both CD4 and CD8, undergoing TCRα chain rearrangement and then exiting the thymus as either naïve CD4+ or CD8+ T cells (Klein et al., 2014; Starr et al., 2003). Although CD8+ T cells are critical for mediating clearance of viral, bacterial and protozoic infections, one of the earliest understood functions of T cells was

to provide support to B cell activation, resulting in the term ‘T-helper’ (Th) cell from the CD4+ lineage. Initial cell-transfer experiments in mice recognized the role of thymus-derived cells in augmenting antibody responses against immunization of sheep erythrocytes (Crotty et al, 2015).

1.3.3 B cell development

In parallel, B cell precursors also arise from a lymphocyte progenitor within the bone marrow, characterised by expression of CD19, CD24, CD43 and CD127 (Rumfelt et al., 2006). Following pre-B cell assembly, which is crucial to remove cells unable to assemble a functional B cell receptor (BCR), immature IgM+ B cells are the first cells in the B cell lineage capable of recognising an antigen. After undergoing rigorous checks for self-reactivity, they exit the bone marrow and then utilise chemokine gradients including the CCL2/CCR2 axis to migrate towards the spleen (Loder et al., 1999; Shahaf et al., 2016). Here, they develop into transitional 1 (T1) cells, expressing an IgM^{hi}, $IgD^{low}CD21^{low}CD23\text{-}CD24^{hi}$ phenotype, and are exposed to self-antigens in the periarteriolar lymphoid sheaths (PALS) of the spleen to ensure sufficient tolerance. T1 B cells that survive this stage move towards the primary follicles of the spleen and transition into $IgMl^{ow}IgD^{hi}CD21^{high}CD23+CD24^{low}$ T2 B cells (Loder et al., 1999). Broadly, mature naïve B cells can be grouped into three populations: follicular (FO) B cells, marginal zone (MZ) B cells, and B-1 cells. FO cells reside within the primary follicles of the spleen, where they are exposed to cognate antigen from follicular dendritic cells (FDCs) (Riedel et al., 2020). Primed B cells can either differentiate into short-lived extrafollicular plasma cells, which are responsible for the majority of IgM+ plasma cells, or differentiate into large centroblasts, initiating the germinal centre (GC) reaction. MZ B cells are located in the marginal zone of the spleen, at the outer limit of the while pulp, and bordered by the red pulp. They are efficient antigen presenting cells, and a strong defensive line against blood-borne pathogens, rapidly differentiating into low-affinity plasma cells when needed. B-1 B cells represent a small fraction

of splenic B cells and are predominantly located in the pleural and peritoneal cavities. They represent an early antibody response against bacterial antigens, secreting IgA within the intestinal lamina propria and other mucosal sites (Popi et al., 2016; Shahaf et al., 2016). A summary of B cell development is shown in Figure 1.

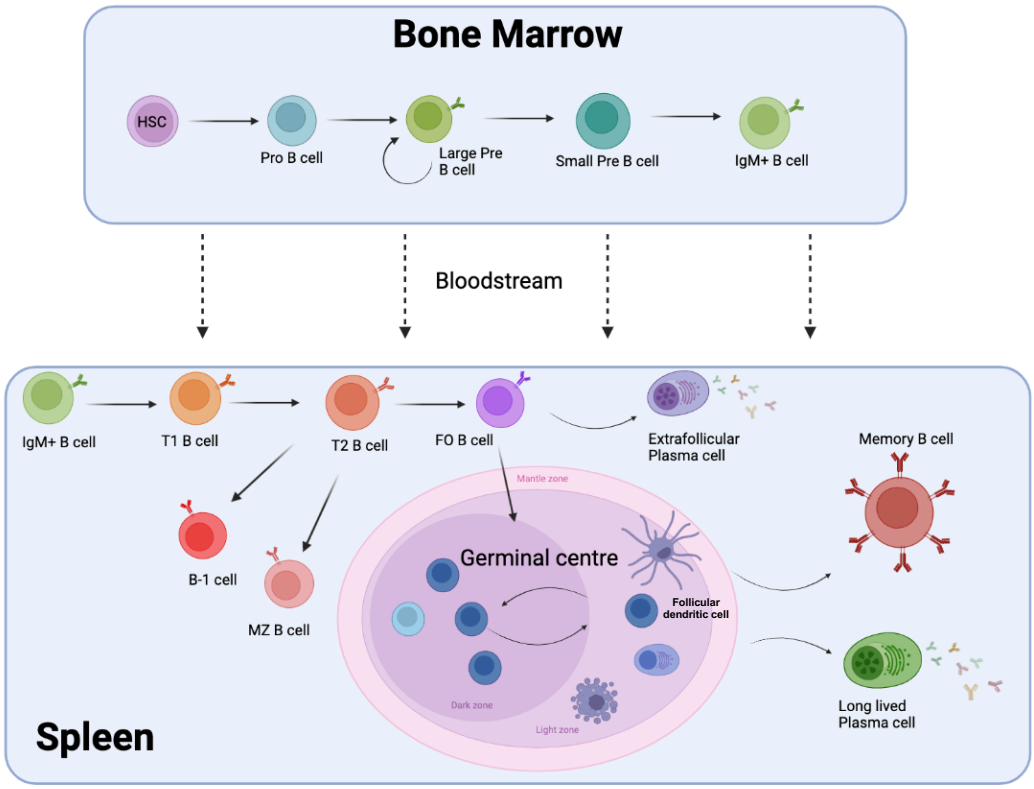

Figure 1: B cell development and differentiation. B cells primarily originate from CD34+CD19- hematopoietic stem cells within the bone marrow, where rearrangement of immunoglobulin heavy and light chains through VDJ recombination leads to the development of functional IgM+ immature B cells. Those that survive tolerance checks to prevent autoreactivity migrate through the bloodstream or lymphatics to secondary lymphoid organs. Following exposure to cognate antigen, mature B cells can undergo plasmocytic differentiation to generate short-lived plasma cells or establish a germinal center reaction. Within the germinal center, B cells undergo iterative rounds of somatic hypermutation and selection through interactions with follicular T helper (Tfh) and follicular dendritic cells (FDC). The resultant B cell pool will exit the germinal center as high affinity memory B or plasma cells.

1.4 Lymph node and lymphatics

LNs are secondary lymphoid organs like that of spleen, and provide a platform for B cell maturation, facilitating antigen dispersal and promoting interactions between immune cell subsets. In response to disease, inflammatory chemokines and cytokines mediate recruitment of lymphocytes and antigen-presenting cells that access the LNs via lymphatic vessel-mediated lymph drainage. Passing through the subcapsular sinus, these lymph-borne solutes disseminate into the cortex where B cells, intrafollicular T cells and dendritic cells are strategically compartmentalised, before moving through conduits to reach the T cell zone of the LN paracortex. Depending on the nature of the stimuli, these compartments can expand or diminish to generate an optimal B cell response. Eventually, lymphocytes exit the LNs via efferent lymphatic vessels and the LNs return to a non-reactive state (Willard-Mack, 2006).

1.4.1 The germinal centre reaction in LNs

GCs are immunological sites in the LN and spleen within which BCR affinity maturation occurs to generate long-lived memory B and plasma cells (Nakagawa et al., 2021; Victora and Nussenzweig, 2012). Tightly regulated mechanisms within the GC promote targeted responses to pathogens whilst ensuring elimination of autoreactive clones. B cells retrieve antigen via their BCR from FDCs and present the antigen to follicular T helper (Tfh) cells (Victora and Nussenzweig, 2012). GC B cells compete for Tfh derived signals critical for positive selection, which culminates in the upregulation of the transcription factor MYC (Calado et al., 2012; Dominguez-Sola et al., 2012). BCR affinity maturation in GC B cells occurs through iterative rounds of clonal expansion, somatic hypermutation (SHM) and selection to generate fine-tuned humoral responses (Victora and Nussenzweig, 2012).

1.4.2 Transcriptional profiling of the GC reaction and of GC B cell derived subsets

Tightly controlled transcriptional profiles govern the formation and development of GCs. In the LN, GC B cells transit between two functionally distinct compartments, the dark zone (DZ) and light zone (LZ) which represent polarized areas in which gene expression patterns drive SMH and selection, respectively, (Calado et al., 2012; Dominguez-Sola et al., 2012; Victora and Nussenzweig, 2012). By utilising single-cell RNA-sequencing (scRNA-seq) on tissue derived from human and mouse, a plethora of transcriptional changes occurring in GCs has been revealed, and with-it novel cell populations have been defined. This includes DZ and LZ subsets, intermediate populations bearing expression of markers associated with both, and pre-memory B cells (Holmes et al., 2020; Kennedy et al., 2020; H. King et al., 2021; McHeyzer-Williams et al., 2015; Nakagawa et al., 2021). Whilst the functional roles for some of these populations remains to be determined, the identification of defining markers provides the opportunity to determine their spatial distribution within the GC and LNs, and possible isolation for further functional studies. scRNA-seq experiments have also tentatively identified the gene expression profile of memory B and plasma cell precursors in the LZ of GCs (Holmes et al., 2020). The differentiation of LZ B cells towards the plasma cell fate is associated with increased Tfh help that enhances NF-κB signaling, *Irf4*, *Xbp1*, *Fkbp11* and *Prdm1* expression (Heise et al., 2014; Holmes et al., 2020; Nutt et al., 2015). In contrast, memory B cell differentiation from LZ B cells is restricted to positively selected cells, seemingly requires minimal Tfh help and is associated with increased *Bach2* and *Hhex* expression levels (Laidlaw et al., 2020; Laidlaw and Cyster, 2020; Nakagawa et al., 2021; Sidwell and Kallies, 2016; Toboso-Navasa et al., 2020).

1.4.3 Germinal center initiation

1.4.3.1 Initiation at the T/B border

Whilst the accepted dogma of GC initiation and development involves the interactions between dendritic cells, T cells and B cells, the inscrutable characteristics of the developmental steps that precede the appearance of fully matured GCs make it difficult to delineate the exact mechanisms that contribute to B cell survival and fate decisions. Typical GC markers include high levels of CD95 (Fas), GL7 and downregulation of IgD, however discrepancies between human and mouse in the expression patterns of markers such as CD38 add to the complexity of the lineage development and the type of antigenic stimulation (Cervenak et al., 2001; Oliver et al., 1997; Smith et al., 1995). The first mouse experiments describing the role of the transcriptional repressor BCL6 and its requirement for Tfh and GC B cells illuminated previously poorly understood mechanisms that are involved in GC cell commitment. While BCL6 acts as a transcriptional regulator in repressing transcription factors including IRF4 and BLIMP1, high levels can reciprocally repress BCL6 and promote an antibody secreting cell phenotype (Basso et al., 2010; Ye et al., 1997). Paradoxically, studies have shown that IRF4 promotes BCL6 and is essential for GC B cell development, emphasising the multifunctional roles of these proteins (Kwon et al., 2009; Ochiai et al., 2013). It is also important to consider what drives the necessity for GC formation during the immune reaction. Historically, SHM and class switch recombination (CSR) were considered to both be reliant on the formation of the GC, due to their dependence on the activity of activation-induced cytidine deaminase (AID) (Muramatsu et al., 2000), which is expressed at its highest level by GC B cells. Early studies by Shinkura *et al.,* described mice with impaired follicular development elicited weak antibody responses and defective CSR. Despite this, the extrafollicular response is widely accepted to produce class switched antibodies as early as day 2 post immunisation (Shinkura et al., 1996), and Roco *et al.,* elegantly presented evidence of germline transcripts within B cells prior to differentiation to GC B cells or

plasmablasts, and evidence of these cells aggregating at the T/B border (Roco et al., 2019). Together, these findings highlight decision points at B cell developmental stages that may not require a GC response.

1.4.3.2 Chemotactic localisation

Secondary lymphoid organs including both the LN and the spleen are highly organised structures, and naïve T and B cells are localised to T cell zones and B cell follicles respectively based on surface receptor expression. FDC secreted CXCL13 recruits B cells by virtue of CXCR5 expression, while T cell localisation is mediated via CCR7 and CCL19/21. Stromal cells secreting chemoattractants including EBI2 line the medullary, subcapsular and cortical sinuses, constructing distinct architectural zones (Ansel et al., 1999; Cyster et al., 2000). As inflammatory material passes through the lymph to LN or bloodstream to the spleen, T and B cells specific for cognate antigen will become activated. Subcapsular sinus macrophages carry antigen via lymphatic vessels and present antigen to naïve B cells localised within primary follicles. BCR crosslinking and exposure to pattern-associated molecular patterns (PAMPs) stimulates an increase in CCR7, CD86, MHC II, and an elevated sensitivity to CD40 signalling (Batista and Harwood, 2009). In parallel, activated CD4+ T cells presented antigen by dendritic cells within T cell zone upregulate levels of CXCR5 and follow the CXCL13 gradient towards the B cell follicles (Lund and Randall, 2010). Engagement of activated T and B cells at the T/B border represents the earliest evidence of BCL6 upregulation (Kerfoot et al., 2011).

1.4.3.3 Commitment to the extrafollicular or intrafollicular pathway

Whilst fate decisions that drive B cells towards an extrafollicular or intrafollicular response are still being elucidated fully, there is evidence that extrafollicular responses are predominantly diverse and of a low affinity. B cells that are bound for a GC response increase their expression of the transcription factor BCL6, while those that are destined for an extrafollicular response immediately begin to express BLIMP1. This upregulation of BLIMP1 directly suppresses PAX5, which is a transcription factor that has both activating and suppressive functions.

The mechanisms in place that drive GC initiation may be driven by early antigen presentation responses between dendritic cells and CD4+ T cells (Elsner and Shlomchik, 2020; MacLennan et al., 2003). PD-1 and CXCR5 upregulation occurs at a very early stage on activated CD4+ cells and then is only sustained on those that gain entry to the follicle for continued activation with B cells. This suggests a potential antigenic stimulation that affects how resultant pre-Tfh cells interact with cognate B cells at the T/B border and subsequently influence the initiation or suppression of the GC response (Baumjohann et al., 2011; Choi et al., 2011). Other antigenic features including T independent type 2 (TI-2) antigens that do not require T cell help to produce an antibody response and induce abortive GCs that fail to produce any long-lived memory or plasma cells (Vos et al., 2000).

1.4.3.4 Antigenic initiation of GC responses

Early B cell activation events are consistently difficult to study due to the downregulation of the BCR post cross-linking of antigen. As the nature of the epitope presented can challenge whether a GC is formed, it is important to consider tumour associated antigens (TAA) and tumour specific antigens (TSAs) present within TNBC and other solid cancers that will influence the immune responses and how this can be manipulated therapeutically. TAAs are

proteins that are upregulated by malignant cells compared to normal cells, however TSAs, also called neoantigens, are selectively expressed only by tumour cells (Apavaloaei et al., 2020). Despite their prevalence, TAAs originate as self-antigens which limits the efficacy of immune responses due to self-tolerance mechanisms. Neoantigens, determined through whole exome and RNA sequencing of tumour tissue, are characterised based on their predictive HLA binding affinity. Although hypothesised to initiate a robust immune response, many studies suggest little to no association between tumour infiltrating lymphocytes (TIL) infiltration and neoantigen load. As the immune response within the TME of TNBC patients is often heterogenous and complex, the number of neoantigen-specific TILs rather than bulk immune infiltration may provide insight into the functionality and maturity of the immune response in patients with opposing outcomes (Peng et al., 2019). Thus, the nature of the antigenic stimuli required to initiate a GC B cell response remains an important consideration and is currently unknown in the context of solid tumours.

1.4.4 GC collapse and shutdown

1.4.4.1 GC B cell apoptosis and proliferation

Control of apoptosis and proliferation are both mechanisms by which B cell levels are maintained within the GC reaction. Apoptosis occurs in both the LZ and DZ due to lack of survival signals, induction of deleterious BCR mutations resulting from SHM, or complete loss of FDCs and Tfh due to lack of antigenic stimuli (Mayer et al., 2017). In parallel, proliferation of B cells is controlled by the levels of C-MYC induced by signals from Tfh (Finkin et al., 2019). Changes in the expression of C-MYC, and other factors including mTORC1 and FOXO1 that are involved in the cell growth ahead of clonal expansion rapidly induces GC collapse if critically low (Calado et al., 2012; Ersching et al., 2017). The autosomal recessive form of hyper-IgM syndrome (HIGM2) develops in patients with

mutations in *AID* and results in intrinsic deficiencies in CSR, with excessively larger GCs in secondary lymphoid organs. It is hypothesised that uncontrollable proliferation of B cells is triggered due to lack of Ig variable region gene somatic mutations, and continuous exposure to antigen (Kuraoka et al., 2009; Revy et al., 2000). In this way, the balance between proliferation and apoptosis within the GC represents a tolerance system to prevent the production of autoreactive or dysfunctional B cells (Mayer et al., 2017).

1.4.4.2 Negative feedback via soluble antibodies

Other proposed mechanisms involved in GC collapse and shutdown include negative feedback regulation by soluble antibodies. Exogenous soluble antibodies secreted by plasma cells can infiltrate the GC and localise on the FDC network (Yang Zhang et al., 2013). Here, it is theorised that antibodies may mask epitopes on antigens and decrease available antigen over time. Mathematical modelling has predicted that high concentrations of antibody can contribute to GC shutdown, and that epitope specific antibodies shift the immune response away from immunodominant epitopes (Arulraj et al., 2019; Yang Zhang et al., 2013). In this way, GCs maintain adequate selection pressure during an immune response to generate high affinity B cells (Forsell et al., 2017). Dysregulation or heightened responses in this nature may contribute to premature shutdown or chronic GC formation.

1.4.4.3 Regulation through regulatory and helper follicular T cells

Whilst Tfh, alongside FDCs, are responsible for presenting cognate antigen to B cells within the GC, the strength and affinity of the TCR of Tfh may contribute to GC longevity. The mechanisms underlying this are currently unknown, but it has consistently been shown that lack of IL-21 signalling or CD40L blockade leads to early GC collapse (Han et al., 1995; Kishi et al., 2010). Paradoxically, constitutive activation of CD40L on B cells also results in premature termination in the GC response. Expression levels of checkpoint markers PD-1

and ICOS on Tfh can also contribute to GC downregulation, due to increased B cell apoptosis and lack of Tfh:B cell interactions (Yang Zhang et al., 2013). miRNA-146a, which regulates ICOS-ICOSL signalling within the GC is shown to peak at late stages of GC responses as numbers of Tfh reduce and might be involved in influencing GC termination (Good-Jacobson et al., 2010). Regulatory follicular T cells (Tfr) that also express Tfh markers CXCR5, PD-1, ICOS but also the transcription factor FOXP3, exert immunoregulatory effects on the GC response. Although shown to employ inhibitory action directly on B and Tfh cells via CTLA-4 signalling, it is unclear what the mechanisms are that specifically lead to Tfr-mediated GC termination. It is difficult to study the functional capabilities of Tfrs, due to the transient nature of FOXP3 expression, and more work is needed to determine their role in GC shutdown (Sage et al., 2014; Wing et al., 2014).

1.5 Immune responses within TNBC

1.5.1 Tumour infiltrating lymphocytes in TNBC

Despite its aggressive phenotype, TNBC is known to be more immunologically 'hot' than other breast cancers, as such, it often presents with high levels of TILs (Loi et al., 2020). A pivotal study by Salgado *et al.,* led to the development of scoring methodologies to assess TIL density within breast cancer, outlying the specificity to report for TILs in the stromal compartment (sTILs) (Salgado et al., 2015). These criteria advise the methods to assess sTILs within the borders of the invasive tumour as a continuous parameter, for example, 80% sTILs would indicate that 80% of the stromal area displays concentrated mononuclear infiltration (Salgado et al., 2015). Whilst not routinely used a diagnostic marker, increased levels of sTILs in both HER2+ and TNBC displays dominance over TNM staging when predicting outcome and response to chemotherapy, anti-HER2 therapy and immunotherapy (Loi et al., 2019; Salgado et al., 2015).

More recently, the in-depth characterisation of spatial TIL organisation has led to the broad classification of tumours into 4 subsets; desert tumours, with a notable absence of TILs, excluded tumours, which present with immune cells at the tumour border but none within the malignant tissue, inflamed/dispersed, in which immune cells infiltrate through stromal and intratumoral tissue but lack aggregates, and finally inflamed/stroma restricted, where TILs form definite organised structures (Hammerl et al., 2021). TNBCs with an inflamed phenotype demonstrate significantly improved distant metastasis-free survival, disease-free survival and overall survival compared to the other subtypes (Hammerl et al., 2021; Nederlof et al., 2021). However, prognostic differences between inflamed/dispersed and inflamed/stroma restricted subtypes highlights the importance of assessing TIL spatial arrangement in TNBC.

1.5.2 TIL-B responses at the primary tumour

In contrast to the longstanding characterization and manipulation of tumour infiltrating T cells (TIL-Ts) for clinical research, the potential of tumour infiltrating B cells, denoted (TIL-Bs), has only recently gained interest amongst breast cancer researchers. The majority of breast carcinomas present with relatively low levels of TIL-Bs (~ 20%), yet this is heightened compared to healthy breast tissue (Garaud et al., 2019). A variety of TIL-Bs at multiple stages of differentiation, including naïve, GC-like, memory-like and plasma cells (Chung et al., 2017; Garaud et al., 2019) have been reported within and around the TME of breast tumors, with a high percentage of TIL-B exhibiting a memory-like phenotype (Buisseret et al., 2017). Notably, the occurrence of GC-like B cells consistently correlates with numbers of Tfh cells, signifying an active and constantly evolving humoral response (Garaud et al., 2019). Despite assessment of TIL-Bs exhibiting stand-alone prognostic value, scoring of TNBC tumors often fails to include the spatial distribution of B cells. B cells in TNBC are often depleted along the borders of TNBC tumours, and dispersed infiltration of B cells is associated with a lower incidence of recurrence within 5 years (Keren et al., 2018). Clusters of heterotypic lymphocytic

infiltration containing B and T cells that form in high numbers and near cancer cells are more prevalent within tumors with improved outcome, compared to those that are fewer, larger and at a distance from malignant cell islands (Wortman et al., 2021). Although not classed as tertiary lymphoid structures (TLS), these spatial differences emphasize the importance of assessing B cell location and proximity to other immune and cancerous cells. The spatial patterns and co-localisations with other cell types further indicate the involvement of TIL-Bs in humoral immunity, with possible roles in antigen presentation and modulation of other immune populations with relevance to tumour progression.

1.5.3 TIL-Bs in tertiary lymphoid structures

In addition to antibody production and antigen presentation, B cells may also contribute to peritumoral immunity by associating with T cells to form organised structures known as TLS (Germain et al., 2015; Shen et al., 2014). When TLS are present around the carcinoma, TIL-B levels are higher in the peritumoral area and are frequently associated with superior disease free and overall survival (Figenschau et al., 2015; Sautès-Fridman et al., 2019).

TLS bear similar morphological and molecular characteristics to secondary lymphoid follicles, forming a definitive marginal zone, mantle zone and a central GC-like structure in which B cell centroblast, centrocyte subsets and Tfh cells are found (Garaud et al., 2019). Somatic mutations of the Ig variable domains of TIL-Bs isolated from T/B clusters in ductal carcinomas reveals evidence of local oligoclonal expansion of cells that have previously undergone antigen-driven hypermutation, proliferation and affinity maturation, much like within a GC (Nzula et al., 2003). To facilitate recruitment, positioning and interactions within GCs, Tfh cells can express ICOS and PD-1 that engage with cognate ICOSL+PD-L1+ centrocytes (Shi et al., 2018). Although the global proportion of PD-1+ and PD-L1+ TILs is low in breast cancers, much of the PD-1 is primarily expressed on T cells that localize within the TLS. This brings to light the impact of PD-1 as a marker of immune activation in contrast to its connotations with

immune exhaustion in the context of cancer. Moreover, gene expression of *PD-1* and *PD-L1* in TILs is significantly associated with improved clinical outcome in basal-like and HER2 enriched breast cancers (Schmid et al., 2018; Solinas et al., 2017). The transposition of these datasets to TLS in breast cancer, together with the ability to record the temporal, spatial and transcriptional profiles of GCs and TLS may further our understanding of the TIL-B populations within the TME and provide a rationale for their contribution to disease progression.

1.6 Crosstalk between primary tumour and LN within TNBC

1.6.1 Clinical assessment of the axillary LNs

Despite serving as transportation channels essential to an effective immune response, the lymphatics also act as corridors for cancerous cells to pass through into the LNs (Ji, 2016; Stacker et al., 2014). Typically presenting as the initial seeding site outside of the primary tumor, the presence of metastatic growth within LNs has been associated with both shortened disease-free survival and a heightened risk of developing metastases in distant organs. Therefore, the incidence of cancer cells within the LNs, the number of metastatic LNs and the occurrence of extra nodal extension have formed essential assessment parameters for routine pathological diagnosis of several cancers, including breast cancer.

Historically, axillary LN clearance was undertaken for all patients with invasive breast cancer. Today, the standard treatment of care for patients with clinically and radiologically negative nodes prior to surgery is surgical resection of only the nodes adjacent to and draining from the tumor bed, the so-called sentinel LNs. It is also becoming more common for breast cancer patients to receive neoadjuvant chemotherapy, which presents new challenges for assessment of the LNs. Treatment induced fibrosis and reactive changes can obscure the local environment and prevent an accurate diagnosis of LN metastasis (Brown et al., 2010).

1.6.2 Antibody production in breast cancer

As a product of the GC response, plasma cells that have undergone SHM and affinity maturation are typically long lived and capable of evoking a humoral response for many years (Brynjolfsson et al., 2018). In contrast, those that develop in extrafollicular foci do not undergo SHM, are typically short-lived, and secrete a combination of switched or unswitched antibodies (Paus et al., 2006). Comprehensive gene expression studies of TIL-B populations in breast cancer identified IgG-associated gene sets in primary carcinomas indicative of pathological complete response to trastuzumab combination therapies and superior overall survival in TNBC (Carey et al., 2014; Iglesia et al., 2014; Perou et al., 1999). Spatial analysis of such antibody responses revealed that breast lesions with high levels of tumor infiltrating plasma cells present with antibodies in their tumour core, at the invasive margin and also within the stromal compartments (Seow et al., 2020). Some of these antibodies are capbale of binding to tumour cells and display a clonal relationship with those present in the axillary LNs, indicative of a systemic response beyond the local TME (Novinger et al., 2015). Supporting a functional role for antibodies in breast cancer, mice deficient for antibody production display a more aggressive disease progression, and the adoptive transfer of IgG secreting plasma cells present in tumor draining LNs (td-LNs) limits metastatic spread (Brynjolfsson et al., 2018; Hollern et al., 2019; Li et al., 2011; Tao H. et al., 2013). However, the antigen specificity of these functionally relevant antibodies is not completely understood. Conversely, the analysis of the IgG and IgA autoantibody repertoire in breast cancer patients revealed that autoantibodies to one or more tumor-associated antigens occurred in most patients. Notably, patients with a higher level of IgG reactivity to breast cancer-associated antigens have significantly shorter recurrence free survival (Garaud et al., 2018). These findings align with studies of spontaneous LN metastasis in breast cancer mouse models. Here, the presence of IgG antibodies to a breast cancer antigen promoted tumor progression through the lymphatics (Gu et al., 2019). Many breast cancer patients demonstrate elevated levels of intratumoral and circulating IgA antibodies, shown to be associated with poor

prognosis and a reduced survival rate in patients with melanoma, colorectal and bladder cancer (Bosisio et al., 2016; Chiaruttini et al., 2017; Liu et al., 2018). As Treg mediated TGF-β can promote IgA class switching in an immune-modulatory fashion (Feng et al., 2011), further work is required to elucidate the role of plasma cells and antibody diversity within the TME of TNBCs. It remains unclear whether GC reactions contribute to the production of protective and/or tumour promoting antibodies, and the extent to which GC reactions in the context of breast cancer follow the canonical checkpoints that curb self-reactivity in physiology. This knowledge is clinically relevant as it may provide insight for strategies that selectively inhibit the development of tumour promoting antibodies and enhance cancer-protective humoral immunity.

1.6.3 Immune tolerance and regulation

An appropriate immune response to pathogens relies on a 'goldilocks window' of checkpoint inhibitor control; too little regulation promotes expansion of autoreactive cells, whereas exacerbated expression leads to anergy and exhaustion. Tolerance of GC responses is in part maintained by Tfr levels, that dampen immune responses by preventing CD28-B7 co-stimulatory interactions through CTLA-4 engagement (Miles and Connick, 2018). Circulating Tfr and Treg cells are found enriched in breast cancer patients, particularly in more aggressive cancers (Kohrt et al., 2005a; Núñez et al., 2020; Song et al., 2019). This may correlate with the knowledge that Tfr cells potently inhibit antigen-specific antibody responses (Linterman et al., 2011). Tfr and Treg cells can also induce an immunosuppressive microenvironment, often through IL-10 production, and promote the expansion of immunosuppressive B cells, so-called Bregs. In a cyclical fashion, IL-10 secreting Bregs support the Treg pool and can impede Tfh responses within the GC (Achour et al., 2017; Liu et al., 2016; Song et al., 2019). The number and localisation of Bregs in breast carcinomas strongly fluctuates with levels of Tregs, notably in and around B and T cell TIL aggregates (Guan et al., 2016; Ishigami et al., 2019). Supporting

a relationship between Bregs and Tregs, a B cell deficient breast cancer model displayed a reduced fraction of Tregs in tumor draining LNs and peritumoral areas (Tadmor et al., 2011). Further, accumulation of Tregs and Bregs within the cancer-free LNs (cf-LNs) of breast cancer patients correlates with fewer class-switched B cells in adjacent LNs with cancerous growth, indicative of a possible role in GC suppression (Mehdipour et al., 2016). This synergistic relationship between Bregs and Tregs, their ability to promote a tolerant environment, and suppress Tfh cells may influence the efficacy of GC reactions within breast cancer patients. Supporting this hypothesis, IL-10 blockade *in vivo* stimulates IgG production and enhances immune infiltration within primary breast carcinomas (Li Q. and Xia Y., 2015, 2015; Tao et al., 2015; Zheng F. et al., 2012). Bregs express PD-1 and PD-L1 which have immunomodulatory functions (Sun et al., 2019). The emerging role of Bregs in promoting immunosuppression in breast cancer may indicate these cells as candidate targets in immune-checkpoint blockade therapy. However, a potential effect of immune checkpoint inhibitors on the GC reaction should also be considered given that GC B cells themselves express PD-L1 (Good-Jacobson et al., 2010b; Hams et al., 2011).

1.7 The prognostic value of GCs in TNBC

Owing to their highly organised structures, morphological alterations in GCs could indicate fluctuations in their molecular mechanisms and polarisation ultimately impacting the quality and quantity of the resulting memory B and plasma cell populations (Bannard et al., 2013; Toboso-Navasa et al., 2020; Victora et al., 2010). Early autochthonous models of breast cancer exhibited enlarged GCs in regional LNs with increased levels of lymphoblasts, a sign of active lymphopoieses, and clusters of dividing plasma cells in the vicinity of the GC (Ciocca, 1980). Based on extensive H&E histopathological data of immune and stromal features at primary breast carcinomas, our group has previously reported histological changes in cancer-free LNs carrying additive risk predictive value for developing distant metastasis. Development

of an immune-stroma-histological (ISH)- risk score, that incorporated the number and size of GCs in cf-LNs, sTILs at the primary tumour, the presence of lymphocytic lobulitis and GC location within the involved LNs (in-LNs), was able to provide further prognostic insight when assessing outcome in TNBCs (Grigoriadis et al., 2018; Loi et al., 2020). These findings have been replicated within multiple cohorts of TNBC patients, harnessing the relationship between the LN and primary tumour to investigate potential crosstalk and communication. Whilst consistent findings have elucidated the strong association between sTILs and disease trajectory within TNBC and other cancers, we have further demonstrated the concordance between number of GCs within the draining LNs (d-LNs), sTIL infiltration at the primary tumour, and the formation of TLS (Grigoriadis et al., 2018; Liu et al., 2021).

1.8 Considerations within TNBC and purpose of thesis

There is growing evidence of the predictive and prognostic role for B cells in TNBC and other solid cancers, which warrants further investigation. Whilst their presence attributes to an improved disease trajectory, there is little information surrounding the functional capacities of GCs within the LNs. Key questions that are yet to be answered include in what capacity is there crosstalk between the B cells within the LN and primary tumour, and how may this be dysfunctional in some patients that leads to little or no anti-tumour response.

This thesis aims to address further the role of GC-derived B cell subsets within TNBC primary tumours and draining axillary LNs, harnessing transcriptional, spatial, and clinical information to determine novel factors that may attribute to distant metastasis progression. To assess the longitudinal response of B cells, *in vivo* models of TNBC were utilised to create a platform on which we can study further the initiation and collapse of GCs within td-LNs. Together, this work explores the molecular drivers and development of tumour induced GC formation and GC derived B cell populations within TNBC.

Chapter 2:
Materials and Methods

2.1 Patient sample collection

Primary breast tissue, cf-LNs and in-LNs were collected from neoadjuvant treatment naïve clinically invasive TNBC (ER-, HER2- by IHC) patients to perform immunofluorescence and imaging mass cytometry (IMC) analyses. Tissue was obtained through the King's Health Partner's Breast Cancer Tissue and Data Bank, Breast Cancer Now Tissue and Data Bank at Bart's Cancer Institute, and Tianjin Medical University Cancer Institute. Research ethics approval was obtained from the respective local research ethics committees (KHP Cancer Biobank REC ref 18/EE/0025, Barts Cancer Institute REC ref 21/EE/0072 and Medical Ethics Committee of Tianjin Medical University Cancer Institute and Hospital Ek2020021).

2.1.1 Sample collection for immunofluorescence analyses

FFPE blocks from 16 neoadjuvant treatment naïve TNBC patients that were classified as low sTILs (≤10%) were chosen as part of this study. 5μM sections from primary tumour, cf-LNs and in-LNs were sectioned by a member of the Tianjin Medical University Cancer Institute.

2.1.2 Sample collection for imaging mass cytometry

FFPE blocks from 2 neoadjuvant treatment naïve TNBC patients were chosen as part of this study. 5μM sections of their respective in-LNs were sectioned by a member of the BCN Barts cancer institute and sent via courier to Guy's Hospital for downstream processing.

2.1.3 Sample collection for microarray analyses

Microarray data was obtained for this work from 124 neoadjuvant treatment naïve clinical invasive TNBC (ER, HER2- by IHC) patients treated between 1984 and 2002 at Guy's Hospital London, UK.

2.2 Immunofluorescence staining

2.2.1 Rehydration and antigen retrieval

Tumour and LN slides were baked for 1 hour at 60°C before dewaxing and rehydration of tissue using the Tissue Tek DRS 2000 (Sakura)**,** on the 'dewax' method for 27 minutes. Samples underwent 5x dips in Xylene, 2x rounds of Xylene washes for 5 minutes, 2x rounds of 100% ethanol for 5 minutes, 1 round of 70% ethanol for 5 minutes and 1 round of tap water for 2 minutes. Heat mediated antigen retrieval was performed using the MenaPath Access Retrieval Unit (Menari Diagnostics). Sections were placed in citrate buffer pH 6.0 (DAKO) and heated to 125°C and 27 PSI for 2 minutes before cooling.

2.2.2 Blocking of tissue and antibody staining

After allowing time to cool, slides were washed 2x 5 mins with PBS (Gibco) in a clean coplin jar on an orbital shaker at room temperature (RT). After drying with tissue paper, a wax ring was drawn around the tissue using a PAP pen (Abcam). Sufficient blocking buffer was prepared to encompass blocking time, primary antibody incubation and secondary antibody incubation. Blocking buffer was prepared as follows; PBS (Gibco) with 5% Donkey serum (Jackson ImmunoResearch), and 0.5% Triton-X100 (Sigma Aldrich). 250µl of blocking buffer (adjusted accordingly for tissue size) was loaded onto the slides. The slides were incubated at RT for 30 minutes in a humidified chamber (slide box with wet paper towel inside). During blocking incubation time, the primary antibody mix was prepared, diluting the antibodies in blocking buffer. Antibodies used are shown in the table below.

Target	**Clone**	**Host species**	**Dilution**	**Manufacturer**	**Cat #**
CD20	Polyclonal	Goat	1:200	Abcam	ab194970
CD27	EPR8569	Rabbit	1:500	Abcam	ab131254
CD138	B-A38	Mouse	1:500	Novus Biologics	NB100-64980
IGF1R	JBW902	Rabbit	1:200	LSBio	LS-B2905

Table 1: Primary antibodies used in immunofluorescence B cell phenotyping of human primary tumours and axillary lymph nodes.

After 30 minutes, blocking buffer was aspirated and slides were incubated with 25µl of primary antibody master mix in a humidified chamber at 4°C overnight (in fridge). The next morning, the antibody mix was removed, and slides were washed with PBS (Gibco) in a

clean coplin jar on an orbital shaker at RT. During washing, the secondary antibody master mix was prepared, using clones and dilutions shown in the table below.

Target	Clone	Host species	Dilution	Fluorophore	Manufacturer	Cat #
Goat IgG	Polyclonal	Donkey	1:600	Alexa Fluor 594	Jackson Immunoresearch	705-585-147
Rabbit IgG	Polyclonal	Donkey	1:600	Alexa Fluor 488	Jackson Immunoresearch	711-476-152
Mouse IgG	Polyclonal	Donkey	1:600	Alexa Flour 647	Jackson Immunoresearch	715-607-003

Table 2: Secondary antibodies used in immunofluorescence B cell phenotyping of human primary tumours and lymph nodes.

Sections were incubated with the secondary antibody mix for 2 hours at RT in a humidified chamber ensuring no exposure to light, before being washed in PBS (Gibco) for 2x 5 mins in a clean coplin jar protected from light at RT. DAPI nuclear stain (Cell Signalling) was prepared at a dilution of 1:2000 in PBS (Gibco). After drying the slide carefully with tissue paper, 250ul of diluted DAPI solution was added to the sections and incubated at RT for 5 minutes in the dark. The slides were then washed 3x in PBS (Gibco) for 5 minutes in a clean coplin jar covered in foil on an orbital shaker, before dipped 5 times in distilled water. Slides were dried before adding 1 drop of mounting medium (Millipore), gently adding a coverslip (VWR) and left to dry overnight at 4°C.

2.2.3 Immunofluorescence imaging

Whole slide images were taken using the Olympus VS120 (Olympus). A 4X overview image was taken using the nuclear staining on the Alexa Fluor 405 channel to obtain an understanding of the tissue morphology. Once the tissue was identified, the LNs and tumours were imaged at 20X magnification using Alexa Fluor 405, Alexa Fluor 488, Alexa Fluor 594 and Alexa Fluor 647. Exposure time were set based on the negative control LN tissue which was stained with no secondary antibody to determine background autofluorescence. Images were exported as VSI files.

2.2.4 Image analysis

Images were opened in Olympus OlyVIA software (Olympus) for general observation of staining quality before exporting the files to (Quantitative Pathology & Bioimage Anylysis) QuPath software (Bankhead et al., 2017). Cell segmentation was performed using the cell selection tool on the nuclear staining. Manual annotations were drawn for staining on each channel and assigned a classifier name corresponding to the antigen that was stained for e.g., CD27. These classifiers were trained based on 3 LNs in the dataset and 3 tumours before being applied to all images. The numbers of positive cells for each classifier were calculated, enabling quantification of CD20+, CD27+, CD138+, CD20+CD27+, CD27+CD138+ and CD20+CD27+CD138+ cells.

2.3 Imaging mass cytometry

2.3.1 Rehydration and antigen retrieval

LN and tumour sections were baked at 60C for 1 hour to ensure adhesion to slides, before proceeding to rehydration and antigen retrieval. Slides were manually incubated in 3 rounds of xylene, replacing with fresh xylene each time, 10 minutes in each coplin jar at RT. The slides were then incubated for 10 minutes in a solution of 50% xylene and 50% 100%

ethanol at RT. Periodic agitation of the slides was performed to efficiently remove wax from the tissue. Next taken through sequential steps of 5 minutes each, the slides were passed through 96% ethanol, 90% ethanol, 80% ethanol, 70% and finally DPBS (Gibco) for 10 minutes. Heat mediated antigen retrieval was performed using the MenaPath access retrieval unit (Menari Diagnostics). Sections were placed in antigen retrieval solution pH 9.0 (R&D systems) and heated to 125°C at 27 PSI for 2 minutes before cooling. When cooled, slides were washed in DPBS (Gibco) for 5 minutes at RT, dried with Kim-Tech tissue paper (Kimberly-Clark) and the tissue encircled with wax using a PAP pen (Abcam).

2.3.2 Permeabilisation and blocking

Permeabilisation buffer was prepared and warmed to 37°C in advance, adding 0.1% Tween-20 (Sigma Aldrich) to PBS (Gibco). The slides were flushed twice using a Pasteur pipette and then washed 2x in 50ml of warm buffer on an orbital shaker for 8 minutes. Blocking buffer was made using two stock solutions: 10% BSA (Sigma Aldrich) in Superblock (Thermofisher) and 1% Tween-20 (Sigma Aldrich) in Superblock (Thermofisher). From these stocks, the working blocking buffer solution was prepared as shown in the table below.

	Per 100ul
10% BSA stock solution	50ul
Superblock	30ul
FcR block (Biolegend)	5ul
1% Tween-20 stock solution	10ul

Table 3: Composition of blocking buffer used in imaging mass cytometry protocol.

2.3.3 Antibody staining

After permeablisation, slides were dried using Kim-Tech tissue (Kimberly-Clark), transferred to a humidified box, and incubated with blocking buffer for 2 hours. A master mix of metal-conjugated antibodies was prepared in blocking buffer as shown in the table below.

Target	Clone	Metal	Dilution	Incubation	Manufacturer	Cat #
Pan keratin	C11	148 Nd	1:00	4 hours RT	Fluidigm	3155016D
CD19	6OMP31	142 Nd	1:100	4 hours RT	Fluidigm	3142016D
IgM	IM260	176 Yb	1:100	4 hours RT	Abcam	ab233886
CD38	EPR4106	141 Pr	1:100	Overnight 4°C	Fluidigm	3141018D
FoxP3	236A/E7	155 Gd	1:50	Overnight 4°C	Fluidigm	3155016D
CD4	EPR6855	156 Gd	1:100	Overnight 4°C	Fluidigm	3156033D
CD8	D8A8Y	162 Dy	1:50	Overnight 4°C	Fluidigm	3162035D
PD1	EPR4877(2)	165 Ho	1:50	Overnight 4°C	Fluidigm	3165039D
Ki67	B56	168 Er	1:50	Overnight 4°C	Fluidigm	3168022D
CD3	Polyclonal	170 Er	1:100	Overnight 4°C	Fluidigm	3170019D
CD20	H1	161 Dy	1:200	Overnight 4°C	Fluidigm	3161029D
CD27	EPR8569	171 Yb	1:100	Overnight 4°C	Fluidigm	3171024D
CD45	D9M8I	152 Sm	1:1000	Overnight 4°C	Fluidigm	3152018D
CD45	HI30	152 Sm	1:1000	Overnight 4°C	Biolegend	304045

CD138	EPR6454	164 Dy	1:100	Overnight 4°C	Abcam	ab226108
IgG	EPR12700	145 Nd	1:500	Overnight 4°C	Abcam	ab250451
IgA	EPR5367-76	149 Sm	1:100	Overnight 4°C	Abcam	ab214003
IgD	EPR6146	160 Gd	1:500	Overnight 4°C	Abcam	ab236778
CD21	EP3093	166 Er	1:500	Overnight 4°C	Abcam	ab271855
CD23	5	154 Sm	1:200	Overnight 4°C	Sinobiological	10261-MM05
PD-L1	1300021	150 Nd	1:100	Overnight 4°C	R&D Systems	MAB1561
CD11c	EP1347Y	173 Yb	1:100	Overnight 4°C	Abcam	ab52632
CD68	KP1	116 Cd	1:100	Overnight 4°C	Abcam	ab955

Table 4: Metal conjugated antibodies used for imaging mass cytometry staining of human TNBC tumours and lymph nodes. RT = Room temperature.

Slides were incubated with the antibody master mix overnight at 4°C or RT for 4 hours (indicated in Table 4), then flushed with warm permeablisation buffer and then washed with fresh permeablisation buffer on an orbital shaker for 2x 8 minutes. The tissue was then flushed with DPBS (Gibco) and washed in a clean coplin jar for 8 minutes in fresh DPS (Gibco). Iridium (Fluidigm) was prepared in DPBS (Gibco) at a final concentrate of 1.25 μM. Excess DPBS (Gibco) was dried from the slides, iridium loaded onto the wax ring and slides placed into a humidified box for 30 minutes at RT. Finally, slides were flushed with RT DPBS (Gibco), washed with DPS (Gibco) on an orbital shaker for 5 minutes at RT and then washed with Milli-Q water for a further 5 minutes at RT. Slides were air dried at RT and kept for ablation at a later date.

2.3.4 Ablation and data acquisition

24 ROIs (regions of interest) across 2 in-LNs from 2 patients were chosen based on location: GC or stroma. ROIs were ablated and data acquired using the Hyperion Imaging System in the BRC Flow Cytometry Core at Guy's Hospital. Data was obtained in the mcd and text format for downstream processing.

2.3.5 Data visualisation and analysis

Files were visualised in MCD viewer (Fluidigm) to assess staining quality across all ROIs. Each channel was viewed individually to check expected staining and overall distribution. ROIs were then exported from MCD viewer as OME.TIFF files and loaded into cell profiler. Cell profiler (Stirling et al., 2021) and Ilastik (Berg et al., 2019) were used to train image crops and subsequently segment cells based on expression of nuclear markers (iridium) and cell membrane makers (CD45). This generated probability masks representing downscaled pixel probabilities after Ilastik pixel classification. The output was subsequently loaded into Rstudio (RStudio Team, 2020), and the downstream analyses were followed as per the pipeline developed by the Bodenmiller lab (Windhager et al., 2021)

2.4 Microarray analyses

2.4.1 Plasmablast gene signature

The plasmablast gene signature was obtained from (H. King et al., 2021). The signature consisted of 32 genes: *IGHG, IGHVDJsum, JCHAIN, MZB1, SSR4, XBP1, HSP90B1, DERL3, FKBP11, SEC11C, SDF2L1, PPIB, PRDM1, PRDX4, SSR3, AC012236.1, PDIA4, MYDGF, SELENOS, HERPUD1, FKBP2, HSPA5, KDELR2, ITM2C, HM13, SUB1, IGKsum, IGLsum, CCL3, IGHD, IGHA, IGHM.* The ssGSEA method (Subramanian et al., 2005) was

applied to patients with low histological sTILs (≤10%) and high histological sTILs (>10%) to categorise the patients into those with a high plasmablast score and those with a low plasmablast score. Cox proportional hazards regression models were used to determine the optimal cut-off of 0.135 for the plasmablast score.

2.4.2 Z-score normalisation

Gene expression was z score transformed and the mean and standard deviation summarised before visualising the normalised gene expression across each patient group using the r package ggplot2. The package rstatix (Kassambara et al., 2022) was then applied to determine significant changes between of the mean expression of key genes.

2.4.3 Kaplan-Meier analyses

Cox proportional hazards regression models were used to determine the optimum cut-off for the average number of GCs, histological sTIL scores and plasma cell gene signature scores. Kaplan-Meier estimators were used, and the likelihood ratio test performed to test differences amongst groups of patients.

2.4.4 Differential gene expression

Differentially expressed genes between TNBC patients with histologically low sTILs and a high plasma cell gene score (IThP) vs all other groups were identified using the limma package (Ritchie et al., 2015), which uses linear models, and can be applied to microarray and RNA sequencing data. Samples were assigned to different groups based on a design matrix and linear models fitted for each gene. A contrast matrix determines the appropriate comparison, and log-fold change standard errors are controlled using an empirical Bayes method. Genes with a Q value < 0.05 were considered differentially expressed.

2.4.5 Gene set enrichment analyses

The fgsea package (Korotkevich et al., 2021) was applied to differentially expressed genes to determine augmented pathways of interest within the IThP, and enriched pathways filtered for an enrichment score > 0. Significant pathways were identified based on a p adjusted value < 0.05.

2.4.6 TNBC clinical characteristics

PAM50 and Lehman's classifications for all 124 TNBC patients were generously provided by other members of the cancer bioinformatics group. Classifications were summarised for each patient group, and a Fisher's exact test performed to determine significant differences in the TNBC subtypes across the cohort.

2.4.7 Histological features of the LNs

Clinical data was generously provided by the KHP Biobank including number of positive LNs, and LN GC number, normalised sinus area and number of available LNs was identified by machine learning methods by other members of the cancer bioinformatics group. Data was visualised using ggplot2 (Wickham et al., 2016) to assess absolute counts of all factors across patient groups.

2.5 *In vitro* TNBC tumour cell line culture

The 4T1, 4T1.2 and 67NR cell lines were gifted from Tony Ng (King's College London). The E0771 cell line was gifted from Adrian Hayday (King's College London/The Francis Crick Institute). All lines were thawed at speed in a 37°C water bath before the addition of 1ml of pre-warmed media and then added to flasks. 4T1 and 4T1.2 cell lines were grown *in vitro* in

T75 flasks in RPMI 1640 (Gibco) supplemented with 10% FBS (Gibco) and 1% penicillin-streptomycin (Sigma-Aldrich) at 37°C with 5% CO_2. Cell lines were allowed to grow to 70% confluency and passaged 2x weekly depending on growth, using 0.05% trypsin-EDTA (Gibco). 67NR and E0771 cell lines were grown *in vitro* in T75 flasks in DMEM (Glutamax) (Gibco), supplemented with 10% FBS (Gibco) and 1% penicillin-streptomycin (Sigma-Aldrich). Cells were allowed to grow to 70% confluency and passaged 2x weekly depending on growth using 0.05% trypsin-EDTA (Gibco). E0771 cell lines grew partially in suspension, so at every passage the supernatant was removed and centrifuged at 1200 RPM for 7 minutes, and then resuspended in fresh media and added to the newly split flasks.

2.6 *In vivo* study of TNBC tumours

2.6.1 Preparation of cell lines for injection

Supernatant from cell lines, except for the E0771 line was aspirated and 2ml of 0.05% trypsin-EDTA was added to the flasks, before placing inside the incubator at 37°C for 5 minutes. For the E0771 cell line, the supernatant was removed and centrifuged at 1200 RPM for 7 minutes and kept on ice until needed. Once cells had been displaced from the flasks, they were placed in 5 ml of fresh media. This media for the E0771 was used to resuspend the pellet previous obtained from the supernatant, to ensure all cells were together. Cells were counted using the Vi-CELL (Beckman Coulter). 4×10^5 cells were separated for each cell line, placed in 15ml falcon tubes (Appleton Woods) and centrifuged at 1500 RPM for 5 minutes. The supernatant was aspirated, and the cells resuspended in 1ml of pre-thawed Matrigel (Corning). Cells were kept on ice and taken to the Biological Research Unit (Francis Crick Institute) for injections.

2.6.2 Mammary fat pad injections

7–12-week-old BALB/c or C57BL/6 mice were placed under anaesthetic for 5 minutes using isoflurane. Once mice were safely anaesthetised by checking foot reflexes, paper towel soaked with 5% ethanol was used to douse the mammary fat pad on the right-hand side of the mouse and reveal the skin. Matrigel-cell line mix was drawn up using 1ml insulin needles (BD Bioscience). Pinching the skin to prevent injections into the peritoneum, 10ul of the cell line (4×10^5 cells) was injected into the 4^{th} mammary fat pad, adjacent to the nipple. The mice were then exposed to pure oxygen for 2 minutes, ear marked and weighed before being allowed to recover in a separate area to the rest of the cage. BALB/c mice were used for 4T1, 4T1.2 and 67NR cell lines and C57BL/6 for the E0771.

2.6.3 Monitoring of tumour growth and mouse mass

Mice were checked every other day for weight loss and tumour growth. Tumours measured as soon as palpable using callipers.

2.6.4 IGF1 administration *in vivo*

10 7–11-week-old BALB/c were administered 4×10^5 67NR cells on day 0, under isoflurane anaesthetic as described above. IGF1 (1mg/kg) was injected subcutaneously into the right flank of the mice close to the tumour site daily from day 1-4, and then on day 6, day 8 and day 10. This change in injection frequency was due to unexpected inflammation at the injection site.

2.6.5 Organ harvesting and cell staining

At day 7, 10, 14, 21, and day 28, mice were sacrificed and the tumours, td-LNs from the right-hand side of the mouse (d-LNs for control mice), non-draining LNs (nd-LNs) from the opposite side of the mouse, and the spleen were removed. Organs were immediately placed in ice cold PBS, before being weighed. The tumours were then placed in 10% neutral buffered formalin. LNs and spleens were dissociated using plungers from 2.5ml syringes (BD Biosciences) and filtered through 70μM pre-equilibrated filters (BD Biosciences) into 50ml falcons (Fisher Scientific) containing 1 ml ice-cold facs buffer (PBS supplanted with 1% FBS and 0.5% EDTA). Filters were flushed with 2ml of facs buffer, and the cells centrifuged for 5 mins at 1500 RPM and the supernatant aspirated. LN cells were then counted using the Vi-CELL (Beckman Coulter) and kept on ice until needed. Red blood cell lysis buffer was prepared using the volumes of buffers provided by the Francis Crick Institute as shown in table 5.

Buffer A	Buffer B	Buffer C	Final Volume
1.5ml	1.5ml	2.0 ml	5ml

Table 5: Volumes of buffers used to prepare red blood cell lysis buffer (representative of 1 sample).

5ml of red blood cell lysis buffer was added to each spleen sample and incubated at RT for 5 minutes, before quenching with 5ml of facs buffer and centrifuging for 5 mins at 1500 RPM.

The supernatant was aspirated, and the cell pellet resuspended in 5ml of facs buffer, before counting the cells using the Vi-CELL (Beckman Coulter). 5x 10^5 cells from each LN (if possible, otherwise the total number obtained was added), and spleen sample were added to a v-bottom 96 well cell culture plate (Thermofisher Scientific). Antibody mixes for the GC/Plasma cell panel were prepared as shown in table 6.

Channel	Fluorophore	Target	Dilution	Manufacturer	Cat#
530/30 Blue	FITC	IgM	1:200	BD Biosciences	553437
710/50 Blue	ef710	CXCR4	1:200	Thermofisher	46-9991-82
586/15 Yellow	PE	CD273	1:200	Biolegend	107206
780/60 Yellow	PECy-7	B220	1:200	Biolegend	103221
395/15 UV	BUV395	IgD	1:200	BD Biosciences	564274
530/30 UV	BUV737	IgG1	1:200	BD Biosciences	741733
670/14 Red	APC	CD19	1:200	Biolegend	115512
780/60 Red	ef780	Viability	1:500	Biolegend	423106
450/50 Violet	BV421	CD38	1:200	Biolegend	102732
525/50 Violet	BV510	CD95/Fas	1:200	BD Biosciences	740507
610/20 Violet	BV605	CD86	1:200	Biolegend	105014
670/30 Violet	BV786	CD138	1:200	BD Biosciences	740880

Table 6: Antibodies used for flow cytometric staining of lymph nodes and spleens.

The antibody master mix was made up in facs buffer, with the addition of murine fc block (Biolegend) at a concentration of 1:200. 80µl of this mix was then added to each well containing LN and spleen samples, accounting for a negative control of unstained spleen cells. Cells were stained for 30 minutes at RT in the dark before washing with 100ul PBS (Gibco) and centrifuging for 5 mins at 1500 RPM. This was then aspirated, and the cells resuspended in 100ul of facs buffer.

2.6.6 Flow cytometric analysis

Compensation beads were prepared for each fluorophore used in the experimental design, using single fluorophore labelled antibodies with anti-rat and anti-Armenian hamster beads (BD Biosciences) at the time of antibody incubation for samples. Beads not labelled with any antibody were used as negative controls to set where the negative populations would lie. Compensation was performed in BD FACSDiva (BD Biosciences), which determined the spectral intersection between each single stained fluorophore, and this was manually adjusted when necessary to minimize the overlap in fluorescent emission.

Samples were acquired on the BD LSR Fortessa (BD Biosciences) flow cytometer, utilising lasers at 355nm (UV), 405nm (violet), 488nm (blue), 561nm (yellow green) and 633nm (red). All flow cytometry was performed within the Flow Cytometry STP at the Francis Crick Institute. Data were recorded in the FCS 3.0 file format within the BD FacsDiva 6.0 programme (BD Biosciences).

2.6.7 Data analysis

FCS files were imported into FlowJo version 10.7.2.(Dickinson and Company, Becton, 2023) For flow cytometry experiments, lymphocytes were identified based on their forward and side-scatter properties, single cells and then dead cells eliminated. B cells were gated on based on co-expression of CD19 and B200, and GC B cells as CD38 low, Fas/CD95 high. Plasma cells were located when expressing high levels of CD138 and low B220. Further, more extensive phenotypic analysis was undertaken to check the immunoglobulin isotypes and GC B cell populations.

2.7 *In vitro* studies

2.7.1 Enzyme-Linked Immunosorbent Assays (ELISA)

Supernatant taken from 4T1, 4T1.2 and 67NR tumour slices kept in culture for 48 hours was frozen at -80°C until needed for further experiments. Conditioned media was also taken from the 4T1, 67NR and CAF cell lines, and uncultured media for negative controls. Aliquots from each sample was then taken and thawed on ice, ensuring enough for 3 replicates per cell line. The mouse/rat IGF1 Quantikine ELISA kit (R&D systems) was then used to detect the presence of IGF1 in all the supernatants, as per the manufacturer's instructions.

2.7.2 Isolation of B cells for co-culture experiments

Spleens and inguinal LNs from 12–16-week-old BALB/c mice were harvested and processed to obtain single cell suspension. Cells were washed in PBS (Gibco) and then centrifuged at 1500 RPM for 5 minutes at RT. Cells were then incubated with anti CD43-biotin(cat no: 553269, BD Biosciences) and anti-TER-119-biotin (cat no: 116204, Biolegend) antibodies at 1:200 dilution in facs buffer for 30 minutes at 4°C, before washing in PBS (Gibco) and centrifuging at 1500 RPM for 5 minutes at RT. Cells were then incubated with macs biotin separation beads (Miltenyi Biotec) as per the manufacturer's instructions and incubated for a further 30 minutes at 4°C. A final wash was performed with PBS (Gibco) before again centrifuging for at 1500 RPM for 5 minutes at RT. The cells were then resuspended in 1ml of facs buffer. Magnetic selection was then performed using LS columns as per the manufacturer's instructions (Miltenyi Biotec) and the flow through collected for downstream experiments.

2.7.3. Plasmid design and preparation

The IGF1 plasmid vector was designed using Vectorbuilder as shown in Figure 2. The mouse IGF1 gene was inserted, alongside an EF1A (eukaryotic translation elongation factor 1 α1) promoter, a SV40 (simian virus 40 late) polyadenylation signal, a CMW (cytomegalovirus) promoter, and an ampicillin resistance gene. determine successful transfection, a EGFP (enhanced green fluorescent protein) ORF (open reading frame) was further added.

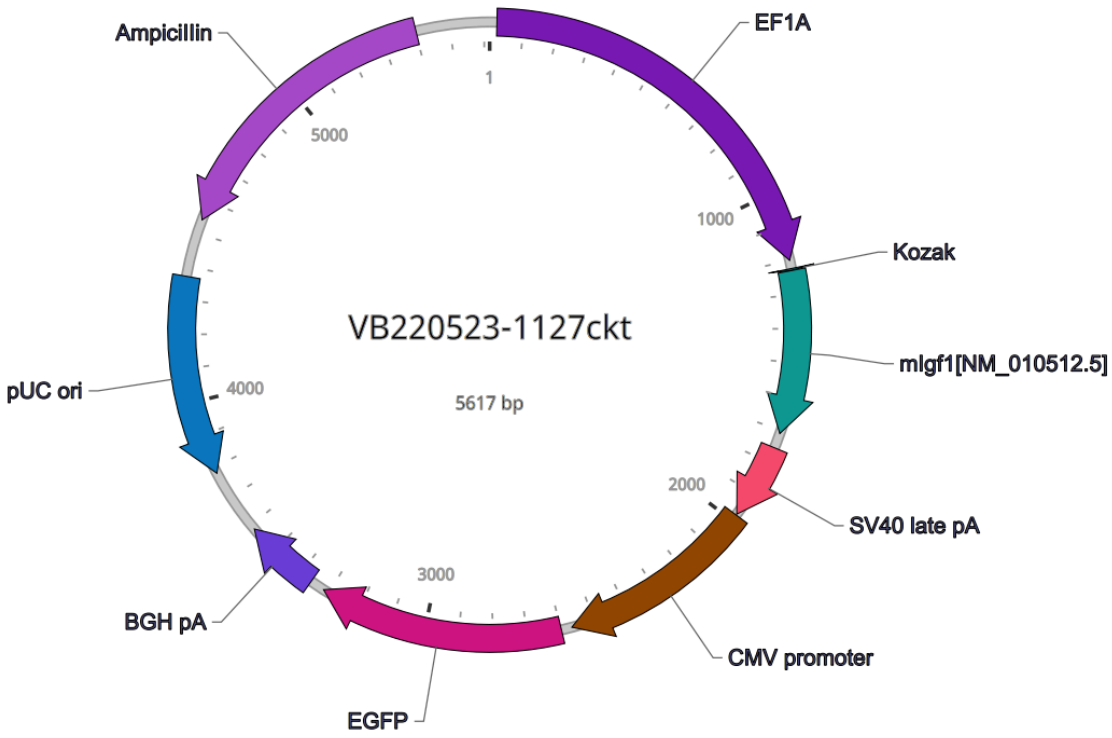

Figure 2: IGF1 plasmid design. Vector map of gene expression vector used for transfection of IGF1, showing key genes and selected resistance genes. Indicated on the map are EFIA (eukaryotic translation elongation factor 1 α1 promoter), Kozak (Kozak translation initiation sequence), SV40 late pA (simian virus 40 late polyadenylation signal), mIGF1 (mouse IGF1 gene), CMV promoter (cytomegalovirus immediate early enhancer/promoter), EGF (enhanced green fluorescent protein), BGH pA (bovine growth hormone polyadenylation signal), pUC ori (pUC origin of replication), Ampicillin. The size of the vector is indicated in bp (base pairs).

2.7.3.1 Plasmid extraction

1µl of the glycerol stock of vector was added to a 250 ml LB (lysogeny broth) liquid culture and incubated in a shaking incubator overnight, supplemented with 100 µg/ml of ampicillin. After 12 hours, the culture was centrifuged at 6000 x g for 15 minutes at 4°C, and the plasmid DNA extracted using the HiSpeed Plasmid Maxi kit (Qiagen), as per the manufacturer's instructions. The final concentration was then measured using a NanoDrop spectrophotometer (Thermo Fisher Scientific).

2.7.4 CAF transfection

Cancer associated fibroblast (CAF) cells were allowed to grow to 70% confluency before transfection. On the day of transfection, media was replaced with serum free media (Opti-MEM (Gibco). Lipofectamine 3000 (Invitrogen) was diluted in Opti-MEM (Gibco). Plasmid DNA was diluted in Opti-MEM and added to P3000 reagent (Invitrogen) as per the manufacturer's instructions and mixed well. Diluted DNA was subsequently added to diluted Lipofectamine 3000 (Invitrogen) at a 1:1 ratio and incubated at RT for 5 minutes. The DNA-lipid complex was then added to the CAF cells and incubated for 4 days at 37°C before analysing using an EVOS imaging microscope.

2.7.5 Cell line spheroids

4T1.2 and 67NR cell lines were resuspended in Matrigel (Corning) and seeded at $5x10^4$ cells per well as Matrigel domes. Domes were allowed to set in the incubator at 37°C for 30 minutes before 500µl of organoid media administered to each well.

2.7.5.1 Spheroid media

Spheroid media was prepared as a stock solution of ADDF containing 10mM HEPES (Sigma), 1x Glutamax (Gibco) and 100 U/ml Penicillin/Streptomycin (Gibco) in advanced DMEM/F-12 (Gibco). 50ml ADDF was then supplemented with 1x B27 (Gibco), 50ng/ml mouse epidermal growth factor (EGF) (Sigma) and 125μM N-Acetylcysteine (Sigma).

2.8 Statistical analysis

All *in vivo work* was analysed using GraphPad Prism Version 9 (GraphPad Software Inc). If data was normally distributed, a student's t-test was used for comparison between the two groups. If the data was non-normally distributed, a Mann-Whitney U (non-paired data) or Wilcoxon matched-paired signed rank test (paired data) was applied. Data is present as medians with interquartile ranges unless specified, and a p value of < 0.05 was considered statistically significant. All other statistical testing was performed in Rstudio (RStudio Team, 2020) and the test used stated for each figure.

Chapter 3:

Characterisation of molecular features and B cell populations in human TNBC tumours and axillary LNs

Introduction

Despite TNBC exhibiting the most aggressive characteristics and poor disease trajectory, it is known to be more immunologically hot than other breast cancer subtypes. Therefore, sTIL density within these tumours has been employed for its ability to predict outcome and response to chemotherapy, anti-HER2 therapy and immunotherapy (Ignatiadis et al., 2019; Loi et al., 2020). This has led to an increased interest in defining the immune populations in the TME of these patients that may be subsequently harnessed for therapeutic potential.

Unlike characterisation of TIL-Ts, the potential applications of TIL-B infiltration have only recently gained interest within the breast cancer field (Garaud et al., 2019). There is strong concordance between TIL-B infiltration and TIL-T density within breast cancers, and an increased presence of TIL-B is consistently associated with a significantly favourable prognosis. B-cell gene signatures and CD20+ infiltration scoring using IHC have affirmed association with improved overall survival and distant disease-free survival time. (Arias-Pulido et al., 2018; Harris et al., 2021; Hu et al., 2021; Schmidt et al., 2021) . Furthermore, utilising a univariate Cox regression model, a 14 gene immunoglobulin (IGG) gene signature displayed a significant association with overall survival in breast cancer patients (Schettini et al., 2022).

Alongside antibody production, antigen presentation and cytokine secretion, B cells within the TME may also contribute to peritumoral immunity by associating with T cells to form TLS' (Germain et al. 2015; Shen et al. 2018). When TLS are present around the tumour, TIL-B levels are higher in the peritumoral areas and are frequently associated with superior distant

disease free survival and overall survival (Figenschau et al., 2015; Lee et al., 2016; Sautès-Fridman et al., 2019).

The most characterised B cell population within TNBC and other breast cancer subtypes is that of memory B cells, whereby an elevated density of memory B cell infiltration within the primary tumour is consistently associated with prolonged survival and longer time to distant metastasis development (Harris et al., 2021). However, the role of plasma cells is more poorly understood. In breast cancer, mice deficient for antibody production display a more aggressive disease phenotype, and the adoptive transfer of IgG secreting plasma cells from td-LNs limits metastatic spread (Brynjolfsson et al., 2018; Hollern et al., 2019; Li et al., 2011; Tao H. et al., 2013). However many breast cancer patients demonstrate elevated levels of systemic IgA antibodies, which are frequently associated with poor prognosis and a reduced survival rate in patients with melanoma, colorectal and bladder cancer (Bosisio et al., 2016; Chiaruttini et al., 2017; Liu et al., 2018). Furthermore, work by Gu *et al.,* has suggested that pathogenic IgG antibodies can facilitate LN metastasis by harnessing the CXCR4/CXCL12 axis (Gu et al., 2019).

Whilst many of these studies address gene signatures, density of cell infiltration and spatial organisation, many do not encompass the overall sTIL score of the tumour and therefore do not distinguish between immunologically hot or cold tumours. Moreover, sTIL scoring using conventional histopathological methods is not an exact reflection of the immune composition within the TME. Tumour associated macrophages (TAMs) and tumour associated neutrophils (TANs) present in a high abundance can exert immunosuppressive mechanisms, and a correlation between EMT and macrophage subsets is associated with metastasis development within breast cancer patients (Su et al., 2014; Wu and Zhang, 2020). This accumulation of TAMs and TANs leads to an antigen presentation deficit which in turn results in an absence of T cell priming within the adjacent LN (Figure 3). Due to the positive correlation between sTILs and outcome, this therefore implicates the ratio of pro- and anti-tumour immune subsets as a possible biomarker of disease trajectory. This contrasts with

immune-hot tumours with high levels of sTILs, where adequate tumour antigen and an increased T cell activation leads to systemic priming of adjacent LNs and, in turn can initiate GC formation.

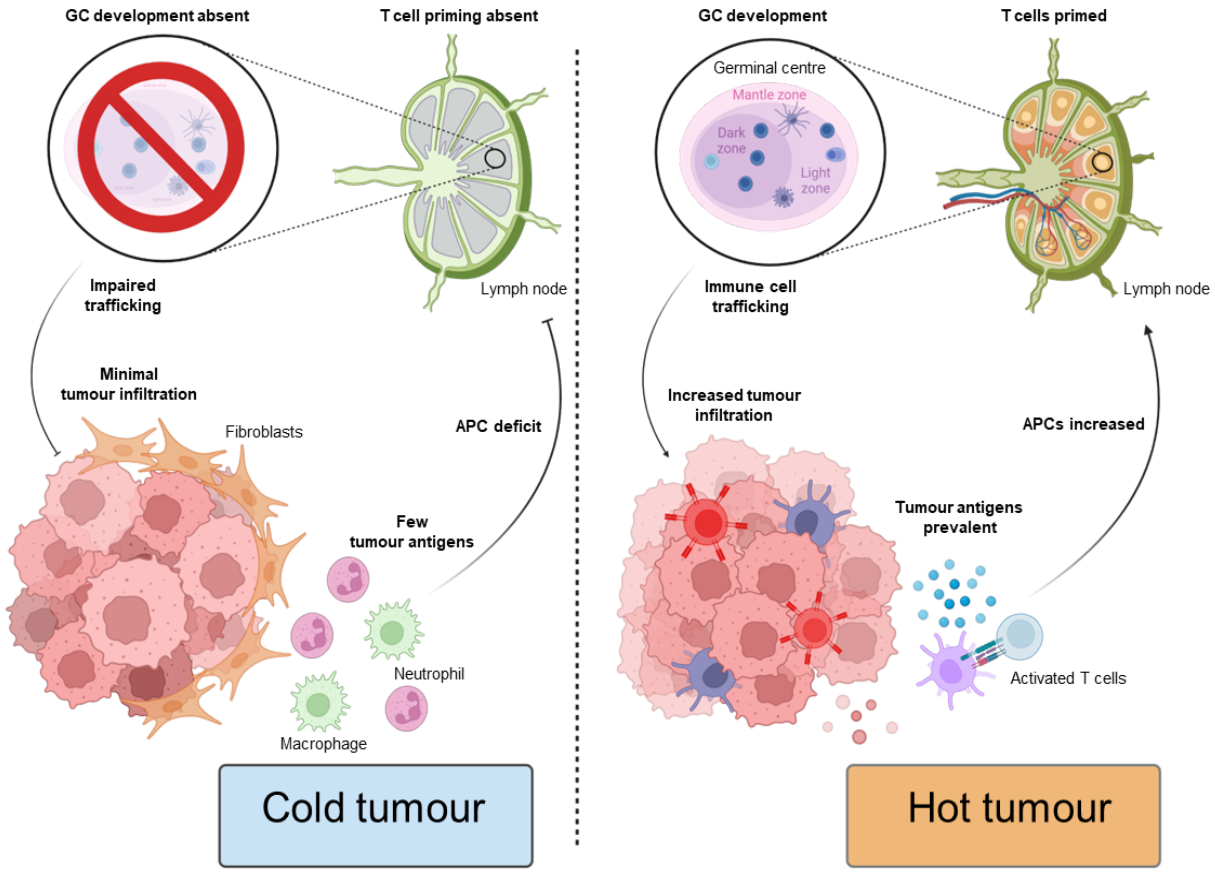

Figure 3: Visual representation of immune cold and hot tumours. Adapted from Bonaventure *et al*., 2019. Lack of T cell infiltration in cold tumour may be due to reduced tumour antigen, antigen presentation deficit, absence of T cell priming within peripheral lymph nodes and impaired tracking to the tumour (left panel). This is in concordance with an increased fibroblast network and accumulation of immunosuppressive myeloid and neutrophil subsets. This is contrast to hot tumours (right panel), where increased tumour antigen leads to the activation of T cells through antigen presentation and germinal centre (GC) formation within peripheral lymph nodes. Adequate priming of T and B cells within the lymph nodes further leads to increased T cell tumour infiltration at the primary tumour.

Despite extensive analyses of immune infiltration within triple negative tumours, the relationship between TIL-B and B cells within adjacent LNs has not been fully investigated. Histopathological assessment of morphological features using whole slide images (WSI) of LNs by our group has previously shown a relationship between sTILs at the primary tumour, the formation of TLS, and the number of GCs. Furthermore, incorporating GC and sinus information provided additive prognostic insight when assessing distant disease-free survival and overall survival in TNBC (Grigoriadis et al., 2018; Liu et al., 2021). High throughput BCR sequencing by McDaniel *et al*., has subsequently revealed evidence of B cell affinity maturation and IgG antibody production against the cancer-testis antigen NY-ESO-1 within sentinel LNs and peripheral blood. This provides potential evidence of a systemic immune response that may originate from adjacent LNs (McDaniel et al., 2018). Furthermore, although studies have been performed to assess immune cell populations within the LNs, high throughput analyses of the GC, the subsets that are required for their function and the consequent GC output has not previously been investigated. Determining this will further our understanding of how tumour infiltrating immune responses may be attributed to B cell mechanisms within the LNs, and how the TME can influence both local and systemic responses, affect sTIL infiltration and regulate metastasis development. Considering the potential deficiencies in GC responses of patients that develop distant metastasis, this may be representative of a systemic immune suppression between primary tumour, periphery, and LN (Alberts et al., 2021).

Aims and objectives:

In this chapter, I characterised GC and B cell immune subsets within the primary tumour, cf-LNs and in-LNs, and their association with disease progression within TNBC patients, considering sTIL scoring of the tumour. Data and samples were available from 3 TNBC cohorts: Bart's, Guy's and Tianjin, which enabled profiling of GCs using imaging and gene expression modalities.

To characterise GCs and immune cell subsets within the axillary LNs of TNBC patients that may be attributed to outcome, IMC and immunofluorescence techniques were performed.

This enabled:

- the characterisation of lymphoid (B, T, and plasma cells) and myeloid populations involved in the GC reaction, their spatial arrangement within the LNs of TNBC patients, and how their prevalence is associated with the risk of developing distant metastasis

This answered the following questions:

1. Are there differences in lymphoid and myeloid populations in the in-LNs of TNBC patients that are associated with the risk of developing distant metastasis?
2. Do these changes exhibit spatial properties which may influence GC functions within these LNs and contribute to or impede distant metastasis development?

To assess immune populations associated with the GC response within the primary tumour of TNBC patients, immune deconvolution from a published single cell dataset was applied to bulk gene expression data available from Guy's cohort, while considering sTIL infiltration. To investigate these patients in more depth, outcome analyses, molecular subtyping and clinical features were extracted to determine if these were associated with immune features and risk of developing distant metastasis.

This answered the following questions:

1. Is gene expression of GC immune populations within TNBC tumours associated with higher risk of developing of distant metastasis?
2. Are these phenotypes attributed to TNBC tumours with low or high sTILs?
3. Are these phenotypes associated with a specific molecular breast cancer subtype and number of in-LNs?

Finally, findings were corroborated on an external cohort of TNBC patients (Tianjin cohort), where immunofluorescence methods were used to profile GC B cell subsets within the tumour and paired axillary cf- and in-LNs.

This answered the following questions:

1. What is the relationship between the frequency of these immune populations between the primary tumour, cf-LNs, and in-LNs?
2. Are increased or decreased levels of these immune populations associated with a risk of developing distant metastasis?
3. What is the spatial distribution of these immune subsets?

3.1 Data collection

Data was obtained from three cohorts of TNBC patients: Bart's, Guy's and Tianjin, as shown in Figure 4. In-LN tissue sections within the Bart's cohort were available as a pilot study, encompassing 1 patient with high sTILs at the primary tumour that did not develop distant metastasis (patient 1) and 1 patient with low sTILs at the primary tumour that developed distant metastasis (patient 2). Within the Guy's cohort, microarray gene expression data from the primary tumour and whole slide images (WSI) of paired axillary LNs was available, totalling 124 patients. Within this group, 48 patients had low sTILs at the primary tumour, and 76 patients had high sTILs at the primary tumour. Patients were dichotomised based on distant metastasis development within either a low or high sTILs setting. This subsequently resulted in 30 patients within the low sTILs group that did not develop distant metastasis and 18 that did develop distant metastasis. Within the high sTILs patients, 59 did not develop distant metastasis and 17 did develop distant metastasis. Finally, the Tianjin cohort was chosen as a validation cohort, which incorporated primary tumour and paired cf- and in-LN sections from low sTILs TNBC patients. Within this group, 8 of the patients did not develop distant metastasis and 8 did develop distant metastasis. Clinical and histological features (if available) are described in more detail below.

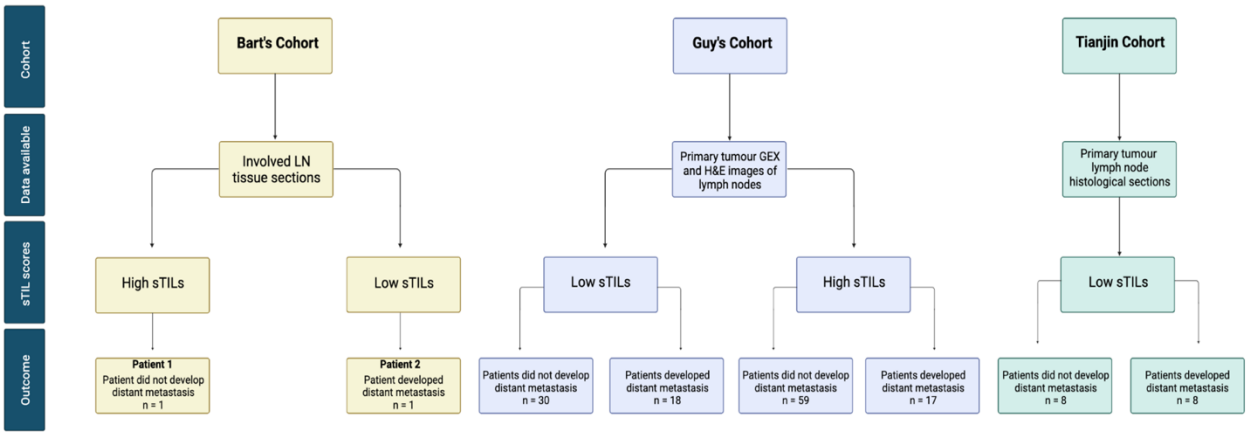

Figure 4: Overview of data collected from Bart's, Guy's and Tianjin cohorts. Consort diagram of cohorts collected for downstream analyses using imaging mass cytometry, gene expression and immunofluorescence. From top to bottom: cohorts used, type of data available, histological sTIL score classification and outcome of patients, including number of samples available for analysis.

3.1.1 Bart's breast cancer cohort

3.1.1.1 Clinical characteristics of tumour and lymph node

The Bart's TNBC cohort consisted of the LNs of 2 patients with invasive TNBC, used a pilot study for the IMC panel staining, ablation with the Hyperion mass cytometer and spatial profiling of immune cell subsets involved in the GC reactions. TNBC patient 1 was free of distant metastasis, whilst TNBC patient 2 developed distant metastasis within 48 months. Patient 1 was slightly younger (55 vs 79 years old at diagnosis) and had a pTstage 1 tumour compared to a pTstage 2 tumour in the patient 2. The tumour of patient 1 had a considerably lower sTILs score (20% vs 80%). Both patients had a pNstage of 2, whereby patient 1 had fewer in-LNs (4 vs 6). Both patients were treatment naïve at time of analyses. The clinical characteristics are outline in Table 7.

3.1.2 Guy's breast cancer cohort

3.1.2.1 Clinical characteristics of tumour and lymph nodes

Patients with invasive TNBC treated between 1984-2002 at Guy's hospital were selected for microarray analysis of the primary tumour and histological characterisation of the paired LNs, totalling 124. Patient age at diagnoses was comparable between the group that did not develop distant metastasis and those that did (55.66 vs 54.2). The pTstage of the tumours within the group that did not develop distant metastasis was primarily pTstage 2 (55%), whereas within the patients that did develop distant metastasis, there was a similar amount that were pTstage 2 and pTstage 3 (37% and 31% respectively). There were more tumours within the group that did not develop distant metastasis exhibiting the highest sTIL score of 4 compared to those that did develop distant metastasis (16% vs 3%), and more tumours within the group that developed distant metastasis exhibited an sTIL score of 0 compared to those from the group that did not (6% vs 1%). LN metastasis was present in 52/124 (44%) patients, 52/124 were LN-negative (43%). LN status was unavailable for 18/124 (15%) of patients. Patients that developed distant metastasis had a higher incidence of pNstage 3 compared to those that did not develop distant metastasis (9% vs 0%) with fewer patients exhibiting pNstage 0 in the group that developed distant metastasis compared to the group that did not (46% vs 63%). Notably, 38% of patients within the group that developed distant metastasis had ≥ 4 in-LNs compared to 4% in the group that did not. The distant metastasis free survival time in the group that developed distant metastasis was 12.9 months, and these patients exhibited an overall survival time of 20.9 months compared to the group that did not develop distant metastasis (36.1 months) (Table 7).

3.1.2.2 Histological characteristics of tumour and lymph nodes

Whole slide images (WSIs) of H&E stained LNs were available for 47 of the 124 patients as shown in Table 7. LN involvement was present in 31/47 of cases with paired WSI data available. Data was obtained from work done by other members of the group, in which digitalised WSIs were assessed using a multiscale embedded deep learning (DL)-framework to capture GCs and sinuses across 5 LNs per patient (Gregory Verghese and Mengyuan Li). The average GC number within each LN ranged between 0 and 74 but was predominantly ≤ 5 (77%). Notably, the range of the maximum number of GCs within 1 LN was large, with 26% exhibiting ≤ 5 but 1 LN presenting with as many as 238. Normalised sinus area ranged from 1.52 – 24.7μm across all LNs, with the maximum area detected within 1 LN between 16-35 μM.

3.1.3 Tianjin breast cancer cohort cohort

3.1.3.1 Clinical characteristics of tumour and lymph nodes

Within the Tianjin TNBC cohort, 16 patient matched primary tumours, cf-LNs and in-LNs were stained for analysis using immunofluorescence. All tumours within this cohort were low sTILs, scoring 0, 5 or 10% sTILs by independent histopathologists. The patients were subsequently split into 2 groups based on distant metastasis development, and the average time to distant metastasis progression was 29.5 months. The mean overall survival time for patients that did not develop distant metastasis was 130.1 months compared to 46.9 months in the group that did not. Notably, 25% of patients that did not develop distant metastasis were alive at the end of the study compared to 0% of patients that had tumour progression to distant sites. Both patient groups had predominantly tumours with a pTstage of 2 (87.50% in both groups), however 1 patient within those that developed distant metastasis presented with a pTstage 3 tumour and 1 in the group that did not develop distant metastasis was

classed as pTstage 1. Whilst patients that developed distant metastasis had no TLS scored at their primary tumours, there was evidence of TLS formation within 3 patients in the group that did not develop distant metastasis (37.5%). The pNstage in both the patients that developed distant metastasis and the group that did not was primarily pNstage 2 (62.5% vs 50%), with both groups exhibiting similar degrees of number of in-LNs (Table 7).

Bart's Cohort			Guy's Cohort			Tianjin Cohort		
	No distant metastasis (Patient 1)	Distant metastasis (Patient 2)		No distant metastasis	Distant metastasis		No distant metastasis	Distant metastasis
Patient age at diagnosis			**Patient age at diagnosis**			**Patient age at diagnosis**		
	55	79	Median (range)	55.66 (24.10 - 84.36)	54.2 (27.35 - 86.86)	Median (range)	56 (35-68)	55.5 (36-64)
pTstage			**pTstage**			**pTstage**		
1	100%	0%	1	26%	29%	1	12.5%	0%3
2	0%	100%	2	55%	37%	2	87.5%	93.75%
3	0%	0%	3	17%	31%	3	0%	6.25%
Unknown	0%	0%	Unknown	2%	3%	Unknown		
sTILs (%)			**sTILs**			**sTILs (%)**		
	80%	20%	0	1%	6%	0	12.5%	25%
			1	11%	17%	5	50%	25%
			2	21%	26%	10	37.5%	50%
			3	51%	46%			
			4	16%	3%			
TLS	NA	NA	**TLS**	NA	NA	**TLS**		
Absent			Absent			Absent	62.5%	100%
Present			Present			Present	37.5%	0%
pNstage			**pNstage**			**pNstage**		
0	0%	0%	0	63%	46%	0	0%	0%
1	0%	0%	1	33%	17%	1	50%	62.5%
2	100%	100%	2	4%	29%	2	25%	25%
3	0%	0%	3	0%	9%	3	25%	12.5%
# involved lymph nodes			**# involved lymph nodes**			**# involved lymph nodes**		
0	0%	0%	0	63%	46%	0	0%	0%
1-3	0%	0%	1-3	33%	17%	1-3	50%	62.5%
4-9	100%	100%	4-9	4%	29%	4-9	25%	12.5%
≥ 10	0%	0%	≥ 10	0%	9%	≥ 10	25%	25%
DMFS time (months)	NA	48	**DMFS time (months)**	NA	12.9 (0.1 -167.5)	**DMFS time (months)**	NA	29.5 (12-50)
OS time (months)	NA	48	**OS time (months)**	36.1 (4.6 - 266.7)	20.9 (2.4 -177.3)	**OS time (months)**	136.1 (4.6 - 266.7)	46.9 (34-72)

Table 7: Clinical characteristics of TNBC patients from the Bart's, Guy's and Tianjin cohort. Patient information for those within the three cohorts. Age is shown as median and range for each group (where applicable). Percentages shown for proportion of patients graded according to pathological tumour staging (pTstage) and pathological nodal staging (pNstage). Stromal tumour infiltrating lymphocyte (sTIL) scores shown for each patient group, as a percentage, or as quantitative score for Guy's cohort. Number of involved lymph nodes shown as percentage within each group. Distant

metastasis free survival (DMFS) time and overall survival (OS) time recorded as median and range in brackets.

3.2 Spatial and cellular characterisation of in-LNs in Bart's TNBC cohort

3.2.1 Outline of imagine mass cytometry experiment

The Bart's breast cancer cohort was used as a pilot study for the IMC experiment, which was chosen to profile multiple immune cell subsets associated with the GC response and their spatial arrangement within the LNs. A panel encompassing a DNA marker and the following 23 markers was designed: Pan-cytokeratin, CD19, IgM, CD38, FoxP3, CD4, CD8, PD1, Ki67, CD3, CD20, CD27, CD45, CD138, IgG, IgA, IgD, CD21, CD23, PDL1, CD11c and CD68, (see also chapter 2, materials and methods, section 2.3.2). To investigate immune subset differences within areas containing a GCs and non-GC areas of the LN, 12 ROIs were chosen within an in-LN from each patient. Therefore, GC containing ROIs and non-GC ROIs of an in-LN could be assessed from 1 patient with high sTILs that did not develop distant metastasis compared to another patient with low sTILs that did develop distant metastasis. It was also possible to compare GC ROIs with non-GC ROIs to define immune cell subsets present in and around the GC but not within the non-GC of the LN, and vice versa. ROIs were ablated using the Hyperion mass cytometer and downstream analyses performed, as outlined in chapter 2, materials and methods, sections 2.3.4 and 2.3.5 (Figure 5).

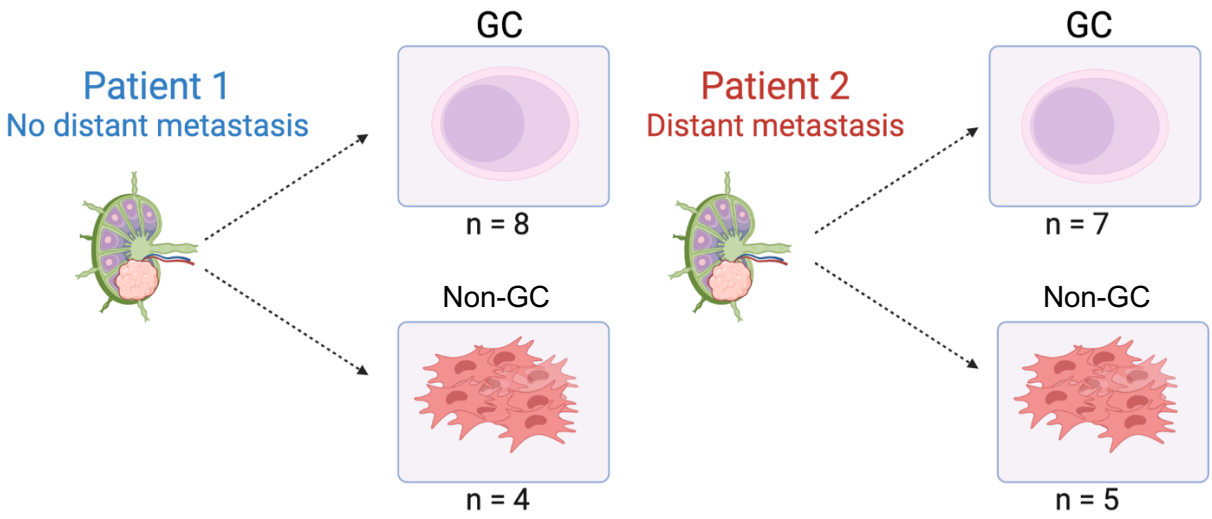

Figure 5: Schematic of IMC experimental outline.12 ROIs were identified from involved lymph nodes from one patient that did not develop distant metastasis (patient 1) and one that did (patient 2). Within each patient, ROIs were split into whether they contained a germinal centre (GC) or did not (non-GC).

3.2.2 Quality control of marker staining and cell segmentation

To avoid analysis biases from a small number of cells expressing high expression of certain markers, IMC counts are commonly transformed or clipped. Here, counts transformation was applied using an inverse hyperbolic sine function which is routinely applied to flow cytometry data (Folcarelli et al., 2022). This ensures that the distribution of counts across each ROI for each marker is normalised. CD20 expression is shown in Figure 6, as an example. Manual assessment of the area of cells across each ROI was performed to avoid any cell segmentation issues. Despite each ROI containing some tumour cells, in addition to the fact that tumour cells are substantially larger than lymphocytes, the cell area across each ROI

was consistent (Figure 7A). Visualisation of the cell masks generated during the analysis process were mapped onto ROIs, confirming expression levels of markers known to be highly expressed within these areas e.g., CD20, CD23, CD3 and Pan-keratin (Figure 7B).

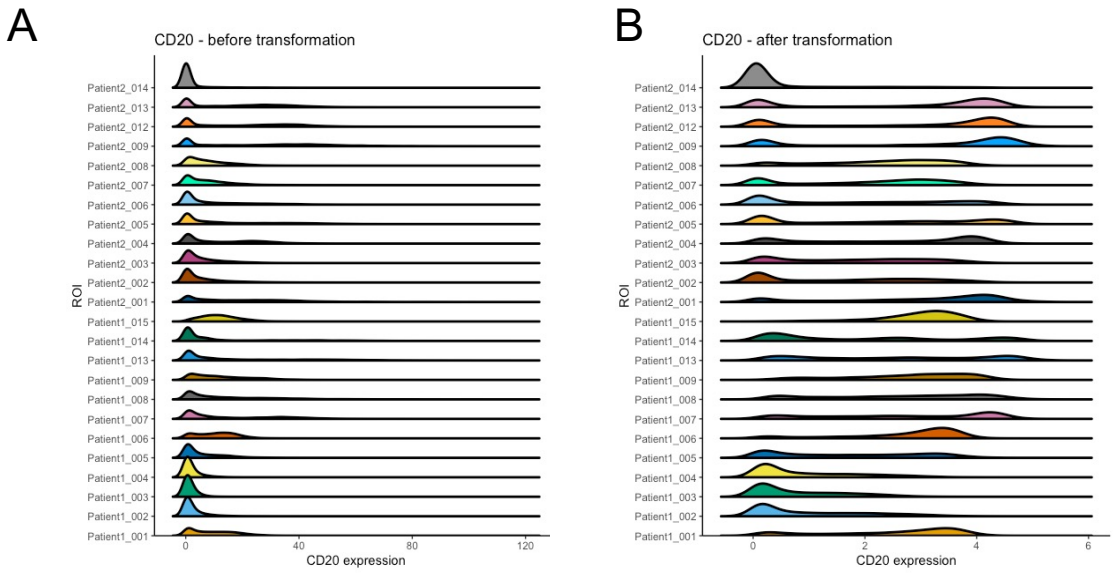

Figure 6: Arcsine transformation of marker expression. (A) Expression of CD20 across patient ROIs before inverse hyperbolic transformation. (B) Expression of CD20 across patient ROIs after inverse hyperbolic sine transformation.

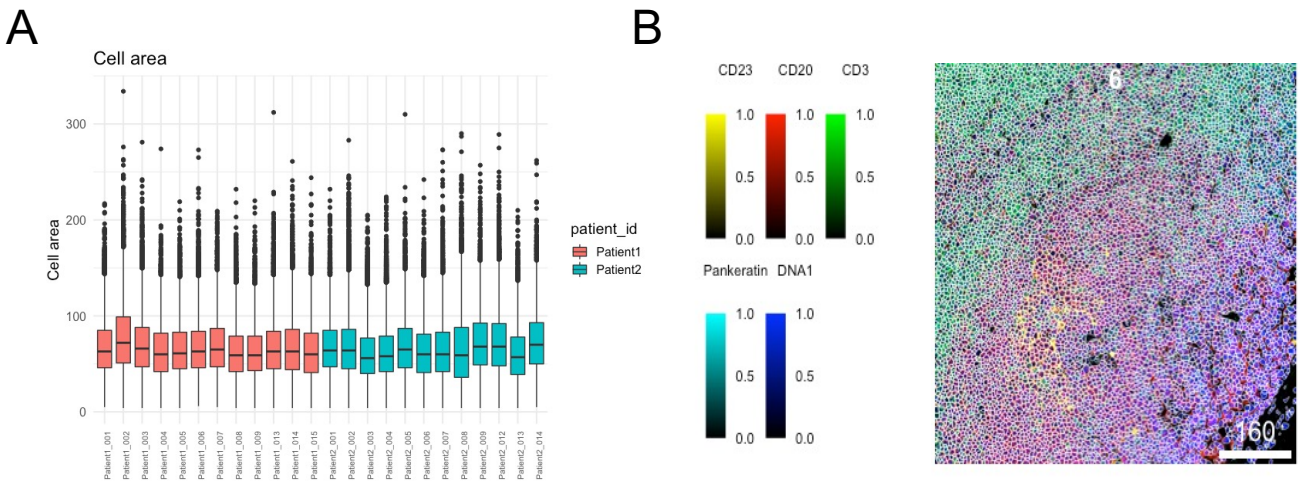

Figure 7: Cell area across patient ROIs. (A) Distribution of cell area in pixels across each ROI. Cell areas from ROIs visualised in red from patient 1 and blue from patient 2. (B) Segmentation mask on a representative ROI with expression markers CD23 (yellow), CD20 (red), CD3 (green), Pankeratin (cyan) and DNA (blue). Scale bar shown in μm.

3.2.3. Establish differences between GC and non-GC ROIs

High dimensional reduction analyses using UMAP of all segmented cells showed subtle but notable differences between the patients (Figure 8A), which seemingly was more apparent when stratifying based on ROI type: GC or non-GC. There were areas of cells that were not prevalent within ROIs non conataining a GC compared to that of GC ROIs (Figure 8B) and prominent differences between patients when focusing on GC ROIs (Figure 8C) and non-GC ROIs separately (Figure 8D).

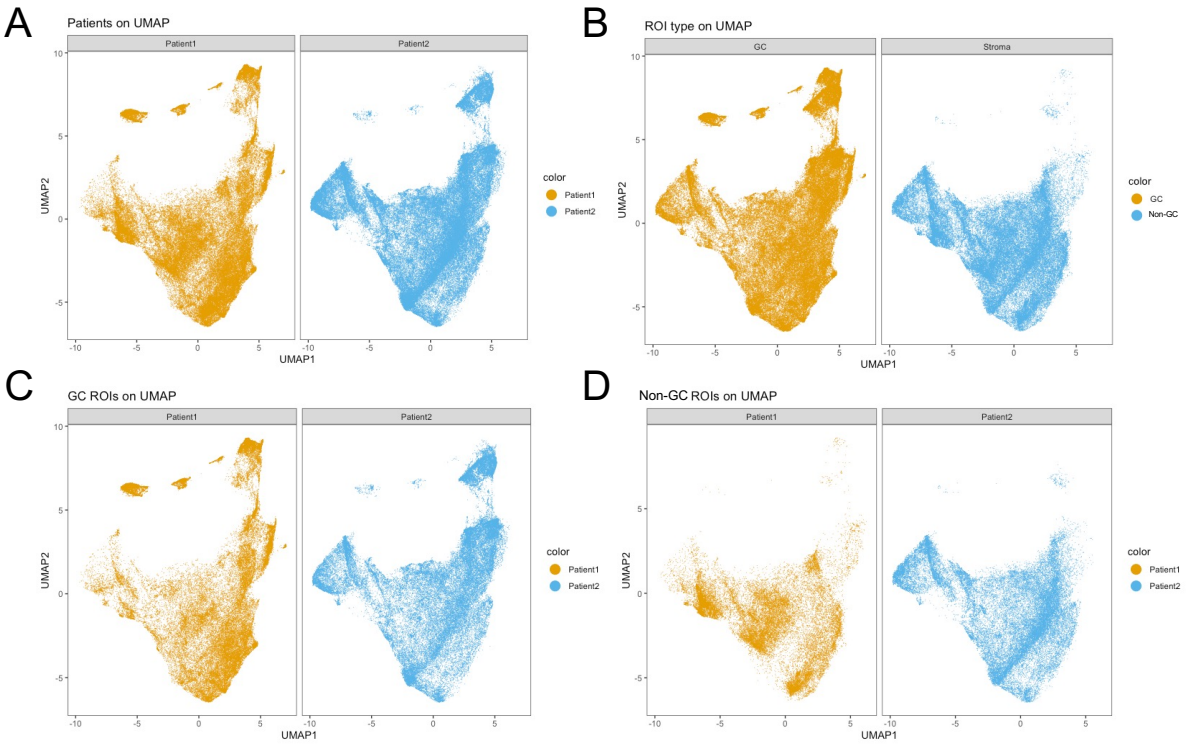

Figure 8: UMAP projections for segmented cells within germinal centre and non-GC ROIs. (A) UMAP projections of segmented cells within ROIs from patient 1 (yellow) and patient 2 (blue). (B) UMAP projections for segmented cells from ROIs containing a germinal centre (GC) (yellow) and those from non-GC areas (blue) across both patient samples. (C) UMAP projections of segmented cells from GC ROIs within patient 1 (yellow) and patient 2 (blue). (D) UMAP projection of segmented cells from non-GC ROIs within patient 1 (yellow) and patient 2 (blue).

3.2.4 A random forest classifier accurately detects immune cell subsets

To define the cell subsets that were present within these ROIs, a cell type classification approach based on ground truth labelling and random forest classification was applied. This utilised information contained in the pre-defined markers to detect cells of interest, used by Hoch *et al*., to classify cell types in a metastatic melanoma IMC dataset (Hoch et al., 2022). The cytomapperShiny function within the cytomapper package (Eling et al., 2020) allowed manual gating of cells based on their marker expression. The random forest classifier was applied to all segmented cells in all ROIs to define cell types based on marker expression levels. A cross-validation model was applied, within which different portions of the data are selected, tested and trained on different iterations. This sampled 11 randomly selected predictors to establish previously defined cell subsets (Figure 9A). The dataset of all segmented cells was split into 5 partitions, training on 4 partitions, testing on 1 partition and repeated 5 times, changing which partition was tested on each time. This resulted in classification of 17 cell types: CD4+T cells, CD8+ T cells, double negative (DN) 1 cells, DN2 cells, follicular B cells, IgA+ plasma cells, IgG+ plasma cells, IgM+ plasma cells, macrophages, marginal zone (MZ) B cells, naïve B cells, switched B cells, PD-1+ CD4+ T cells, CD8+ PD-1+ T cells, Tregs, unswitched B cells and tumour cells. Defining markers used for these cells are laid out in Table 8. Cells with a maximum probability of 0.4 were classed as ‘undefined’, which was 15% of all segmented cells (Figure 9B).

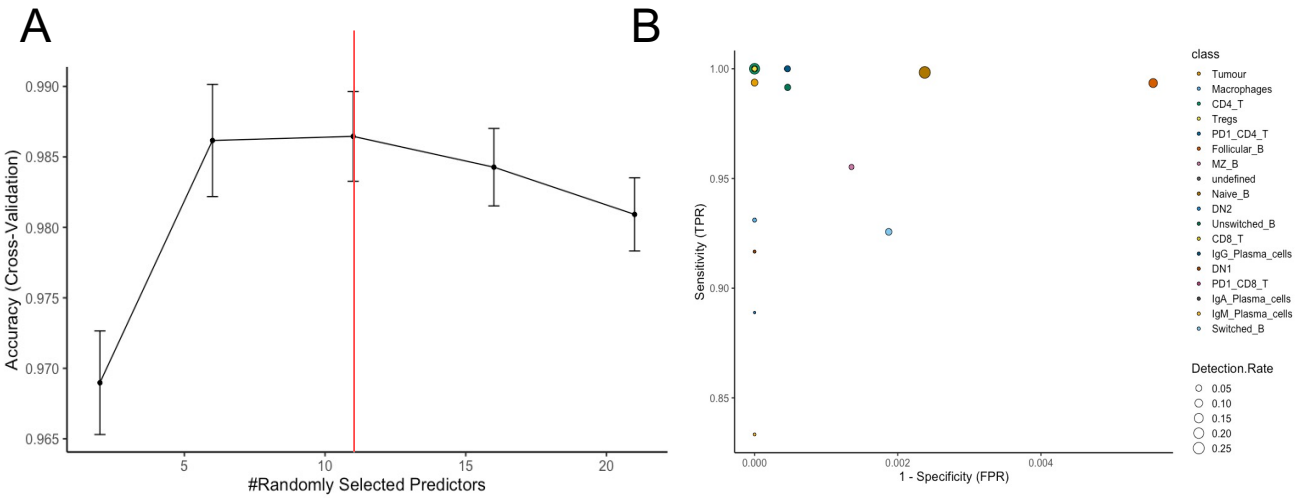

Figure 9: Immune cell type detection in ROIs of involved lymph nodes. (A) Cross-validation accuracy of random forest classifier when randomly sampling predictors between 0 and 20. The final value used for the model was mtry = 11 (red line). (B) True positive rate (TPR) of sensitivity and false positive rate (FDR) specificity of 17 cell types identified using a random forest classifier.

Cell type	Defining marker expression
CD4_T	CD45+CD3+CD4+
CD8_T	CD45+CD3+CD8+
Tregs	CD45+CD3+CD4+FoxP3+
PD1_CD4_T	CD45+CD3+CD4+PD-1+
PD1_CD8_T	CD45+CD3+CD8+PD-1+
Unswitched_B	CD45+CD20+IgD+CD27+
Switched_B	CD45+CD20+IgD-CD27+
Naïve_B	CD45+CD20+IgD+CD27-
Double_negative_1	CD45+CD20+IgD-CD27-CD21+
Double_negative_2	CD45+CD20+IgD-CD27-CD11c+
Follicular_B	CD45+CD20+IgD-CD23+CD21+
Marginal_zone_B	CD45+CD20+IgM+IgD^{low}CD23-CD21+
IgA_plasma_cells	CD45+CD20-CD38+IgA+
IgG_plasma_cells	CD45+CD20-CD38+IgG+
IgM_plasma_cells	CD45+CD20-CD38+IgM+
Macrophages	CD45+CD20-CD3-CD68+
Tumour	CD45-Pankeratin+

Table 8: Markers used to define 17 cell types classified within Bart's TNBC lymph nodes. Immune cell populations identified using cell classification based on positive or negative expression of key defining markers.

3.3 Establish differences in immune cell types across patient ROIs and ROI types

Using UMAP projections, cell types were mapped to compare cell type differences between all ROIs taken from patient 1 compared with those taken from patient 2. This showed a potential increase in MZ B cells within the LN from patient 2, increased macrophage cells, and a decrease in PD-1+ CD4+T cells across all ROIs within patient 1 (Figure 10A-B). To further compare cell composition across cell types present in GC ROIs compared to non-GC ROIs within these patient's LNs, UMAP projections for the 17 cell types were mapped to all GC ROIs compared to all non-GC ROIs from both patients. As expected, GC ROIs presented with a smaller population of follicular B, naïve B, unswitched B and MZ B compared to ROIs in non-GC areas (Figure 10C-D). Mapping these cell types back onto the ROIs showed GCs ROIs as follicular B and naïve B rich areas, and non-GC ROIs more densely populated with tumour, macrophage, and mixture of T cell and plasma cell subsets (Figure 11). Further comparing cell types as a percentage of each ROI between patients suggested a substantial decrease in PD1+ CD4+ T cells, PD1+ CD8+ T cells and an increase in macrophages in patient 2 (Figure 12-13A/B).

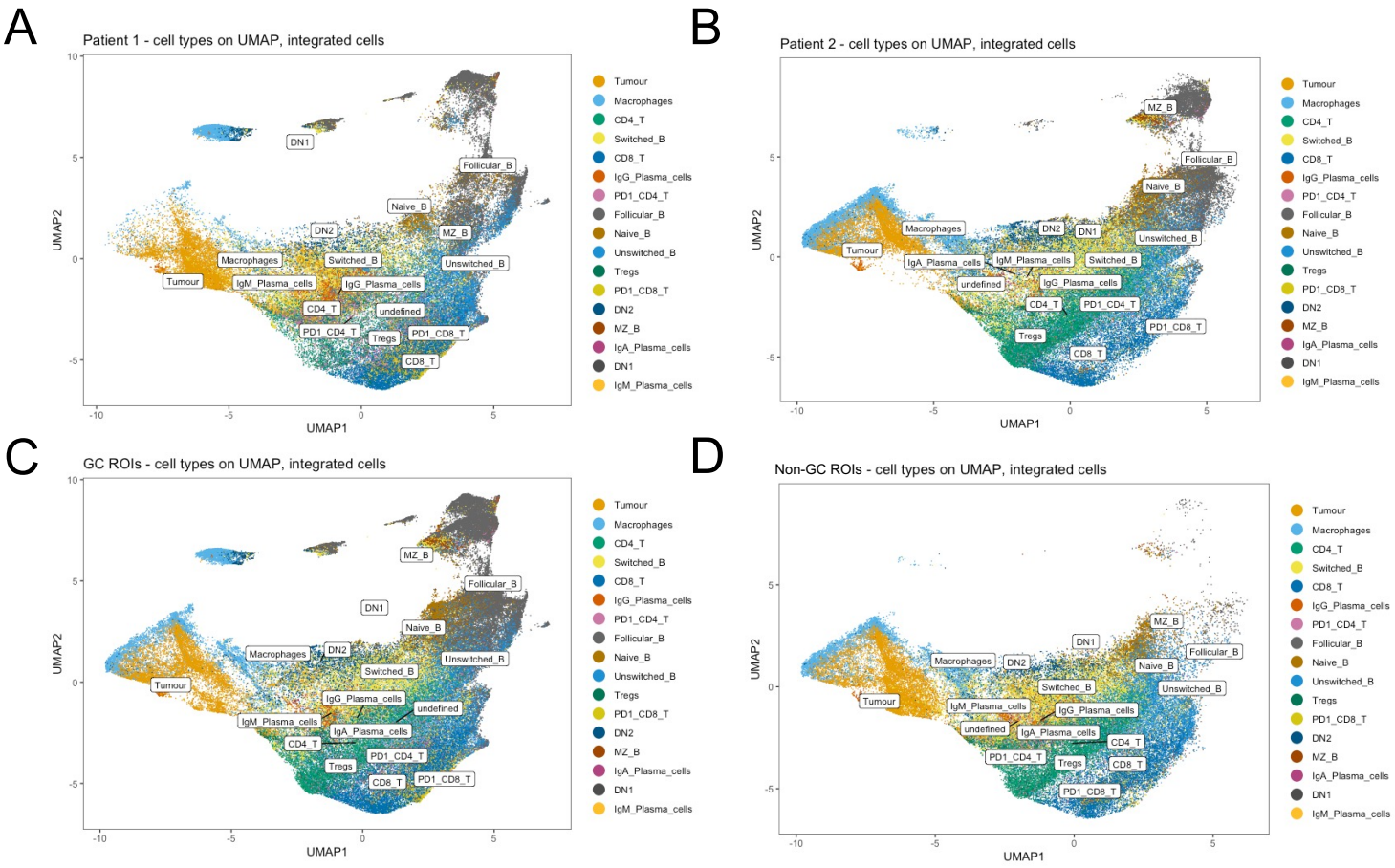

Figure 10: Cell types on germinal centre and non-GC ROIs within lymph nodes. (A) UMAP projection of segmented cells from lymph node ROIs from patient 1, labelled by cell type. (B) UMAP projection of segmented cells from lymph node ROIs from patient 2, labelled by cell type. (C) UMAP projection of segmented cells from lymph node ROIs containing germinal centres (GCs) from both patients, labelled by cell type. (D) UMAP projection of segmented cells from lymph node ROIs containing germinal centres (GCs) from both patients, labelled by cell type.

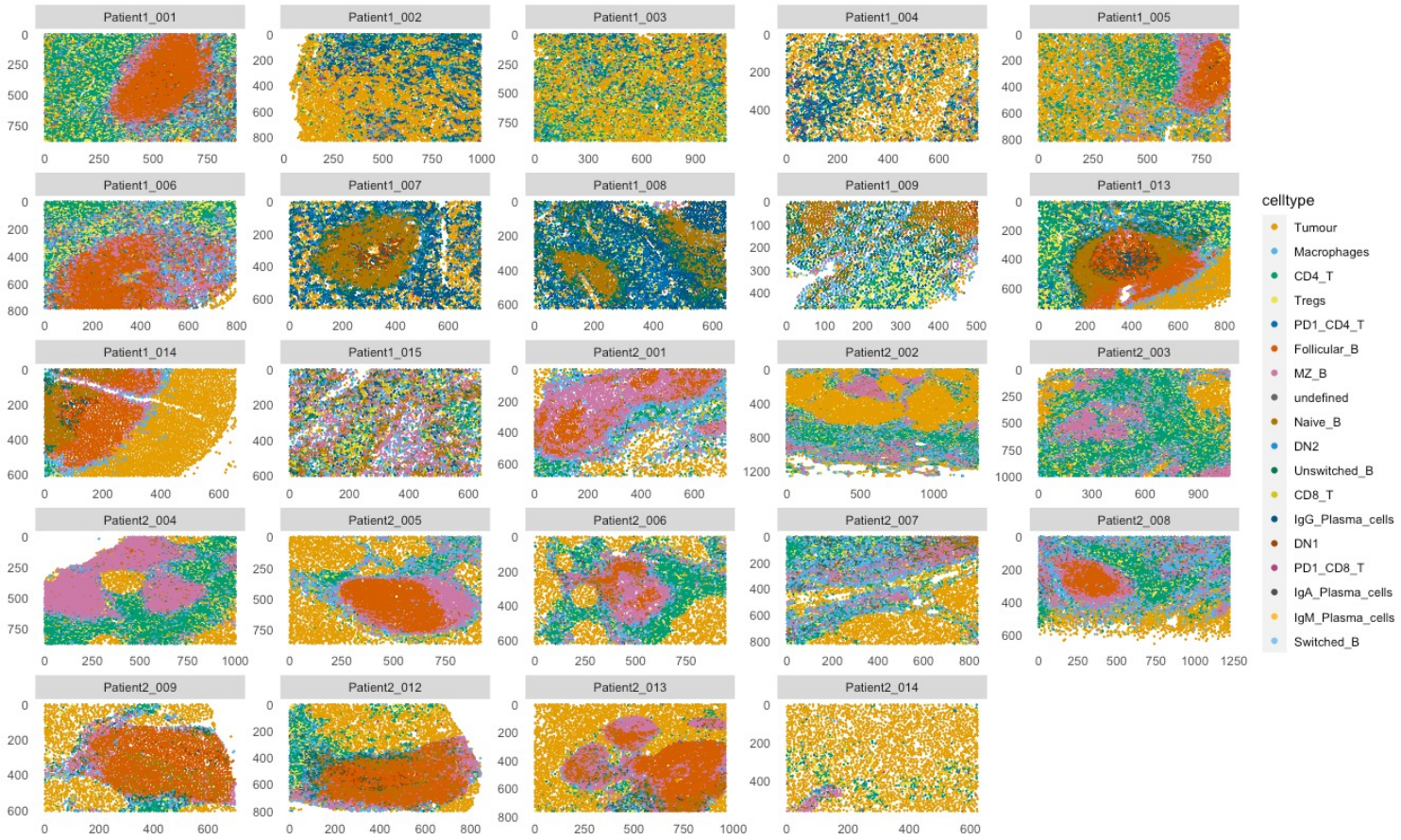

Figure 11: Spatial mapping of 17 cell types across patient ROIs. Spatial distribution of the 17 cell types identified across all patient ROIs, coloured by cell type.

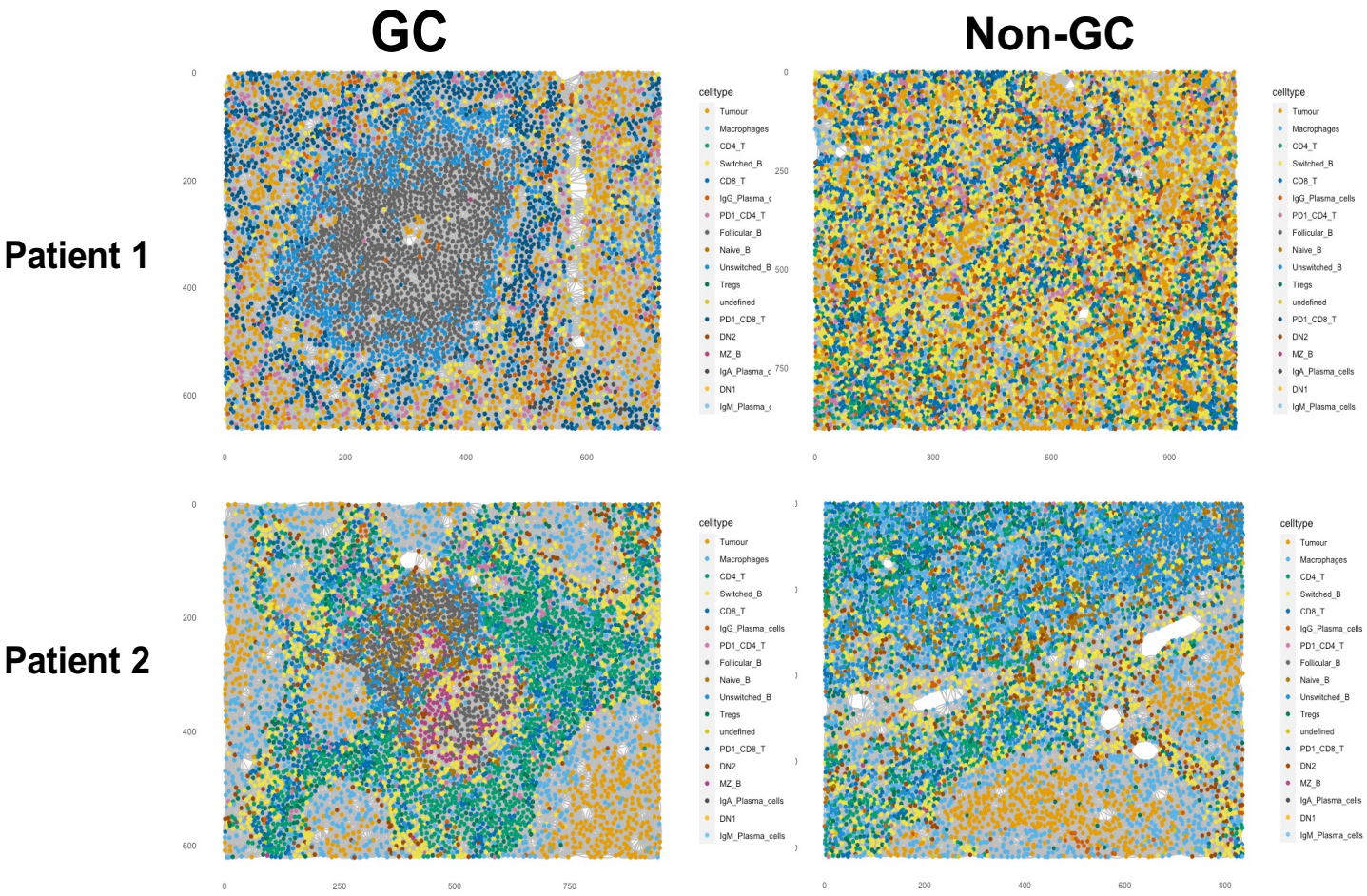

Figure 12: Representative GC and non-GC ROIs. Representative GC and non-GC ROIs from patient 1 that did not develop distant metastasis and patient 2 that did, coloured by cell type.

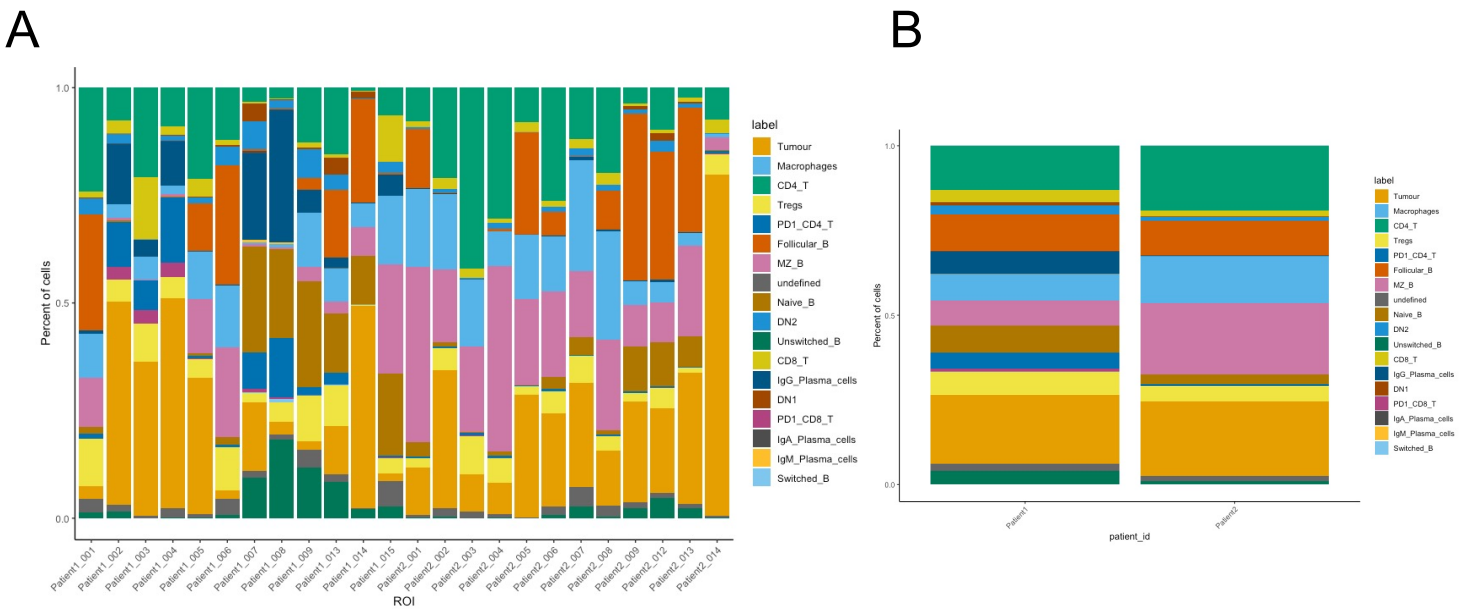

Figure 13: Cell types as a percentage of all cells detected within patient ROIs. (A) Cell types as a percentage of segmented cells within all lymph node ROIs, coloured by cell type. (B) Cell types as a percentage of segmented cells within lymph node ROIs from patient 1 and patient 2, coloured by cell type.

3.3.1 Cellular composition in LNs differs in between patients with different disease trajectories

To correctly quantify these cell types further, cell type numbers/mm^2 were normalised to the area of each ROI and compared between patients. This revealed no differences in the numbers of overall T cells (CD4+ T cells and CD8+ T cells combined), however there was a significant increase in CD4+ T cells within patient 2 accompanied by a decrease in CD8+ T cells (Figure 14A-D). This is in accordance with data showing an increase in CD8+ T cell infiltration at the primary tumour being associated with a better prognosis, including improved overall, distant metastasis free survival and response to immunotherapy (Ali et al., 2014; Jin and Hu, 2020,; Joseph et al., 2021), in addition to a high CD8/CD4 ratio in the TME of breast carcinoma being indicative of a superior disease trajectory (Wang et al., 2017).

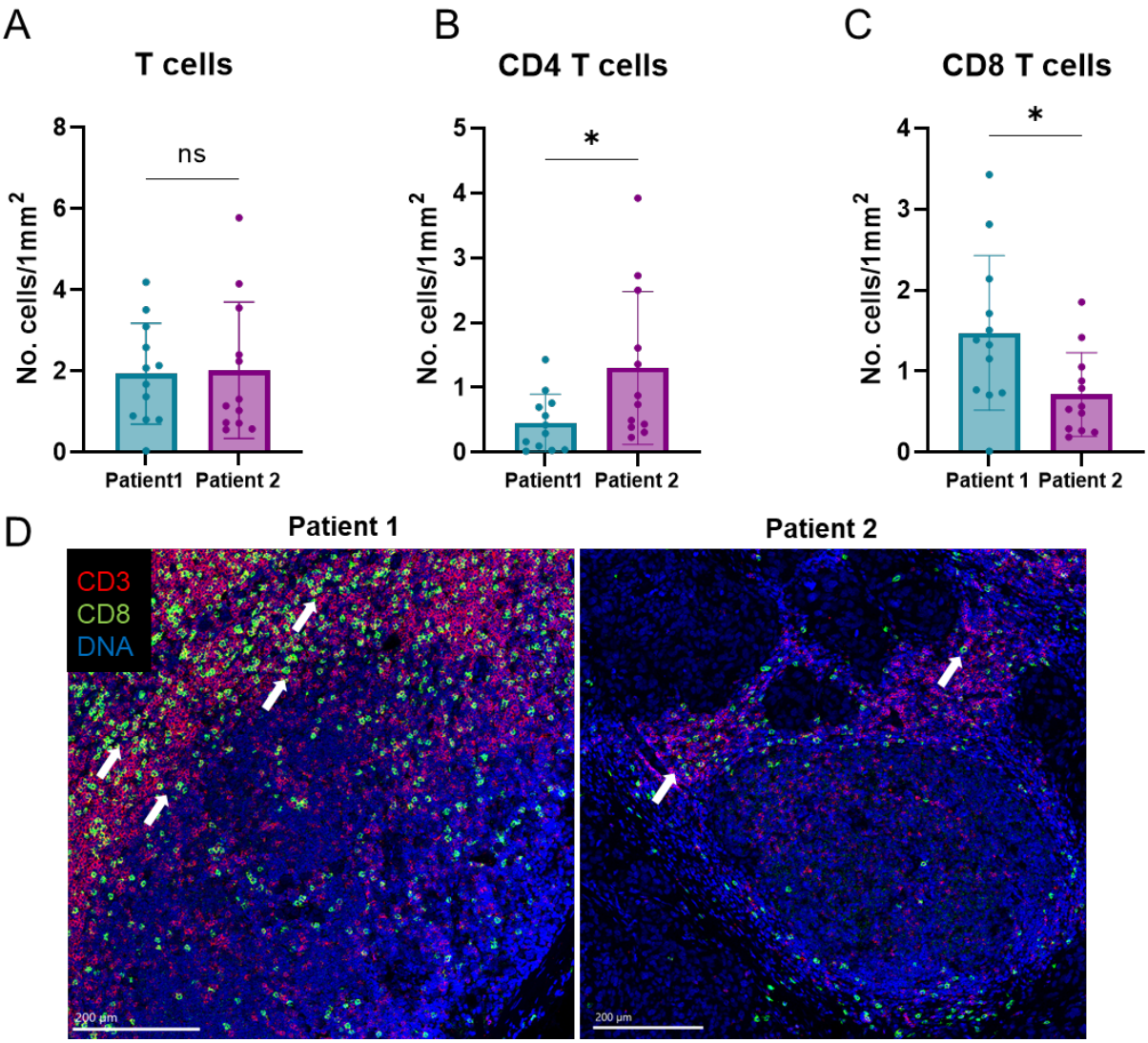

Figure 14: T cells distribution in lymph nodes of patients with different disease trajectories. (A) T cells per mm^2 within ROIs from patient 1 that did not develop distant metastasis and patient 2 that did develop distant metastasis. (B) CD4+ T cells per mm^2 within ROIs from patient 1 that did not develop distant metastasis and patient 2 that did develop distant metastasis. (C) CD8+ T cells per mm^2 within ROIs from patient 1 that did not develop distant metastasis and patient 2 that did develop distant metastasis. (Mann-Whitney U tests, * = $p < 0.05$). (D) Representative images of a ROI from the lymph nodes of patient 1 and patient 2. White arrows indicate CD8+ T cells.

Within the LNs, the PD1/PDL1 axis is critical to the GC response, modulating interactions between pre-Tfh and B cells at the T/B border, and selection processes within Tfh and B cells within the LZ of the GC itself (De Silva and Klein, 2015). A significant depletion in both the number of PD1+CD4+ T cells and PD1+ CD8+ T cells within the LN of patient 2 was observed (Mann-Whitney U test, $p < 0.01$, $p < 0.0001$) (Figure 15). The difference in PD1+ CD4+ T cells was specific to GC regions (Mann-Whitney U test, $p < 0.05$) (Figure 16A-B), potentially suggesting a depletion of Tfh cells. This was also represented in the images, which identified this reduction in PD-1+CD4+ T cells to be prominent within the GC, as opposed to the areas surrounding it. PD1+CD8+ T cells, although more prominently lacking in the GC ROIs of patient 2 (Mann-Whitney U test, $p < 0.01$), was also significantly depleted within non-GC ROIs (Mann-Whitney U test, $p < 0.05$).

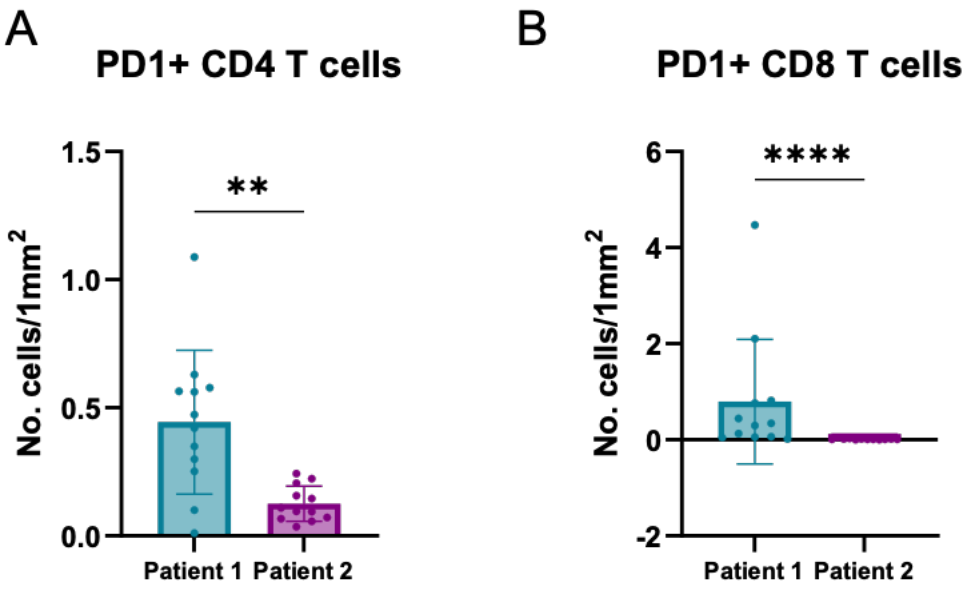

Figure 15: PD1+ CD4 and PD1+ CD8 T cells depleted within lymph node ROIs. (A) PD1+ CD4+ T cells per mm^2 within all ROIs from patient 1 and patient 2. (B) PD1+ CD8 T cells per mm^2 within ROIs from patient 1 and patient 2 (Mann-Whitney U tests, ** = $p < 0.01$, **** = $p < 0.0001$).

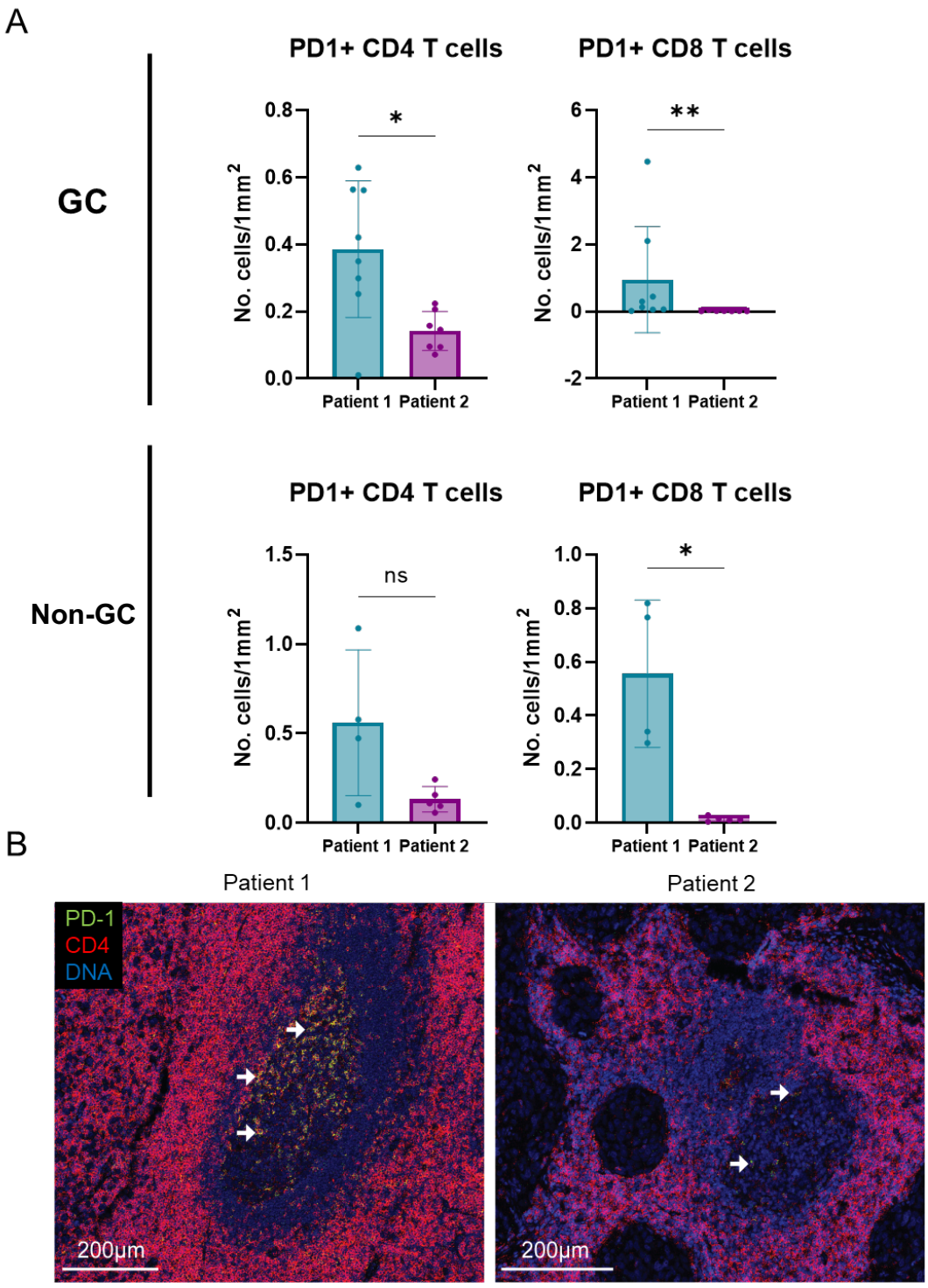

Figure 16: PD1+ CD4 and PD1+ CD8 T cells predominantly depleted within GC ROIs of patient 2. (A) PD1+ CD4 T cells and PD1+ CD8 T cells per mm^2 within GC and non-GC ROIs from patient 1 that did not develop distant metastasis (-) and patient 2 that did develop distant metastasis (+). Mann-Whitney U tests, * = $p < 0.05$, ** = $p < 0.01$. (B) Representative images of a GC ROI from the lymph nodes of patient 1 and patient 2. White arrows indicate PD1+CD4+ T cells.

To investigate other B cell subsets integral to the GC response, the numbers of naïve B, unswitched B, and switched B cells were evaluated. This revealed an increase in naïve B cells within patient 2 (Mann-Whitney U test, $p < 0.05$) (Figure 17A), but no differences in numbers of unswitched and switched B cells within the LNs of these patients (Figure 17B-C). Further, evaluation of follicular B cells (CD20+CD23+CD21+) showed no significant differences (Figure 18A), but there was a notable increase in MZ B cells (CD20+CD21+IgD-CD23-) within patient 2 (Mann-Whitney U test, $p < 0.05$) (Figure 17B). As expected, these changes were unique to GCs for both naïve B (Mann-Whitney U test, $p < 0.05$) and MZ B cells (Mann-Whitney U test, $p < 0.05$) compared to those present within the stroma (Figure 19A-B).

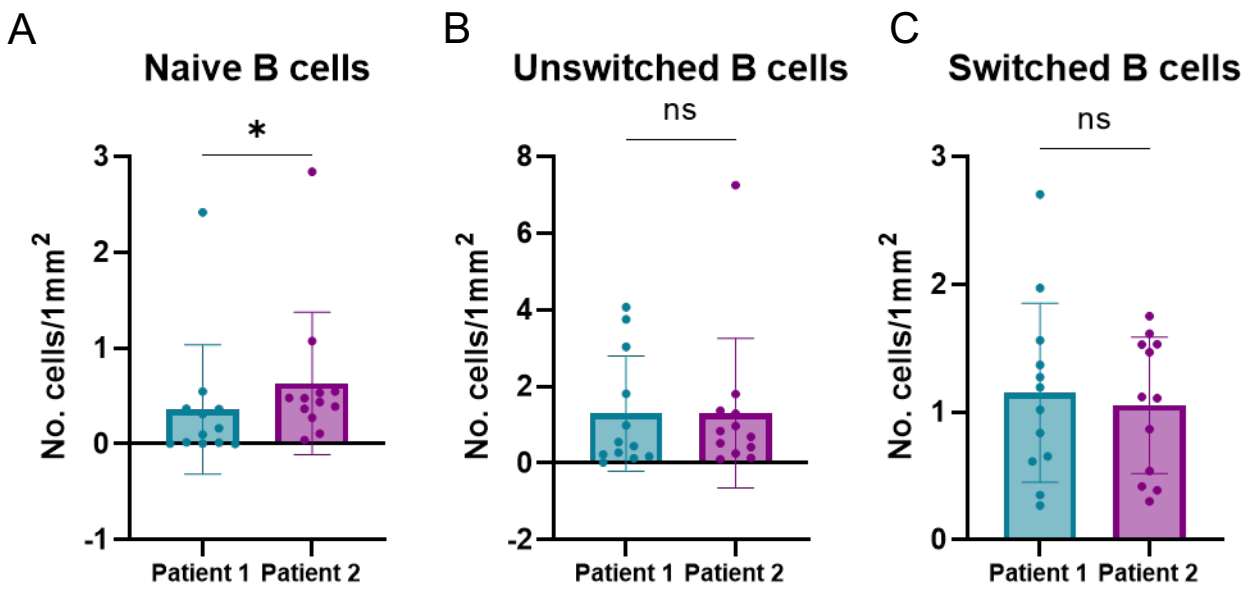

Figure 17: Naïve B cells enriched in the lymph nodes of ROIs from the patient that developed distant metastasis. (A) Naïve B cells per mm^2 within ROIs from patient 1 that did not develop distant metastasis (-) and patient 2 that did develop distant metastasis (+). (B) Unswitched B cells per mm^2 within ROIs from patient 1 that did not develop distant metastasis (-) and patient 2 that did develop distant metastasis (+). (C) Switched B cells per mm^2 within ROIs from patient 1 that did not develop distant metastasis (-) and patient 2 that did develop distant metastasis (+). (Mann-Whitney U tests, * $p < 0.05$).

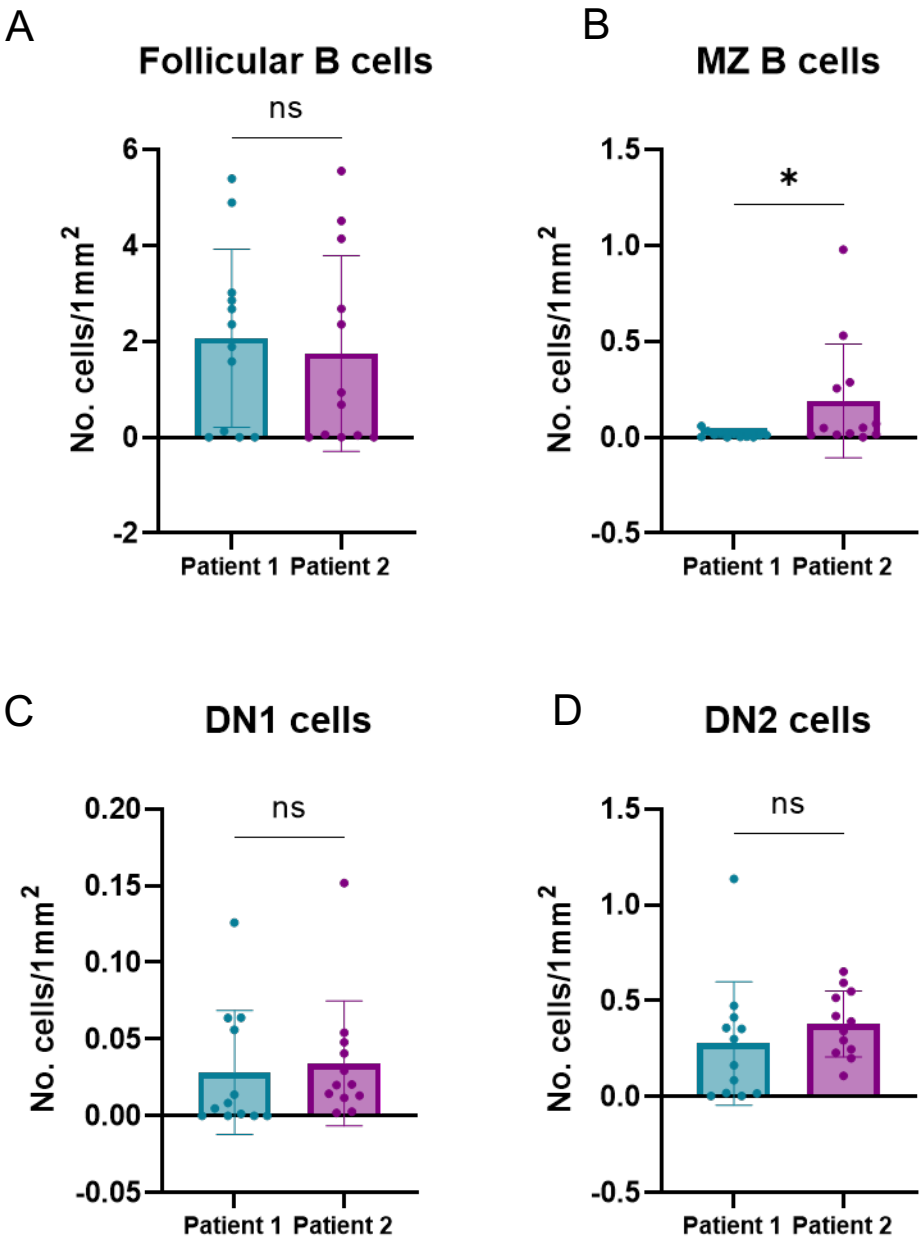

Figure 18: Marginal zone B cells are enriched in the lymph node ROIs of the patient that developed distant metastasis. (A) Follicular B cells per mm^2 within ROIs from patient 1 that did not develop distant metastasis (-) and patient 2 that did develop distant metastasis (+). (B) Marginal zone (MZ) B cells per mm^2 within ROIs from patient 1 that did not develop distant metastasis (-) and patient 2 that did develop distant metastasis (+). (C) Double negative 1 (DN1) B cells per mm^2 within ROIs from patient 1 that did not develop distant metastasis (-) and patient 2 that did develop distant metastasis (+). (D) Double negative 2 (DN2) B cells per mm^2 within ROIs from patient 1 that did not develop distant metastasis (-) and patient 2 that did develop distant metastasis (+). (Mann-Whitney U tests, * = $p < 0.05$).

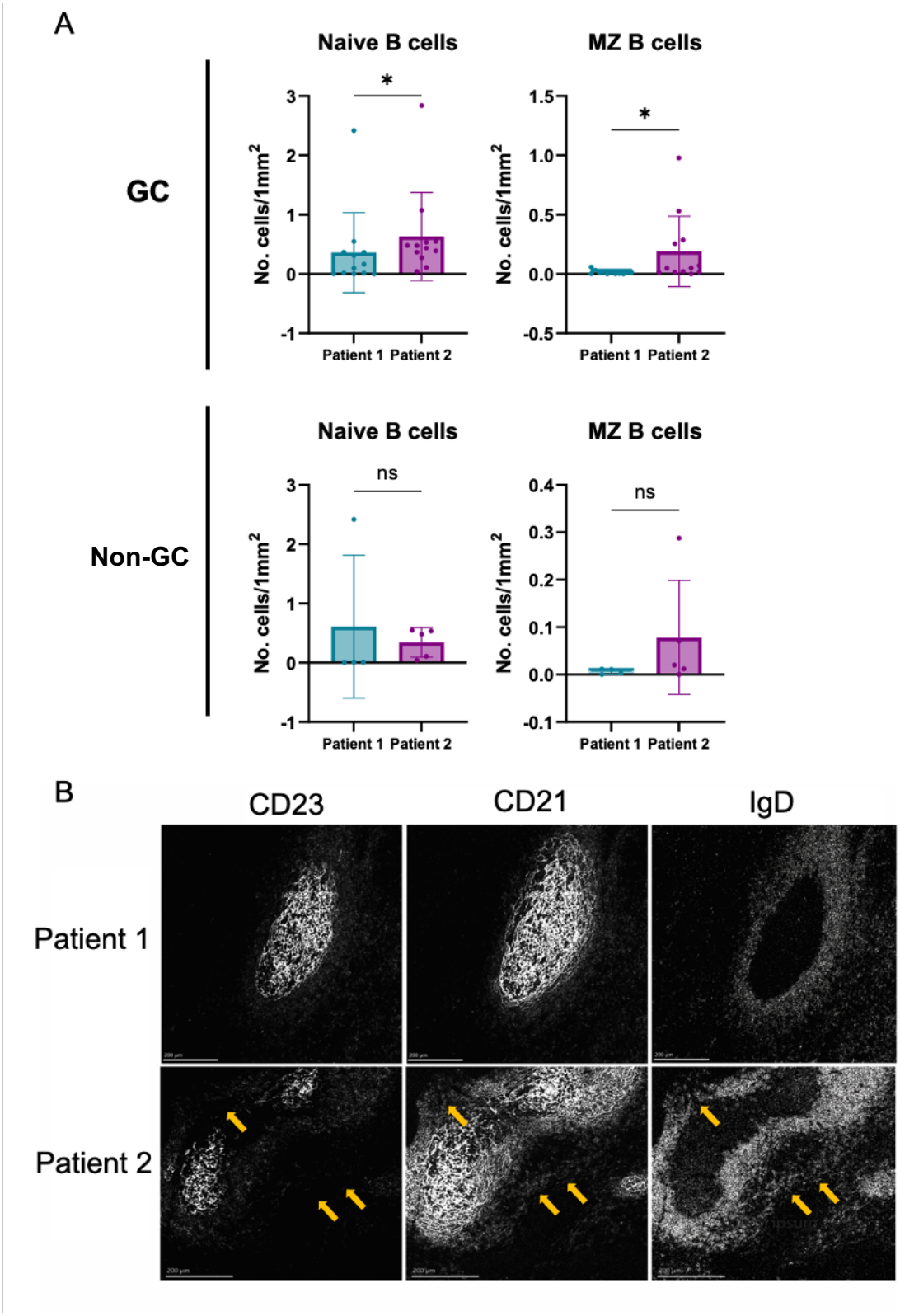

Figure 19: Marginal zone B cells are enriched in the GC ROIs of patient 2. (A) Naïve B and marginal zone (MZ) B cells per mm^2 within GC and non-GC ROIs from patient 1 that did not develop distant metastasis (-) and patient 2 that did develop distant metastasis (+). Mann-Whitney U tests, * = $p < 0.05$. (B) Representative images of CD23, CD21 and IgD staining from GC ROIs in the lymph nodes of patient 1 and patient 2. Yellow arrows indicate CD23-CD21+IgD^{low} marginal zone B cells.

3.3.2 DN 2 B cells, Tregs and macrophages increased in non-GC areas of LN of patient 2

Other cell populations of interest were DN cells, which have gained traction within the oncology field as a hallmark of B cell exhaustion, often prevalent in autoinflammatory and chronic infectious diseases (Li et al., 2021). They are so named due to the lack of expression of IgD and CD27, indicating a class switched phenotype without expression of traditional activation markers. Of interest within the GC field, there is accumulating evidence to suggest subsets of DN originate from different pathways. DN1 cells (CD19+CD20+IgD-CD27-CD21+) are thought to be derived from the GC, differentiating into switched memory cells through upregulation of *TCF7* and subsequently antibody secreting plasma cells. In contrast, DN2 cells (CD19+CD20+IgD-CD27-CD11c+) may stem from TLR7+ activated B cells within the extrafollicular regions and lead to plasma cell production in the absence of a GC (Jenks et al., 2018). When assessing DN1 and DN2 levels within the LNs of the patients within this cohort, there was no significant differences in the number of both DN1 and DN2 between patient 1 and patient 2 (Figure 18). However, there was a trend of increased DN2 cells in patient 2 (Mann-Whitney U test, $p = 0.0635$) when specifically focusing on non-GC ROIs (Figure 20A). This is suggestive of plasma cell derived responses that may be initiated in the absence of a GC to be more prevalent in patient 2 that developed distant metastasis. This increase was in parallel with populations with immunosuppressive tendencies; there was a trend towards an increase in Tregs and a significant enrichment of macrophages within the non-GC ROIs of patient 2 (Mann-Whitney U test, $p = 0.0635$, $p < 0.05$ respectively) (Figure 20A-B).

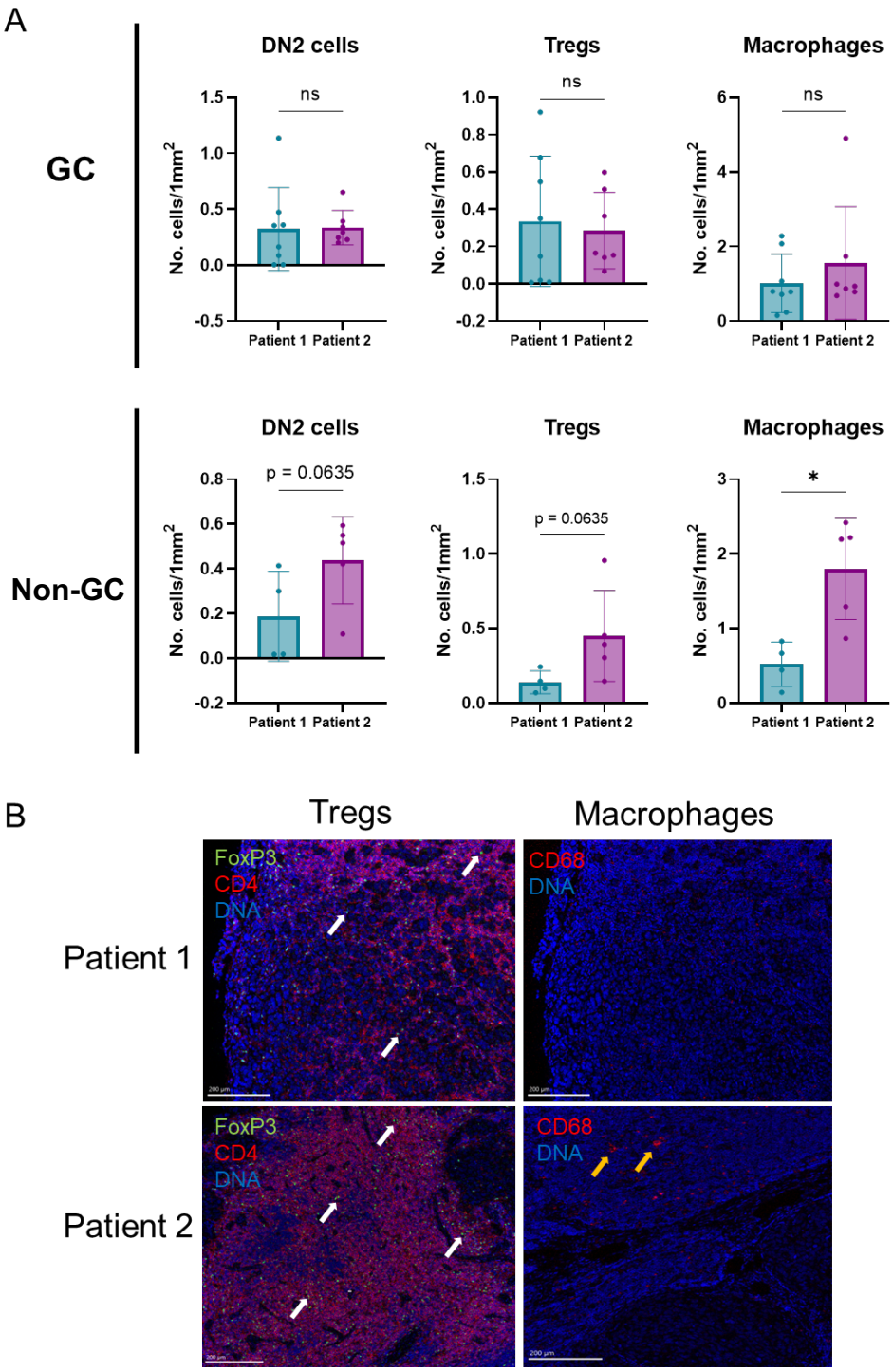

Figure 20: Tregs, DN2 and macrophages enriched in non-GC areas of patient 2. (A) Double negative 2 (DN2), Tregs and macrophages per mm^2 within GC and non-GC ROIs from patient 1 that did not develop distant metastasis (-) and patient 2 that did develop distant metastasis (+). Mann-Whitney U tests, * = $p < 0.05$. Numbers depicted when p values were close to significance. (B) Representative images of CD4+FoxP3+Tregs and CD68+ macrophages in non-GC areas of patient 1 and patient 2. White arrows indicate Tregs, and yellow arrows indicate macrophages.

3.3.3 IgG+, IgA+ and IgM+ plasma cells depleted in LNs of patient 2

Having ascertained that the LN from patient 2 was enriched for immunomodulatory subsets and DN2 cells, the density of IgM+, IgA+ and IgG+ plasma cells was assessed. There were no significant differences between the numbers of IgM+ and IgA+ plasma cells (Figure 21A-B), however a significant enrichment of IgG+ plasma cells within patient 1's LN compared with patient 2's LN (Mann-Whitney U test, $p < 0.01$), (Figure 21C). When evaluating the spatial arrangement of these subsets, there was an increased number of IgM+, IgA+ and IgG+ plasma cells within the non-GC ROIs of patient 1's LN compared to patient 2's LN (Mann-Whitney U test, $p < 0.05$), however only IgG+ plasma cells were significantly expanded within the GCs ROIs of patient 1 (Mann-Whitney U test, $p < 0.01$) (Figure 22A). This expansion of IgG+ plasma cells in the patient 1's LN was notably primarily within the GC itself, inferring that these are predominantly GC derived, whereas this localisation to the follicle was not evident within the LN of patient 2.

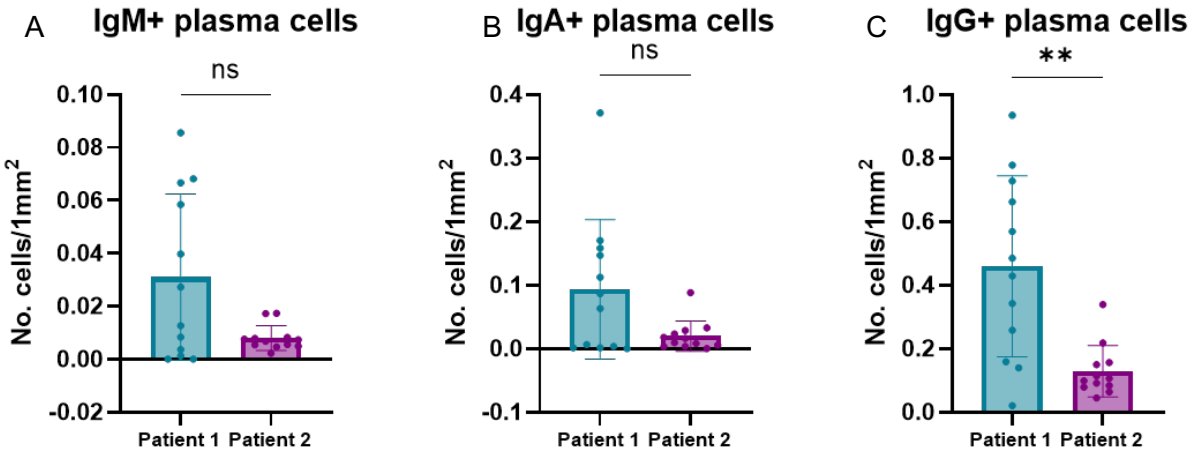

Figure 21: IgG plasma cells are depleted in the lymph node ROIs of the patient that developed distant metastasis. (A) IgM+ plasma cells per mm^2 within ROIs from patient 1 that did not develop distant metastasis (-) and patient 2 that did develop distant metastasis (+). (B) IgG plasma cells per mm^2 within ROIs from patient 1 that did not develop distant metastasis (-) and patient 2 that did develop distant metastasis (+). (C) IgA plasma cells per mm^2 within ROIs from patient 1 that did not develop distant metastasis (-) and patient 2 that did develop distant metastasis (+). (Mann-Whitney U tests, ** = $p < 0.01$).

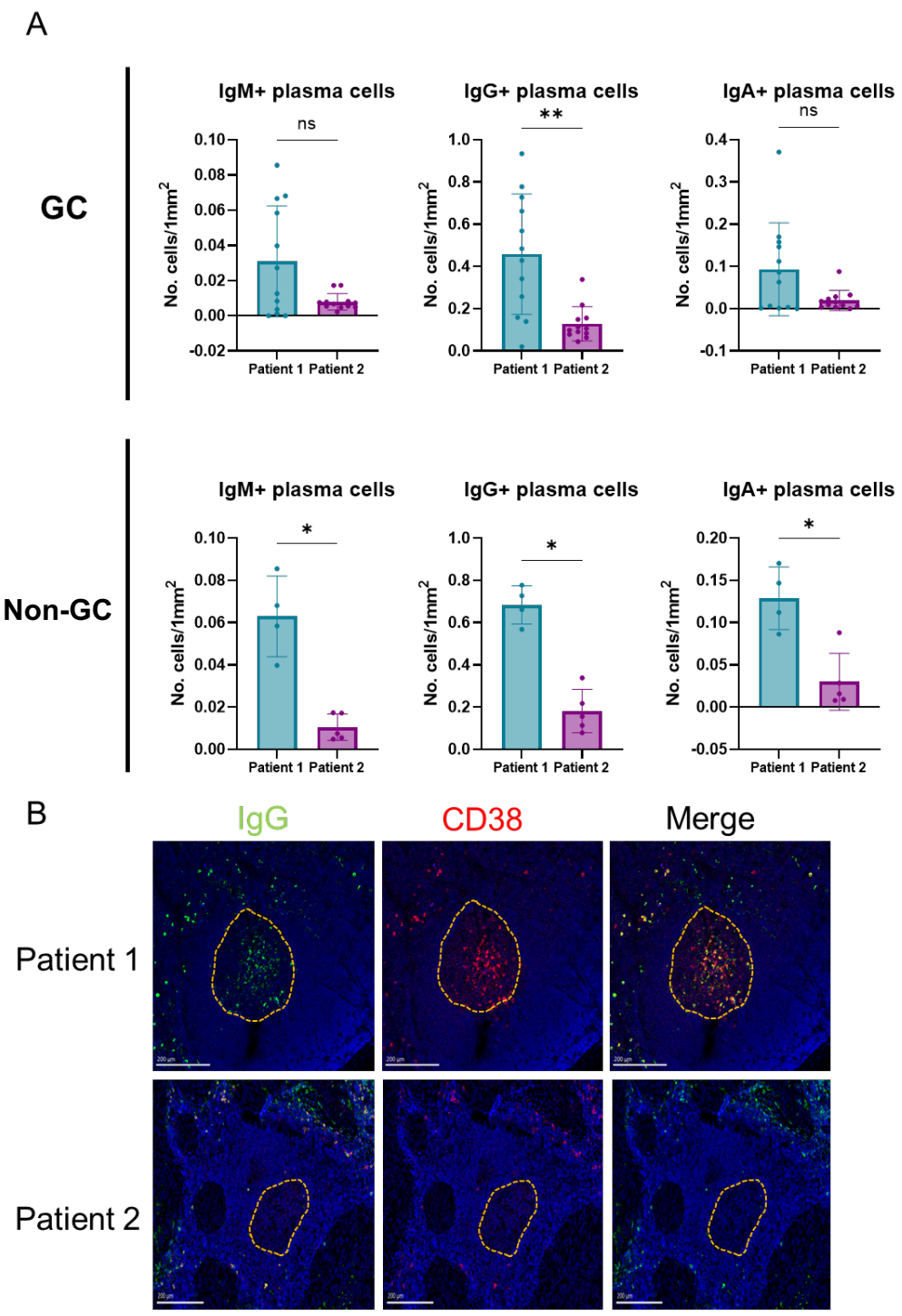

Figure 22: Plasma cells enriched in patient 2 compared to patient 1. (A) IgM, IgA, and IgG+ plasma cells per mm^2 within GC and non-GC ROIs from patient 1 that did not develop distant metastasis (-) and patient 2 that did develop distant metastasis (+). Mann-Whitney U tests, * = $p < 0.05$.(B) Representative images of IgG+ CD38+ plasma cells in the GC ROIs from the lymph nodes of patient 1 and patient 2. Yellow dashed line indicates the outline of the GC.

3.4 Spatial analyses identifiies distinct cellular neighbourhoods

To further assess the spatial communication between these cell types and how this might be relevant to the ROI type, GC or stroma, and patient outcome, Kmeans clustering with a k value of 20 was used to determine cellular neighbourhoods (cn). This identified 12 unique neighbourhoods, with distinctive spatial patterns across the ROIs. GCs were comprised of cn_3, cn_4 and cn_1, whereas non-GC areas appeared to have more cn_6, cn_9 and cn_5 (Figure 23A). Cn_1 was enriched for MZ B cells, follicular B cells and DN1 cells, cn_2 for macrophages and tumour cells, and cn_3 follicular B cells alone. Cn_4 contained follicular B cells and naïve B cells, cn_5 predominantly IgM+ plasma cells, IgG+ plasma cells, IgA+ plasma cells and switched B cells. Cn_6 defined areas which were tumour cells alone, and cn_7 as unswitched B cells alone. Cn_8 consisted of a CD4+ T cell population, also enriched for Tregs, and cn_9 containing low levels of switched B, and CD4+ T cells. cn_10 was predominantly the DN populations; DN1, DN2 but also a switched B cell phenotype, and cn_11 consisted of mainly DN1 and naïve B. Finally, cn_12 was defined by PD1+ CD4+ and CD8+ T cells, as well as PD1-CD8+ T cells, IgA+ plasma cells and IgG+ plasma cells (Figure 23B).

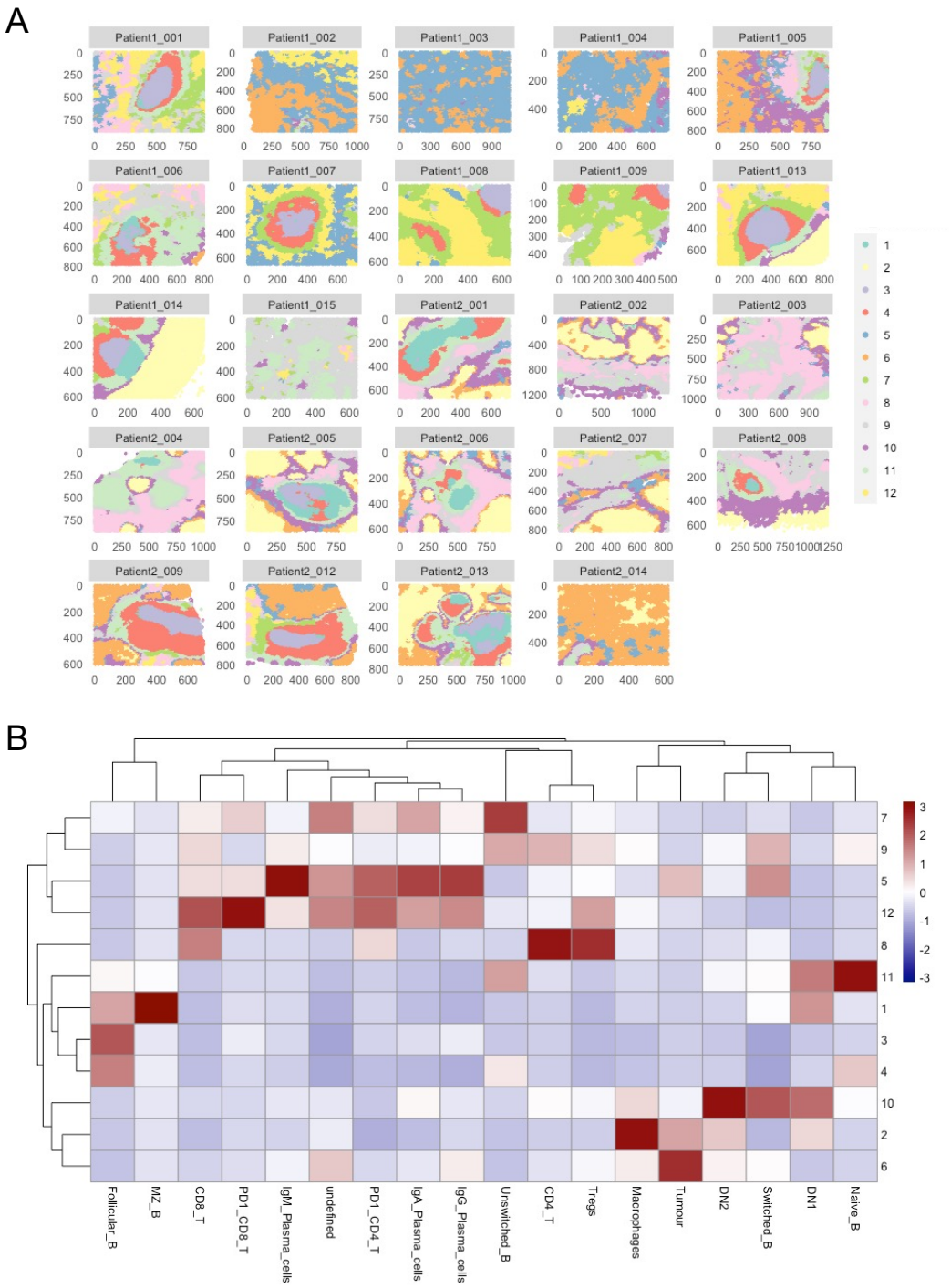

Figure 23: Immune cells form distinct cellular neighbourhoods in the LNs of Bart's TNBC cohort. (A) Spatial visualisation of cellular neighbourhoods (cn) within all ROIs across patient lymph nodes, numbered 1-12 and coloured by cellular neighbourhood. (B) Heatmap of cell types prevalent or lacking within each cellular neighbourhood, numbered 1-12.

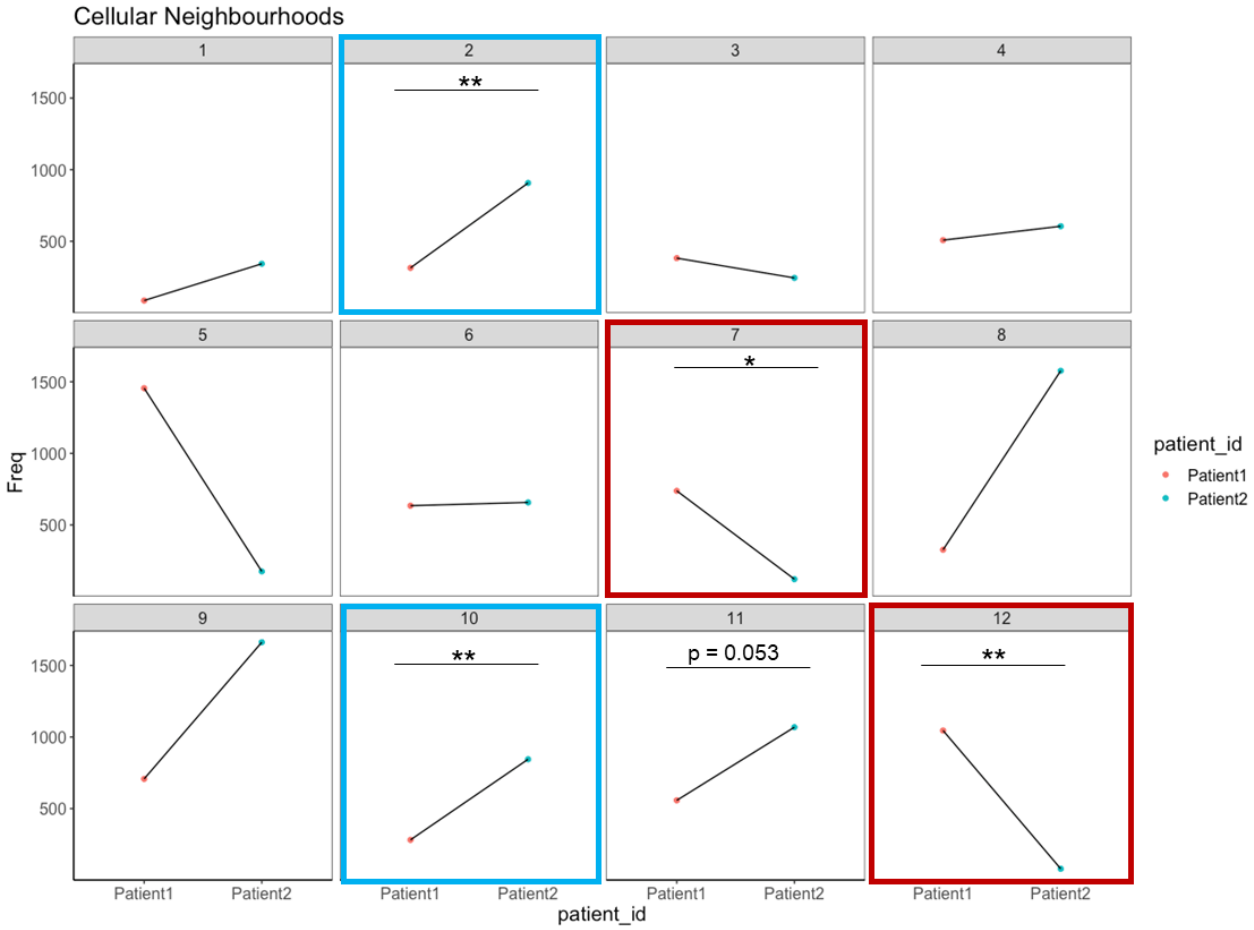

Figure 24: Cellular neighbourhoods differ in LNs of patients with or without distant metastasis. Mean cellular neighbourhood changes between patient 1 that did not develop distant metastasis and patient 2 that did. Cellular neighbourhood differences that were significantly altered are outlined in red (Wilcoxon rank sum test, * = $p < 0.05$, ** = $p < 0.01$).

3.4.1 Patient 1 and patient 2 exhibit differences in spatial neighbourhoods of immune cell subsets

When investigating how these neighbourhoods changed within the LNs of these patients, it was apparent that patient 2 was enriched for cn_2 (Kruskal-Wallis, $p < 0.01$), cn_10 (Kruskal-Wallis, $p < 0.01$), and was trending towards increased levels of cn_11 (Kruskal-Wallis, $p = 0.053$). Conversely, patient 1 LNs contained more cn_7 (Kruskal-Wallis, $p < 0.05$), and cn_12 (Kruskal-Wallis, $p < 0.01$) compared to patient 2 LNs (Figure 24). These changes were reflective of cell type differences, indicating a crosstalk between tumour cells and macrophages, and prevalence of DN subsets to localise near each other within patient 2. In contrast, patient 1 exhibited enrichment of neighbourhoods indicating T cell and plasma cell interactions, which was absent within patient 2. This was also specific to ROIs containing GCs (Figure 25), which is suggestive of a level of communication between these cell types related to the GC reactions that may contribute to a superior disease outcome. In contrast, the potential tumour-macrophage interactions and DN crosstalk in patient 2 were enriched in non-GC ROIs compared to those containing a GC (Figure 25).

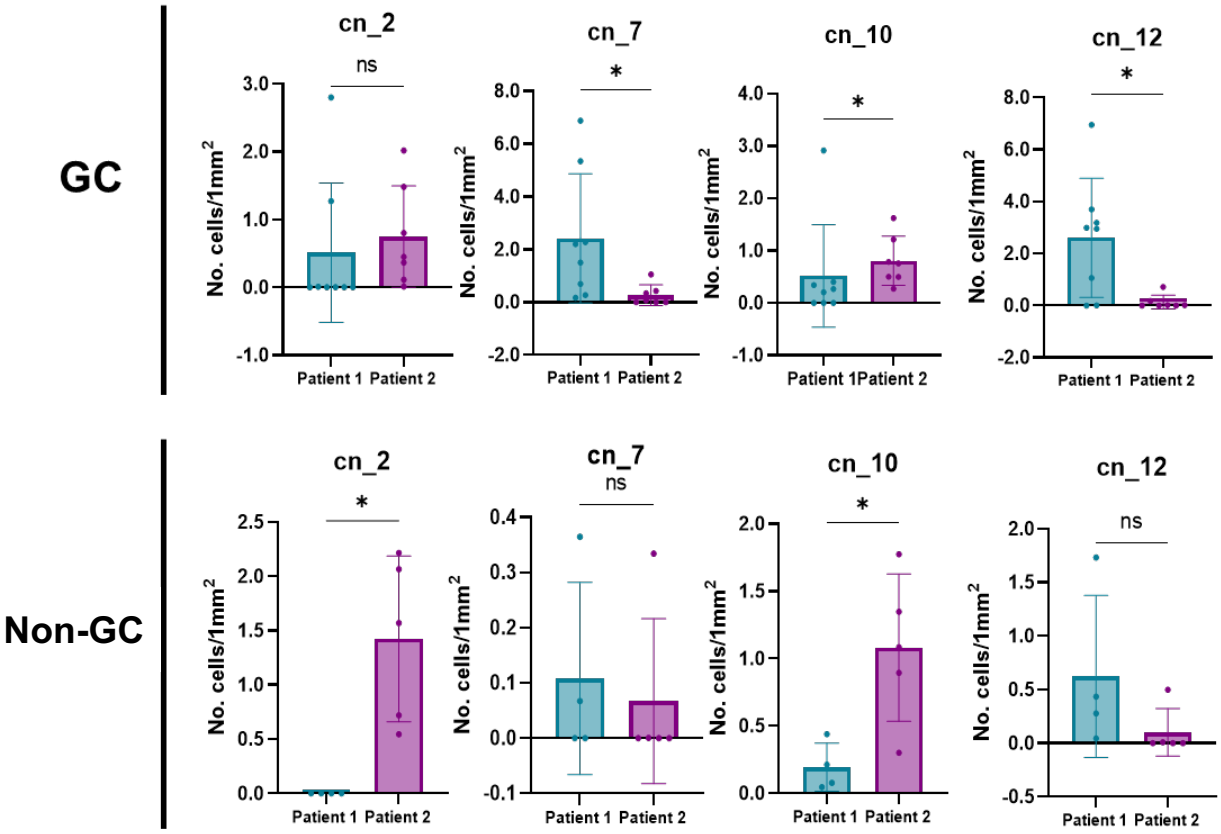

Figure 25: Patient 1 enriched for interactions within plasma cells and T cells within GC ROIs and patient 2 exhibits upregulated localisation of macrophages and tumour cells within non-GC ROIs. Normalised cellular neighbourhoods within GC and non-GC ROIs of patient 1 and patient 2 lymph nodes. Mann-Whitney U tests, * = $p < 0.05$.

3.5 Cellular neighbourhoods demonstrate patterns of spatial context

To elucidate the communication between these cns further, a k-nearest neighbour algorithm was applied to calculate spatial contexts (SCs). Cn fractions were sorted from high-low and the SC of each cell assigned as the minimal combination of SCs that additively surpasses a threshold of 0.9, aiming to represent the dominant cns in a given window (Bhate et al., 2022). SCs were further filtered for those that had a minimum of 100 cells per SC. This identified 43 unique SCs, with those that did not meet the filter criteria defined as NA. SC nomenclature was described as the cns involved, for example, if there were interactions between cn_2, cn_4 and cn_5 this would be shown as sc_2_4_5. The spatial orientation of these SCs could then be mapped back to each ROI as shown in Figure 26. This revealed GCs with very few SCs (ROI 10) and those with many (ROI 23).

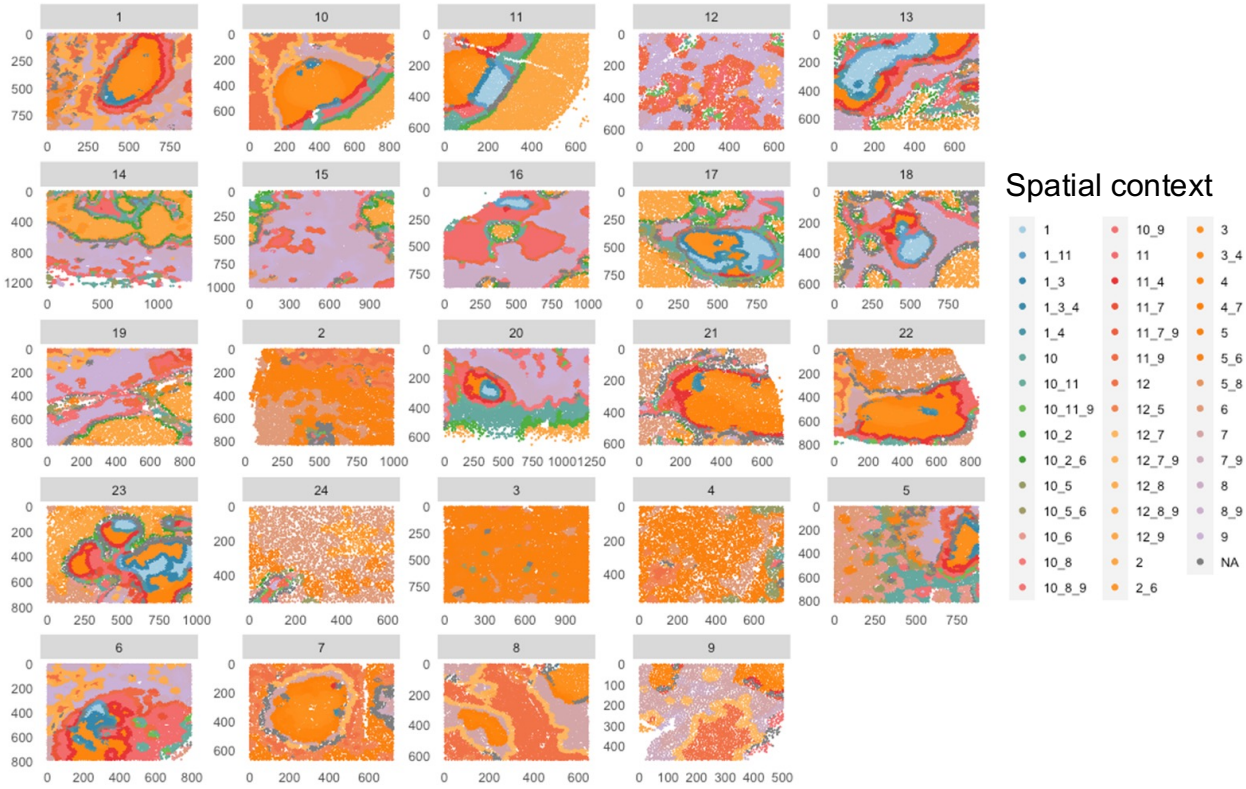

Figure 26: Unique spatial contexts of cellular neighbourhoods identified within ROIs of patient 1 and patient 2 lymph nodes. Spatial contexts depicting cellular neighbourhood interactions within the ROIs of patient 1 and patient 2. Colours indicate unique spatial contexts (SCs).

3.5.1 Enrichment of macrophage and Treg clusters in the LN of patient 2

As shown in Figure 27, there was enrichment of sc_2 in patient 2, defined as cn_2 alone (Mann-Whitney U test, $p < 0.01$) and sc_2_6, indicating interactions between cn_2 and cn_6 (Mann-Whitney U test, $p < 0.0001$). There were also potential interactions between cn_2 and cn_10 as well as between cn_2, cn_10 and cn_6, which was significantly increased in patient 2 compared to patient 1 (Mann-Whitney U test, $p < 0.0001$) (Figure 27A). This is a suggestive of a crosstalk of clusters of macrophages, Tregs, DN populations and tumour cells that is highly upregulated in patient 2 but absent in patient 1. There was also an enrichment of sc_10 (Mann-Whitney U test, $p < 0.05$), sc_10_11_9 (Mann-Whitney U test, $p < 0.05$), sc_10_9 (Mann-Whitney U test, $p < 0.001$), sc_10_8 (Mann-Whitney U test, $p < 0.05$) and sc_10_8_9 (Mann-Whitney U test, $p < 0.01$) in patient 2. This further signified communication between the DN B cells, macrophages (cn_10), a naïve B (cn_11) and CD4+ T/Treg (cns_8 and 9) (Figure 27A). Clusters of macrophages and Tregs were further visible in tumour infiltrated areas of the LN from patient 2, that were distinctly absent in patient 1 (Figure 27B). Taken together, these data suggest within the non-GC areas of the LN of patient 2, the localisation and communication between tumour cells, macrophages, DN B cells, and Tregs may contribute to distant metastasis development.

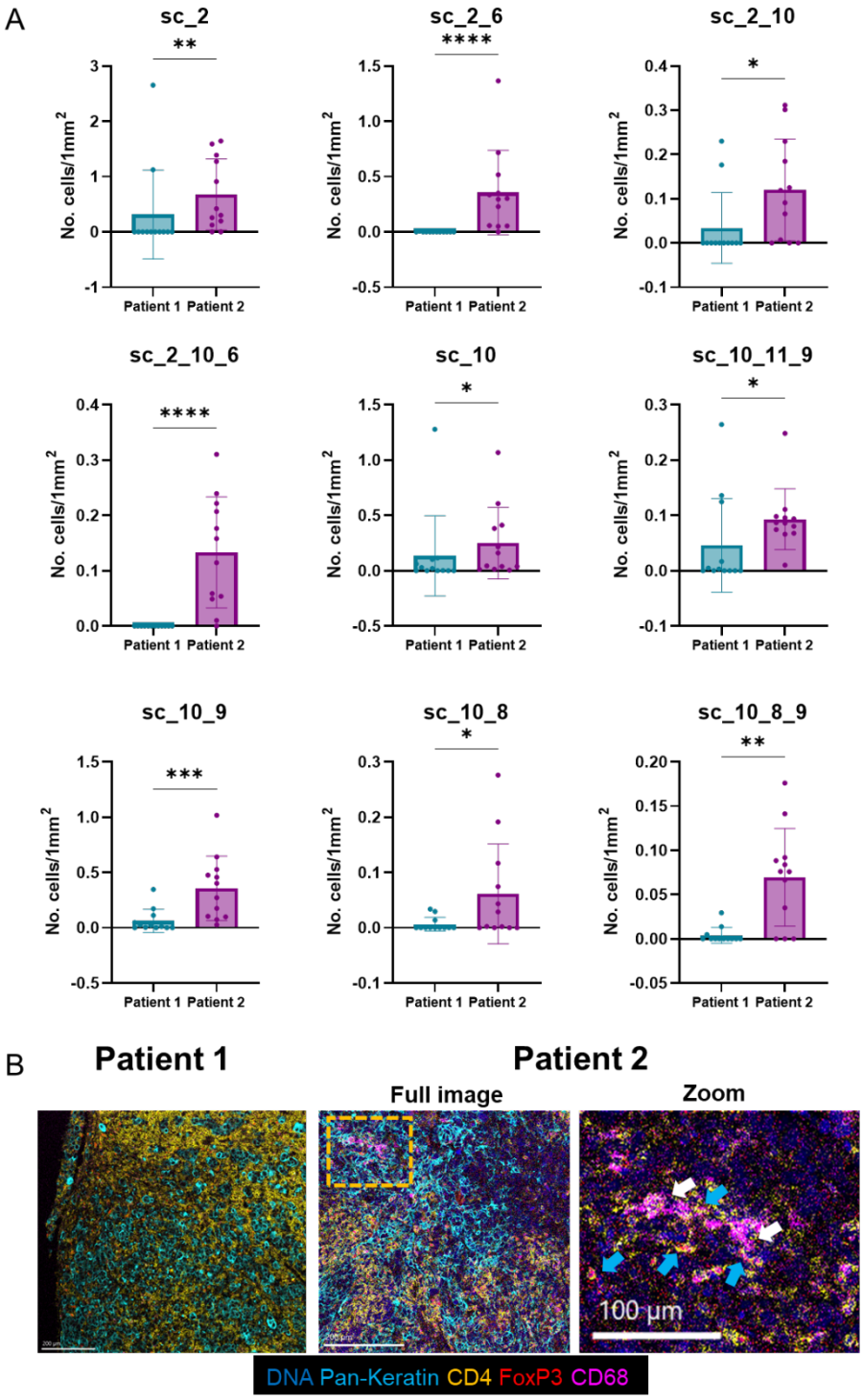

Figure 27: Spatial contexts upregulated within patient 2. (A) Normalised spatial contexts within non-GC ROIs of patient 1 and patient 2 lymph nodes. Mann-Whitney U tests, * = $p < 0.05$, ** = $p < 0.01$, *** = $p < 0.001$, **** = $p < 0.0001$.(B) Representative images showing increased localisation of CD68+ macrophages, CD4+FoxP3+ Tregs and tumour cells in non-GC ROIs of patient 2. Yellow arrows depict macrophages and blue arrows indicate Tregs.

3.5.2 T cells, plasma cells and tumour cells co-localise in GC ROIs of patient 1

In contrast, within the GC ROIs of patient 1 there was enrichment of sc_7 (Mann-Whitney U test, $p < 0.05$), sc_12_7_9 (Mann-Whitney U test, $p < 0.05$), sc_12 (Mann-Whitney U test, $p < 0.01$), sc_12_7 (Mann-Whitney U test, $p < 0.05$) and sc_12_5 (Mann-Whitney U test, $p < 0.05$). This suggested communication between cns containing multiple immune subsets including unswitched B (cn_7), plasma cells, PD1+ CD4 T cells, tumour cells (cn5), CD8+ T cells, PD1+ CD8+ T cells and Tregs (cn_12) (Figure 28A-B). This is suggestive of an active GC immune response, in which PD1+CD4+ T cells are interacting with unswitched B cells to induce differentiation into antibody-secreting plasma cells. These interactions in turn may facilitate an anti-tumour response. Notably, this process was not observed in the LN from patient 2 GC ROIs, and may be indicative of immune suppression, which is perhaps facilitated by the increased macrophage and Treg presence within the non-GC areas of these LNs.

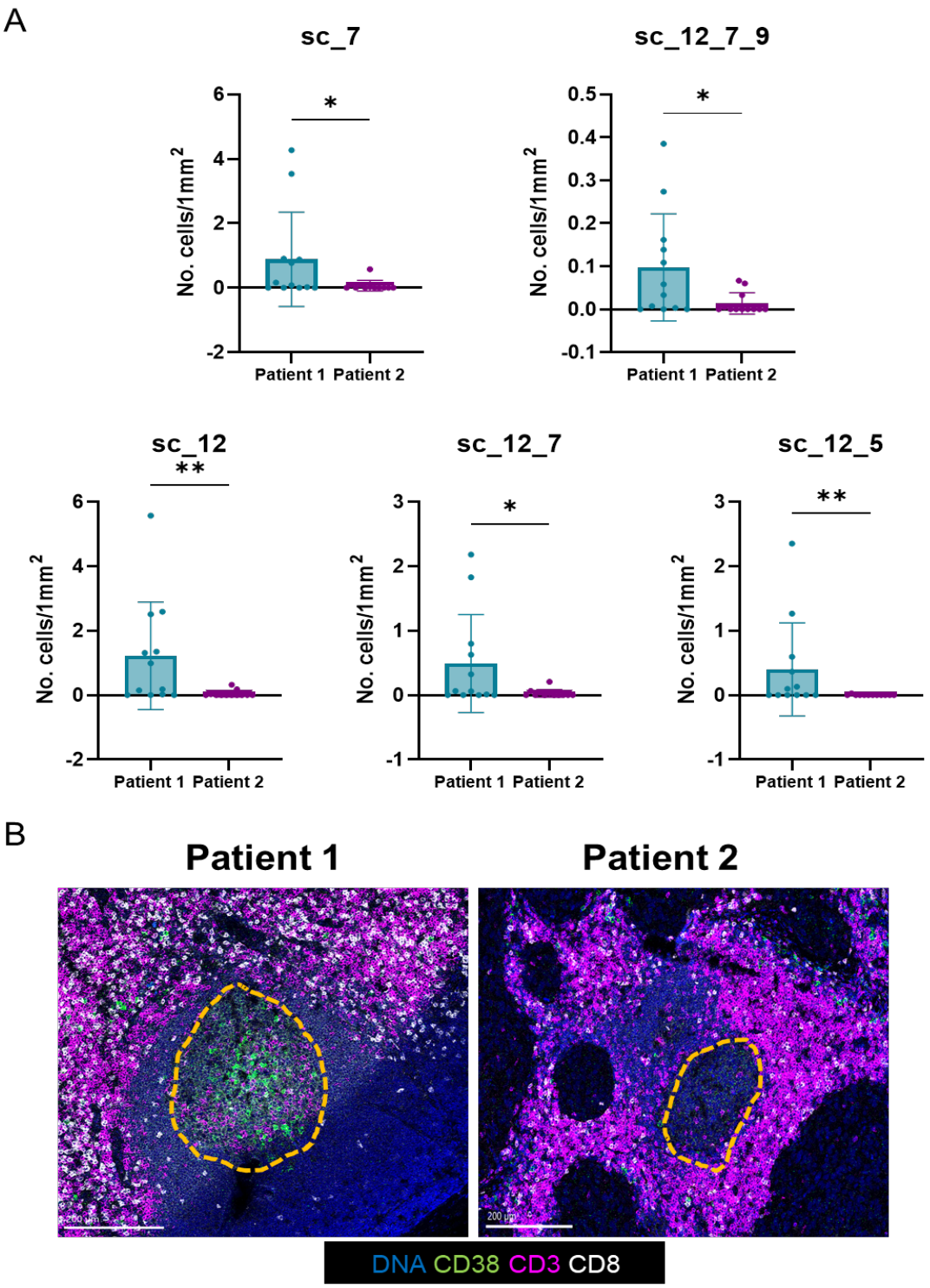

Figure 28: Patient 1 enriched for GC spatial contexts between cellular neighbourhoods containing T cells and plasma cells. (A) Normalised spatial contexts within GC ROIs of patient 1 and patient 2 lymph nodes. Mann-Whitney U tests, * = $p < 0.05$, ** = $p < 0.01$, *** = $p < 0.001$, **** = $p < 0.0001$. (B) Representative images showing increased localisation of plasma cells and T cells in GC ROIs of patient 1. Yellow dashed line indicates the outline of the GC.

3.6 Summary of spatial IMC-based profiling of LNs

In summary, accumulation of potentially immunosuppressive subsets including macrophages, Tregs and DN B cells were enriched within the in-LN of patient 2, who developed distant metastasis with 48 months. In the stroma of this LN, a prevalence for spatial interactions between these cell types was found. In contrast, the LN from patient 1 who did not develop distant metastasis. exhibited an increased level of T cell subsets associated with an anti-tumour and GC response, including CD8+ T cells, PD1+CD4+ T cells and plasma cells. There was also a spatial predisposition for these cells to localise closely to each other in and around the GC. As these tumours exhibited extreme differences in sTIL infiltration; the tumour from patient 1 was scored as having 80% sTILs and patient 2 with 20% sTILs, it was important to consider the relationship between these subsets and histological sTIL scoring and how this may have contributed to distant metastasis development.

3.7 sTILs scores are prognostic for distant disease-free survival in Guy's TNBC cohort

To expand on these immune cell subsets, their prevalence within the primary tumour and the relationship with sTIL infiltration, gene expression data of 124 TNBC tumours was subsequently analysed in a subset of retrospective breast cancer Guy's cohort (Brasó-Maristany et al., 2016). To examine these immune responses further and within the context of immune-hot and cold tumours, sTILs were first classified as per Salgado's criteria (Salgado et al., 2015) within the Guy's breast cancer cohort (Figure 29A). This method assesses the percentage of stroma occupied by concentrated mononuclear cells as a continuous parameter. Percentage sTILs were semi quantitatively graded; 0 = absence of lymphocytes, 1 = minimal (1-10% of surface area in given location), 2 = mild (10-20%), 3 = moderate (>20-50%) and 4 = strong (≥ 50%). Patients were dichotomised depending on their

levels of TILs at the primary carcinoma, and Kaplan-Meier survival analyses performed. Patients with tumours showing equal or more than 20% sTILs had a significantly reduced distant disease-free survival over 20 years (Figure 29B).

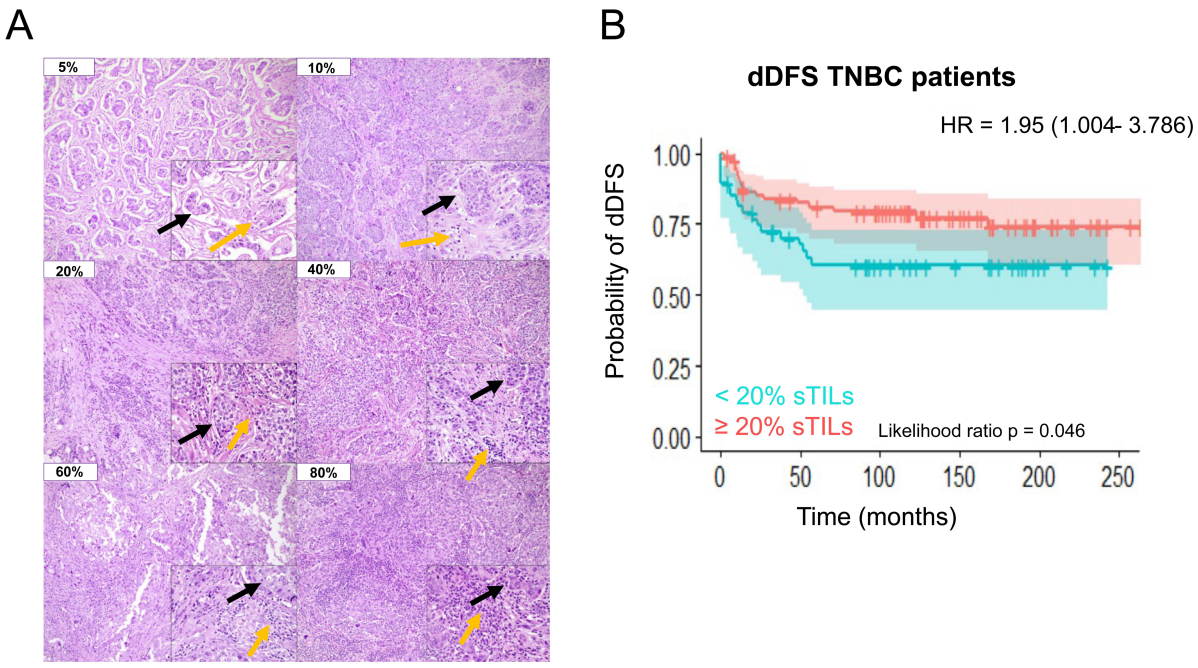

Figure 29: sTILs are prognostic in Guy's cohort. (A) Representative H&E images of stromal infiltrating lymphocytes (sTILs) in triple negative breast cancer (TNBC) (adapted from Fuchs et al., 2020). TILs were scored according to the International TILs Working Group (ITWG). Yellow arrows depict lymphocytes and black arrows indicate clusters of tumour cells. (B) Kaplan Meier distant-disease free survival (dDFS) analyses of 124 TNBC patients. The red line indicates patients with ≥ 20% sTIL infiltration (n = 76) and the blue line patients with < 10% (n = 48). Survival curves were compared using the log-rank test. HR = Hazard ratio with confidence interval shown in brackets.

3.8 Assessing prognostic factors in the Guy's TNBC cohort

Next, clinicopathological characteristics including age, tumour size, histological grade and number of in-LNs were compared within the Guy's TNBC cohort using univariate and multivariate Cox proportional hazard regression models. Age has been studied heavily with regards to immune specificity and function, and ageing has an impact on T cell repertoire diversity and B cell function. Specifically, CD8+ T cell diversity decrease with age, and frequencies of clonal populations expand in contrast to a reduction in CD4+ T cells (Yoshida et al., 2017). Studies in nonhuman primates have shown a reduced follicular area in older animals, significantly diminished numbers of Tfh cells, and an increase in $FoxP3^{high}Lag3^{high}$ CD4+ T cells with potential suppressive capabilities (Shankwitz et al., 2020). Further, our group has shown that there is an inverse linear relationship between the number of GCs in LNs and the age of the patient at diagnosis (Liu et al., 2021). In this way, it was important to evaluate the age of the patients at diagnosis as a confounding factor in the outcome analyses. In the univariate analysis, only tumour size and number of in-LNs were indicative of distant metastasis development (hazard ratio (HR) = 1.35, 95% confidence interval (CI) = 1.13 - 1.61, p = 0.001, and hazard ratio (HR) = 1.09, 95% confidence interval (CI) = 1.04 - 1.13, p < 0.001 respectively) (Figure 30A). This was also apparent in the multivariate analysis, where only tumour size and number of in-LNs was indicative of distant metastasis development (hazard ratio (HR) = 1.51,95% confidence interval (CI) = 1.04 - 1.13, p < 0.001, and hazard ratio (HR) = 1.12, 95% confidence interval (CI) = 1.07 - 1.17, p < 0.001 respectively) (Figure 30B). This therefore demonstrates that tumour size and number of in-LNs within this breast cancer cohort are significant elements that contribute to a shorter distant metastasis free survival time, and further highlights the importance of the LN status within TNBC.

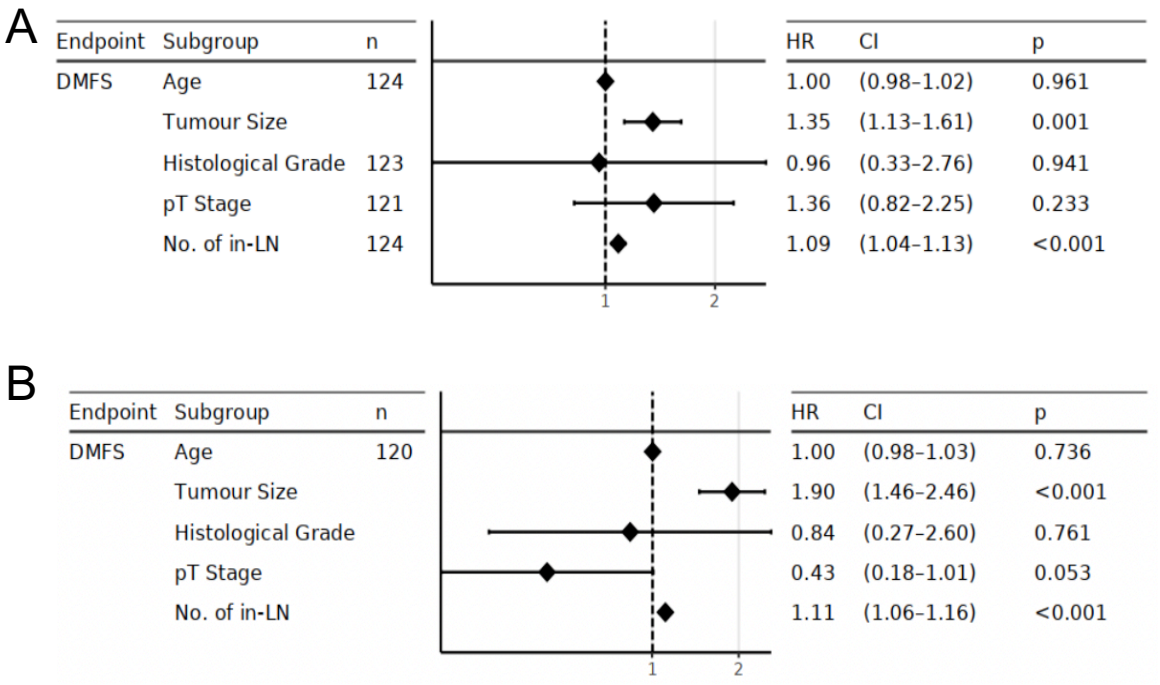

Figure 30: Univariate and multivariate cox proportional hazard regression distant metastasis free survival analyses. (A) Univariate Cox proportional hazard regression distant metastasis free survival analyses of age, tumour size, histological grade and number of in-LNs. HR hazard ratio, CI = confidence interval, p = p value. (B) Multivariate cox proportional hazard regression distant metastasis free survival analyses of age, tumour size, histological grade and number of in-lymph nodes (positive LN). HR hazard ratio, CI = 95% confidence interval, p = p value.

3.9 Prognostic significance of immune signatures in the Guy's TNBC cohort

To estimate immune population prevalence related with the GC response, a published scRNAseq dataset was used to deconvolute microarray data sequenced from histological sections of these immune-hot and cold tumours. Whilst single cell information from cf-LNs would have been used, this was not available at the time of the study, therefore scRNAseq from a tonsil dataset was applied (H. W. King et al., 2021). In this study, immune cells were isolated from tonsils of patients with recurrent tonsilitis and sleep apnoea, where the authors performed scRNAseq, V(D)J sequencing and high dimensionality reduction analyses to determine 25 subsets associate with the GC reactions. Multiple univariate Cox proportional hazards analyses of these GC signatures on the Guy's TNBC microarray data revealed that high expression of populations previously characterised in breast cancer including CD4+ T cells, CD8+ T cells and memory B cells were associated with a longer distant metastasis free survival time (hazard ratio (HR) = 0.37, 95% confidence interval (CI) = 0.19-0.72, p = 0.003, hazard ratio (HR) = 0.30, 95% confidence interval (CI) = 0.15 – 0.62, p = 0.001, and hazard ratio (HR) = 0.39, 95% confidence interval (CI) = 0.19-0.81, p = 0.012 respectively) (Figure 31). This is in alignment with published data that indicates high memory B cell infiltration consistently shows relevance for overall survival and distant disease-free survival in TNBC patients, and memory B cell signatures have exhibited prognostic potential within the context of low and high sTIL TNBC. Particularly within immunologically hot TNBCs, an increased memory B cell phenotype is significantly associated with a longer distant disease free survival time (Harris et al., 2021). In contrast, a high plasmablast signature exhibited the largest hazard ratio (HR) within this cohort, although not reaching significance (HR = 1.22, 95% confidence interval (CI) = 0.63-2.36, p = 0.560). Immunoglobulin signatures including the immunoglobulin kappa C (IGKC) metagene have been linked to longer disease free survival within TNBC patients (Iglesia et al., 2014; Schmidt et al., 2021), however plasmablast gene signatures have so far not been frequently assessed, and have not been described in detail when the prognostication of sTIL was performed (Figure 31).

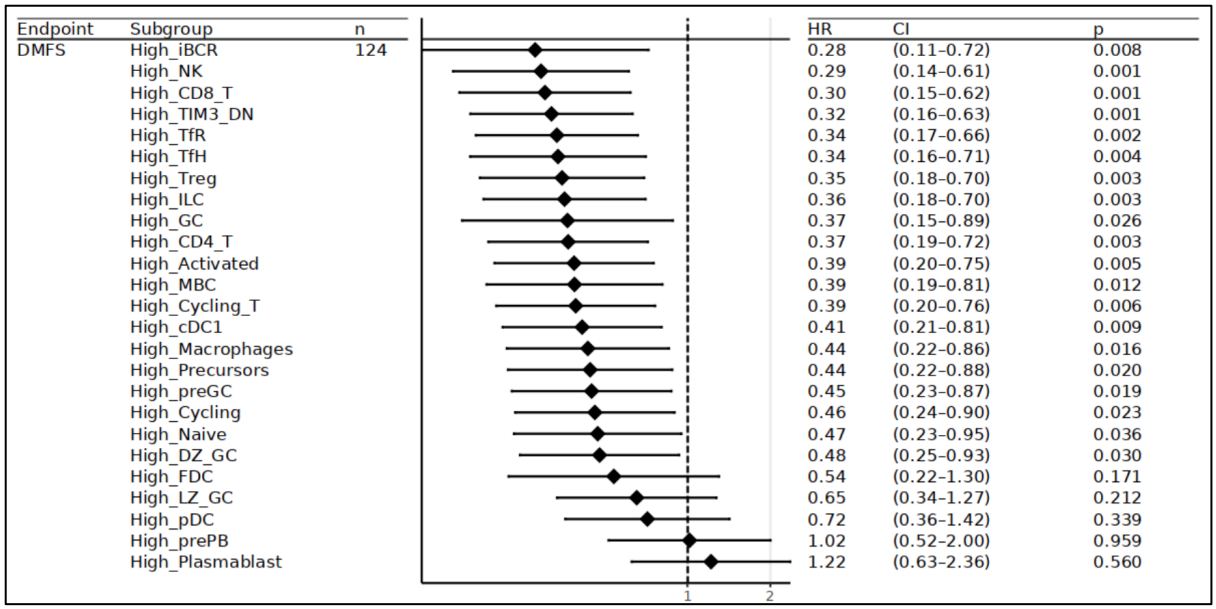

Figure 31: Forest plots of univariate cox proportional hazards regression distant metastasis free survival analyses of tonsil gene sets. Multiple univariate cox proportional hazard regression distant metastasis free survival analyses of gene sets from single cell tonsil dataset (H. King et al., 2021). HR = hazard ratio, CI = 95% confidence interval, p = p value.

3.9.1 Plasmablast gene signature prognostic within low sTILs tumours

To determine if high expression of these gene signatures were indicative of distant metastasis development in a sTIL-dependent manner, multiple univariate Cox proportional hazards regression analyses were applied to the Guy's cohort, looking at patients with low and high sTILs at the primary tumour. This revealed that within low sTILs tumours, there was a trend towards a high plasmablast gene signature being associated with the risk of developing distant metastasis (hazard ratio (HR) = 2.53, 95% confidence interval (CI) = 0.95-6.75, p = 0.080) (Figure 32A). This, however, was not the case in high sTILs tumours, where a high plasmablast gene signature demonstrated a hazard ratio of 0.53 (95% confidence interval (CI) = 0.16-1.77, p = 0.3). Conversely, many of the T cell subsets including CD8+ T cells were associated with a longer time of developing distant metastasis in patients with high sTILs TNBC (hazard ratio (HR) = 0.30, 95% confidence interval (CI) = 0.16-3.27, p =

0.041) (Figure 32B). This suggests that a high plasmablast or plasma cell infiltration within low sTILs tumours may be indicative of patients that develop distant metastasis.

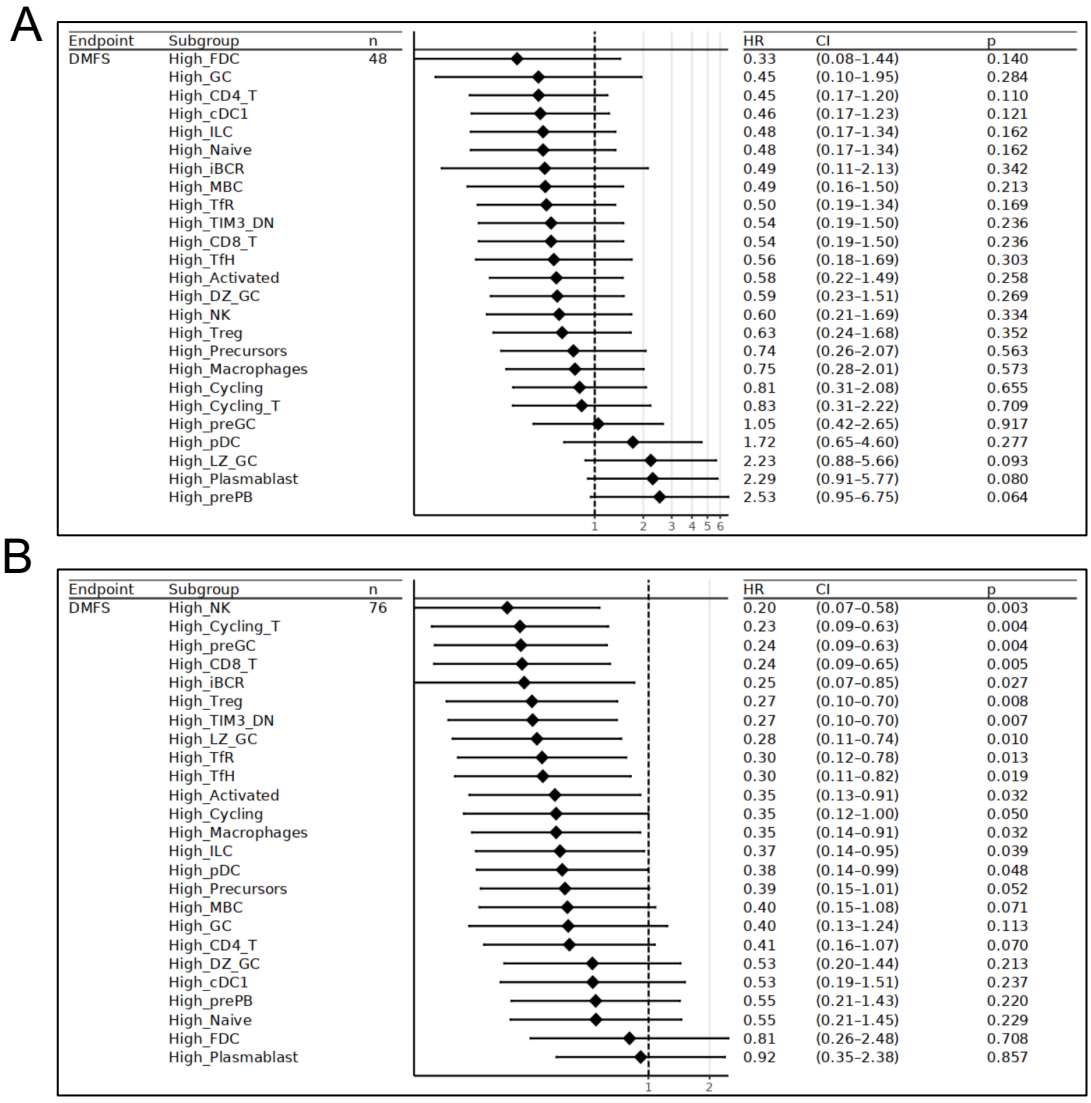

Figure 32: Forest plots of univariate cox proportional hazards regression distant metastasis free survival analyses of tonsil gene sets in low and high sTILs tumours. Multiple univariate Cox proportional hazard regression distant metastasis free survival analyses of gene signatures from single cell tonsil dataset (H. King et al., 2021) in low sTILs (A) and high sTILs tumours (B). HR = hazard ratio, CI = 95% confidence interval, p = p value.

3.10 Deconvolution of Guy's breast cancer cohort using plasmablast gene signature and histological sTIL scoring

To investigate the role of this plasmablast gene signature further within the context of immune-cold tumours, patients from the Guy's cohort were split into 4 subgroups based on ssGSEA enrichment scores and paired histological scoring. Cox proportional hazard regression models were applied to identify an optimal cut-off of 0.135 to determine high and low plasmablast gene scores within these samples. This identified 4 groups: patients with low sTILs and a high plasmablast enrichment score (lThP), those with low sTILs and a low plasmablast enrichment score (lTlP), those with high sTILs and a high plasmablast enrichment score (hThP), and finally patients with low sTILs and a low plasmablast enrichment score (hTlP) (Figure 33A). These subgroups of patients were explored of their molecular features to characterise further those with possible plasma cell infiltration within the context of immune-hot and cold tumours.

Next, key genes involved in plasma cell differentiation were examined individually. *JCHAIN* is a small polypeptide that is required for multimerization of secretory IgM and IgA, generally assumed to be highly expressed on all plasma cells (Castro and Flajnik, 2014), was upregulated in both lThP and hThP groups compared to those with a low plasmablast enrichment score (paired T test, $p < 0.01$). Other typical B and plasma cell genes including *CD79a*, which associates with membrane-bound immunoglobulin to stabilise the B-cell receptor complex, was also significantly increased in the lThP and hThP groups (paired T test, $p < 0.01$, $p< 0.05$ respectively). However, there were marked differences between the lThP group and hThP group. lThP patient tumours showed significantly decreased levels of *PRDM1*, a transcriptional repressor, and *IRF4*, a multifunctional transcriptional regulator that both can drive terminal differentiation of B cells to plasma cells (Nutt et al., 2011) (paired T test, $p < 0.001$). In comparison, these tumours exhibited higher expression of *XBP1* than hThP patients, which is a mediator of the mammalian unfolded protein response (UPR), and upregulated in antibody secreting cells (Nutt et al., 2011) (paired T test, $p < 0.01$). (Figure

33B). The differences between plasma cell related gene expression in IThP patients and hThP patients may suggest plasma cells of different maturity. Whilst *JCHAIN* expression was similar, heightened *XBP1* but lack of *PRDM1* and *IRF4* within the IThP group may indicate that plasma cells infiltrating these tumours are of a more immature phenotype, as *PRDM1* and *IRD4* are well known to be attributed to terminal differentiation of plasma cells, compared to XPB1, upregulated at earlier stages (Nutt et al., 2011).

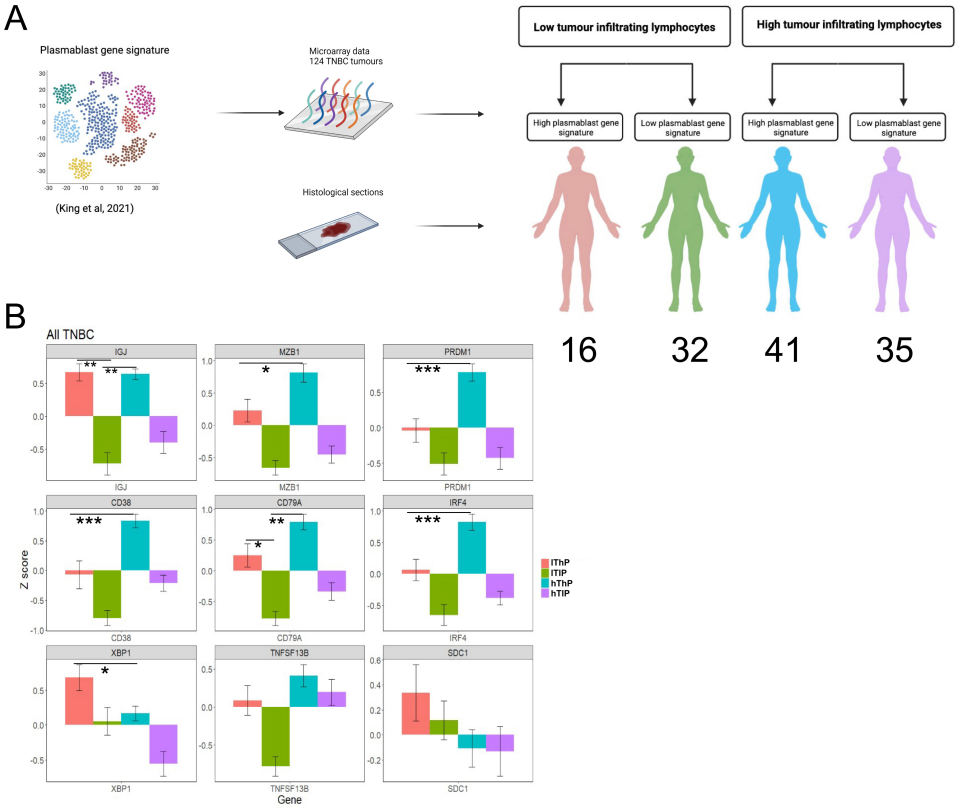

Figure 33: Deconvolution of TNBC tumours using sTILs and a plasmablast gene signature reveals distinct subtypes. (A) Schematic illustration of how the plasmablast gene signature based on single cell RNA-sequencing data from tonsils (King et al., 2021) was used in combination with histological sTIL scoring to identify subgroups amongst 124 TNBC tumours. High sTILs was determined as sTIL infiltration ≥ 10%. Cox proportional hazard regression models were used to determine the optimal cut-off of 0.135 for the plasmablast signature. Classification of these tumours stratifying patients into 4 groups; those with low TILs and a high plasmablast score (IThP, red), low TILs and a low plasmablast score (ITIP , green), high TILs and a high plasmablast score (hThP, blue) and high TILS with a low plasmablast score (hTIP, purple). (B) Barplots showing the normalised Z score gene expression of key plasmablast genes across the 4 groups.

3.10.1 Plasmablast gene signature associated with distant metastasis development in low sTILs tumours

Kaplan-Meier survival analyses were then used to determine how sTIL specific expression of the plasmablast gene signature could potentially contribute to distant metastasis development. IThP patients exhibited a significantly reduced distant disease-free survival time compared to all other groups: hazard ratio (HR) = 2.907, likelihood ratio test, p = 0.01 (Figure 34A). Furthermore, high expression of this plasmablast gene signature within low sTILs tumours was attributed to a shorter distant disease-free survival time: hazard ratio (HR) = 2.288, likelihood ratio test, p = 0.074 (Figure 34B).

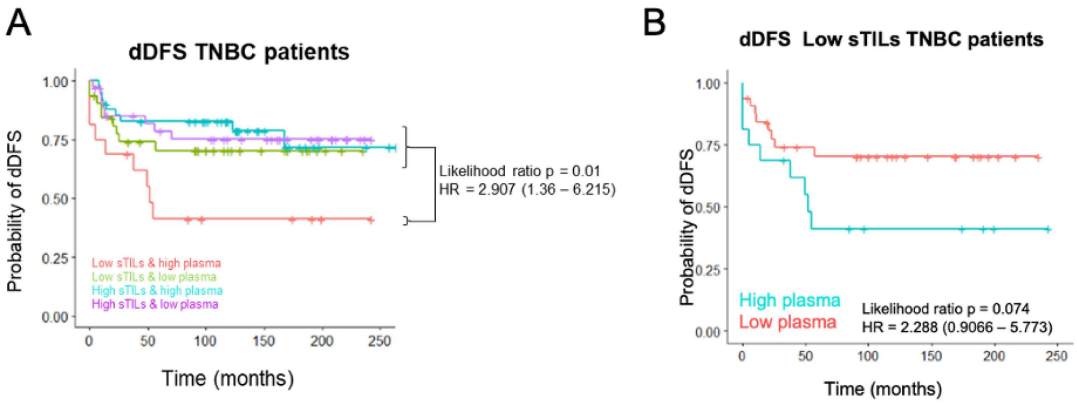

Figure 34: Low sTILs and high plasmablast gene signature is associated with worse outcome in TNBC patients. (A) Kaplan Meier graphs distant disease-free survival (dDFS) of 124 TNBC patients. Patients with low TILs and a high plasmablast gene signature are shown in red (n = 16), those with low TILs and low plasmablast gene signature are shown in green (n = 32). Patients with high TILs and a high plasmablast gene signature are depicted in blue (n = 41), whereas those with high TILS and a low level of plasmablast gene signature are shown in purple (n = 35). Survival analyses were compared using the Likelihood ratio test. HR = Hazard ratio with confidence interval shown in brackets. (B) Kaplan Meier graph showing dDFS of TNBC patients with low sTILs (n = 48). Patients with a low plasmablast score are shown in red (n = 32) and those with a high plasmablast score are shown in blue (n = 16). Survival curves were compared using the Likelihood ratio test. HR = hazard ratio with confidence interval shown in brackets.

3.10.2 lThP tumours exhibit low histological incidence of necrosis and fibrosis

TNBC is more likely to exhibit necrosis compared to other breast cancer subtypes, with an incident rate of 35-56% (Abdelhafez et al., 2021), but there is controversy surrounding the impact this may have on tumour progression. Studies have shown that the presence of tumour necrosis is linked to accelerated tumour growth and poor outcome (Abdelhafez et al., 2021), however Pu *et al*., showed that elevated necrosis was linked to complete pathological response (pCR) after neoadjuvant chemotherapy in breast cancer patients (Pu et al., 2020). Necrosis may augment an immune response through triggering inflammation, after rupturing cells release their intracellular contents into the microenvironment (Yang et al., 2015). Damage associated molecular patterns (DAMPs) secreted during necrosis can stimulate toll-like receptor (TLR) signalling on dendritic cells (DCs) or macrophages, but also through ligation of TLR4 and TLR9 on B cells, resulting in IgM+ plasmablast expansion (Genestier et al., 2007).

To assess, if TNBC with low TILs and a high plasmablast gene expression are more likely to be necrotic, histopathological assessment of necrosis was incorporated into the analyses. This revealed that lThP tumours had the lowest incidence of necrosis compared to the other groups (25% vs 39%, 70% and 40%) (Figure 35A). This may be reflective of tumour cells proliferating at a lower rate and may contribute to the low sTIL environment. hTlP tumours presented with the highest incidence of necrosis (70%) followed by lTlP tumours (40%), and hThP tumours (39%). This is perhaps increased with high sTILs tumours as chemotactic gradients initiated by high levels of inflammation from cell death may lead to the recruitment of sTILs.

High fibrosis levels, characterised histopathologically by elevated levels of collagen, is often seen in TNBC, and is known to be associated with rapid tumour progression and unfavourable outcome (Basso et al., 2010). Histological assessment of primary tumours of

the IThP subgroup, did, however, not show any increased levels of fibrosis in comparison to other subgroups (Figure 35B).

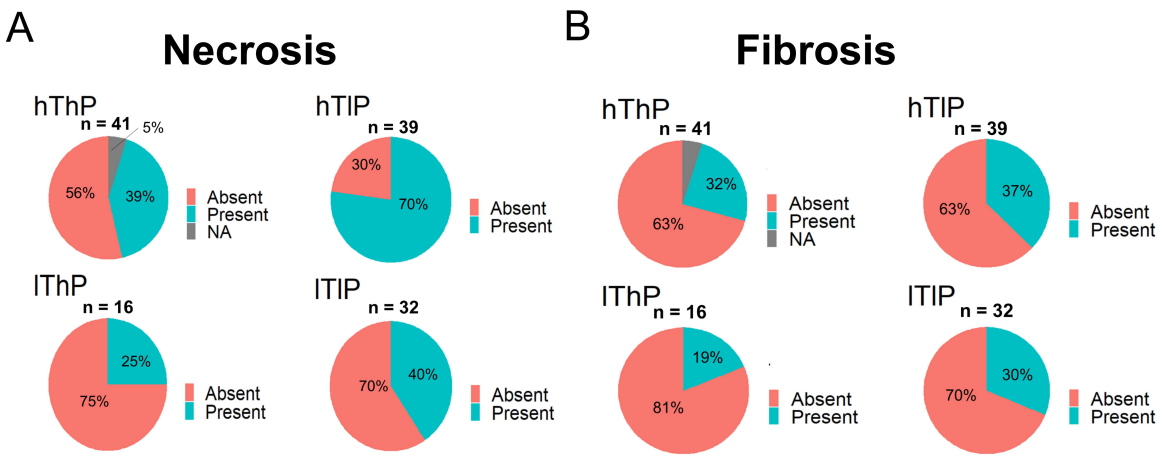

Figure 35: Necrosis and fibrosis status of TNBC tumours within each subgroup. Pie charts showing the percentage TNBC exhibiting necrosis (A) and fibrosis (B), within patients with high TILs and a high plasmablast gene signature (hThP), high TILs and low plasmablast gene signature (hTIP), low TILS and a high plasmablast gene signature (IThP), and low TILs with a low plasmablast gene signature (ITIP).

3.10.3 lThP tumours for the luminal androgen receptor subtype

To determine the molecular profiles of the tumours stratified by sTILs and the plasmablast signature, molecular subtypes of classification, namely PAM50, Lehman's, Burstein, four-gene decision tree, and integrative clusters (IntClust) were applied (Figure 36). Within the lThP patient group, 8/16 (50%) were of the LAR subtype based on the Burstein classification, and 6/8 (75%) were LAR based on the Lehmann-TNBC typing. In concordance with published data, LAR tumours within the lThP group were predominantly HER2- enriched by PAM50 subtyping (62.5%) (Ahn et al., 2016). The lThP group were further made up of IntClust 3 (37.5%), IntClust 4 (25%), IntClust 7 (18.75%), IntClust 5 (12.5%), and one sample was IntClust 10 (6.25%). This points to these tumours as exhibiting low genomic instability and the highest frequency of *PIK3CA, CDH1* and *RUNX1* mutations (Dawson et al., 2013). In agreement with this data, subtyping using the four-gene decision tree method revealed that lThP patients were predominantly MC4 (43.75%) and MC5 (43.75%). MC4 tumours are enriched for PI3K/Akt signalling, and MC5 presents with high expression of genes associated with ErbB signalling (Quist et al., 2019). Despite MC1 tumours typically presenting with higher levels of estrogen and AR signalling, none of the lThP tumours within the Guy's cohort were classed as MC1.

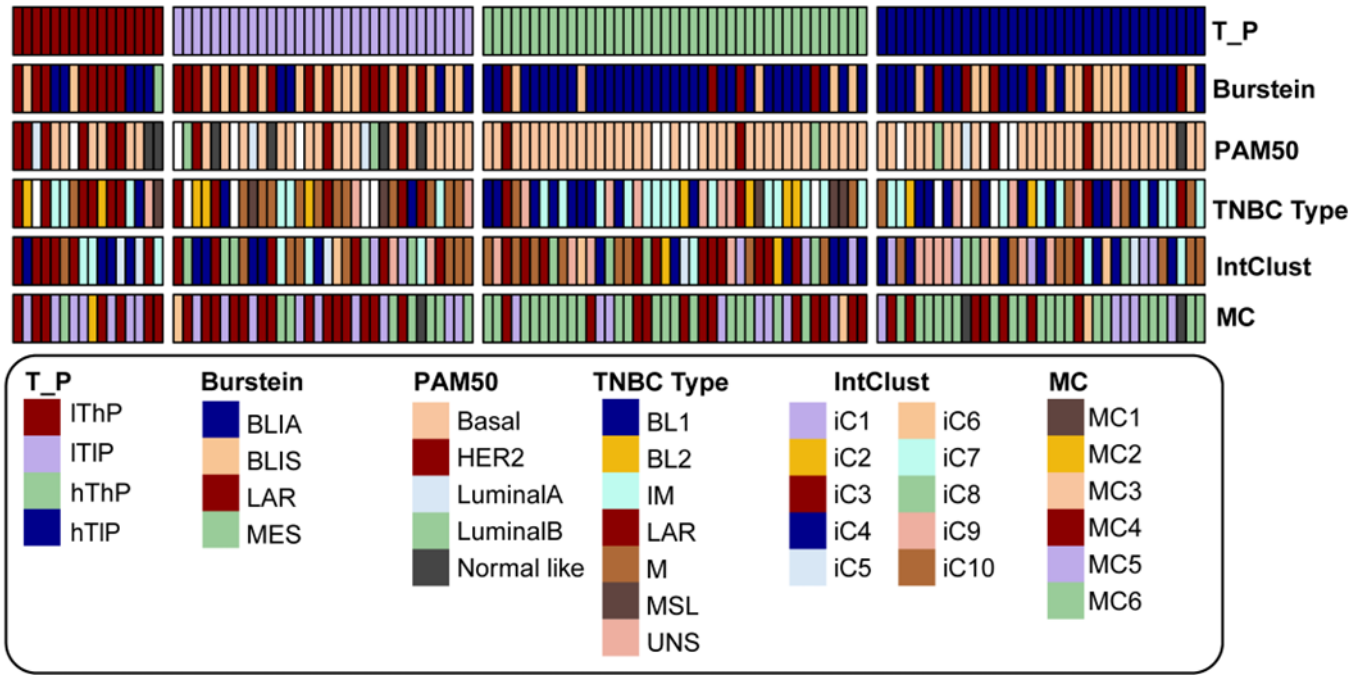

Figure 36: TNBC with low sTILs and high plasmablast signatures are predominantly of the luminal androgen receptor subtype. Molecular characterisation of tumours by sTILs (T) and plasmablast signature (P) scores. Bars represent sample-specific characteristics, including Burstein subtyping (Burstein et al., 2015), PAM50 (Parker et al., 2009), TNBC Type (Lehmanns, (Lehmann et al., 2011)), IntClust (Dawson et al., 2013), and MC (Quist et al., 2019).

3.10.4 Germinal centre numbers and sinus area are reduced in axillary lymph nodes of lThP TNBC patients

Previous data has shown that an increased number of GCs and expanded sinus area in TNBC patients is associated with increased dDFS and overall survival (Grigoriadis et al., 2018; Liu et al., 2021). Extrapolating from data acquired previously using a multiscale embedded deep learning (DL)-framework to capture GCs and sinuses, average GC number, normalised average sinus area and number of in-LNs were assessed within these subgroups (Verghese *et al*., under review).

In concordance with previous data linking sTIL infiltration and GC number in cf-LNs, the hThP group had the highest average number of GCs across their axillary LNs compared to lThP (Wilcoxon signed rank test $p < 0.001$), lTlP (Wilcoxon signed rank test, $p < 0.001$) and compared with hTlP patients (Wilcoxon signed rank test, $p < 0.01$) (Figure 37A). This group of patients also exhibited enlarged average sinus area within all LNs compared with lTlP patients (Wilcoxon signed rank test, $p < 0.01$) lThP patients (Wilcoxon signed rank test, $p < 0.05$), but not relative to those in the hTlP group. hTlP patients had expanded sinus area within all axillary LNs compared to lThP patients (Wilcoxon signed rank test, $p < 0.05$), and the lTlP (Wilcoxon signed rank test, $p < 0.05$), (Figure 37B). Conducive to inferior outcome, the lThP patients had the most in-LNs compared to lTlP (Wilcoxon signed rank test, $p < 0.01$), hThP (Wilcoxon signed rank test, $p < 0.05$), and hTlP (Wilcoxon signed rank test, $p < 0.05$) (Figure 37C). There was no associated between the average GC numbers within the LNs of a patient and the age at diagnosis of a patient within any of the subgroups (Figure 36D). Moreover, these data demonstrated that lThP patients have a low level of immune reactivity and high incidence of tumour involvement within their axillary LNs.

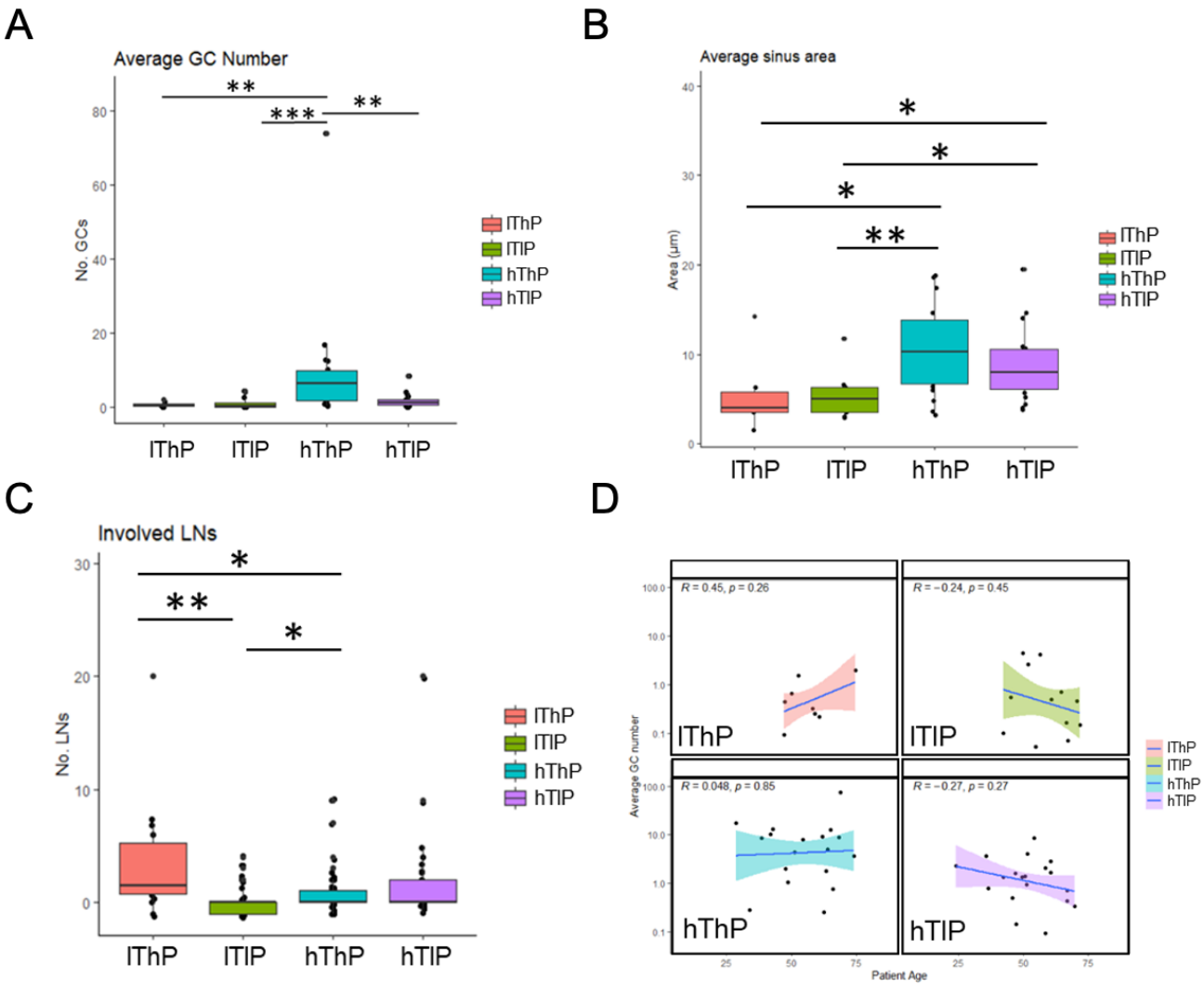

Figure 37: Histological characteristics of axillary lymph nodes across the TNBC cohort. Boxplots showing (A) the number of involved lymph nodes. (B) the average GC number in the axillary lymph nodes; (C) the sinus area in the axillary lymph nodes across the 4 patient subgroups. (D) In each subgroup, Spearman's rank correlation coefficient for correlations between the age of patient at diagnoses and the number of GCs in the axillary lymph nodes. Wilcoxon statistical tests used for (A-C), * = $p < 0.05$, ** = $p < 0.01$, *** = $p < 0.001$.

To explore the role of the GCs in cf- and in-LNs of these patients in more depth, Kaplan-Meier survival analyses were used to separate patients based on low average GC number (<2) and high average GC number (≥2) in all LNs. In agreement with our published data (Grigoriadis et al., 2018; Liu et al., 2021), the patients with high sTILs and more than 2 GCs within the LNs had a significantly longer time to distant metastasis compared to all the other groups hazard ratio (HR) = 10.41, likelihood ratio test, p = 0.001, (Figure 38A). Further to this, a reduced number of GCs within the LNs of patients with a high plasmablast enrichment score had a significantly shorter time to distant metastasis: hazard ratio (HR) = 2.288, likelihood ratio test, p = 0.025, (Figures 38B). Examining the impact of GC in LNs and sTIL levels at the primary tumour site within patients with a high plasmablast gene score showed that patients that exhibited low sTILs within this cohort had a significantly shorter distant disease-free survival time compared to those with high sTILs: hazard ratio (HR) = 3.13, likelihood ratio test, p = 0.0077, (Figure 39A). Crucially, GC counts in LNs alone within this group showed that patients with less than 2 GCs in all LNs had a significantly shorter distant disease-free survival time compared to those with more than 2: hazard ratio (HR) = 9.124, likelihood ratio test, p = 0.008, (Figures 39B). Thus, GC information within the LNs of these TNBC patients could potentially be used interchangeably with sTIL scores to delineate those with a high plasmablast environment and indicate risk of developing distant metastasis.

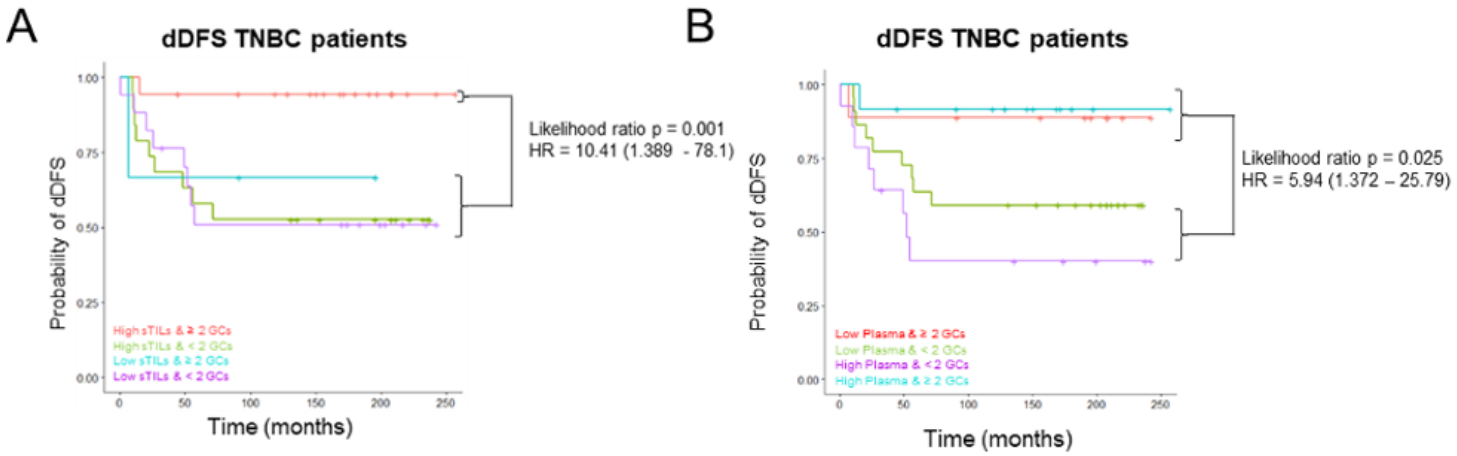

Figure 38: GC number adds prognostic value to outcome in IThP patients. (A) Kaplan Meier distant disease-free survival analyses of TNBC patients. Patients with high TILs and more than 2 GCs in their draining axillary LNs are shown in red (n = 18), those with high TILs and less than 2 GCs in their draining axillary LNs are shown in green (n = 19). Patients with low TILs and more than 2 GCs are depicted in blue (n = 3), whereas those with low TILS and less than 2 GCs are shown in purple (n = 17). Survival analyses were compared using the likelihood ratio test. HR = Hazard ratio with confidence interval shown in brackets. (B) Kaplan Meier distant disease-free survival analyses of TNBC patients. Patients with a low plasmablast score and more than 2 GCs in their draining axillary LNs are shown in red (n = 9), those with a low plasmablast score and less than 2 GCs are shown in green (n = 22). Patients with high plasmablast scores and more than 2 GCs are depicted in blue (n = 12), and those with high plasmablast scores and less than 2 GCs are shown in purple (n = 14). Survival analyses were compared using the likelihood ratio test. HR = Hazard ratio with confidence interval shown in brackets.

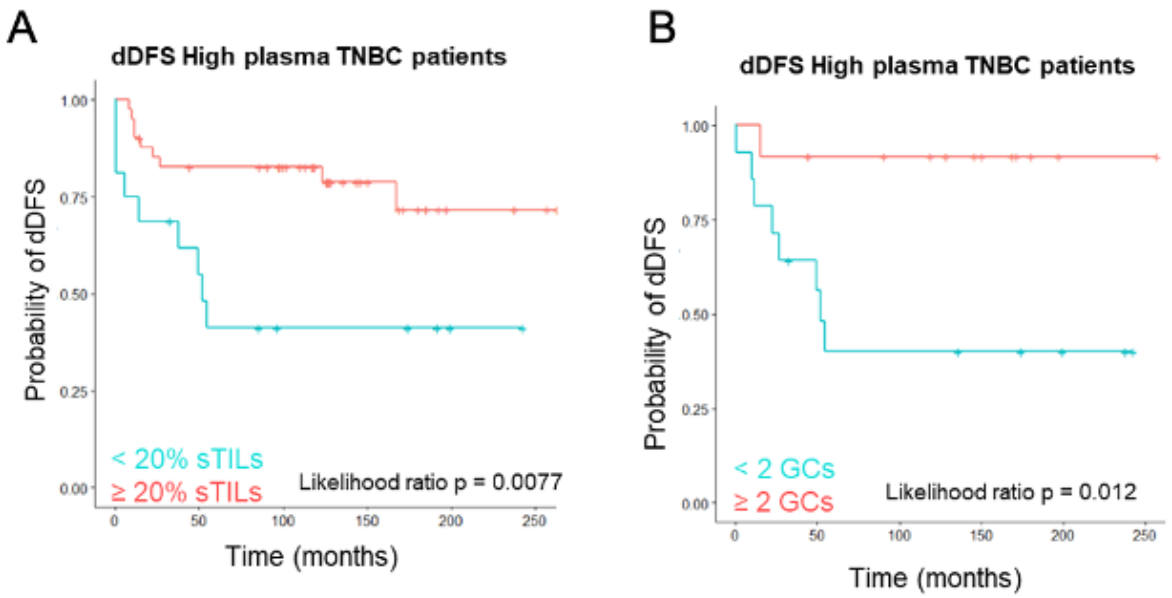

Figure 39: Low sTILs and low GC numbers associated with distant metastasis development in patients with high plasmablast gene score. (A) Kaplan Meier distant disease-free survival analyses of 57 TNBC tumours with high plasmablast gene score. Patients with low sTILs shown in blue (n = 16), and those with high sTILs shown in red (n = 41). Survival analyses were compared using the log rank test. (B) Kaplan Meier distant disease-free survival analyses of 26 TNBC tumours with high plasmablast gene score, comparing low and high GC numbers in adjacent lymph nodes. Patients with less than 2 GCs shown in blue (n = 14) and those with more than or equal to 2 GCs is shown in red (n = 12). Survival analyses were compared using the likelihood ratio test.

3.11 Genes associated with plasma cell migration and LN egress are upregulated in tumours with low sTILs and a high plasmablast gene signature

Next, I asked whether expression of genes associated with LN egress and plasma cell migration may be upregulated in the lThP group, which may suggest that those within the primary tumour are derived from the adjacent LN. The CXCL12/CXCR4 axis is a chemokine gradient essential for plasma cell movement, predominantly to the bone marrow from secondary lymphoid organs for further maturation (Cheng et al., 2018). Further, synergy between CXCL12 and HGF has shown to be implicated in the migration of multiple myeloma cells(Ullah, 2019). KLF2 and S1PR1 are upregulated on plasmablasts and plasma cells in the peripheral blood and are thought to play a role in homing to the bone marrow and tissues (Winkelmann et al., 2011). Within these tumours, *KLF2* was significantly upregulated in lThP patients compared to hThP and hTlP (paired T tests, $p < 0.01$, $p < 0.05$ respectively). This was also the case for *S1PR1*, elevated in lThP tumours compared to lTlP (paired T test, $p < 0.001$), hThP (paired T test, $p < 0.01$), and hTlP (paired T test, $p < 0.001$). There was also an increase in *CXCL12* expression in lThP tumours compared to hTlP (paired T test, $p < 0.05$, which indicates differences in the gene expression profiles of tumours with a high plasmablast environment when comparing low vs high sTILs. Further, *HGF* was upregulated in lThP compared to hThp tumours (paired T test, $p < 0.05$), and lTlP tumours (paired T test, $p < 0.001$) (Figure 40). Taken together, this suggests an overexpression of genes within lThP tumours that are favourable for plasma cell migration and homing from the adjacent LN. A comprehensive analysis looking at differentially expressed genes and pathway analysis of this lThP subgroup was investigated further in chapter 5. Section 5.1.

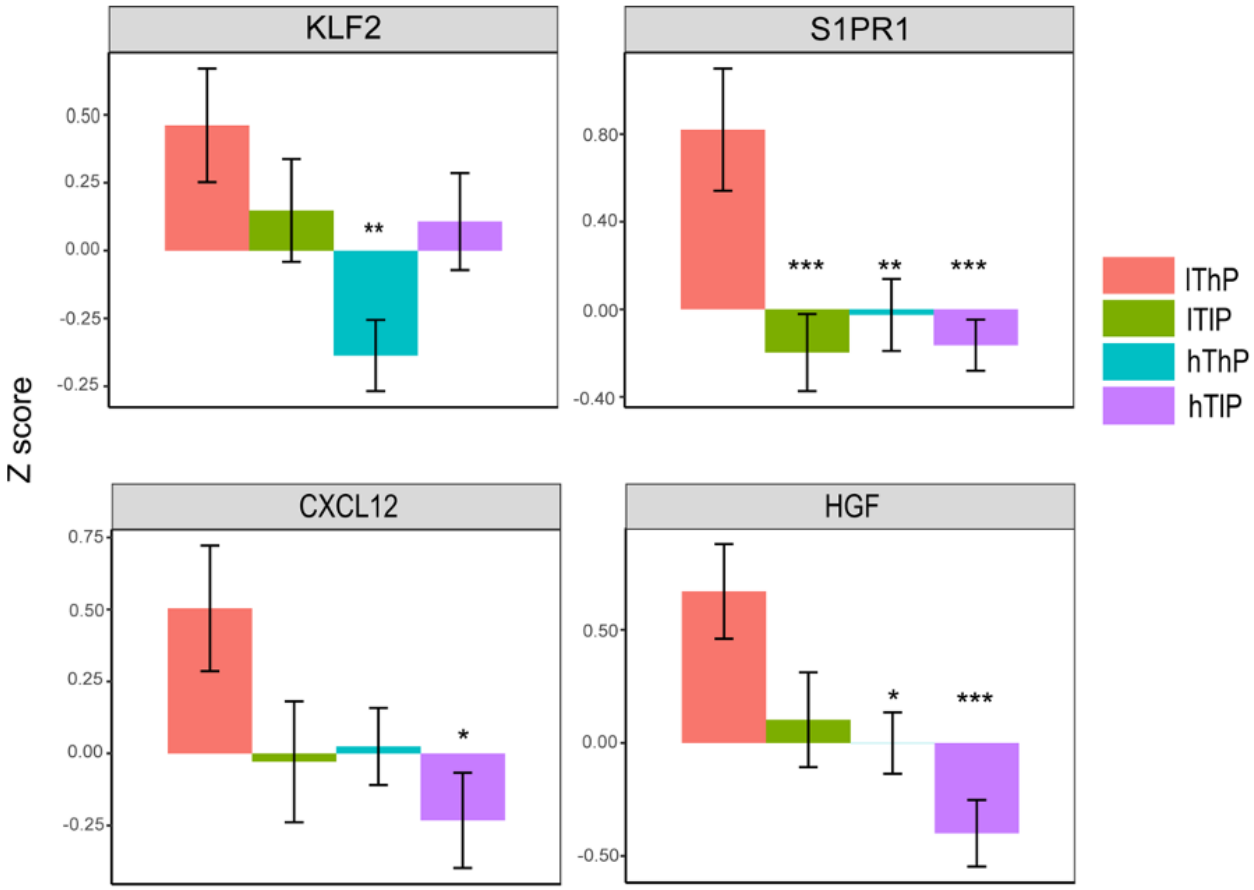

Figure 40: lThP patient tumours upregulate factors associated with lymph node egress and plasma cell migration. Normalised gene expression of KLF2, S1PR1, CXCL12 and HGF within lThP, lTlP, hThP and hTlP patients (paired T tests comparing lThP patients to other groups, * = p< 0.05, ** = p < 0.01, *** =p < 0.001).

3.12 GCs are enriched in in-LNs of patients that did not develop distant metastasis within the Tianjin TNBC cohort

To validate these findings on a protein level and assess the spatial analyses of plasma cells within low sTILs primary tumours and LNs, histological sections were chosen for immunofluorescence techniques. At the time of analyses, sections of the Guy's cohort in which previous gene expression data was performed was not available. We have previously shown that GCs within cf-LNs hold prognostic information within the Tianjin cohort of HER2+ and TNBC tumours (Liu et al., 2021), therefore histological sections of a subset (16) of these patients were selected for subsequent experiments. As previously mentioned, these patients exhibited all low sTILs tumours, scoring $\leq$ 0%, 5% or 10% using Salgado's scoring criteria (Salgado et al., 2015). The number of GCs were scored in cf-LNs and in-LNs across the 16 patients. There was no significant difference between the number of GCs in the cf-LNs and in the in-LNs (Mann-Whitney U test and Wilcoxon rank sum test) (Figure 41A). However, within the in-LNs but not the cf-LNs, a lower number of GCs was associated with distant metastasis development (Mann-Whiney U test, $p < 0.01$) (Figure 41B).

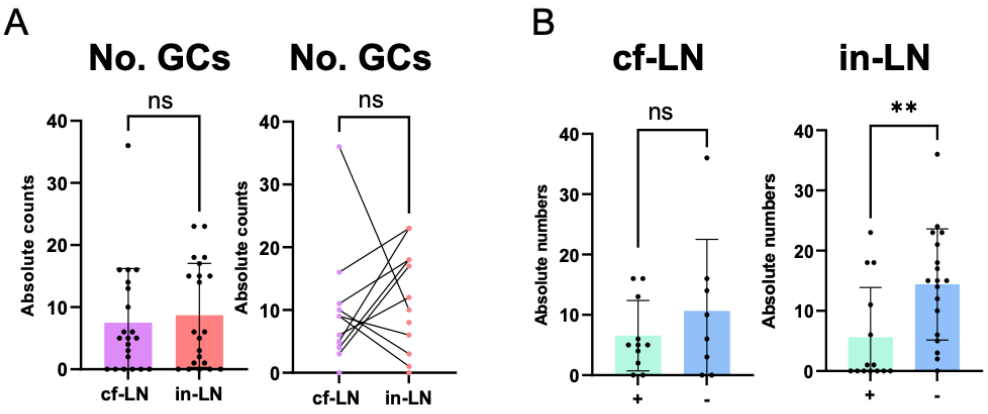

Figure 41: Increased GC number in involved LNs is associated with a better outcome in TNBC patients. (A) Absolute numbers of germinal centres within cancer free lymph nodes (cf-LNs) and involved lymph nodes (in-LNs) shown as independent factors or as patient-paired LNs. A Mann-Whitney U test and Wilcoxon rank sum test were used respectively to calculate statistics. (B) Absolute numbers of germinal centres within cf-LNs and in-LNs of patients that developed distant metastasis (+) and those that did not (-), shown as independent factors or as paired LNs within the same patient. A Mann-Whitney U test and Wilcoxon rank sum Test were used respectively to calculate statistics. * = $p < 0.05$.

3.13 Memory B cells and plasma cells quantification using multiparametric immunofluorescence

Having established that low sTIL tumours with few GCs in their axillary LNs exhibit higher expression of genes associated with plasma cells, the percentages of memory B cells and plasma cells were evaluated within paired patient matched primary tumour, cf-LNs and in-LNs from the Tianjin cohort. IF was utilised to detect the presence of memory B cells by virtue of CD20 and CD27 expression and classed as CD20+CD27+CD138-. Plasma cells were confirmed as CD20-CD27+ CD138+ (Figure 42A). Using QuPath v.0.3.2 (Bankhead et al., 2017) a random forest classifier was applied to IF-stained images of 19 cf-LNs, 23 in-LNs and primary tumour sections from 16 TNBC patients. A mask was generated for each image; CD138+ cells represented in magenta, CD20+ cells in red, CD27+ cells shown in green, CD20+CD27+CD138- as yellow, CD138+CD27+CD20- in grey (Figure 42B).

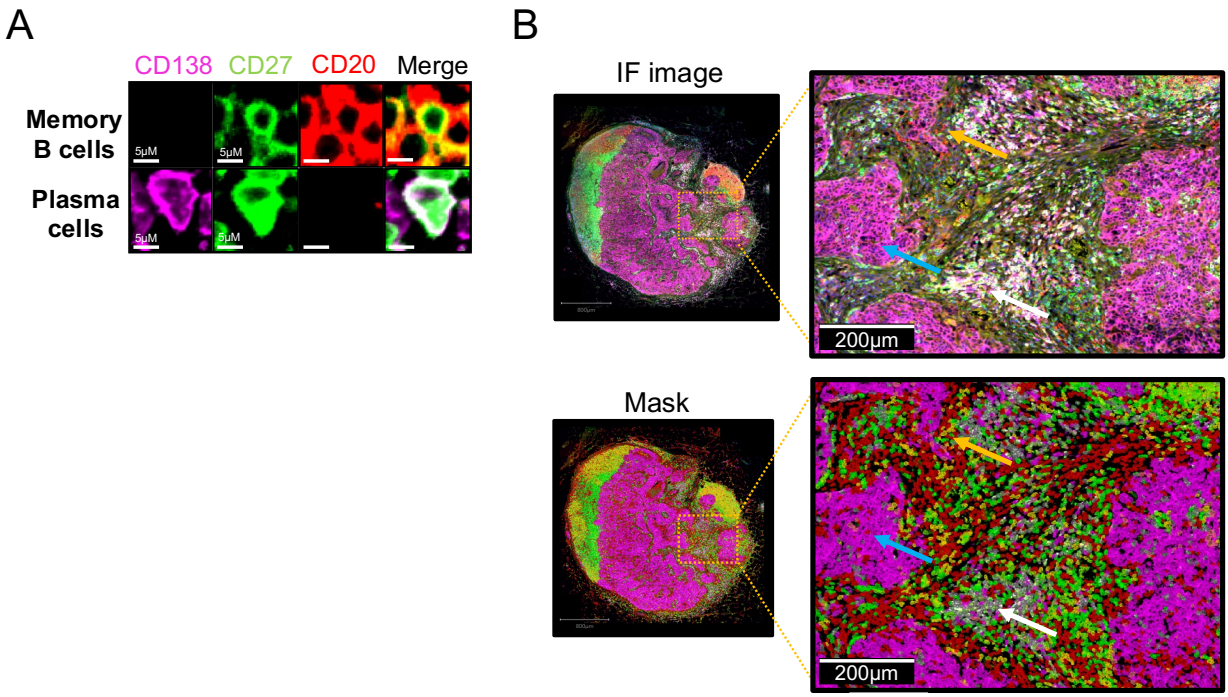

Figure 42: Detection of B cell subsets using immunofluorescence staining. (A) Example images of an involved LN from a TNBC patient stained using immunofluorescence, and its paired mask generated using QuPath. Magenta cells within mask represent CD20-CD27-CD138+ cells (blue arrows). Yellow arrows indicate memory B cells, which are CD20+CD27+CD138- and yellow cells within the mask. White arrows show plasma cells, identified as CD20-CD27+ CD138+and grey cells in the mask. Red cells picked up by the mask are CD20+CD138-CD27- within immunofluorescence staining.

3.13.1 Plasma cells are enriched, and memory B cells are depleted in involved lymph nodes compared to cancer-free lymph nodes

Quantification of CD20+CD27+ memory B cells within the cf-LNs and in-LNs revealed an enrichment for memory B cells within the cf-LNs compared to the in-LNs both independently and when compared on between paired LNs within a patient (Mann-Whitney U test, $p < 0.05$, Wilcoxon rank sum test, $p < 0.01$, respectively) (Figure 43A). The memory B cells were localised near the follicles and GCs of the cf-LN, with a large proportion of CD20+CD27+ cells residing in close proximity to follicles compared to the in-LN (Figure 43B). Conversely,

CD138+CD27+ plasma cells were increased in the in-LN compared to the cf-LN, when assessing across all cf-LNs and in-LNs and compared between paired LNs within a patient (Figure 44A). Plasma cells were predominantly found in the in-LNs near malignant metastatic cells, enriched in the stromal areas, but within the cf-LN, they were in close proximity to follicles and GCs (figure 44B).

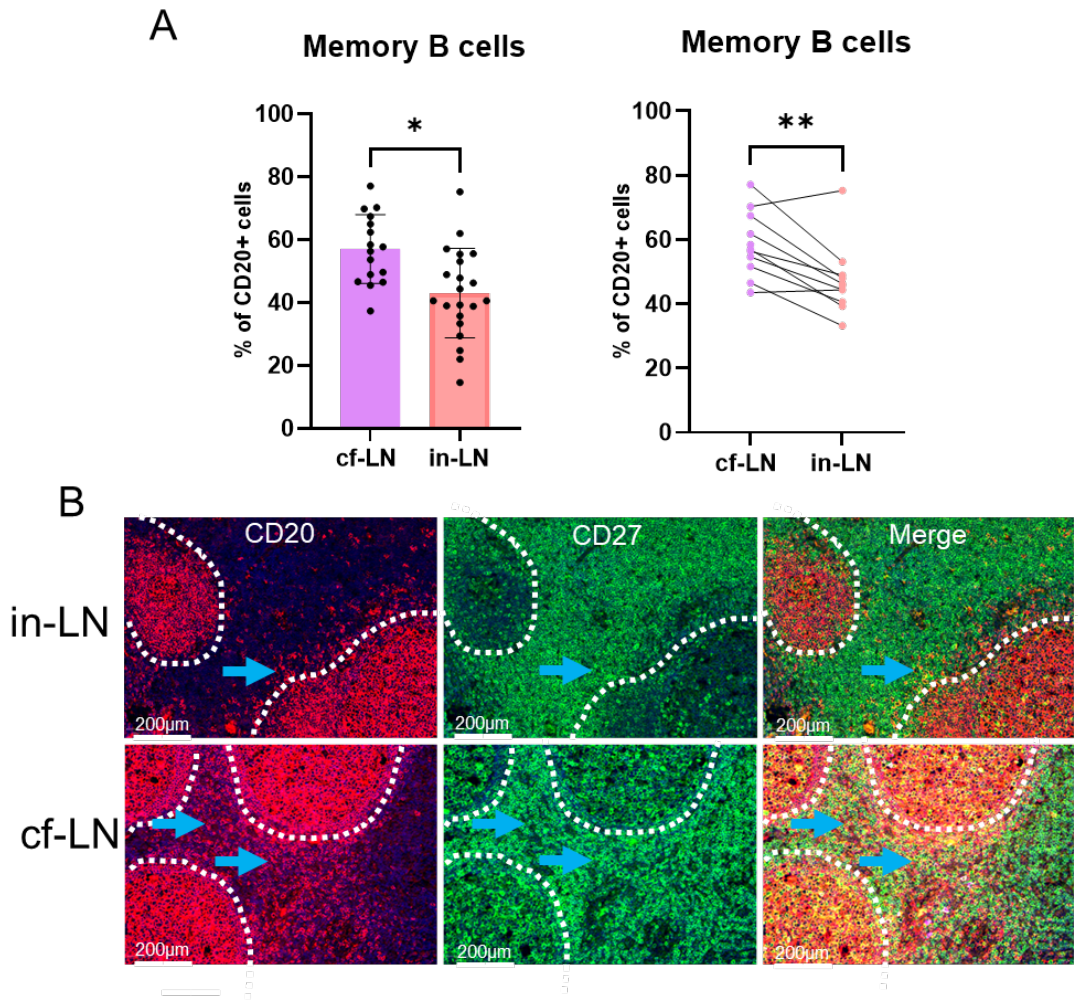

Figure 43: Memory B cells are enriched in cancer-free lymph nodes compared with involved in TNBC patients. (A) Memory B cells as percentage of cells within cancer-free LNs (cf-LNs) and involved lymph nodes (in-LNs) of TNBC patients, shown as independent or patient-paired factors. A Mann-Whitney U test and Wilcoxon rank sum test were used respectively to calculate statistics. * = $p < 0.05$, ** = $p < 0.01$. B) Representative immunofluorescence images of an in-LN and cf-LN from one TNBC patient. White dotted lines indicate the outline of follicles, and blue arrows represent memory B cells.

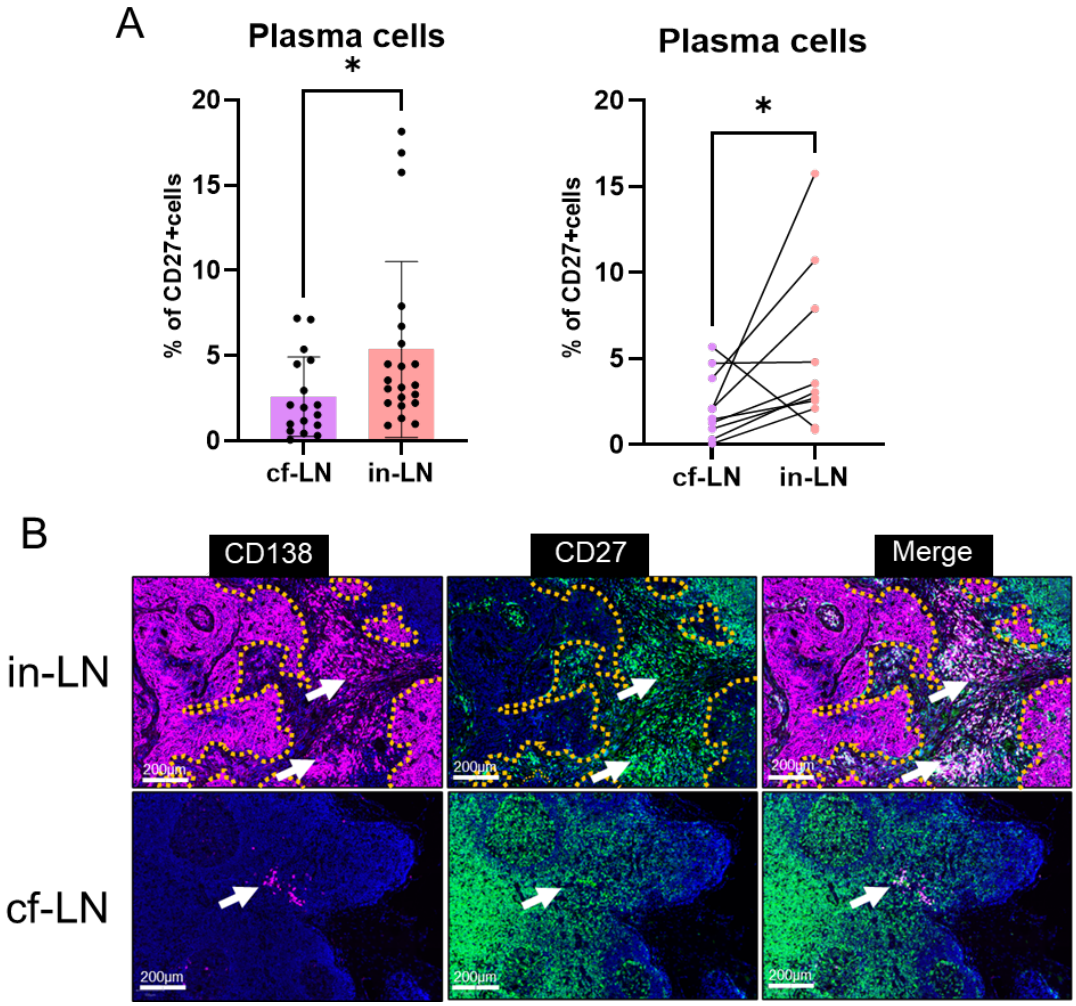

Figure 44: Plasma cells are increased in involved lymph nodes of TNBC patients compared with cancer-free lymph nodes. (A) Plasma cells as % CD27 cells within cancer-free LNs (cf-LNs) and involved lymph nodes (in-LNs) of TNBC patients, shown as independent factors or as paired LNs within the same patient. A Mann-Whitney U test and Wilcoxon Test were used respectively to calculate statistics. (B) Representative immunofluorescence images of an in-LN and cf-LN from one TNBC patient. Yellow dotted lines indicate metastatic tumour border, and white arrows highlight plasma cells. * = $p<0.05$.

3.13.2 Plasma cell frequency is increased in the in-LNs of patients with low sTILs tumours and with a high risk of developing distant metastasis

To determine if the levels of memory B cells and plasma cells in the cf- and in-LNs may be associated with outcome, the proportions of each subset were compared in patients without distant metastasis and those who developed distant metastasis. Memory B cells were enriched in the cf-LNs of patients who did not develop distant metastasis (Mann-Whitney U test, $p < 0.05$), but there were no significant changes within the in-LNs (Mann-Whiney U test) (45A) and they were primarily located near B cell follicles and GCs (Figure 45B). Conversely, CD138+CD27+ plasma cells as a percentage of CD27+ cells were increased within in-LNs of patients who developed distant metastasis (Figure 46A) and were predominantly located near to metastasis deposit in LNs, clustered within the stromal areas (Figure 46B). The enrichment of plasma cells in patients that developed distant metastasis was not observed within the cf-LNs, where there was no difference in percentage of plasma cells between the two patient groups (Figure 45A-B). It was also noted that the percentage of plasma cells within CD27+ cells in the in-LN was negatively correlated with the number of GCs (Spearman corelation, $r = -0.548$, $p<0.01$), but this was not evident with the levels of memory B cells (Spearman corelation $r = 0.37$, $p = 0.0405$) (Figure 47A). There was no correlation between the percentage of memory B cells or plasma cells and the number of GCs within the cf-LNs of these low sTILs patients (Figure 47B). These data collectively suggest that low sTILs patients who develop distant metastasis have low levels of memory B cells within their cf-LNs, high levels of plasma cells within their in-LNs and these frequencies are negatively correlated with the number of GCs in a LN.

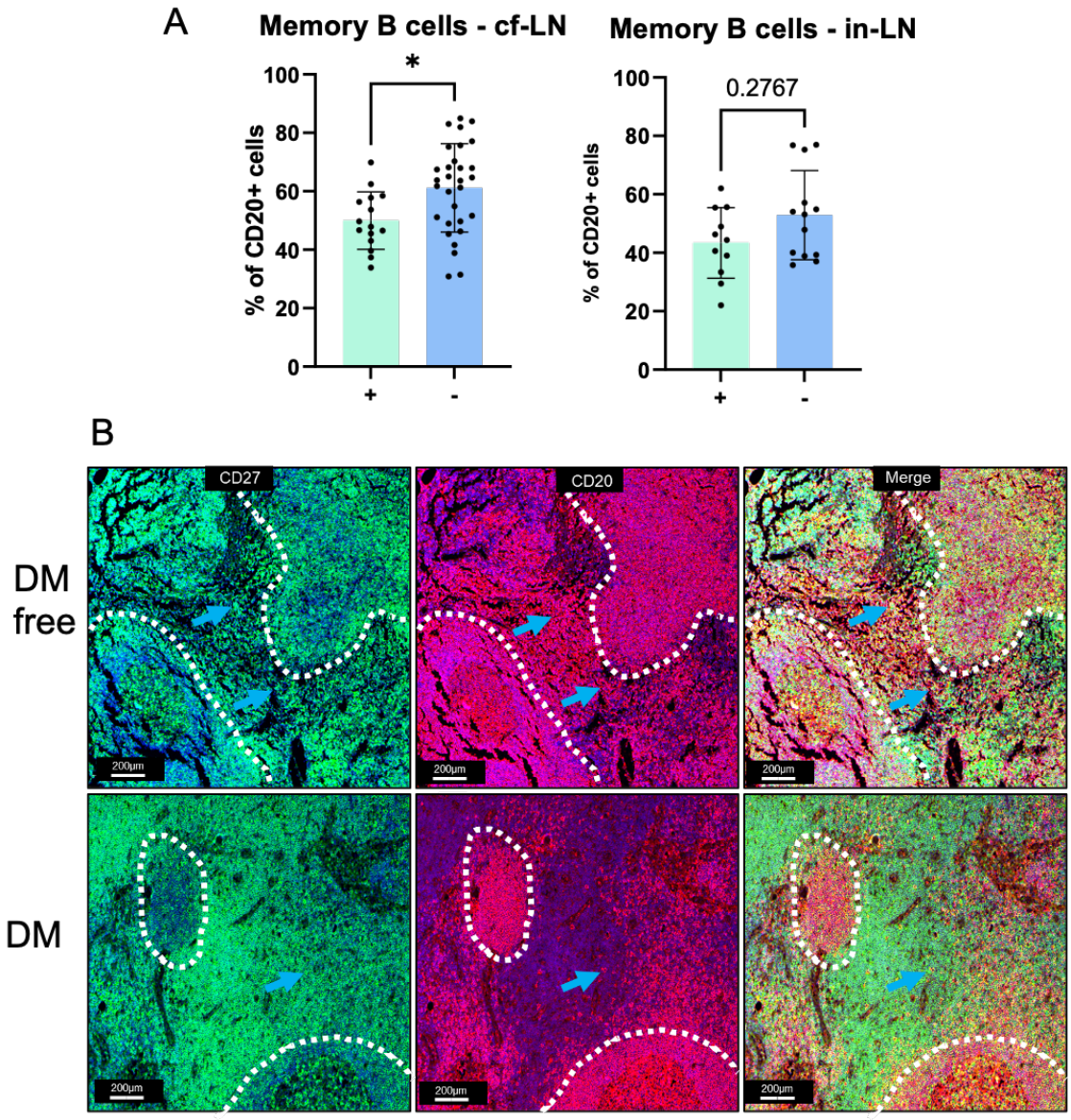

Figure 45: Increased memory B cells in cancer free lymph nodes in TNBC patients with improved outcome. (A) Memory B cells as % CD20 cells within cancer-free LNs (cf-LNs) and involved LNs (in-LNs) of TNBC patients that were distant metastasis free (-) and those that developed distant metastasis (+). (B) Representative immunofluorescence images of a cf-LN from one TNBC patient that developed distant metastasis and one that did not. White dotted lines indicate the outline of follicles, and blue arrows represent memory B cells. Mann-Whitney U tests were used. * = $p < 0.05$. DM = distant metastasis.

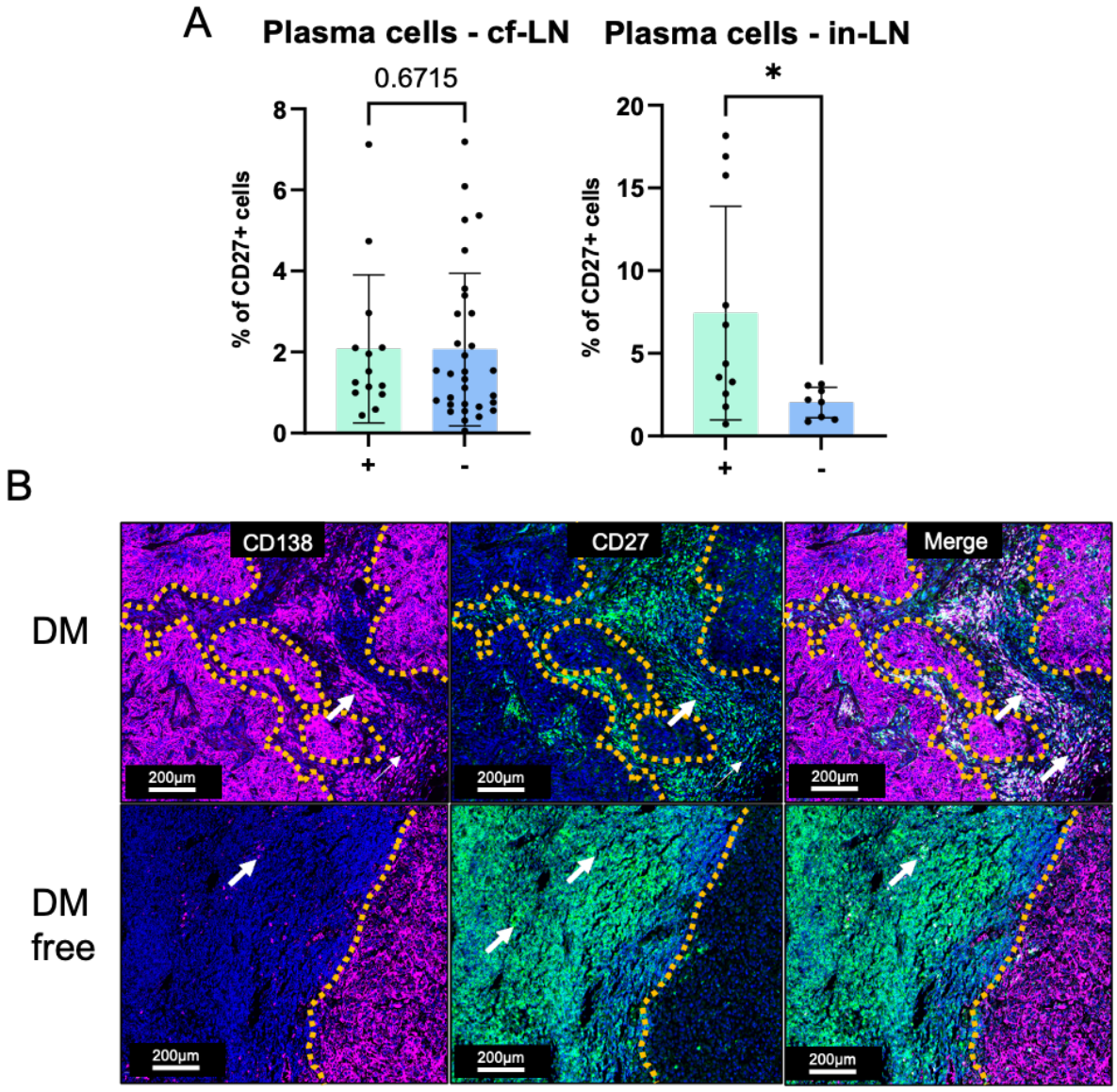

Figure 46: Increased plasma cells in involved lymph nodes in TNBC patients that who had developed distant metastasis. (A) Plasma cells as % CD27 cells within cancer-free LNs (cf-LNs) and involved LNs (in-LNs) of TNBC patients that were distant metastasis free (-) and those that developed distant metastasis (+). (B) Representative immunofluorescence images of in-LNs from one TNBC patient that developed distant metastasis and one that did not. Yellow dotted lines indicate metastatic tumour border, and white arrows highlight plasma cells. * = $p < 0.05$. DM = distant metastasis.

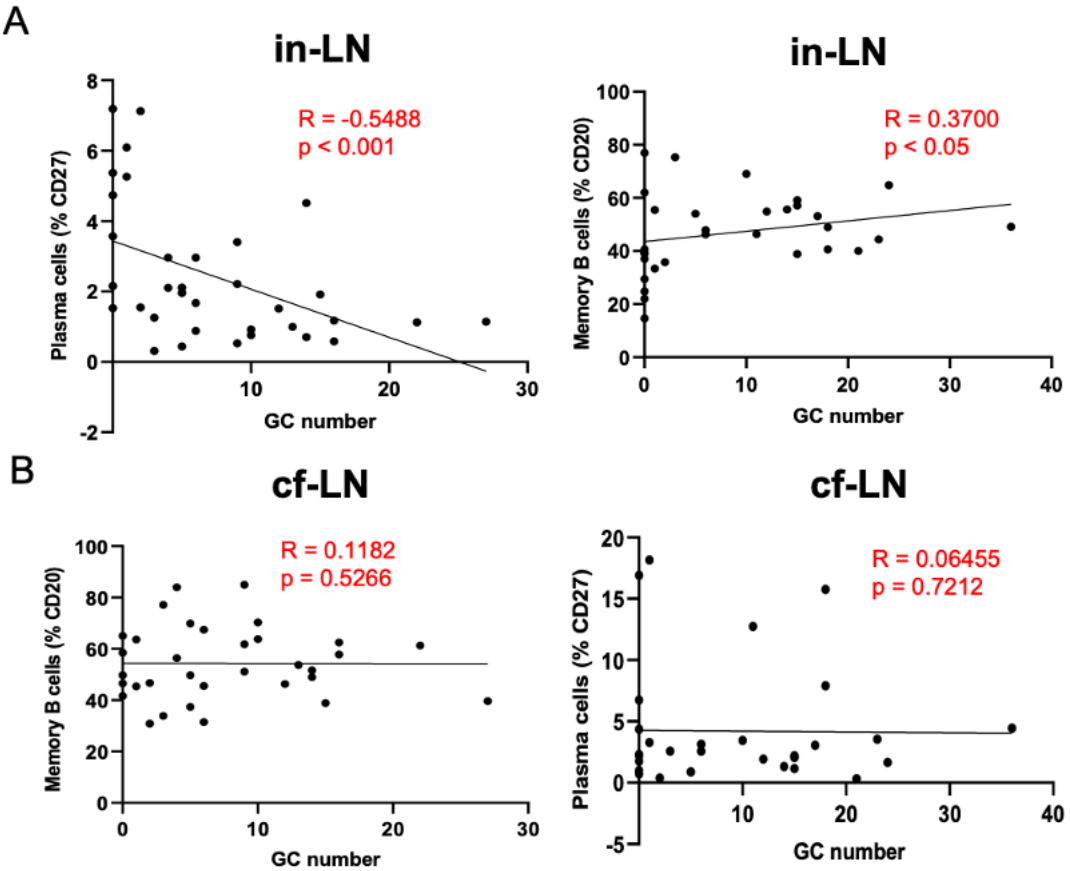

Figure 47: The frequency of plasma cells is negatively correlated with GC numbers in involved lymph nodes of low sTIL TNBC patients. (A) Spearman's rank correlation coefficient for correlations between plasma cells as percentage of CD27+ cells with the average number of germinal centres (GC) within involved lymph nodes (in-LN). (B) Spearman's rank correlation coefficient for correlations between memory B cells as percentage of CD20+ cells with the average number of germinal centres (GC) within involved lymph nodes (in-LN).

3.13.3 Plasma cells are increased but memory B cell levels reduced in primary tumour and in-LNs compared to cf-LNs

To determine if the frequency of memory B cells and plasma cells in primary tumour, cf-LNs and in-LNs were distinctive within a patient, paired analyses were performed. The percentage of memory B cells as a fraction of CD20+ cells was significantly enriched in both the cf-LN and in-LN compared to the primary tumour (Wilcoxon rank sum test, $p < 0.0001$) (Figure 48A). In contrast, plasma cells as a percentage of CD27+ cells were decreased in both the cf-LN and in-LN compared with their patient-matched primary tumour sections (Wilcoxon rank sum test, $p < 0.0001$) (Figure 48B). Memory B cells at the primary tumour lesion localised near clusters of naïve CD20+CD27- B cells and plasma cells were primarily found within the intratumoral stroma (Figure 48C). In concordance to the outcome analyses seen within the cf-LNs and in-LNs (Figures 45 & 46), a strong trend towards memory B cell depletion and plasma cell enrichment was associated with distant metastasis development within these low sTIL primary tumours (Mann-Whitney U test, $p < 0.05$) (49A-B). Plasma cells within the primary tumour of patients that developed distant metastasis were predominantly stroma restricted whereas in metastasis free patients, they were found infiltrated in the tumour (Figure 49C).

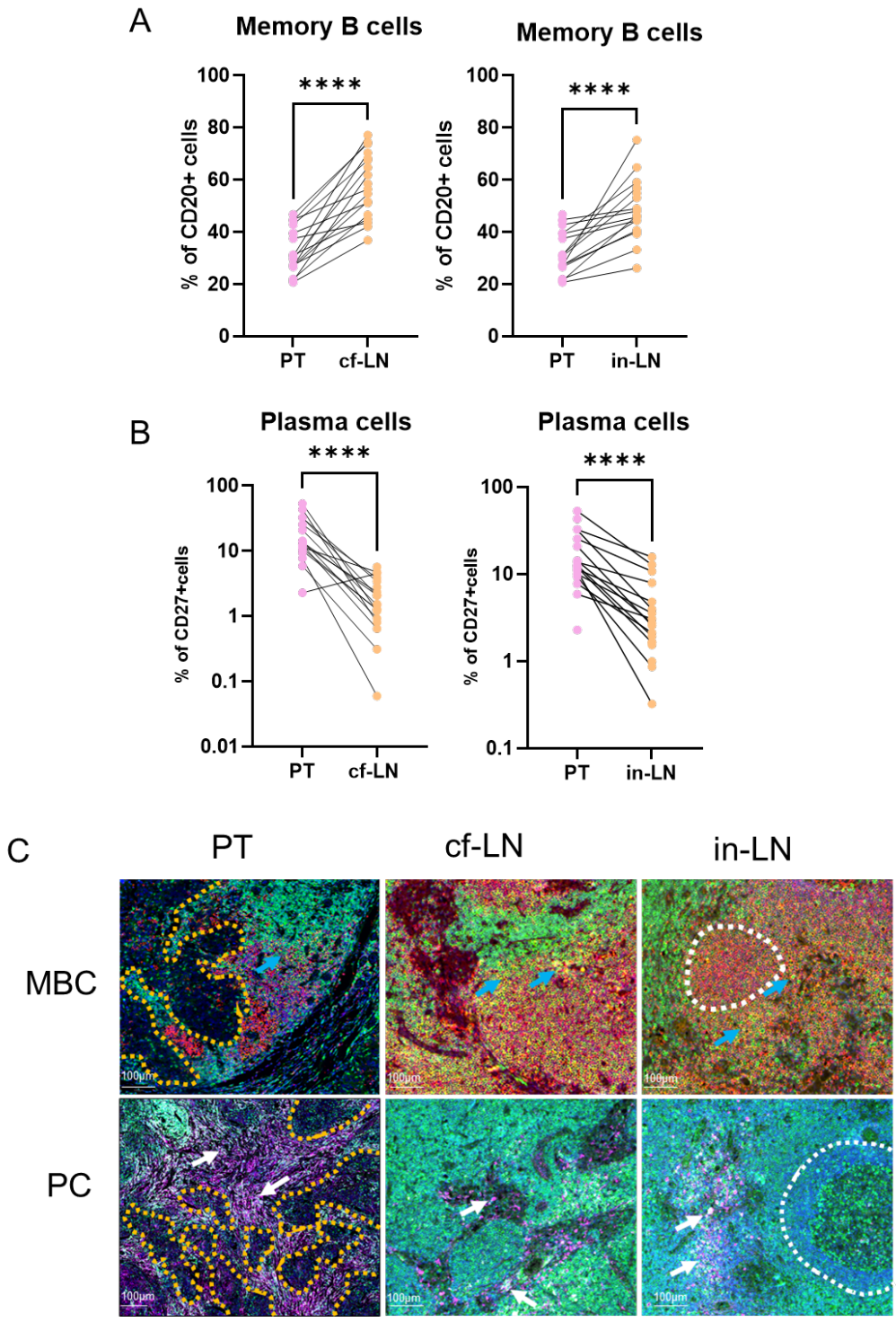

Figure 48: Memory B cells are depleted, and plasma cells enriched in primary TNBC tumours compared to cancer free and involved lymph nodes. (A) Memory B cells as a % of CD20+ cells in matched primary tumour (PT), cancer-free (cf-) and involved (in-) lymph nodes. (B) Plasma cells as % of CD27+ cells in matched primary tumour (PT), cancer-free (cf-) and involved (in-) lymph nodes. **** = $p<0.0001$, paired Wilcoxon test. (C) Representative immunofluorescence images of memory B cells (MBC) and plasma cells (PC) in the primary tumour (PT), cancer-free LN (cf-LN) and involved LN (in-LN). DM = distant metastasis.

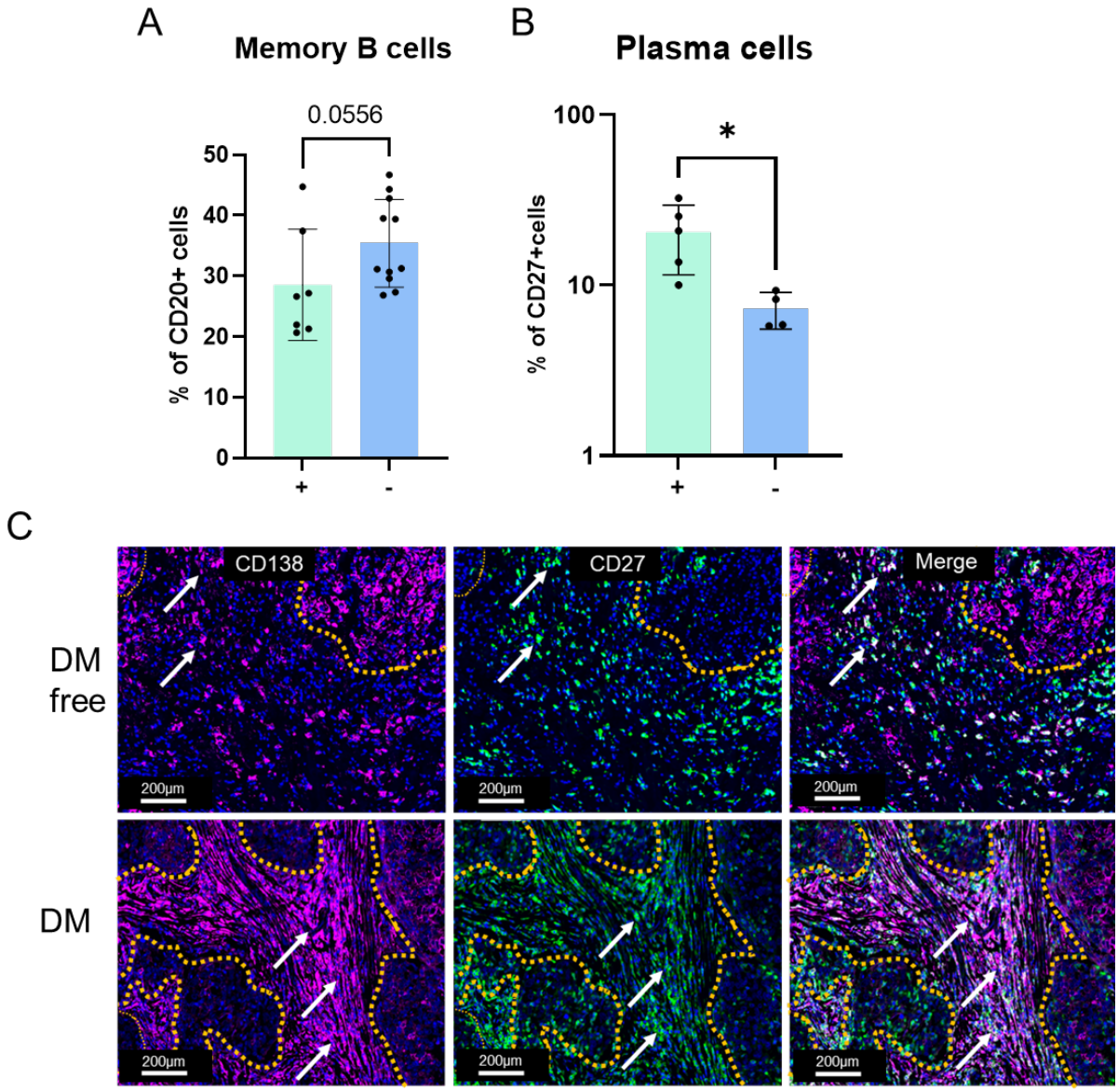

Figure 49: Plasma cells enriched and and memory B cells depleted in low sTIL TNBC tumours that developed distant metastasis. (A) Memory B cells as % CD20 cells within primary tumours in patients that developed distant metastasis (+) and those that did not (-). (B) Plasma cells as % CD27 cells within primary tumours in patients that developed distant metastasis (+) and those that did not (-). (C) Representative immunofluorescence images from a low sTIL TNBC tumour that did not progress to distant metastasis (top row) and a low sTIL TNBC tumour that did progress (bottom row). Yellow dotted lines indicate tumour/stroma border and white arrows highlight plasma cells. *= $p < 0.05$, Mann Whitney U test. DM = distant metastasis.

3.14 Discussion

Our group has consistently shown the additive prognostic value of GC formation within the d-LNs in patients with TNBC, especially within those with low sTILs tumours. However, so far, there is little knowledge on the cellular composition of GCs, their derived B cell populations, and their role in tumour progression in breast cancer. One aim within this chapter was to profile immune cells related to the GC reactions within axillary LNs of TNBC patients and to evaluate whether cellular or molecular composition of primary tumour and LNs differed in subgroups of patients with different disease trajectories. As a pilot study, I used multiplex IMC techniques to explore the cellular composition of an in-LN of a patient with high sTILs within their primary tumour who was distant metastasis free, and an in-LN from a patient with low sTILs within their primary tumour and developed distant metastasis.

The LN of patient 1 (high sTILs) exhibited increased CD8+ T cells and depleted CD4+ T cells levels compared to the LN of patient 2 (low sTILs). Mouse models of TNBC, including the 67NR and 4T1, have previously suggested that CD8+T cells in the LN can prevent metastatic spread from primary tumour to the LNs, although the mechanisms behind these observations are still unclear (Joseph et al., 2021). The most striking differences, however, were that of the enrichment of both PD1+ CD4+ T cells and PD1+ CD8+ T cells within the GCs in the LN of the patient 1 compared to GCs in the LN of patient 2. Although CXCR5 and ICOS, known markers for Tfh cells, were not used in this study, the increased prevalence of PD1+CD4+ T cells within the GCs suggests the presence of Tfh cells, which have a crucial role in antigen presentation and selection of B cells. This suggests an active priming of GC B cell responses occurring within the LN of patient 1 which may limit metastatic spread to distant organs and contribute to high sTIL infiltration at the primary tumour.

Further, despite their association with exhaustion within the context of cancer, PD1+CD8+T cells play a pivotal part in the GC reaction, regulating autoimmunity and maintaining B cell tolerance (Yuhong Chen et al., 2019). This suggests that within the LNs of patient 2, there

may be a deficiency in antigen presentation and maintenance mechanisms by T cells that ensure sufficient maturation of B cells into memory B and plasma cells. In alignment with this, the LN of patient 2 exhibited significantly more naïve B within the GC ROIs compared to patient 1, indicating that the B cells within these GCs may be less likely to undergo class switching. In conjunction with this, the GC ROIs from the LN of patient 2 demonstrated a high prevalence of MZ B cells. MZ B cells are subset of innate like B cells that are predominantly localised to the spleen, however are found in small numbers within LNs and the circulation (Appelgren et al., 2018). MZ B cells can rapidly differentiate into IgM+ plasmablasts in response to type 1 TI antigens including LPS, but also act as a regulator of autoimmunity, secreting regulatory cytokine IL-10 to induce self-tolerance (Appelgren et al., 2018). Although understudied within the context of breast cancer, Mehdipour *et al*., reported a modest increase in MZ B cells in in-LNs compared to cf-LNs within breast cancer patients (Mehdipour et al., 2016). This may indicate that the increased occurrence of MZ B cells within the LN of patient 2 could skew the GC response towards a more immature phenotype which may in turn be associated with poor outcome and lack of immune infiltration at the primary tumour.

Despite relatively fewer plasma cells present in the LN of patient 2 compared to patient 1, the increase in MZ B cells may indicate that some of these plasma cells may be more likely to originate from an extrafollicular pathway, which typically results in predominantly IgM+ antibody secretion (Bortnick and Allman, 2013). Whilst IgM can participate in tumour mediated killing via opsonisation and antibody dependent cellular cytotoxicity, increased levels of somatically mutated and class switched IgG is generally more recognised to have the most potent anti-tumour capabilities (Cui et al., 2021). In parallel, the trend towards an increase in DN2 cells within the non-GC areas of the LN from patient 2 further points towards an extrafollicular response. Potentiated by TLR7 signalling, activated naïve B cells can differentiate into DN2 cells in the absence of a GC reaction, which subsequently will form the basis for extrafollicular plasma cell responses (Fillatreau et al., 2021). Although

relatively understudied in the context of cancer, the DN phenotype has been associated with chronic viral infection and autoimmune disease and suggested to represent exhausted or senescent memory B cells in a similar fashion to exhausted T cells. Within NSCLC, they are enriched in lung tumours compared to normal adjacent tissue and are inversely correlated to the abundance of affinity-matured B cells within the tumour (Centuori et al., 2018). More recently, they have been shown to be expanded within the TME compared to the periphery of breast cancer patients, representing as much as 40% of B cells within treatment naïve tumours (Carpenter et al., 2022). Although the role of these cells has not been fully elucidated within the context of tumour progression, due their exhaustion-like properties they may be representative of a B cell subset that could impede functional anti-tumour B cell responses. Here, this process may indicate an extrafollicular or exhausted phenotype of B cells promoting distant metastasis progression due to inadequate clearance or maintenance of metastatic cells within the in-LNs.

The trend suggesting an enrichment of Tregs within the non-GC areas of patient 2 may further indicate an immunosuppressive environment. Their spatial colocalization subsequently indicates a crosstalk between Tregs and macrophages, forming clusters at close proximity to tumour cells. There has been indication that the poor prognosis of bladder, cervical and breast cancer is attributed in part to TAM infiltration, and high numbers of CD68+ macrophages are associated with a significantly shorter disease free survival in breast cancer, secreting cytokines including IL-35 to promote metastasis (Larionova et al., 2020). Notably, positive-feedback loops have been suggested between tumour infiltrating Tregs and M2 macrophages which facilitates the progression of laryngeal squamous cell carcinoma and TAM derived IL-10, that, in turn, can contribute to the differentiation of Tregs (Li et al., 2022; Rabinovich et al., 2010). Whilst I could not make the distinction between M1-like or M2-like macrophages, the enrichment of Tregs and macrophages in the LN of patient 2, and co-localisation of these 2 subsets is perhaps reflective of a mechanism that facilitates CD8+T cell suppression within the LN. This, in parallel with inadequate antigen presentation

within GCs, and increased extrafollicular responses may facilitate distant metastasis development. Impeded GC B cell response is furthermore possibly mirrored in the reduction of plasma cell production within the LNs of patient 2, which was not immunoglobulin isotype dependent. However, there was a significant enrichment of IgG+ plasma cells within the GCs of LN of patient 1 compared to the LN of patient 2, indicating possible increased IgG responses arising from a GC reaction. There was also a lack of evident communication between key subsets involved in antigen presentation and anti-tumour responses in the LN of patient 2. The indication that PD1+CD4+ T cells in the LN of patient 1 were interacting with CD8+T cells, unswitched B cells and predominantly IgA+ and IgG+ plasma cells suggest an active humoral response within the LN that was distinctly absent in LN of patient 2. Taken together, this is suggestive of immune activation within the LN of patient with high sTIL infiltration, which indicates it may be able to potentiate responses at the primary tumour and prevent distant metastasis development.

Harnessing gene expression signatures of many of these subsets within the primary tumours of an independent cohort revealed that a high level of NK cells, T cell and B cell subsets, namely CD4+ T cells, CD8+ T cells, Tfh and memory B cells was predictive of a longer distant disease-free survival time. This is in concordance with published data, showing that an increased infiltration of T cells and memory B cells are associated with an improved survival and longer time to distant metastasis in TNBC patients (Chumsri et al., 2020; Harris et al., 2021; Oshi et al., 2020). This phenomenon was only significant within the context of high sTIL tumours, which suggests that within immunologically cold tumours, an increase in these subsets is not enough to prevent tumour evolution and distant metastasis development. Notably, an upregulation of the plasmablast gene signature, specifically within low sTILs tumours (lThP) was associated with a shorter distant metastasis free survival time, potentially reflecting on an exhausted or dysfunctional plasmablasts/plasma cells. As aforementioned, many breast cancer patients present with high levels of intratumoral and circulating IgA antibodies within the periphery, which are shown to be associated with poor

prognosis and a reduced survival rate in other solid cancers (Bosisio et al., 2016; Chiaruttini et al., 2017; Liu et al., 2018). IgA infiltration is uncommon within healthy breast tissue, as it plays a role in modulating mucosal immune responses within the gut. However, viral antigenic responses, including that of SARS-Cov2, present with heightened levels of peripheral neutralising IgA responses at early stages of infection (Sterlin et al., 2021). This potent but short-lived antibody response highlights the role of broadly neutralising antibody responses that are perhaps disadvantageous for anti-tumour immunity. Other regulatory immune cell subsets, including Tregs have been found to be increased within the TME of TNBC patients, similarly to their enrichment in the in-LNs. As Treg mediated TGF-β can promote IgA class switching in an immune-modulatory fashion (Feng et al., 2011), I hypothesise that Treg mediated cytokine secretion may modulate the plasma cell response towards an IgA-bias compared to that of an anti-tumour IgG one. Further work is therefore required to elucidate the role of plasma cells and antibody diversity within the TME of TNBCs.

A large proportion of the patients in the lThP group were classified as the LAR group. Whilst only encompassing 10% of all TNBC tumours, this subtype presents with characteristics that include refractory behaviour to chemotherapy treatments (Nedeljković and Damjanović, 2019). As a subtype it has gained interest in breast cancer, highlighting the AR as a potential biomarker for targeted therapies. AR is a steroid nuclear receptor that binds to androgens, namely testosterone and dihydrotestosterone, before translocating to the nucleus to modulate gene expression. Whilst it is essential for normal breast development, it is overexpressed in many breast carcinomas and predominantly co-localises with ER in luminal cells. In its inactive state, it is bound to heat shock proteins (HSP), including HSP70, which has a role in cell survival and carcinogenesis. Binding of circulating antigens to the HSP70:AR complex causes conformational changes allowing displacement of this pairing and AR dimerization (Brumec et al., 2021). Despite several clinical trials targeting AR with antiandrogens including bicalutamide and enzalutamide, response rates have been

consistently low (Gucalp et al., 2013). Although the LAR subtype is classified as TNBC, it has been shown that AR expression within these tumours correlates with that of HER2, luminal and steroid genes. (Vidula et al., 2019). This may indicate that these tumours are molecularly similar to HER2-low breast cancers, which express low levels of HER2 by IHC staining however are negative for the ISH score. This subgroup represents a group of tumours that have previously been overlooked when considering traditional HER2-targeting therapies, and potentially indicates that they may biologically similar to those within the LAR subgroup (Zhang et al., 2022).

Although it is recognised that AR has a role in promoting tumourigenesis and enhancing treatment resistance, there have been few studies to determine the role of androgen signalling on the immune microenvironment. Kwon *et al*., described how androgen signalling can facilitate CD8+ T cell exhaustion and has a role in regulating transcriptional trans-activator TCF7/TCF1. Notably, as aforementioned, TCF7 is paramount for the development of DN cells, which may indicate AR can promote B cell responses towards this phenotype. Further, the ablation of the androgen-AR axis *in vivo* augmented effector T cell differentiation and potentiated the response to PD-1 immune checkpoint blockade (Kwon et al., 2022). AR activity can further promote neutrophil activity and a higher neutrophil/lymphocyte ratio is considered to be a poor prognostic biomarker in several solid tumours (Templeton et al., 2014). Moreover, gender-bias within tumour immunity has gained interest due to a significant higher incidence rate of cancers of non-reproductive organs including colon, skin, head and neck and liver in male populations compared to female. The majority of accrued information draws parallels between this susceptibility and the sex steroid hormones; ERα, Erβ and AR (Clocchiatti et al., 2016). Whilst there has been no work to date focusing on AR signalling and GC derived responses within the context of solid tumours, AR plays an important role in regulating Tfh differentiation, and can inhibit B cell class switching (Olson et al., 2020).

Other histological characteristics including fibrosis and necrosis are routinely assessed within TNBC tumours, and there is debate how they can influence tumour growth as well as

their role in modulating infiltrating immune cells. Both features are often developments of chronic inflammatory diseases; therefore, it was in part expected that there were the lowest levels of both phenotypes present within the lThP patients. Although fibrosis notoriously contributes to a stiffened extracellular matrix (ECM) and heightened angiogenesis, it can also provide a niche for antigen presentation and immune stimulation within the TME (Chandler et al., 2019). Inflammatory immune subsets including M1 and M2 macrophages can further facilitate the development of fibrosis through secretion of cytokines and chemokines while promoting an anti-tumour response (Wynn and Barron, 2010). However, the role of necrosis and fibrosis, and what impact this may have on the role of plasma cell responses, is unknown.

In parallel, the lThP group presented with the highest number of in-LNs, which is characteristic of the LAR subgroup (Yang et al., 2022). In concordance with our previous data, these patients had the lowest number of GCs and reduced sinus area within their axillary LNs. From this, the hypothesis is that there may be some level of immune suppression within the primary tumour that prevents the necessary antigenic stimulation required to induce an initial GC response, or that GC responses in the LNs are not sustained during disease progression. As there are plasma cells present within these tumours but not a substantial GC response, this may be further be reflective of those that are derived from extrafollicular pathway. Although yet to be shown within the context of solid tumours, mice infected with the mouse mammary tumour virus (MMTV) induce a substantial level of plasmablasts, differentiating from early infected B cells that migrate from the draining LN via adhesion molecules $\alpha_4\beta_1\beta_2$ to the mammary gland (Finke et al., 2001). Plasma cells that develop in extrafollicular foci do not undergo SHM, are typically short-lived, and secrete a combination of switched or unswitched antibodies (Elsner and Shlomchik, 2020). Whether these cells within human TNBC tumours are derived from an extrafollicular response is yet to be determined but may be intuitive of antibody secretion with minimal priming against TAAS. Furthermore, the molecular features of these low sTILs tumours perhaps have the

propensity to influence the nature of class switching and SHM required to target TAAs. TNBC often display high levels of CXCL12, secreted by the stromal compartment of the TME. Its receptor CXCR4 is utilised by tumour cells to support angiogenesis, tumour growth and metastasis to both LN and distant organs(Guo et al., 2016). However, it is a key cytokine receptor expressed on plasma cells, critical for migration to the bone marrow during later stages of maturation (Nutt et al., 2015). lThP TNBCs had increased levels of *CXCL12* expression comparatively to the other TNBC subsets, in addition to other genes associated with plasma cell migration and LN egress including *S1PR1* and *HGF.* This suggests that although this may be one of the mechanisms used to facilitate the invasion of the adjacent LNs, it also may provide a niche for which plasma cells are recruited to but are not functionally capable of eliciting a sufficient anti-tumour response, or are diverted from their natural course of maturation.

Moreover, there was a strong concordance between paired primary tumour, cf-LN and in-LN with regards to the plasma cell and memory B cell compartments. Memory B cells were heightened in cf-LNs and plasma cells diminished, however plasma cells were enriched and memory B cells depleted within the in-LNs. This could be indicative of an evolving immune response; memory B cells encountering tumour antigen and differentiating into antibody producing plasma cells, however in agreement with the gene expression data, it was evident that large clusters of plasma cells in both the intratumoral stroma within the primary tumour and in-LN was associated with development of distant metastasis in low sTILs patients. Notably, the percentage of plasma cells negatively correlated with the number of GCs formed, which is again a possible indicator of extrafollicular differentiation.

In summary, data of this chapter has highlighted the immunophenotypic differences between GCs and non-GC areas within in-LNs of TNBC patients that had different disease trajectories, with regards to distant metastasis development. There may be intrinsic alterations in key immune cell populations within the GC and adjacent LN, including lack of PD-1+ CD4+ T cells that subsequently will prevent adequate antigen presentation and B cell

maturation into antibody secreting plasma cells. Further, the accumulation of immune subsets that may promote immunosuppressive capabilities, namely macrophages, Tregs and DN B cells, with spatial prevalence to localize near tumour cells, may indicate an environment preventive of GC derived anti-tumour responses. In addition, an increase in plasma cells within a low sTILs TME may be attributed to the LAR subtype of TNBC patients and is associated with both regional and distant metastasis development. However, how they might be modulated by tumour, stroma and other immune cells is yet to be fully elucidated.

3.15 Limitations and future work

One of the main limitations of this work was that of the small sample size available for IMC analysis within the Bart's TNBC cohort. Although profiling of the LNs of these patients including multiple sampling of ROIs from each LN, there was a lack of biological repeats which means that a representative immune environment was not necessarily adequately determined. Despite this, comparisons between multiple types of ROIs, i.e., GC and non-GC areas across each patient allowed for statistical comparisons and identified immune subset differences and spatial interactions that may attribute to disease progression. Applying this to a larger cohort of TNBC patients would confirm if these changes were consistent with those developing distant metastasis and further provide a better understanding as to the immune composition of the LNs within those with an inferior disease trajectory. Another limitation was lack of paired samples available for both gene expression and immunohistochemical analyses. Therefore, although the plasma cell gene signature could be attributed to distant metastasis development and reduced GC response within the adjacent LNs, infiltration of plasma cells and other B cell subsets could not be investigated histologically within the same samples. This meant that an independent cohort was used, and therefore it was not possible to ascertain if the tumours within this cohort with a high

plasma cell and low memory B cell phenotype were of the LAR subtype. To overcome these limitations, low sTIL tumours exhibiting the LAR phenotype should be profiled with the IMC panel, alongside paired involved LNs, histological quantification of GC numbers and clinical outcome data including distant disease-survival and overall survival. This would delineate the plasma cell phenotype, spatial interactions with other immune subsets, and immunoglobulin phenotypes within this subset of patients in both the tumour and paired LNs that may be attributed to distant metastasis development and poor disease trajectory.

Chapter 4: Profiling GCs and B cell responses in mammary gland tumours and lymph nodes of *in vivo* TNBC mouse models

Introduction

Multiple challenges exist when studying the development of the pre-metastatic niche when utilising human samples, as changes within the LN immune environment are proposed to occur early in tumour progression (Rye et al., 2022). Analysis of these samples provide only a snapshot of potentially fluid phenotypes of which some may be key to prevent tumour dissemination to distant organs. Tumour bearing mouse models can be harnessed to study the temporal changes of the adjacent LN as it responds to the presence of tumour cells within the mammary gland (Bos et al., 2010). These models provide a platform to assess the systemic immune responses within the LNs at proximity to the tumour, in parallel to those at range, something that is not currently possible within humans.

Transplantation models to study breast cancer metastasis *in vivo*

Breast cancer growth and metastasis can be mimicked in various ways *in vivo* and the use of transplantation models has been frequently employed to examine tumour progression. Murine breast cancer cell lines can be ectopically or orthotopically implanted into the skin or mammary fat pad, which will in part recapitulate tumour growth and metastasis development in humans (Bos et al., 2010). Injections via tail or portal vein will predominantly result in colonisation of the lung and liver respectively, whereas intracardiac infusion has a broader metastatic tropism of target organs (Goddard et al., 2016; Jenkins et al., 2005; Richert et al., 2005). However, there are limitations of introducing cancer cells directly into the blood circulation, primarily that it cannot be considered a system of true metastasis, instead that of an organ colonisation assay.

Syngeneic transplantation mouse models

Syngeneic models, in which the cancer cells from one mouse are transplanted into another with an identical genetic background, form the basis for many tumour transplantation models. This bypasses immunologic host-versus-graft reactions and concomitantly allows in depth analyses of an intact immune system, something that is often considered essential when studying the progression of breast carcinomas (Gravekamp et al., 2004). The 4T1 cell line has been commonly used, derived from a single spontaneous arising mammary tumour within a BALB/c mouse (Miller, 1983; Tao et al., 2008). It is resistant to 2'-deoxy-6-thioguanosine triphosphate treatment and has mutations within frequently affected genes in breast cancer;*Tp53, Pik3cg* but not *Brca1* or *Brca2* (Schrörs et al., 2020). Proliferation markers including *Mki67*, *Birc5* and *Top2a* are upregulated, alongside *Msln*, *Ect2* and *Plk1*, which drive metastatic ability to LN, lungs, and bone (Monteran et al., 2020; Schrörs et al., 2020). TNBC markers, when compared to mammary gland control samples, are comparably low (*Erbb2*), lower (*Esr1*) or not found to be expressed (*Pgr*), making this a suitable system to study TNBC progression *in vivo* (Schrörs et al., 2020). The 4T1.2 line is a highly metastatic derivative of the 4T1, isolated from a single metastatic clone within the lungs. In contrast, the 67NR cell line, although derived from the same autochthonous tumour as the 4T1, harbours no metastatic properties (Dexter et al., 1978). This, in turn with nuclear ERα positivity observed by immunohistochemical assessment, suggests that it has less of a triple negative phenotype in comparison to 4T1 and 4T1.2 tumours (Johnstone et al., 2015). Despite discrepancies in the HR characteristics of these cell lines, the comparison of these models provides the opportunity to study clonally related tumours with a range of metastatic characteristics.

Other syngeneic models include the E0771 and its metastatic counterpart, the E0771.LMB, originally isolated from a spontaneous tumour that arose within a CB57BL/6 mouse, and a single metastatic clone from the lung respectively (Le Naour et al., 2020). Despite the well

described characteristics of these cells, the data are contradictory. Indeed, the classification of the HR status of this model is divergent amongst researchers. Despite multiple publications recognising this model as triple negative, others have observed transcription of the gene encoding ERα on multiple occasions. This has been met with some controversy due to the weak expression within protein assays and the localisation of the receptor within the cytoplasm but not the nuclear compartment (Le Naour et al., 2020). Similarly, the PR status and *Erbb2* expression is poorly described and conflicted. Work by Johnstone *et al.,* did not find expression of *Erbb2* by gene expression or immunohistochemical analyses (Johnstone et al., 2015) whereas Hiraga *et al.,* and Zou *et al.,* respectively identified transcriptional evidence and protein expression by western blot (Hiraga and Ninomiya, 2019; Zou et al., 2013).

Xenograft transplantation methods of breast cancer

To examine the development and migration capacity of human breast cancer cell lines *in vivo*, xenograft transplantation methods can be harnessed using immunocompromised mice. The most commonly used cell line is the MDA-MB-231, derived from the pleural effusion of a breast cancer patient which can be injected subcutaneously, intravenously, intracardially or orthotopically into the mammary fat pad of mice (Hurst et al., 1993; Kim et al., 2004). After intravenous injection, it has the propensity to metastasise to bone, liver, lung, adrenal glands and brain, and has been used to identify factors with a potential functional role in breast cancer migration. These include IL-11, osteopontin and connective tissue growth factor (CTGF) with proclivity to drive osteolytic metastasis, as well as CXCL1, matrix metalloproteinase-1 (MMP-1) and cyclo-oxygenase-2 (COX-2) that may facilitate migration to the lungs (Adwan et al., 2004; Kang et al., 2003; Minn et al., 2005).

However, an impaired immune response within these models is restrictive in recapitulating the TME and the mechanisms behind which immune cell subsets may impede or facilitate metastasis. Further, stromal cell compartments within the tumour originate from the host and may not fully support transplanted tumour growth and development as effectively as is

routinely observed within human carcinomas. CAFs in particular, can modulate CXCR4/CXCL12 mediated chemokine signalling, which has been shown to recruit and promote endothelial progenitors, enhancing angiogenesis and subsequent metastasis (Orimo et al., 2005). There are also fundamental differences in the receptor expression of target organs within mice that may prevent tumour cell and host interactions critical in humans for the facilitation of tumour cell migration and entry into target organs (Kuperwasser et al., 2005).

The use of genetically engineered mouse models in breast cancer

To eliminate the discrepancies discussed above, genetic manipulation using several promoters can drive expression of known oncogenes within the mammary epithelium, and effectively mimic breast carcinogenesis in mice. This reduces error introduced when administering cell lines into the target site, which can account for differing rates of metastasis due to proximity to blood vessels and depth of implantation. Common promoters used in genetically engineered mouse models (GEMMs) include mouse mammary tumour virus-long terminal repeat (MMTV-LTR) , whey acid protein (WAP) , C3(1), bovine β-lactoglobulin (B-LG) and metallothionein (MT), which facilitate expression of genes such as *Erbb2/Neu*, polyoma middle T (*PyMT*) antigen, *SV40*)T antigen, *Ha-Ras*, *Wnt-1*, *Tgf-α* and *c-Myc* (Cardiff et al., 2000). The MMTV-LTR system is most frequently used, and MMTV-PyMT transgenic mice exhibit hyperplasia, adenoma/mammary intra-epithelial neoplasia, followed by early and eventually late carcinoma. It effectively recapitulates the gradual loss of steroid hormone receptors (estrogen and progesterone) seen in humans, and will develop metastasis in the lungs and LNs, primarily due to hormonal changes after the first pregnancy (Lin et al., 2003; Maglione et al., 2001).

Whilst many of these models provide effective systems to study the growth and metastatic capabilities of breast cancer, the propensity for GEMMs to develop LN metastasis is relatively low compared to transplantation systems. MMTV-Wnt1 and MMTV-PyMT exhibit

metastatic lesions within the td-LNs, but this is not consistent and often at low levels. (Attalla et al., 2021).

Transcriptional analyses indicate immunological reprogramming within the tumour draining lymph nodes of 4T1.2 and 67NR mouse models

Recent work by our group has confirmed the prognostic value of GCs and sinuses within the axillary LNs, and subsequent relationship with TIL infiltration at the primary tumour lesion (Grigoriadis et al., 2018; Liu et al., 2021). Further, transcriptional analyses by Dr Thomas Hardiman, a previous PhD student in the group have examined gene expression of immunological subsets within the td-LNs of the 4T1.2 and 67NR models in a time-series fashion. This has revealed a deviation of the transcriptional landscape in LNs from tumour bearing mice compared to control within 7 days of injection. Notably, a reduction was seen in genes associated with T cell function in the 4T1.2 model, including *Cd3e, Cd3g, Cd4,* and *Cd8b1* between days 3-7, sustained over subsequent timepoints (unpublished data). This has been observed in human analyses of axillary LNs, associated with an inferior disease trajectory, and levels of CD4 T cells allowed significant stratification of tumour size, extent of nodal metastasis and disease-free survival (Kohrt et al., 2005). This depletion of T cell genes within the d-LNs of the 4T1.2 and 67NR models was accompanied by an increase in those with immunoregulatory capabilities, including *Foxp3*, a marker of Tregs (Hardiman, 2022). This is in concordance with human single cell profiling of cf- and in-LNs which has identified increased frequencies of CD8 T cells expressing the exhaustion marker TIGIT (T-cell immunoreceptor with Ig and ITIM domains) and Tregs within in-LNs (Rye et al., 2022).

Whilst the LNs within these mouse tumour models appeared to exhibit a decrease in T cell responses with tumour progression, there was an upregulation in genes critical to B cell function at early timepoints. A striking observation of those associated with GC responses was apparent by day 7, including *Aicda*, *Il21*, *Fasl*, and *Pou2af1* in parallel with B cell genes *Cd79a* and *Btk*. This was accompanied by those essential for the maintenance and differentiation of plasma cells; *Irf4*, *Prdm1* and *Xbp1.* These results are reflective of work by

Allen *et al.*, who comprehensively assessed the immune landscape of the 4T1, AT3 and MMTV-PyMT breast cancer mouse models and showed that within the td-LNs of the 4T1 mice, there was a reduction in T cells in parallel with a progressive expansion of B cells.

Given the prominent role for GC development within the tumour-adjacent LNs of breast cancer patients, and the indication that tumour-bearing *in vivo* mouse models upregulate genes associated with a GC B cell response in the td-LNs, I asked whether orthotopic tumour models can drive formation of GCs within the LNs, the nature of GC derived B cell populations and how they evolve in response to a developing tumour. Here, experiments harnessed the syngeneic metastatic 4T1 and 4T1.2 models compared with the non- and poorly metastatic 67NR and E0771. I evaluated how colonisation of the td-LNs may influence the development of GC B cell populations in response to invading tumour cells.

Aims and objectives

Mouse breast cancer cell lines were utilised *in vitro* and *in vivo* models of breast cancers to capture tumour cell mediated B cell activation and development in a longitudinal fashion. This enabled the:

- Investigation of the effect of the 4T1.2 cell line on LN and splenic cell populations *in vitro* to assess B cell activation and plasma cell differentiation

- Characterisation of GC B cells within the td-LNs, nd-LNs and spleen of pre-clinical mouse models of breast cancer to explore possible tumour induced GC responses and their development against tumour progression

- Determination of the immunoglobulin phenotypes of GC derived B cells that may be associated with the different metastatic abilities of pre-clinical mouse models.

This answered the following questions:

1. Do GCs develop in the td-LNs of mice upon implantation of tumour cell lines, and in nd-LNs indicating a systemic response?
2. Are there differences in the kinetics of GC formation across mouse models?
3. Is there a formation of memory B cell and plasma cell populations within the td-LNs and nd-LNs of these tumour bearing mice?
4. What is the immunoglobulin phenotype of GC B cells, memory B cells and plasma cells within the td-LNs and how does this evolve in response to the developing tumour?

4.1 Characteristics of mouse TNBC cell lines

The 4T1, 4T1.2, 67NR and E0771 cell lines were harnessed within this chapter to study their effects on B cell development both *in vitro* and *in vivo.* Characteristics of the cell lines are laid out in table 9. The 4T1, 4T1.2 and 67NR were originally obtained from BALB/c mice, in comparison to the E0771 which arose from a spontaneous tumour on a C57BL/6 background. The 4T1, 4T1.2 and 67NR tumours exhibit a basal-like phenotype which is typical for TNBC tumours (Yin et al., 2020), compared to the E0771 tumours which present with some heterogeneity, as basal-like/luminal B. The 67NR and E0771 consistently present as slower growing compared to the 4T1 and 4T1.2, bearing palpable tumours at ~10 days post inoculation compared to ~ 7 days respectively. This is also in alignment with the metastatic potential of these cells; the 4T1 and 4T1.2 tumours will readily metastasise to the LN, lungs and bone, whereas the 67NR and E0771 will on rare occasion spread from the primary lesion.

Genetics	Strain	Format	BC subtype	Tumour formation	Origin of cell line	Metastatic ability
4T1	BALB/c	Cell line	Basal-like	~ 7 days	Spontaneous tumour	High
4T1.2	BALB/c	Cell line	Basal-like	~ 7 days	Lung metastasis from spontaneous tumour	High
67NR	BALB/c	Cell line	Basal-like	~ 10 days	Spontaneous tumour	Poor/none
E0771	C57BL/6	Cell line	Basal/ Luminal B	~ 10 days	Spontaneous tumour	Poor

Table 9: Characteristics of cell lines used for *in vivo* studies. Feature of tumour models used, including strain of mouse, human breast cancer (BC) subtype, duration from induction to palpable tumour formation, origin of cell line and metastatic characteristics. 4T1 (Aslakson et al., 1991), 4T1.2 and 67NR (Aslakson and Miller, 1992), E0771 (Casey et al., 1951).

4.1.1 Mouse TNBC cell lines exhibit morphological differences *in vitro*

To identify morphological changes present in the tumour cells, cells were cultured *in vitro* (RPMI 1640 + 10% FCS) for 4T1, 4T1.2 and DMEM, high glucose + 10% FCS for 67NR and E0771. Despite the clonally related properties of the 4T1, 4T1.2 and 67NR, there were marked differences in their appearances. The 4T1 cells displayed a typical epithelial phenotype, with tight cell-to-cell contact, whereas the 4T1.2 exhibited trends of a mesenchymal phenotype; loss of cell-cell adhesion and spindle shaped cells. 67NR cells tessellated in the same way as the 4T1, showing limited levels of mesenchymal like properties, which were prominent within the E0771 (Figure 50).

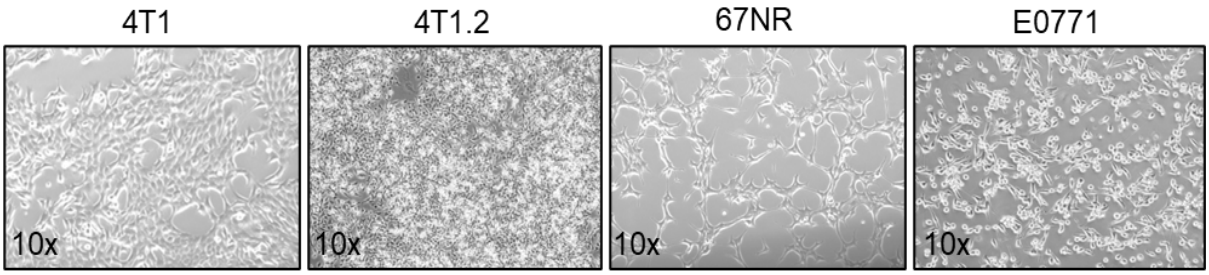

Figure 50: Morphological differences in mouse TNBC tumour cell lines. Images of TNBC cell line growth from left to right; 4T1, 4T1.2, 67NR and E0771 at 60% confluency, taken using the EVOS M5000 imaging system with the 10x objective.

4.2 4T1.2 cell lines induces B cell activation and expansion of CD138^{low} plasma cells

To profile the effect of tumour cell activation on lymphocytes, LN and spleen cells from WT BALB/c mice were harvested and co-cultured with the 4T1.2 cell line, which was chosen due to its highly aggressive properties. LN and spleen cells were co-cultured for 5 days *in vitro* with or without 4T1.2 cells, during which cells were imaged at day 0 and 48 hours, before harvesting for analysis using flow cytometry (Figure 51A). After 2 days, there was clear expansion of the lymphocyte population (white cells) that had clustered closely with the tumour cells (red cells) (Mann-Whitney U test, $p < 0.001$) (Figure 51B-C). At day 5, there was a significantly larger proportion of CD19+B220+ B cells within the LN cells (Mann-Whitney U test, $p < 0.05$) which was trending within the spleen cells (Mann-Whitney U test, $p = 0.0556$) (Figure 52A-B) that were co-cultured with 4T1.2 cell line compared to those cultured alone. There was also a statistically significant increase of CD86+ B cells within the LN population (Mann-Whitney U test, $p < 0.01$), which was trending in the spleen cells (Mann-Whitney U test, $p = 0.1508$) (Figure 52C-D). The percentage of LN cells upregulating a plasma cell like phenotype (CD138^{low}B220-) was enriched within the populations cultured with 4T1.2 cells compared to those that were cultured alone (Mann-Whitney test, $p < 0.01$) and this was trending within the spleen cells (Mann-Whitney U test, $p = 0.074$) (Figure 53A-B). The plasma cell phenotype was enriched for IgM within the LN cells compared to that of

the spleen (Mann-Whitney U test, $p < 0.01$), with a small proportion of plasma cells within the spleen populations expressing IgG1 compared to no evidence of this within the LN cells (Mann-Whitney U test, $p < 0.01$) (Figure 53C-E). Taken together, this suggests the ability of the 4T1.2 tumour cell line to induce B cell activation and an IgM+ plasma like phenotype within the LNs.

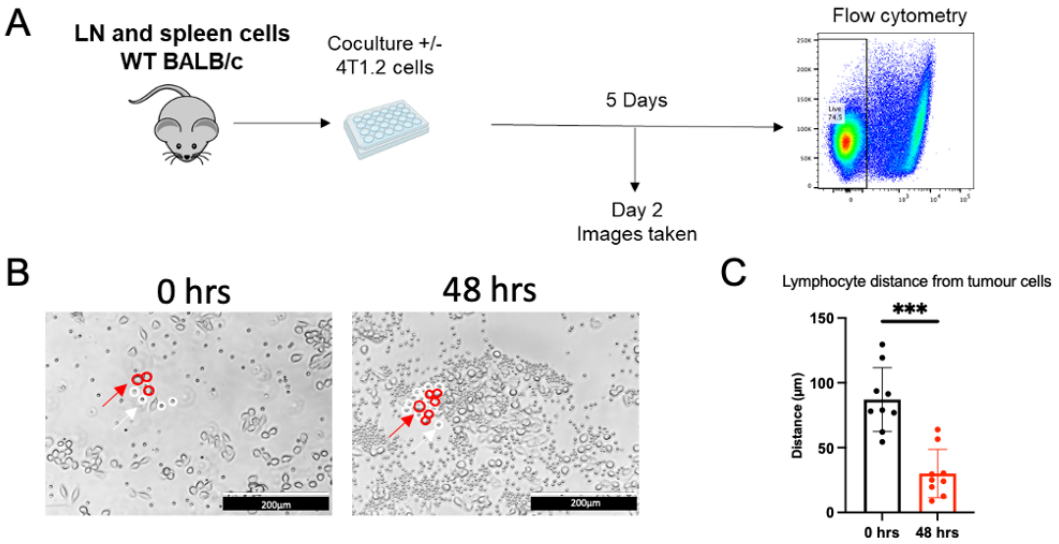

Figure 51: Lymphocytes aggregate around tumour cells within coculture system. (A) Schematic illustration of in vitro coculture experiments harvesting LN and spleen cells from WT BALB/c mice after incubation with the 4T1.2 cell line for 5 days before analysis of populations using flow cytometry. (B) Images of tumour and lymphocytes at 0 hours and 48 hours after experimental setup using the EVOS M5000 imaging system. (C) Quantification of 9 randomly selected areas to determine the proximity of tumour cells to lymphocytes within each well at 0 hours vs 48 hours.

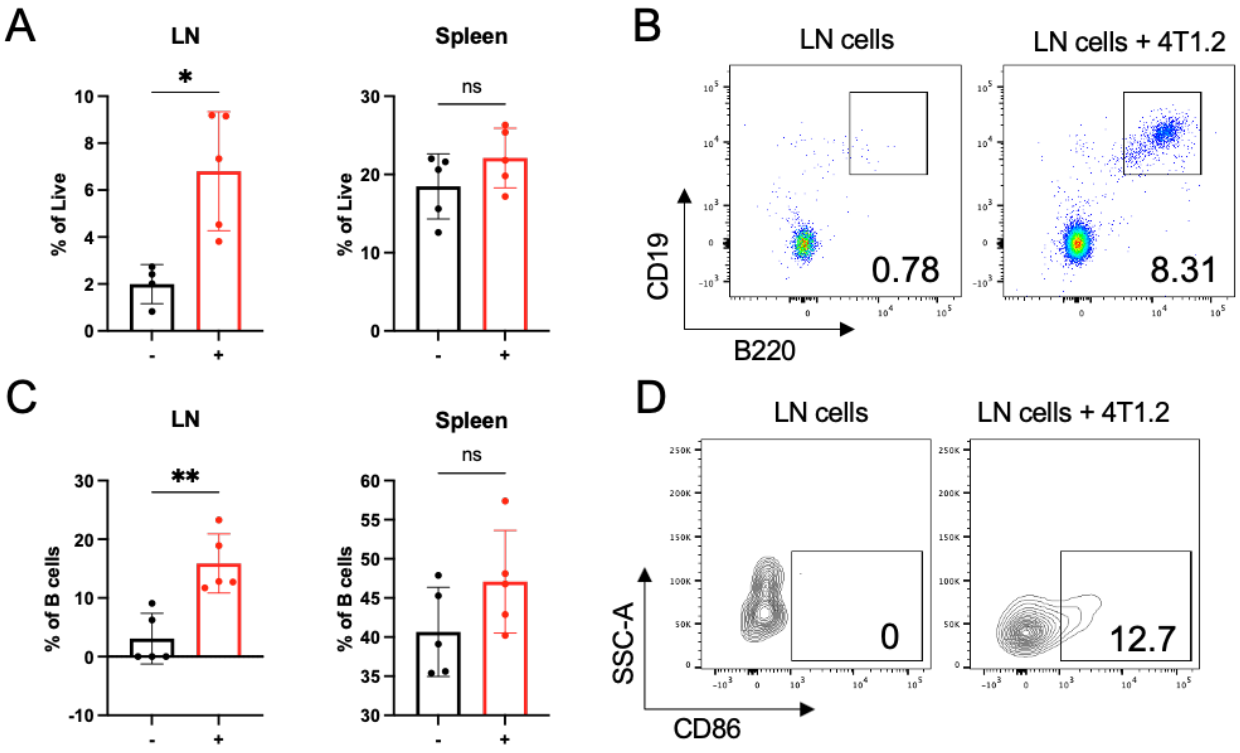

Figure 52: 4T1.2 cell line induces B cell expansion and activation. (A) Graphs showing B cells (defined as CD19+B220+), as % of live cells within wells that contained LN or spleen cells alone (-) and those that were cocultured with 4T1.2 cells (+). (B) Representative flow plots to show the % of B cells within LN cells when cultured alone or with 4T1.2 cells. (C) Graphs showing the % of CD86+ B cells as a % of total B cells from wells that contained LN or spleen cells alone (-) and those that were cocultured with 4T1.2 cells (+). (D) Representative flow plots showing the % of CD86+ B cells within LN cells when cultured alone or with 4T1.2 cells. Mann-Whitney tests used for statistical analysis in each graph. * = $p < 0.05$, ** = $p < 0.01$. p values are shown where statistical significance was not reached.

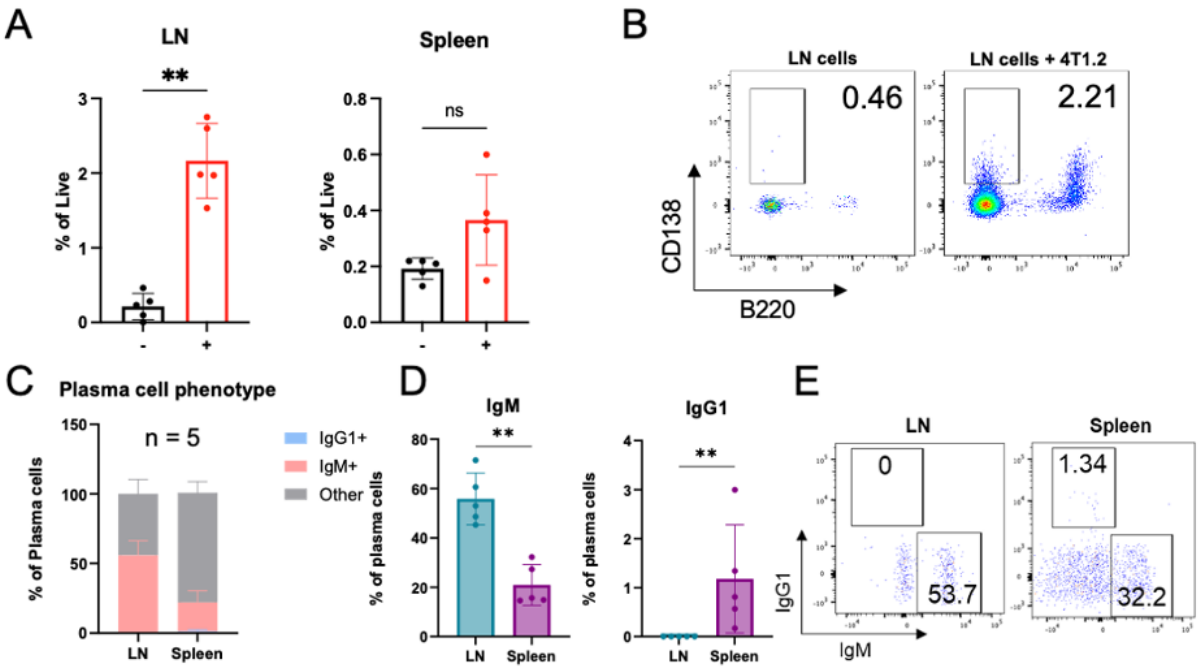

Figure 53: 4T1.2 cell line induces plasma cell expansion and immunoglobulin differences between spleen and LN cells. (A) Plasma cells (defined as CD138+B220-) % of live cells within LN and spleen populations cocultured alone (-) or with 4T1.2 tumour cells (+). (B) Representative flow plots of plasma cells as % of live cells within LN populations cultured alone or with 4T1.2 cells. (C) Proportions of IgM+, IgG1+, and IgM-IgG1- plasma cells from LN and spleens that were cocultured with 4T1.2 cells. (D) Representative flow plots of IgM+ and IgG1+ plasma cells as % of total plasma cells within LN and spleen cells cultured with 4T1.2 cells. Mann-Whitney tests used for statistical analysis in each graph. ** = $p < 0.01$. p values are shown where statistical significance was not reached.

4.3 Assessment of clinical features in breast cancer mouse models

To establish the effect of these murine cancer lines on GC B cell development in LNs *in vivo*, cells resuspended in Matrigel were injected in an orthotopic manner into the 4th mammary fat pad of either BALB/c or C57BL6 mice, depending on the mouse cell line used. Control mice were administered an injection of Matrigel alone. The adjacent inguinal LN was assigned as the td-LN, and the paired inguinal LN on the opposite side of the mouse as the non-draining LN (nd-LN). At the endpoint of each experiment, both inguinal LNs were removed, along with the tumour and spleen for analyses using flow cytometry and histology (Figure 54A). Timepoints looked at post tumour inoculation consisted of day 7, day 10, day 14, day 21 and day 28 (Figure 54B). Due to restrictions within the home office license, day 28 was only analysed within the 67NR and E0771, as the tumour growth for 4T1 and 4T1.2 would surpass limits due to accelerated tumour growth.

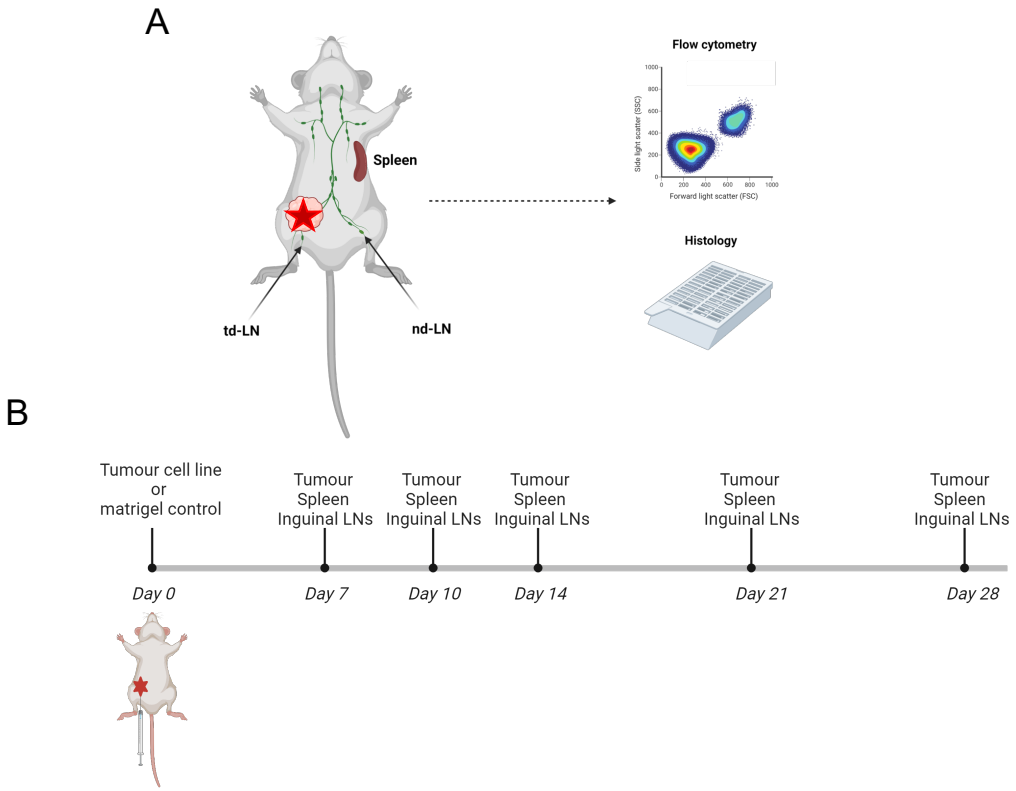

Figure 54: Experimental design for orthotopic mouse models of TNBC. (A) Schematic showing the location of inguinal LNs harvested at completion of experimented, denoted tumour draining lymph node (td-LN) and non-draining lymph node (nd-LN) before analysis using flow cytometry and histology. Red star represents tumour within 4th mammary fat pad. (B) Timeline of experiments from tumour inoculation at day 0 and timepoints at which td-LN, nd-LN, spleen, and tumour were removed for analysis.

4.3.1 Breast cancer tumours do not cause weight loss in mice

Mice were monitored after administration of all cell lines to check weight loss, as a percentage of baseline. Although there were trends within the E0771 and 4T1.2 towards tumour bearing mice gaining weight more slowly, this was not significant at any timepoint. There were no statistically significant changes in the weight of the mice when comparing tumour bearing to control within the 4T1 and 67NR models (Figure 55A-D).

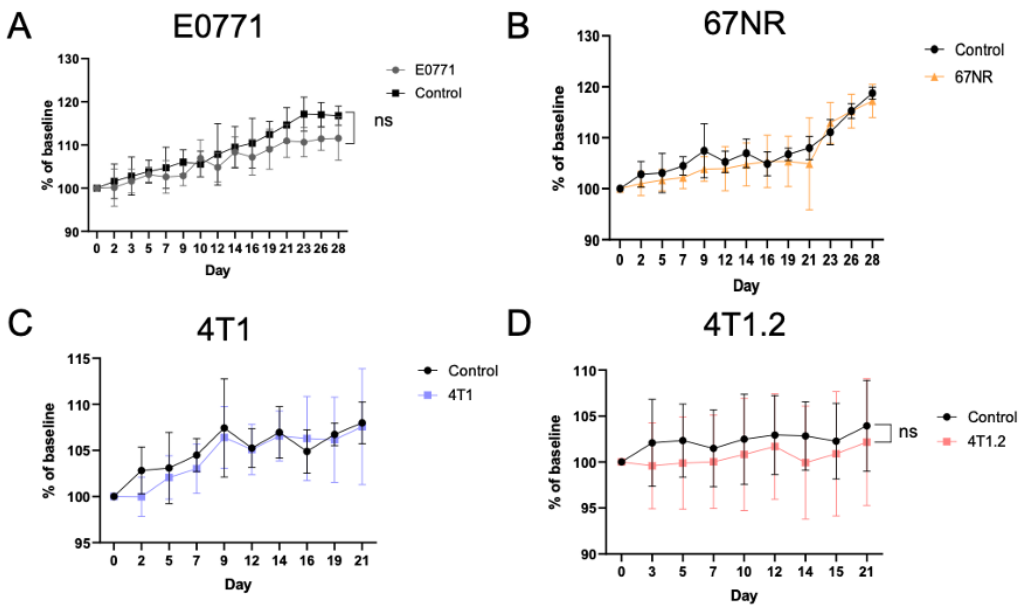

Figure 55: Orthotopic mouse models of TNBC do not affect mouse body weight. (A) Body weight of tumour bearing mice inoculated with E0771 cell line as a % of baseline weight at day 0, compared to control mice injected with Matrigel alone (n = 25). (B) Body weight of tumour bearing mice inoculated with 67NR cell line as a % of baseline weight at day 0, compared to control mice injected with Matrigel alone (n = 12). (C) Body weight of tumour bearing mice inoculated with 4T1 cell line as a % of baseline weight at day 0, compared to control mice injected with Matrigel alone (n = 12). (D) Body weight of tumour bearing mice inoculated with 4T1.2 cell line as a % of baseline weight at day 0, compared to control mice injected with Matrigel alone (n = 12).

4.3.2 Tumour kinetics vary between models

In concordance with published data, the 4T1 and 4T1.2 tumours exhibited the fastest growth kinetics, palpable by day 7 and reaching the maximum volume limit within 21 days post inoculation. Although the E0771 tumours were palpable by day 10, the growth rate was much slower and the tumours at day 28 of the timeseries were below the threshold required to end the experiment. 67NR tumours took the longest time to become measurable within these mice (day 10-14), however upon day 21 there was a sharp increase from ~200 mm^3 to ~1200mm^3 at day 28 (Figure 56A). At day 21 there were evidence of the differences between the models, with 4T1 and 4T1.2 exhibiting significantly larger tumours than the 67NR (Kruskal-Wallis test, $p < 0.05$ and $p < 0.01$ respectively). This was trending between the 4T1, 4T1.2 and the E0771 tumours but not statistically significant (Figure 56B).

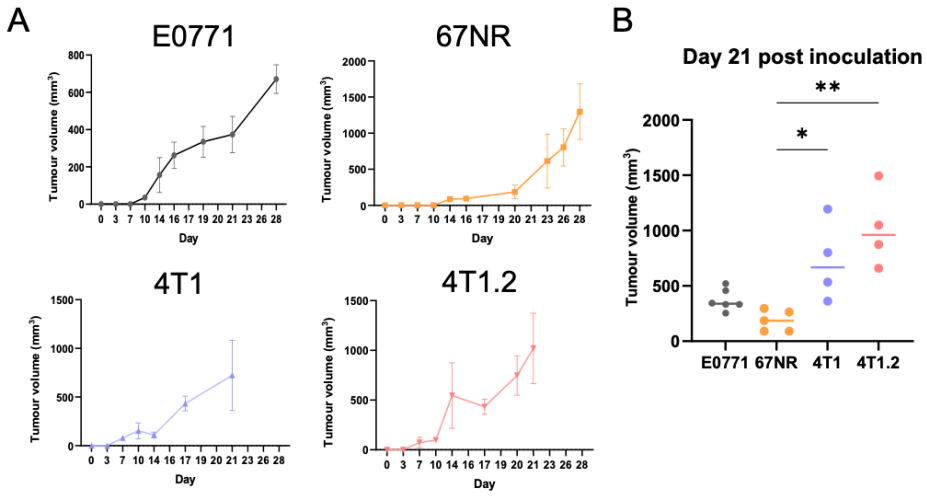

Figure 56: Tumour growth kinetics across TNBC mouse models. (A) Tumour volume from day of inoculation (day 0) to day 28 across E0771, 67NR, 4T1 and 4T1.2 mouse models. (B) Tumour volume at day 21 post administration of cell line across all models. Kruskal-Wallis test with Dunn's multiple comparison post-hoc test * = $p < 0.05$, ** = $p < 0.01$.

4.3.3 Tumour models induce lymphadenopathy and splenomegaly

LN enlargement is characteristic of injury and infection, acting as a platform for B cell maturation, facilitating antigen and promoting interactions between T cells, B cells, DCs and other antigen presenting cells (APCs). Within breast cancer patients and mouse models, LN swelling is often due to the presence of cancerous cells that have spread from the primary tumour to adjacent LNs (Arroyo-Crespo et al., 2019; Dimcić et al., 1997; Lores et al., 1998). Here, the td-LN mass prominently increased compared to the LN from day 0 to day 21 in the 4T1 and 4T1.2 models, potentially associated with their metastatic ability to spread to the td-LNs (Figure 57A-B). However, when comparing the mass of the paired td-LN to the nd-LN within each mouse, there was a significant increase in the td-LN in the non-metastatic 67NR and poorly metastatic E0771 (Wilcoxon signed rank test, $p < 0.0001$ and $p < 0.0001$, respectively) as well as within the 4T1 and 4T1.2 (Wilcoxon signed rank test, $p < 0.0001$ and $p < 0.0001$). Notably, there was no difference in the control mice between the mass of the nd-LN and td-LN (Wilcoxon signed rank test, $p = 0.16$ and $p = 0.77$) (Figure 57C). At day 21 within the 4T1.2 model, the adjacent LN was in full contact with the tumour (Figure 57D). Taken together, this is reflective of LN metastasis that is prevalent within the 4T1 and 4T1.2 model, but suggestive of a level of immune activation that also may be taking place, as this enlargement was also apparent within the non-metastatic 67NR and E0771 models. The 4T1, and 4T1.2 showed signs of splenomegaly by day 14 which increased at day 21, and this was also the case at day 28 for the 67NR (Figure 57E). This has been suggested to be due to an increase in myeloid and granulocyte populations that has been previously seen within the 4T1 model (duPre' and Hunter, 2007).

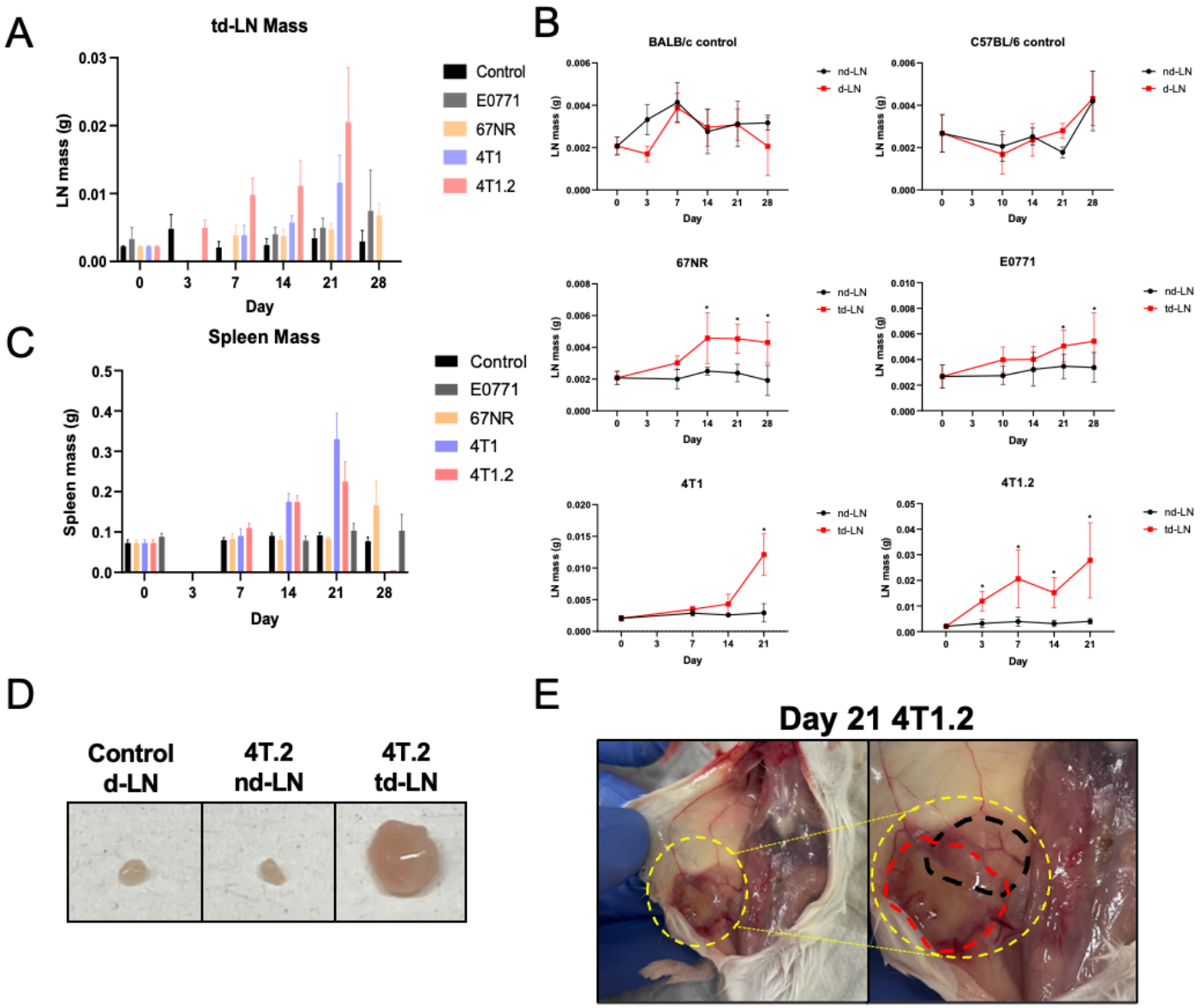

Figure 57: Tumour bearing mice develop enlarged td-LNs and splenomegaly. (A) Mass of td-LNs from control mice or those inoculated with E0771, 67NR, 4T1 and 4T1.2 cell lines from day 0 to day 28. (B) Lymph node mass of draining LNs (d-LN) from control mice, and td-LNs from tumour bearing mice compared with nd-LNs in E0771, 67NR, 4T1 and 4T1.2 models (Wilcoxon signed-rank tests * = $p < 0.05$). (C) Spleen mass in control and tumour bearing mice from E0771, 67NR, 4T1 and 4T1.2 models from day 0 till day 28. (D) Draining LN from a control mouse, nd-LN and td-LN from 4T1.2 mouse 21 days after tumour inoculation. (E) BALB/c mouse 21 days post tumour initiation with 4T1.2 cell line, red circle depicts tumour and black circle outlines the td-LN.

4.4 Flow cytometry panel to assess GC B cell subsets

To assess the GC B cell content present within enlarged td-LNs of mouse models, flow cytometric analyses were performed. The gating strategy to determine the different cell types is shown in Figure 58. Lymphocytes were gated on using forward and side scatter area (FSC-A, SSC-A), and then doublets excluded using forward and side scatter height and width (FSC-H, FSC-W, SSC-H, SSC-W). Live cells were identified as those that did not take up live/dead dye, and plasma cells as B220-CD138+. B cells were defined as B220+CD19+, and GC B cells as the proportion of B cells that expressed CD38 but were low for CD95/Fas. The GC is governed by controlled transcriptional profiles that modulate two functionally distinct compartments, the dark zone (DZ) and light zone (LZ). These represent polarised areas that govern somatic hypermutation and selection of B cells, respectively (Calado et al., 2012; Dominguez-Sola et al., 2012; Victora and Nussenzweig, 2012). Single cell RNA-sequencing (scRNA-seq) has been applied to GCs isolated from human and mouse tonsils and spleens respectively to further delineate these cells into pre-GC, DZ and LZ subpopulations, and those that express genes associated with both, classed as intermediate (Holmes et al., 2020; Kennedy et al., 2020; H. King et al., 2021; McHeyzer-Williams et al., 2015; Nakagawa et al., 2021). Whilst complex phenotyping at this level is not possible using flow cytometric techniques, staining for markers such as CXCR4 and CD86 within GC B cells was applied here to differentiate between DZ ($CXCR4^{high}CD86^{low}$) and LZ ($CD86^{high}CXCR4^{low}$). Memory B cells could be identified as non-GC B cells that were IgD-, and further to this CD273 expression could define a subset of memory B cells. IgM and IgG1 expression were then assessed within the memory B cell, CD273+ memory B cell and plasma cell fractions. IgG1 was chosen in conjunction with IgM, due to its characteristics as the major immunoglobulin subset within sheep red blood cell (SRBC) immunisations that is associated with isotype switching derived from GC B cell responses(McAllister et al., 2017). In summary, flow cytometric techniques could allow profiling of B cell subsets including GC B

cells, memory B cells, plasma cells and their immunoglobulin isotype characteristics within the nd- and td-LNs of *in vivo* mouse models.

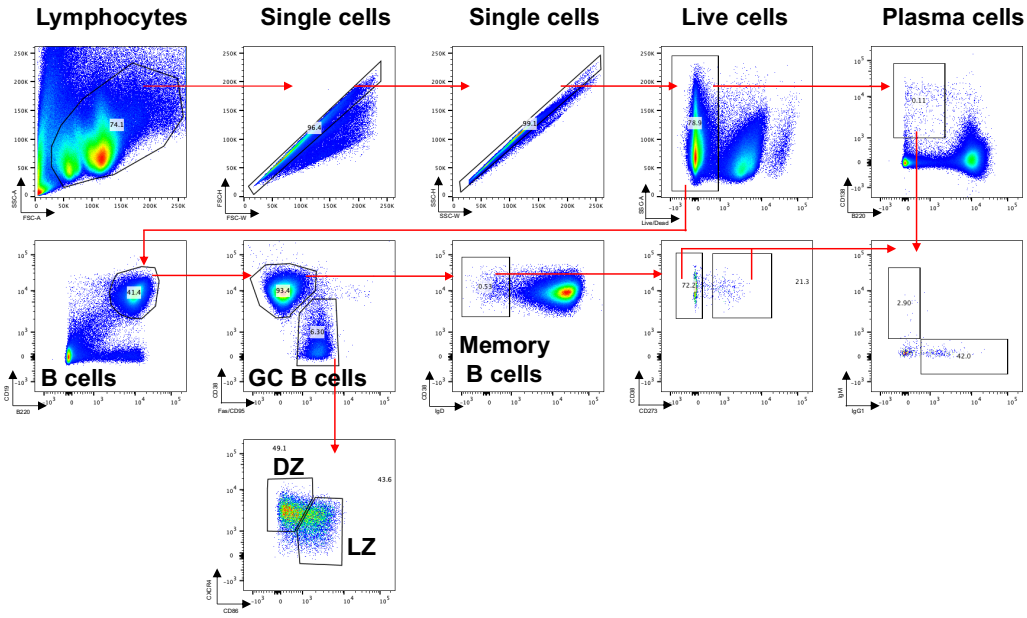

Figure 58: Gating strategy to identify B cell populations. Gating strategy on flow cytometry data to analyse B cell populations within the spleen and LNs. Plasma cells were defined as CD138+B220-, B cells as CD19+B220+ and GC B cells within the B cell fraction as CD38^{low}CD95/Fas^{high}. Dark zone GC B cells were identified as CXCR4^{high}CD86^{low} and light zone GC B cells as CXCR4^{low}CD86^{high}. Memory B cells (MBC) were defined as a subset of the non-GC B cell compartment that were IgD- and could further be subdivided into CD273+ and CD273-. IgM and IgG1 expression were measured for memory B cells and plasma cells.

4.5 B cell proportion increases within increasing tumour draining lymph nodes

The expansion of B cells within spleens and LNs is associated with a response to infection, and often seen within multiple immunisation models (Bergström and Heyman, 2017). To assess if this was the case within these orthotopic tumour models, the percentage of CD19+B220+ B cells out of total live cells was calculated using flow cytometry within the nd-LN, td-LN and spleens of control and tumour-bearing mice of every mouse model tested. Tumour bearing mice inoculated with 67NR, 4T1 and 4T1.2 demonstrated an increase in B cells as a percentage of live cells within td-LNs as early as day 7 compared to d-LN controls (Kruskal-Wallis test, $p < 0.001$). This expansion of B cell frequency within the td-LNs remained consistent for the 4T1 and 4T1.2 models at day 14 (Kruskal-Wallis test, $p < 0.05$), but was not prominent in the 67NR at day 14 or day 21. Although there was an increase in the td-LN of the E0771 model at day 28, this was not significantly different at any other time point assessed compared to d-LN controls (Figure 59A). However, there was an expansion in the percentage of B cells within the td-LNs of mice implanted with E0771, 67NR, 4T1 and 4T1.2 tumours compared to the paired nd-LNs within each mouse (Wilcoxon rank signed test, $p < 0.01$, $p < 0.05$, $p < 0.01$, $p < 0.01$ respectively) (Figure 59B-C). This suggests that the presence of these orthotopic tumours induced B cell reactivity which was specific to the td-LNs.

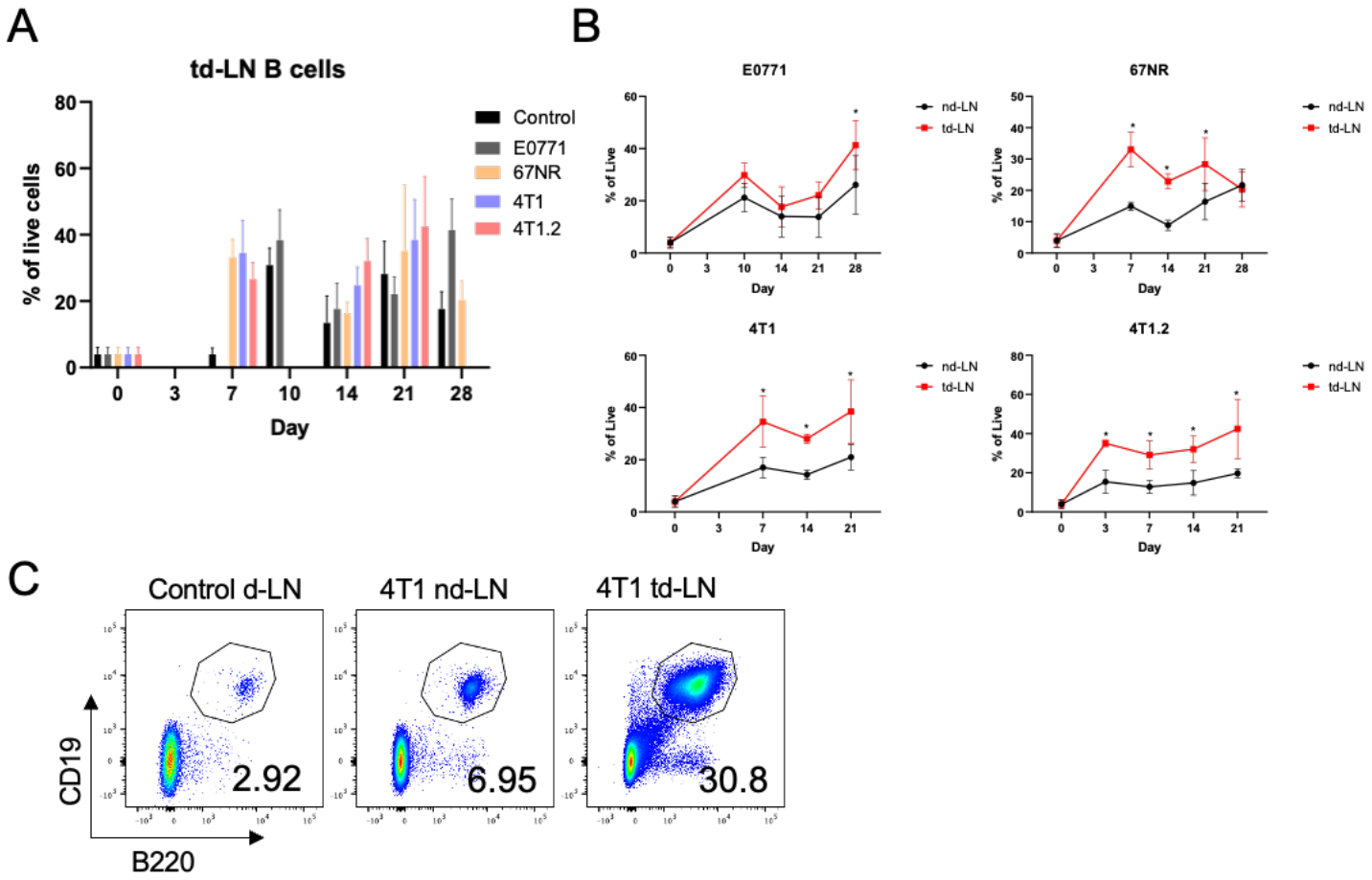

Figure 59: B cells are expanded within td-LNs of tumour bearing mice. (A) B cells (CD19+B220+) as a % of live cells within d-LNs of control and td-LNs of E0771, 67NR, 4T1 and 4T1.2 mice across timepoints from day 0 to day 28. (B) B cells (CD19+B220+) as a % of live cells from d-LNs in control mice, and td-LNs from tumour bearing mice compared with nd-LNs in E0771, 67NR, 4T1 and 4T1.2 models (Wilcoxon signed-rank tests, * = $p < 0.01$). (C) Representative flow cytometry plots of CD19+B220+ cells as % of live from a control d-LN, 4T1.2 nd-LN and 4T1.2 td-LN 14 days after implantation of tumour cell line.

4.6 Germinal centres develop in tumour draining lymph nodes

To determine the phenotype of these B cells, further analyses was performed using flow cytometry to investigate the existence of B cells exhibiting GC like characteristics. B cells that undergo a GC reaction in mice downregulate CD38 and upregulated CD95/Fas (Calado et al., 2012). Fas plays a role within the GC in regulating the production of autoreactive B cells, and those that survive positive selection will upregulate markers including BCL6 to prevent fas-mediated apoptosis (Koncz and Hueber, 2012). Within the nd-LN, there was no difference in the percentage of GC B cells between those mice implanted with a tumour line compared to those mice receiving Matrigel control (Figure 60A). In contrast, a GC B cell population in the td-LNs were observed across all mouse models (Figure 60B). At day 7 post inoculation, a significant enrichment in the GC B cell population as a percentage of B cells within the td-LNs of mice was seen with 67NR, 4T1 and 4T1.2 cell lines (Kruskal-Wallis test, $p < 0.05$, $p < 0.05$, $p < 0.001$, respectively). This was also observed at day 14 (Kruskal-Wallis test, $p < 0.05$, $p < 0.05$, $p < 0.01$ respectively) and day 21 post inoculation (Kruskal-Wallis test, $p < 0.05$, $p < 0.05$ and $p < 0.01$ respectively). The proportion of GC B cells within the B cell fraction peaked at day 7 and appeared to decline by day 21 in the 4T1.2 td-LNs, in contrast the 67NR model retained a strong GC B cell response for 4 weeks post tumour inoculation (Kruskal-Wallis test, $p < 0.001$). td-LNs from E0771 tumour bearing mice, although displayed an enrichment of GC B cells at day 10 and day 14 compared to control d-LNs, this was 7x lower than that of the 4T1.2 at day 7 and was not significantly higher compared to control d-LNs by day 21 or day 28 (Kruskal-Wallis test) (Figure 60B).

When assessing the percentage of GC B cells between paired nd-LNs and td-LNs within each mouse, there was an increase in GC B cells within the td-LNs of E0771, 4T1 and 4T1.2 compared to nd-LNs at day 7 (Wilcoxon rank signed test, $p < 0.05$, $p < 0.05$, $p < 0.01$ respectively). In contrast, the GC B cells within the td-LNs of the 67NR model exhibited a similar trend but only reach statistical significance at day 21 and 28 (Wilcoxon rank signed

test, $p < 0.05$, $p < 0.01$). Whilst the GC B cell response within the E0771, 4T1 and 4T1.2 peaked between day 7-14 and declined by day 21, the percentage within the 67NR model was sustained until day 28. The magnitude and longitudinal patterns of the GC B cell response within the td-LNs of these models may therefore be reflective of their immunogenic potential and metastatic properties.

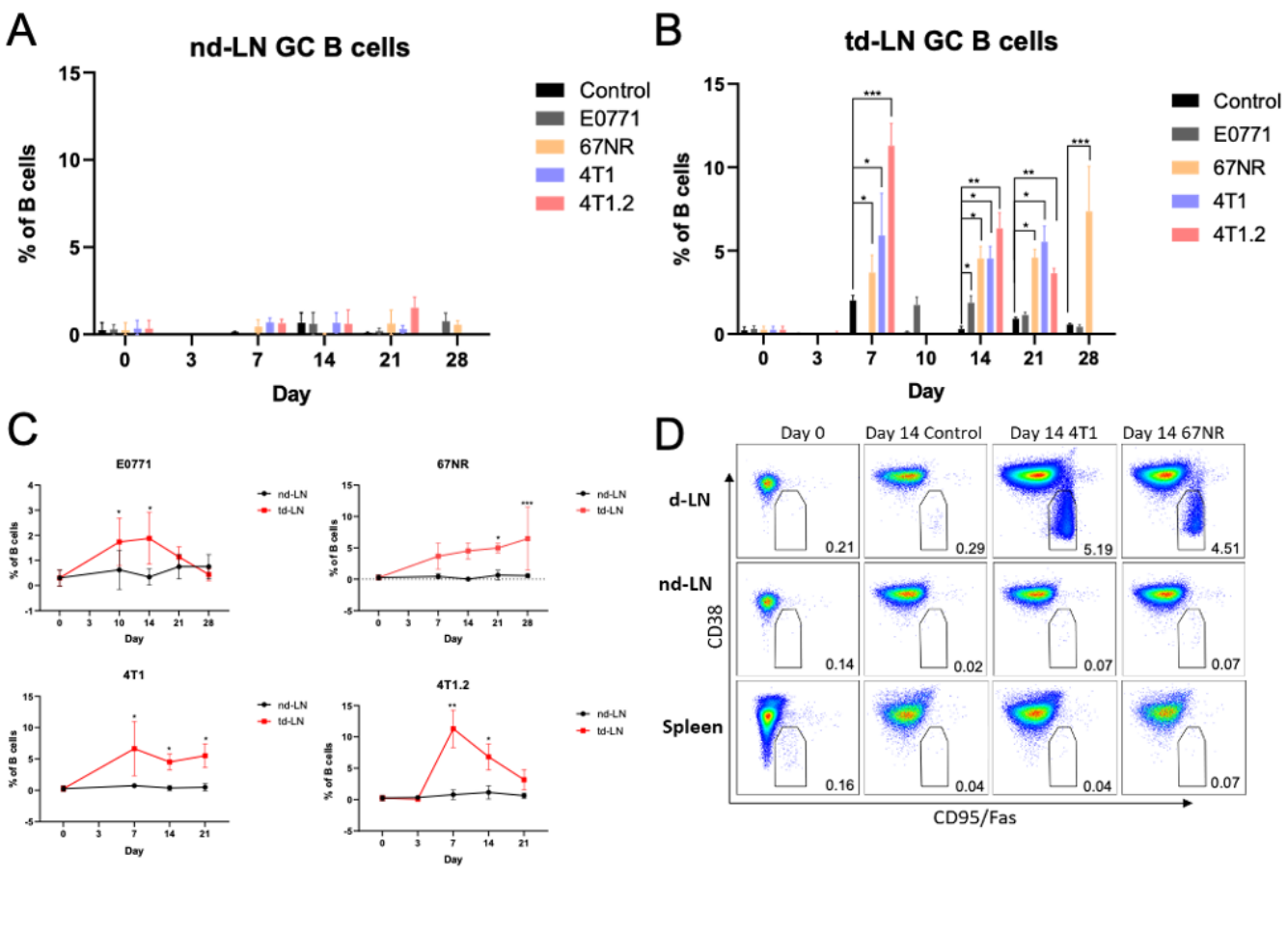

Figure 60: GC B cells are increased within td-LNs of tumour bearing mice. (A) GC B cells as % of total B cells, defined as CD19+B220+CD38^{low}CD95/Fas^{high} within the non-draining LN of control and tumour bearing mice administered the E0771, 67NR, 4T1 or 4T1.2 cell line from day 0 until day 28. (B) GC B cells as % of total B cells, defined as CD19+B220+CD38^{low}CD95/Fas^{high} within the draining-LN (d-LN) or tumour-draining LN (td-LN) of control and tumour bearing mice administered the E0771, 67NR, 4T1 or 4T1.2 cell line from day 0 until day 28 (Kruskal-Wallis test with Dunn's multiple comparison post-hoc tests, * = $p < 0.05$, ** = $p < 0.01$, *** = $p < 0.001$). (C) GC B cells (CD19+B220+ CD38^{low}CD95/Fas^{high}) as a % of B cells from tumour-draining LNs (td-LNs) compared with nd-LNs in E0771, 67NR, 4T1 and 4T1.2 models, (Wilcoxon signed-rank test, * = $p < 0.05$, ** = $p < 0.01$, *** = $p < 0.001$). (D) Representative flow cytometry plots from draining LNs (d-LN), non-draining LNs (nd-LN) and spleens at day 0 of inoculation and day 14 in control mice or those administered the 4T1 or 67NR cell line.

Although flow cytometry can evaluate the fraction of B cells that express GC markers, it cannot be used to determine spatial orientation and the morphological structures of the GCs within these models. BCL6 staining was used to visualise if there was formation of GCs, as it is a master regulatory of GC responses, acting as a transcriptional repressor to ensure sufficient tolerance and prevent premature activation of B cells (Basso and Dalla-Favera, 2010). GCs were visible within the td-LNs as well-defined structures at day 7 and were visible in the 67NR model as late as day 28 post inoculation (Figure 61).

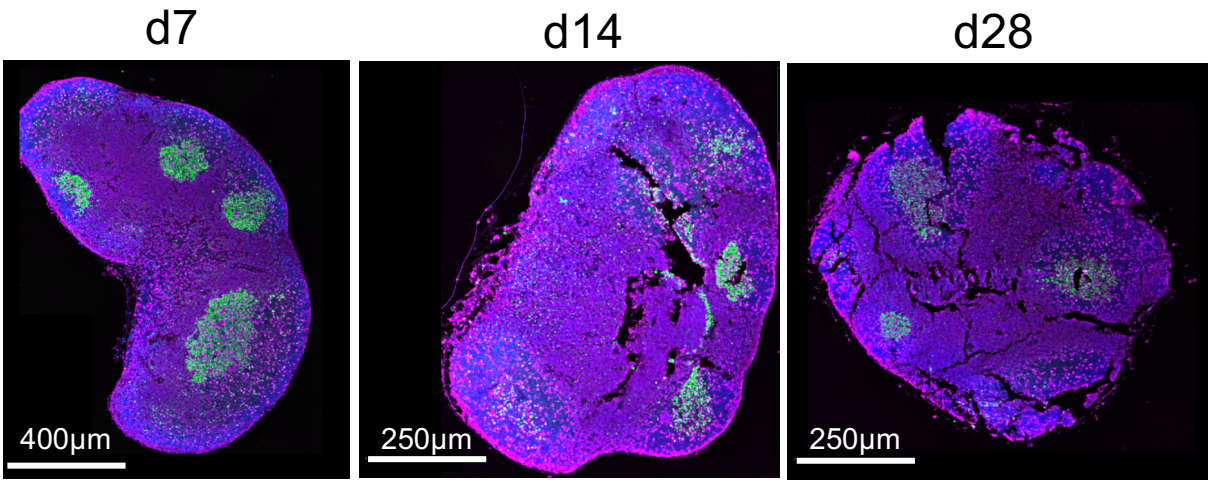

Figure 61: GCs form in tumour draining LN of orthotopic mouse models of TNBC. Immunofluorescence images taken from the tumour draining LNs (td-LN) of the 67NR model at day 7, day 14 and day 28 post tumour inoculation. Images are stained with a nuclear dye (blue), anti-CD4 antibody (magenta) and anti-BCL6 antibody (green).

4.6.1 Dark zone and light zone fractions within the germinal centre are not significantly altered

Within traditional immunisation mouse models, early GCs are visible within follicles using histological methods at day 4. Rapidly dividing B cell blasts begin to populate the network of follicular dendritic cells at the centre of the follicle, which continues until day 7 when the GC develops fully polarised DZ and LZ areas. Following somatic hypermutation (SHM) within the dark zone, GC B cells migrate to the LZ where Tfh cells patrol GC B cells and form transient contacts depending on the antigen available and affinity on MHC complexes. Whilst enhanced GC responses are observed in several pathologies including that of system lupus erythematosus (SLE), the dysregulation of these zones has not been routinely assessed. To determine if there were differences in LZ/DZ polarity within tumour induced GCs, DZ and LZ fractions as a percentage of total GC B cells, as well as the DZ/LZ ratio was assessed within the td-LNs of each model at every timepoint. The td-LNs from the 4T1.2 model demonstrated a trend towards an increase in the DZ fraction compared with 67NR and 4T1, which was sustained between day 7 and day 21, however within the 67NR, this trend was reversed, displaying a possible increase in LZ GC B cells. GC B cells from the td-LNs of E0771 mice followed a similar pattern to the 4T1.2, with an increased DZ fraction and reduced LZ except at day 28 (Figure 62A-B). Therefore, GC B cells within the 4T1.2 and E0771 td-LNs demonstrated a possible decrease in the LZ/DZ ratio compared to those from the td-LNs of 4T1 and 67NR, which was consistent from day 7 to day 21 post tumour inoculation (Figure 62C). This trend may be indicative of a lack of antigen presentation and selection within the 4T1.2 and E0771 models that may affect the subsequent maturation of anti-tumour B cell response.

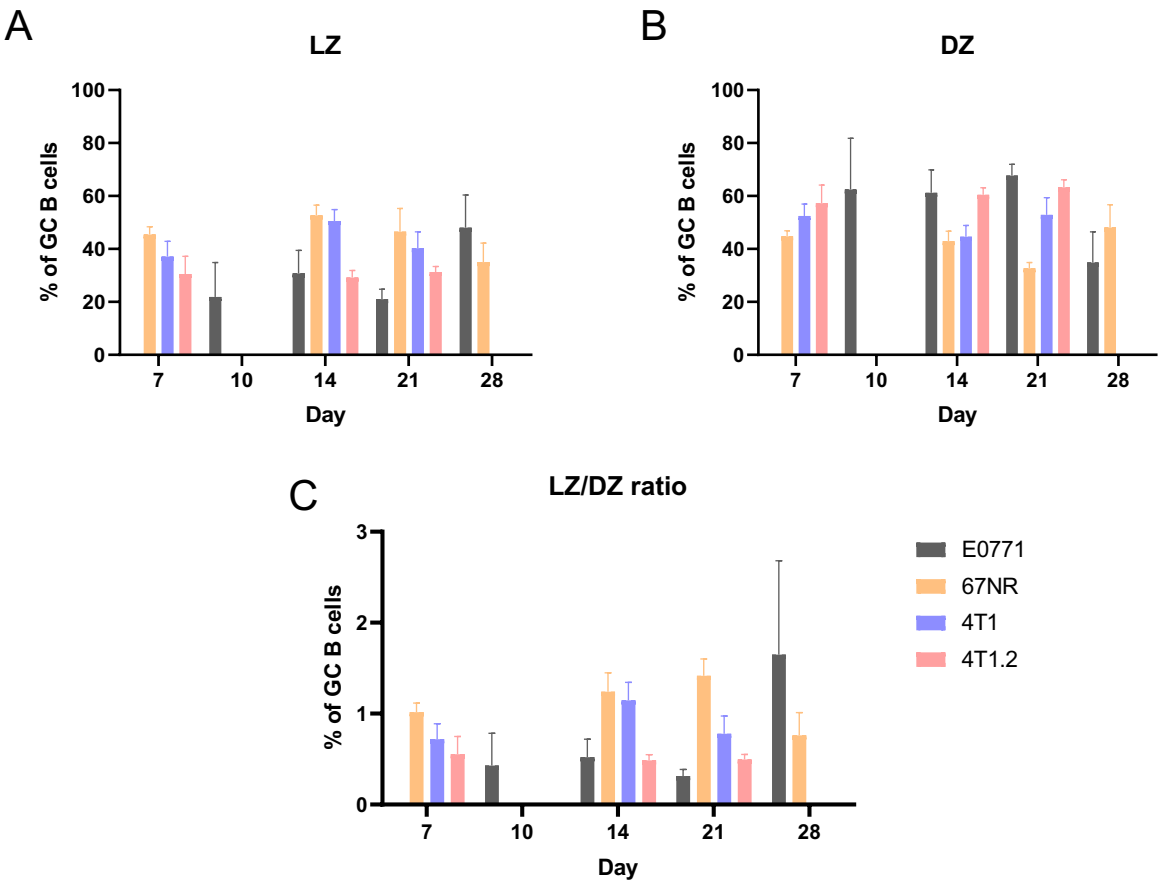

Figure 62: No significant alterations in the light zone to dark zone ratio of GC B cells. (A) Dark zone (DZ) GC B cells as a percentage of total CD19+B220+CD38^{low}CD95/Fas^{high} GC B cells within the tumour draining LNs (td-LNs) of E0771, 67NR, 4T1 and 4T1.2 models between day 7,10 and 21. (B) Light zone (LZ) GC B cells as a percentage of total CD19+B220+CD38^{low}CD95/Fas^{high} GC B cells within the tumour draining LNs (td-LNs) of E0771, 67NR, 4T1 and 4T1.2 models between day 7,10 and 21. (C) The ratio of LZ to DZ GC B cells within the tumour draining LNs (td-LNs) of E0771, 67NR, 4T1 and 4T1.2 models between day 7,10,14, 21 and 28.

4.6.2 IgM+ GC B cells increase in metastatic 4T1.2 accompanied by a reduction in class switched IgG1

Next, the immunoglobulin isotype profiles of GC B cells were evaluated across all mouse models over time. Whilst GC B cells from the E0771, 67NR and 4T1 demonstrated a steady decline in the fraction of GC B cells expressing IgM, this population increased between day 7 and day 21 in the 4T1.2 td-LNs (Figure 63A). In contrast, GC B cells derived from the 67NR td-LNs displayed a class-switched IgG1 phenotype which increased over time. At day 14, percentages of class-switched IgG1 GC B cells plateaued in the 4T1 and E0771 models and started to decrease in the td-LNs of 4T1.2 mice (Figure 63B). This revealed stark differences in the immunoglobulin phenotype of GC B cells between the most aggressive and metastatic tumour model (4T1.2), and the non-metastatic 67NR. There was a significant decrease in IgM+ GC B cells within the td-LNs of 67NR mice, accompanied by an increased fraction expressing IgG1 (Kruskal-Wallis test, $p < 0.05$ and $p < 0.05$ respectively). In contrast, the percentage of IgM+ GC B cells within the td-LNs of 4T1.2 mice was significantly enhanced between day 7 and day 21, whilst the proportion expressing IgG1 was depleted (Kruskal-Wallis test, $p < 0.01$ and $p < 0.01$ respectively) (Figure 63C). These data indicate that the tumour growth kinetics and metastatic ability of these different TNBC mouse models may impact on the functionality of the GC response in LNs and class switching potential of GC B cells.

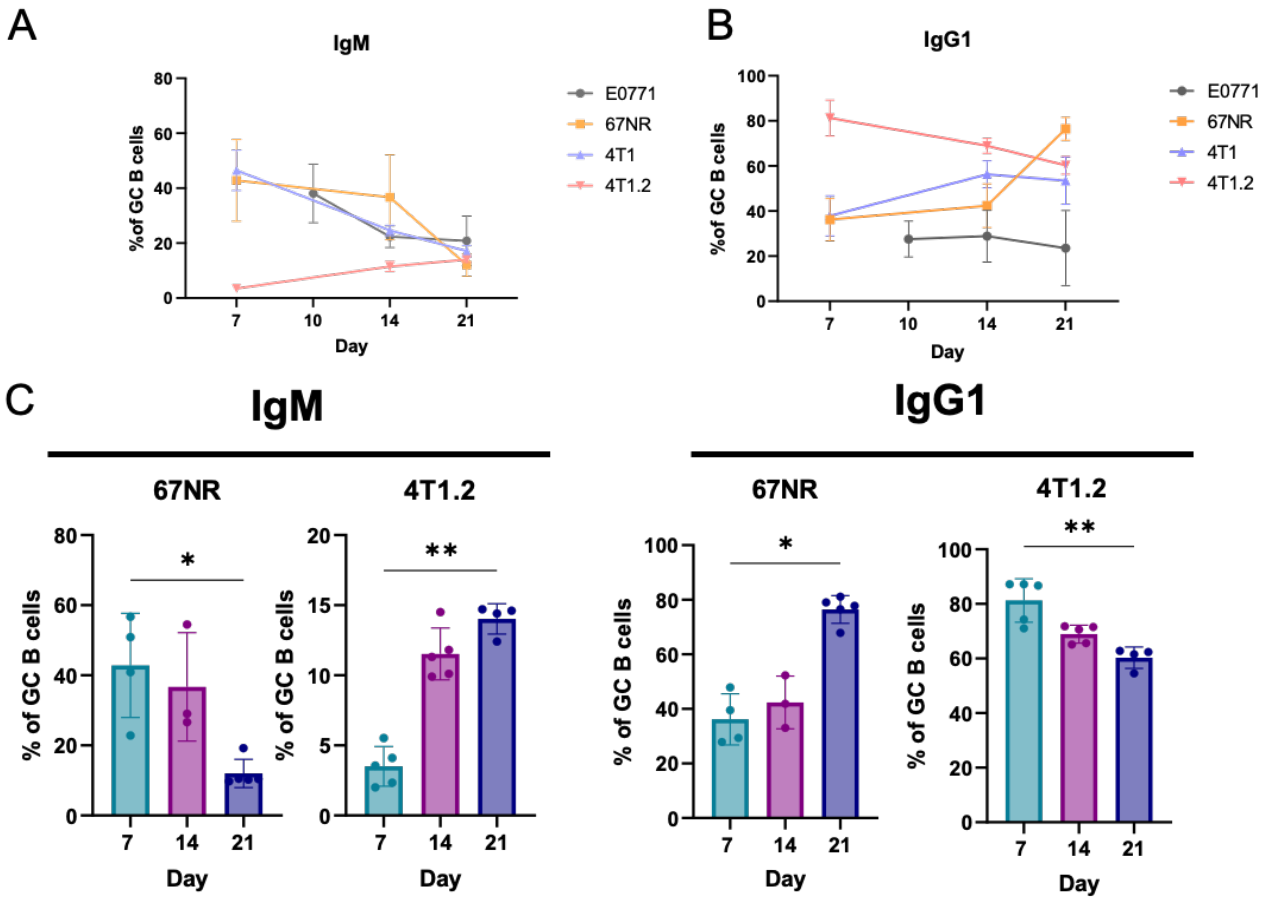

Figure 63: 4T1.2 and 67NR GC B cells within tumour draining lymph nodes exhibit opposing immunoglobulin phenotypes over time. (A) IgM+ GC B cells as a percentage of total CD19+B220+CD38^{low}CD95/Fas^{high} GC B cells within the tumour draining LNs (td-LNs) of E0771, 67NR, 4T1 and 4T1.2 models between day 7,10 and 21. (B) IgG1+ GC B cells as a percentage of total CD19+B220+CD38^{low}CD95/Fas^{high} GC B cells within the tumour draining LNs (td-LNs) of E0771, 67NR, 4T1 and 4T1.2 models between day 7,10 and 21. (C) Barplots to show changes in the frequency of IgM+ and IgG1+ GC B cells between day 7 and day 21 within td-LNs of the 67NR and 4T1.2 model (Kruskal-Wallis test with Dunn's multiple comparison post-hoc test. * = $p < 0.05$, ** = $p < 0.01$).

4.7 Memory B cells are increased in tumour draining lymph nodes

GCs are responsible for the maturation of B cells to produce highly specific memory B cell and antibody producing plasma cells. To determine whether mammary tumour development affects the GC related B cell populations within the td-LNs, the memory B cell levels were assessed, and were defined as the percentage of non-GC B cells (CD19+B220+CD38^{high}CD95/Fas^{low}) that had also downregulated IgD. Although there was some variability in the memory B cell fraction within the nd-LN and td-LN, there was an increase within the td-LNs of 4T1.2 mice at day 7, day 14 and day 21 post inoculation compared to d-LN in control mice. This was also true for the E0771 within the nd-LNs and td-LNs at day 10 and day 14 but not evident within the td-LNs of 67NR or 4T1 models (Figure 64A-B). There was a significant increase in memory B cells within the td-LN of E0771 mice compared to nd-LNs at day 14 (Wilcoxon signed-rank test, $p < 0.01$), and trending at day 7 and day 14 but did not reach statistical significance. This trend was similar to that of the GC B cell response seen in figure 58, which peaked at day 14 and declined by day 28. In contrast, the 4T1 and 67NR models exhibited no differences in memory B cells within the td-LNs at all timepoints compared to the nd-LNs (Figure 64C). The 4T1.2 exhibited the most differences between td-LNs and nd-LNs with a steady increase in memory B cells from day 7 to day 21, which was significantly different to the nd-LN in all time points (Wilcoxon signed-rank test, $p < 0.01$, $p < 0.05$, $p < 0.001$ respectively) (Figure 64C-D). As this response was not reflective of the trend seen in GC B cells for the 4T1.2 model, in which they peaked at day 7 and declined by day 21, this may an indication that the memory B cells may derive from an extrafollicular response.

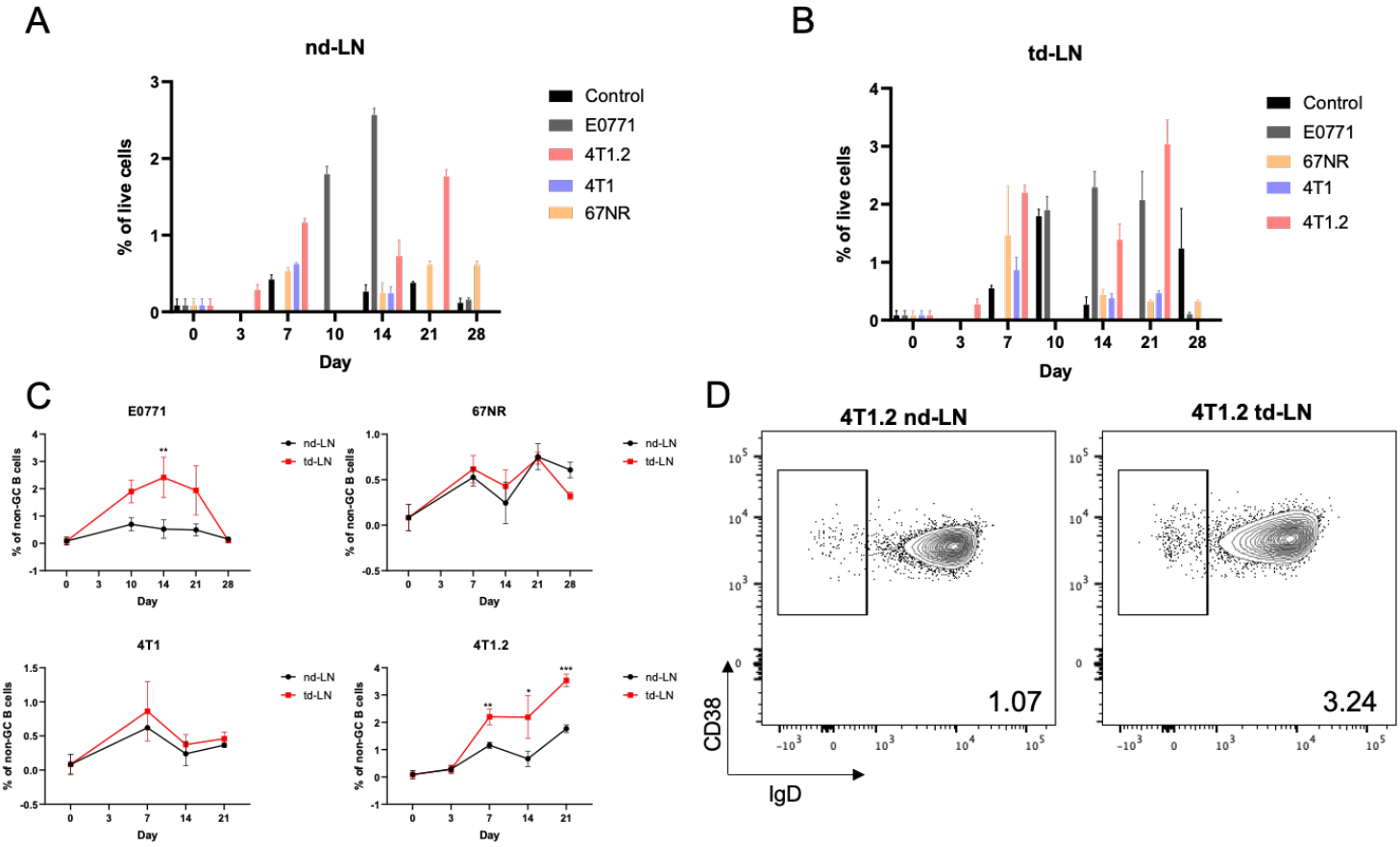

Figure 64: Memory B cells are enriched in td-LNs of E0771 and 4T1.2 mice. Memory B cells (CD19+B220+CD38+CD95-IgD-) as a % of non-GC B cells (CD19+B220+CD38^{high}CD95/Fas^{low}) within the non-draining LN(nd-LN) (A) and tumour draining LN (td-LN) (B) of control, E0771, 67NR, 4T1 and 4T1.2 at day 7, 10, 14, 21 and 28 post tumour induction. (C) Memory B cells (CD19+B220+CD38+CD95-IgD-) as a % of non-GC B cells (CD19+B220+CD38^{high}CD95/Fas^{low}) from td-LNs compared with nd-LNs in E0771, 67NR, 4T1 and 4T1.2 models, (Wilcoxon signed-rank tests * = $p < 0.05$). (D) Representative flow cytometry plots from nd-LNs and td-LNs from 4T1.2 mice at day 21 post tumour inoculation.

4.7.1 Tumour draining lymph nodes in 4T1.2 model are enriched for IgM+CD237+ memory B cells

To determine if there was concordance between the immunoglobulin isotype of the GC B cells and the memory B cell output, the percentage of memory B cells expressing IgM and IgG1 within the td-LNs of 4T1.2 mice was evaluated. Similar to the GC B cells, the fraction of memory B cells expressing IgM was significantly increased between day 7 and day 21 (Kruskal-Wallis test, $p < 0.01$) (Figure 65A,65C). There was also a dramatic reduction in the percentage of memory B cells expressing IgG1 between day 7, day 14 and day 21 (Kruskal-Wallis test, $p < 0.05$) (Figure 65B-C).

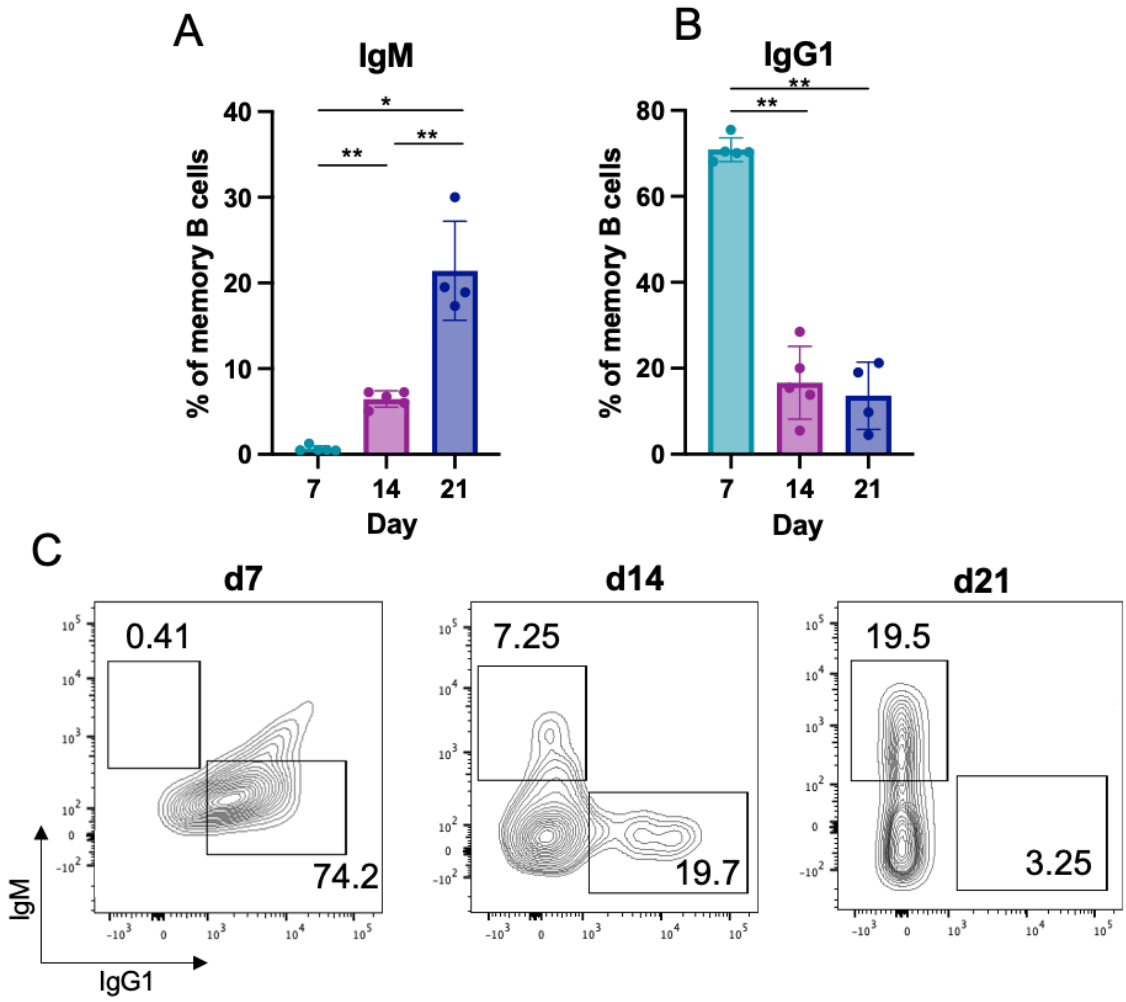

Figure 65: Memory B cells within td-LN of 4T1.2 mice obtain IgM+ phenotype over time. (A) The percentage of IgM+ memory B cells within tumour draining LNs of 4T1.2 mice at day 7, day 14 and day 21 post tumour induction (Kruskal-Wallis test with Dunn's multiple comparison post-hoc test. * = $p < 0.05$, ** = $p < 0.01$). (B) The percentage of IgG1+ memory B cells within tumour draining LNs of 4T1.2 mice at day 7, day 14 and day 21 post tumour induction. Kruskal-Wallis test with Dunn's multiple comparison post-hoc test. ** = $p < 0.01$. (C) Representative flow cytometry plots of IgM and IgG expression within CD19+B220+CD38+CD95-IgD- memory B cells at day 7, day 14 and day 21 in td-LNs of 4T1.2 mice.

Whilst previous data has suggested that the antibody isotype of memory B cells controls whether memory B cells will differentiate upon restimulation or persistent challenge, studies have further shown a role for markers including CD80 and CD273 (PD-L2), that independently of isotype can stratify memory B cell subsets with distinct functional properties. Notably, CD80+CD273+ memory B cells will rapidly differentiate into antibody secreting cells upon rechallenge, and do not generate GCs. On the contrary, CD80-CD273- memory B cells tended to generate very little antibody secreting cells and had the propensity to seed novel GCs (Zuccarino-Catania et al., 2014). These data highlight differences within the memory B cell pool in response to antigen that need to be investigated further within the context of cancer, potentially providing novel avenues of immune response against tumour antigens. Here, CD273 expression on memory B cells within the td-LNs of 4T1.2 mice was assessed to determine if there was a propensity of the memory B cell pool to upregulate CD273.

The percentage and absolute number of memory B cells expressing CD273 was enriched between day 7 and day 21 (Kruskal-Wallis test, $p < 0.01$) (Figure 66A-C). In concordance with the overall phenotype of the memory B cells, the fraction of the CD273+ memory B cells upregulating IgM was also increased between day 7 and day 21 (Kruskal-Wallis, $p < 0.01$) (Figure 67A,67C). This was in parallel with a reduction in CD273+ memory B cells expressing IgG1 between day 7 and day 21 (Kruskal-Wallis test, $p < 0.01$) (Figure 67B-C). This further may indicate that the memory B cells generated in the td-LNs have the propensity to differentiate into plasma cells upon rechallenge without generating a GC response, but what this may indicate in terms of tumour progression needs to be investigated further.

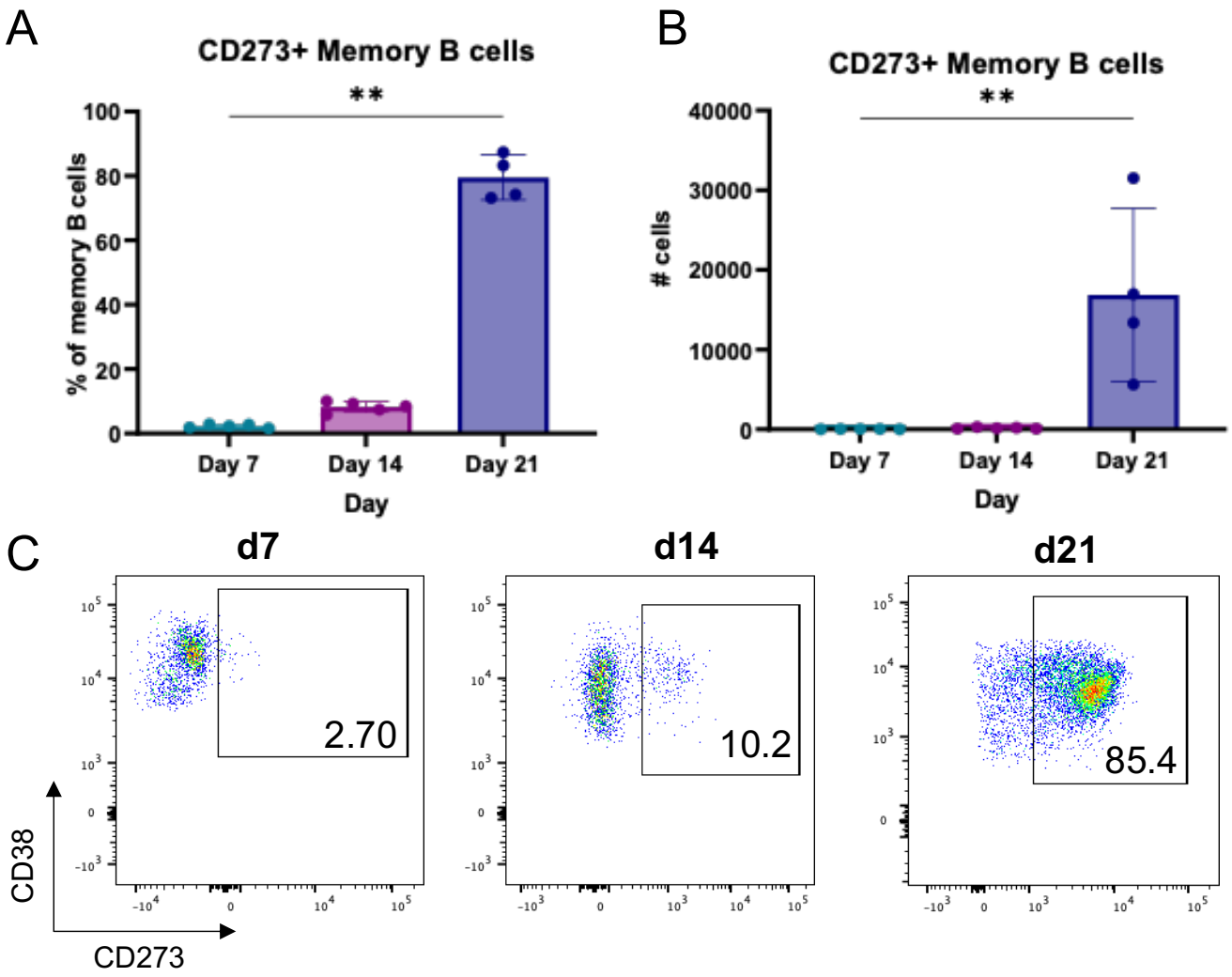

Figure 66: Memory B cells within td-LN of 4T1.2 mice upregulate CD273 over time. (A) The percentage of memory B cells expressing CD273 within tumour draining LNs of 4T1.2 mice at day 7, day 14 and day 21 post tumour induction. Kruskal-Wallis test with Dunn's multiple comparison post-hoc test. * = $p < 0.05$. (B) Absolute numbers of memory B cells expressing CD273 within tumour draining LNs of 4T1.2 mice at day 7, day 14 and day 21 post tumour induction. Kruskal-Wallis test with Dunn's multiple comparison post-hoc test. * = $p < 0.05$. (C) Representative flow cytometry plots of CD273 expression within CD19+B220+CD38+CD95-IgD- memory B cells at day 7, day 14 and day 21 in td-LNs of 4T1.2 mice.

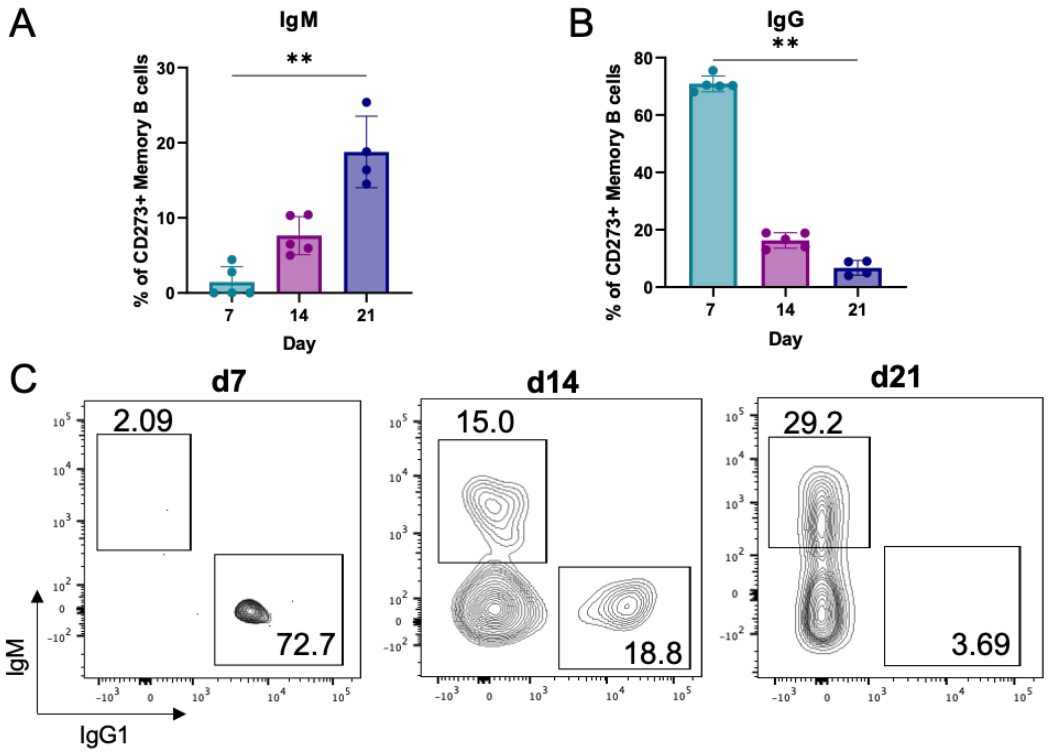

Figure 67: IgM+ CD273+ memory B cells within tumour draining LNs of 4T1.2 mice increase over time. (A) The percentage of IgM+ CD273+ memory B cells within tumour draining LNs of 4T1.2 mice at day 7, day 14 and day 21 post tumour induction. Kruskal-Wallis test with Dunn's multiple comparison post-hoc test. * = $p < 0.05$. (B) The percentage of IgG1+ CD273+ memory B cells within tumour draining LNs of 4T1.2 mice at day 7, day 14 and day 21 post tumour induction. Kruskal-Wallis test with Dunn's multiple comparison post-hoc test. * = $p < 0.05$, ** = $p < 0.01$. (C) Representative flow cytometry plots of IgM and IgG expression within CD19+B220+CD38+CD95-IgD- memory B cells at day 7, day 14 and day 21 in td-LNs of 4T1.2 mice.

4.8 Plasma cells are increased in tumour draining lymph nodes of 4T1.2 mouse models

Having established that orthotopic mouse models of breast cancer could generate GC B cells within td-LNs, the plasma cell production was evaluated, as a percentage of CD138+B220- cells within the live cell pool. There was a substantial increase in the percentage of plasma cells within the td-LNs of mice implanted with the 4T1.2 cell line compared to d-LN controls at day 7 that was sustained until day 21 (Kruskal-Wallis test, $p < 0.01$). This expansion was not evident in any of the other models, with a small increase within the td-LNs of the 4T1 at day 21 and within the E0771 at day 28. (Figure 68A-B). At day 7, day 14 and day 21, the percentage of plasma cells was increased within the td-LNs of 4T1.2 mice compared to the nd-LNs (Kruskal-Wallis test, $p < 0.01$, $p < 0.05$ and $p< 0.05$ respectively) (Figure 68B-C). A Spearman's rank correlation coefficient test was applied to assess the correlation between the proportion of plasma cells and the percentage of GC B cells within the td-LN of 4T1.2 cumulatively across all timepoints. This revealed a possible negative correlation between the plasma cell expansion and the percentage of B cells with a GC-like phenotype within the td-LNs of these mice ($R = -0.51$, $p = 0.06$) (Figure 68D). Visualising the spatial orientation of CD138+ plasma cells within the td-LNs showed a large expansion of plasma cells at day 21 compared to day 7 and day 14, which were predominantly located in the paracortex of the LN (Figure 68E). Akin to the memory B cells and GC B cells, the percentage of IgM+ plasma cells also increased between day 7 and day 21(Kruskal-Wallis test, $p < 0.05$) (Figure 69A, 69C) however, the fraction of plasma cells expressing IgG1 was unchanged (Kruskal-Wallis test) (Figure 69B-C).

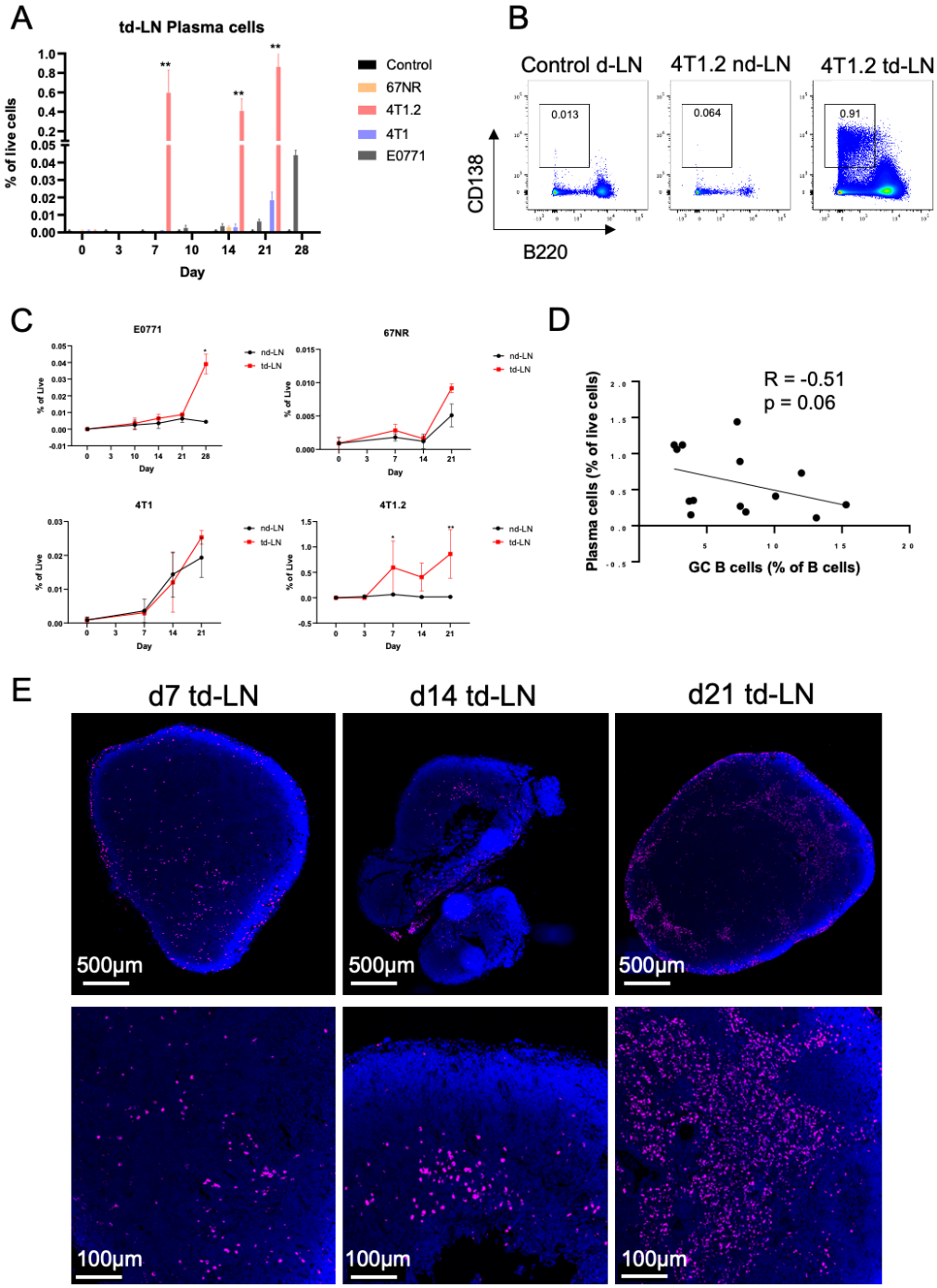

Figure 68: Plasma cells are enriched in the tumour draining lymph nodes of 4T1.2 and E0771 mice. (A) Plasma cells (CD138+B220-) as a % of live cells within the draining and tumour draining LNs of control, E0771, 67NR, 4T1 and 4T1.2 mice between day 0 and day 28 after tumour induction (Kruskal-Wallis test with Dunn's multiple comparison post-hoc test, ** = $p < 0.01$). (B) Representative flow cytometry plots of CD138+B220- plasma cells within the draining lymph node (d-LN) of control mice, non-draining lymph node (nd-LN) and tumour draining lymph node (td-LN) of mice bearing 4T1.2 tumours. (C) Plasma cells (CD138+B220-) as a % of live cells within the nd-LNs and td-LNs of 4T1.2 mice from day 0 to day 21 post tumour induction (Kruskal-Wallis test with Dunn's multiple comparison post-hoc test, * = $p < 0.05$, ** = $p < 0.01$). (D) Spearman's rank correlation coefficient for the correlation between plasma cells as % of live cells compared with GC B cells as a % of total B cells). (E) Representative immunofluorescence images of CD138+ plasma cells (magenta) in the td-LN of a 4T1.2 mouse at day 7, day 14 and day 21 post inoculation.

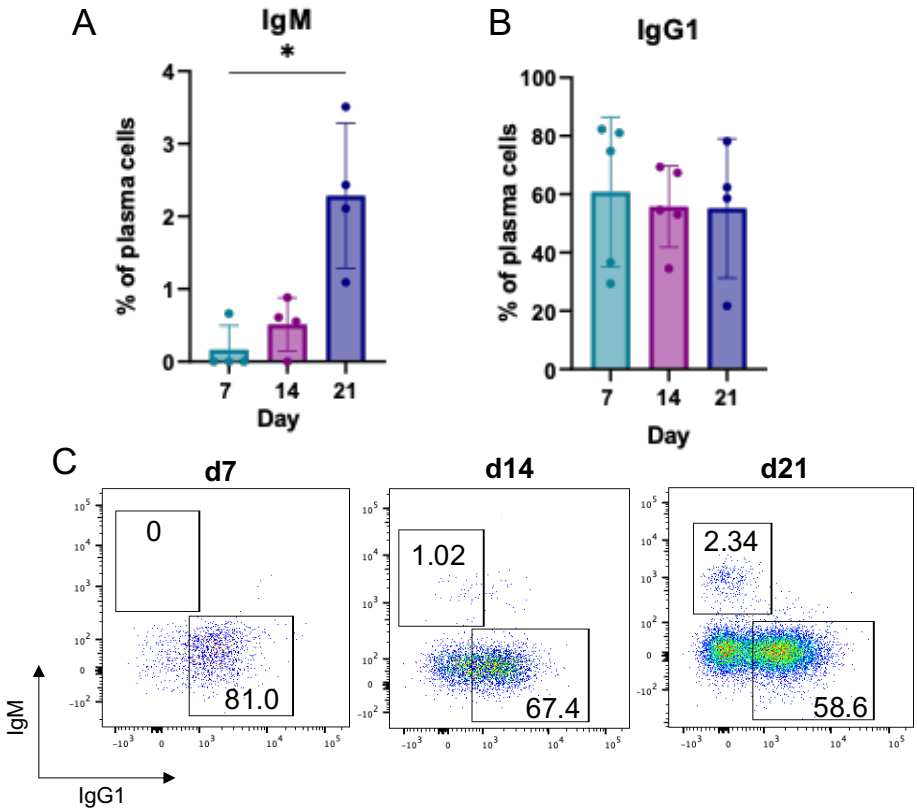

Figure 69: IgM+ Plasma cells increase within tumour draining-LN of 4T1.2 mice over time. (A) The percentage of IgM+ plasma cells within tumour draining LNs of 4T1.2 mice at day 7, day 14 and day 21 post tumour induction (Kruskal-Wallis test with Dunn's multiple comparison post-hoc test. ** = $p < 0.01$) (B) The percentage of IgG1+ plasma cells within td-LNs of 4T1.2 mice at day 7, day 14 and day 21 post tumour induction (Kruskal-Wallis test with Dunn's multiple comparison post-hoc test). (C) Representative flow cytometry plots of IgM and IgG expression within CD138+B220- plasma cells at day 7, day 14 and day 21 in td-LNs of 4T1.2 mice.

4.8.1 Plasma cells express CXCR4 in tumour draining LNs of 4T1.2 mouse model

The CXCR4:CXCL12 axis plays a key role in the migration of plasma cells from secondary lymphoid organs including the spleen and LN to the inflamed tissue and the bone marrow for further maturation. Within the td-LNs of 4T1.2 mouse models, the percentage of plasma cells expressing CXCR4 was between 95-100% and comparable between day 7, day 14 and day 21 (Figure 70A-B). There was also no difference in the median fluorescence intensity (MFI) of CXCR4 on the plasma cells present at day 7, 14 and 21 post tumour induction (Figure 70C).

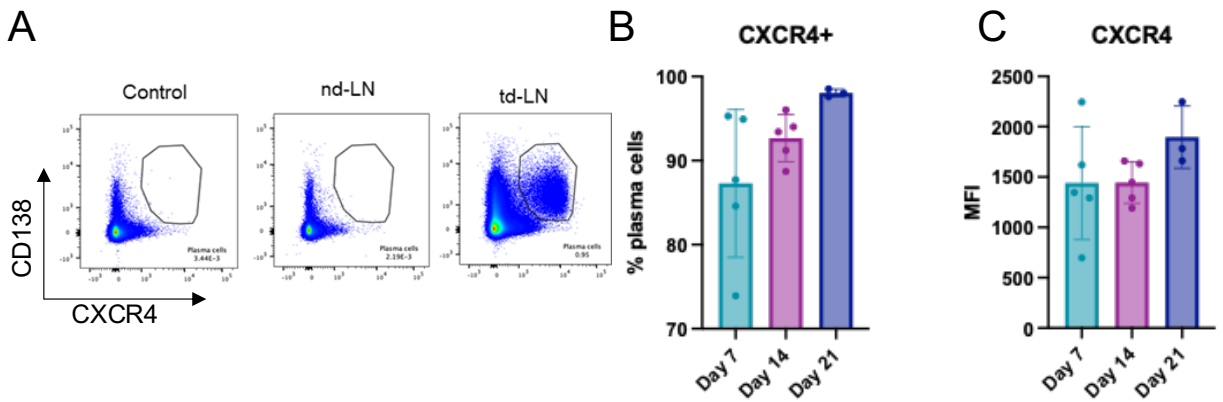

Figure 70: Plasma cells are predominantly CXCR4+ within td-LN of 4T1.2 mice. (A) Representative flow cytometry plots of the 4T1.2 model at day 21 post injection of cxcr4 expression on plasma cells within the draining LN of control mice, non-draining LN (nd-LN) of 4T1.2 mice, and tumour draining LN (td-LN) of 4T1.2 mice. (B) CXCR4+ expression on plasma cells at day 7, day 17 and day 21 after tumour initiation of 4T1.2 mice within td-LNs of 4T1.2 mice. (C) Median fluorescence intensity of CXCR4 on plasma cells day 7, day 17 and day 21 of 4T1.2 mice post inoculation with cell line.

4.9 Discussion

In this chapter, GC derived B cell populations from LNs were assessed in the context of 4 pre-clinical mouse models of breast cancer, in both *in vitro* assays and within a temporal fashion using *in vivo* models. Due to the metastatic variability of the cell lines, parallels could be drawn between the phenotypic nature of these subsets in the context of tumour progression. Data described here shows the ability of 4T1.2 cells to induce activation of LN and splenic B cells, through upregulation of CD86, and the increased presence of $CD138^{low}$ plasma like cells. Whilst co-culture assays have described expansion of IFN-y producing T cells from td-LNs when exposed to tumour cell lines (Okamura et al., 2022), there are few studies investigating the effect on B cells. Studies examining human peripheral blood B cells co-cultured with human breast cancer cells result in the emergence of a $CD20^{low}$ Breg population that expresses TGF-β and is capable of suppressing T cell activity (Yu Zhang et al., 2013). Whist data here does not examine the Breg population, the enrichment of $CD138^{low}$ plasma cells within the LN cells cultured with 4T1.2 cell lines is suggestive of a plasmablast-like population, which expressed high levels of IgM. CD138 is a master regulator of plasma cell differentiation and is highly upregulated upon maturation into antibody secreting cells (McCarron et al., 2017). Whilst not completely representative of a physiological environment within a tumour setting, this provides some evidence that 4T1.2 tumour cells can induce B cell activation and influence the development of early-stage plasma cells.

In agreement with published work, data shown here further describes how the tumour growth kinetics of the 4T1.2 was accelerated comparatively to the 4T1, 67NR and E0771 models. The 4T1 and 4T1.2 models both developed splenomegaly from day 14 post induction, which is suggested to be due to an influx of Gr-1^{dim}/$CD11b^{bright}$ immature granulocytes induced by G-CSF, GM-CSF and M-CSF also present within the tumour and peripheral blood (duPre' and Hunter, 2007). All models presented with a significant lymphadenopathy in the td-LNs

compared with nd-LNs, which has not been routinely assessed by others utilising these orthotopic methods. Studies examining the LNs within the 4T1 and 4T1.2 models have identified the presence of metastasis through immunohistochemical staining of cytokeratin and Ki67 (Arroyo-Crespo et al., 2019), however notably there was an increase in the td-LNs of the non- and poorly metastatic 67NR and E0771 models. This is presumably due to an expansion of the sinuses as a result of increased lymphatic flow from inflammation caused by the tumour. In response to injury and disease, chemokines and cytokines will mediate recruitment of lymphocytes and antigen presenting cells that will access the LNs via lymphatic vessel-mediated lymph drainage. The stimuli present will induce expansion of intrafollicular T cells, dendritic cells, and B cells within the cortex to generate an optimal B cell response (Willard-Mack, 2006).

Using flow cytometric and histological techniques, it was subsequently shown here that the orthotopic implantation of breast cancer tumours within the mammary fat pad leads to substantial B cell and GC response within the td-LNs. Although this has similarly been shown in the 4T07 model, where authors examined the levels of hypoxia among B cells that responded to tumours (Firmino et al., 2021), this is the first study comparing the impact of multiple breast cancer cell lines on GC formation and function within draining LNs. One of the most striking observations was that the td-LN GC B cell fraction within the 4T1.2, which is the most aggressive tumour model, peaked at day 7 but then appeared to decrease by day 21. In comparison, the 67NR and the least aggressive model, maintained constant levels of GC B cells throughout the study timeline.

This was accompanied by a steady decline in the number of IgG1+ GC B cells and an increase in IgM+ GC B cells within the td-LNs of the 4T1.2 mice. Conversely, the 67NR GC B cells lost IgM expression and the fraction of IgG1+ cells expanded. Within traditional immunisation methods used to study GC B cell development in mice, administration of antigen typically results in early GCs containing the most unswitched IgM+ B cells, and IgG responses dominate the GC 14-21 days post challenge. This is indicative of IgG+ B cells

within the GC being positively selected more readily than those that express IgM, in concordance with interactions with cognate T follicular helper (Tfh) cells and selection of high-affinity B cells. Therefore, IgG+ GC B cells further show a greater propensity to differentiate into antibody secreting cells than their IgM+ counterparts (Sundling et al., 2021). Within the context of the 4T1.2 model, it may be that the progression of tumour cells to the LN, which takes place around day 10-14, may interfere with the GC reaction and subsequent development. It is well known that CD8 T cells will develop an exhausted phenotype, upregulating inhibitory molecules such as PD-1, LAG3, T-cell immunoglobulin and mucin-domain containing-3 (TIM3) and CTLA-4 in response to constitutive activation within cancer and other chronic diseases (Wherry and Kurachi, 2015). Although the understanding of CD4 T cell exhaustion is somewhat lacking, Tfh cells from late-stage patients with hepatitis B virus (HBV)-related hepatocellular carcinoma (HCC) demonstrate impaired abilities to induce naïve B cells towards antibody secreting plasma cells, which is correlated with the intensity of PD-L1 expression in the resected tumours (Zhou et al., 2016). Whilst the frequency of Tfh cells was not assessed here, unpublished data from our group suggests a rapid decline in Tfh from day 7 to day 21, and this may provide some explanation as to why the fraction of GC B cells within this highly metastatic model could be impaired, perhaps that td-LN T cells come into direct contact with tumour cells, promoting an exhausted phenotype.

Whilst GC B cell levels remained at a constant level within the 67NR model, there was no indication of an increase in either memory B cells or plasma cells within the td-LNs. This is somewhat surprising, due to the evident class switching taking place within the pool of GC B cells. The control of memory B cell and plasma cell exit from the GC is mediated by the ubiquitin ligase activity of CBL proteins (Li et al., 2018), and whether this process is impaired during the GC development within the td-LNs of 67NR mice, is yet to be explored.

In concordance with the immunoglobulin isotype phenotype of the GC B cells of the 4T1.2 model, there is a rapid decline in the IgG1+ memory B cells present within the td-LNs, accompanied by an expansion of those expressing IgM. Although this reduction in IgG1+

plasma cells was not observed in the same manner, there was also a population of IgM+ plasma cells that appeared by day 21. IgM antibodies are considered to play a major role in humoral immunity in early stages of the primary immune response, however IgM+ memory B cells can develop either from a high affinity situation (GC dependent), or low affinity and lacking somatic hypermutation (SHM) (GC independent). Studies utilising the (4-hydroxy-3-nitrophenyl) acetyl (NP)- hapten system have reported that IgM+ SHM+ memory B cells originating from the GC response are unable to differentiate into IgM+ antibody secreting cells, however IgM+SHM+ memory B cells can differentiate into plasma cells secreting IgM as part of a recall response, providing broad cross-reactivity to microbial infection (Tashiro et al., 2018). This suggests that during tumour progression, the memory B cells produced within the td-LNs may be originating from an extrafollicular response, or as part of a secondary recall system that may be replacing class switched populations with a broadly neutralising response against tumour antigens.

In the same way, many plasma cells expressing IgM typically arise from a T cell independent manner, eliciting a broadly neutralising response in early stages of disease. However, the persistence of long lived plasma cells within secondary lymphoid organs including the spleen, suggest that IgM may serve a non-redundant role in humoral memory by augmenting host IgG responses particularly in the context of viral infection (Bohannon et al., 2016). Within the context of breast tumour immunology, adaptive IgM is consistently higher in breast cancer tissue of patients with stage 1 and stage 2 disease. Whilst IgM can participate in early tumour cell elimination through opsonisation and antibody-dependent cell cytotoxicity, a hallmark of a damaged immunological response within an established tumour is immunosuppression of IgG but constant levels of IgM (Díaz-Zaragoza et al., 2015).

Taken together, these data suggest GC development in adjacent LNs as a direct consequence of TNBC tumour initiation. Discrepancies in the B cell phenotypes between the 67NR and 4T1.2 models indicates the presence of LN metastasis can potentially influence

the maintenance of the GC responses and abilities to produce class switched memory B cell and plasma cell responses.

4.10 Limitations and future work

One limitation to this study is the effect of all cell lines on B cell populations were not initially studied *in vitro*. This would enable comparisons between tumour cell lines with an array of metastatic properties and how they can directly affect LN and splenic B cell populations. This contrasts with the *in vivo* models in which the effect on the LNs and spleens can be studied after implantation of tumour within the mammary gland. There are also further limitations to these models. Although studying these mouse models across a period of four weeks give some indication of the temporal characteristics of the GC B cell populations, the timeframe utilised is acute, which is not representative of analyses performed on human samples taken after tumour and LN resection. Establishing a chronic model of TNBC to study the longevity of GC and GC derived populations, including hallmarks of exhaustion would be more illustrative of the mechanisms that facilitate both local and distant metastasis.

Furthermore, the relationship between the GC B cell subsets within the d-LNs and the primary tumour has not been presented here. This should be investigated in depth to characterise the migration and crosstalk between tumour and LN, and the role of the GC B cell response in promoting tumour infiltration of other immune subsets. Further, the populations studied here have not incorporated other populations present within the GC reactions for analyses, including that of Tfh, dendritic cells and regulatory subsets. Investigating the role of these populations would better our understanding of tumour derived moieties which can directly impact the formation and maintenance of the GC.

To study the impact of LN metastasis on the GC B cell populations, memory B, GC B and plasma cells within the 4T1.2 model should be extracted pre and post tumour invasion for

downstream analyses using sc-RNA sequencing. Resultant gene signatures may indicate how the tumour cells are impacting the formation and maintenance of the GC B cell response, which could be validated *in vitro* and eventually targeted with novel therapies.

Chapter 5

Molecular features of TNBC and their association with germinal centres and plasma cell responses

Introduction

Based on data from chapter 3, patients with low sTILs and a high plasma gene score (lThP) tumours were enriched for tumours of the luminal androgen receptor (LAR) subtype. HER2-enriched cases have frequently been reported in the LAR TNBC (Ahn et al., 2016), and lThP tumours exhibited an increased frequency of the HER2-enriched subtype using the Burstein classification. Moreover, our four-gene decision tree classification assigned these lThP tumours predominantly to the MC4 and MC5 subtypes. As we have shown, MC4 TNBC had higher expression of genes belonging to the PI3K/Akt signalling and ErbB signalling pathways(Quist et al., 2019). Androgen receptor (AR) upregulation points to a gender-biased environment within which androgens, namely testosterone, dihydrotestosterone and androstenedione are overexpressed(Davey and Grossmann, 2016). These sex hormones are increased in both males and females within puberty, however, are consistently upregulated within males in comparison to females throughout life (Handelsman et al., 2018) Previous work studying LAR TNBC revealed these patients are often older, post-menopausal, more involved iLNsand notably have a numerically lower stromal TIL count compared to non-LAR TNBC tumours(Thompson et al., 2022). Further analysis has also shown that these patients have a 2-fold decrease in the likelihood of responding to neoadjuvant chemotherapy, and a subsequently lower pathological complete response rate (pCR) compared to non-LAR TNBC tumours. (Thompson et al., 2022). Transcriptional profiling of these tumours has suggested that they downregulate pathways associated with DNA damage and repair, cell cycle and proliferation, which is suggestive of a poor response to chemotherapy based therapies (Thompson et al., 2022).

LAR tumours often present with an increased prevalence of cancer associated fibroblast (CAF) subsets, namely inflammatory CAFs (iCAFs) and myofibroblast-like CAFs (myCAFs), which can respond to androgens within the stromal compartments of the TME. This is in conjunction with an increased expression of gene related to angiogenesis, stemness and differentiation (Thompson et al., 2022). CAFs are believed to participate in the growth and invasion within the breast tumour microenvironment by producing tumour-promoting mediators and remodelling the extracellular matrix(Sahai et al., 2020).

CAFs can further secrete cytokines, chemokines, and other effector molecules, including TGF-β, CXCL12, collagens, metalloproteinases (MMPs) and laminin, which subsequently modulate immune infiltration. Within this context, studies have primarily focussed on tumour associated macrophages (TAMs), tumour associated neutrophils (TNs), natural killer (NK) cells and T cell subsets including CD4+ T cells, CD4+FoxP3+ Tregs and CD8+ T cells. CAFs can contribute to an immunosuppressive environment by promoting the recruitment of protumourigenic M2 macrophage subsets, Tregs and suppressing effector T cell infiltration (Xing et al., 2010). CAFs have been further implicated in TLS formation within pre-clinical mouse models. In contrast to their role in promoting immunosuppressive setting, CAFs can act as lymphoid tissue organiser cells (LTo) in conjunction with infiltrating CD8+ T cells and B cells. Effector CD8+ T cells recruit FAP-podoplanin+ fibroblasts to high endothelial venules (HEVs) where they differentiate into CXCL13-secreting fibroblast reticular cells (FRCs). This, in turn, will recruit and promote proliferation of $LT\alpha_1\beta_2$ secreting B cells which further stimulates TLS formation and maturation (Rodriguez et al., 2020). These data, therefore, point to CAFs as a heterogenous population that can stimulate both anti- and pro-tumour properties within the TME. and further work is required to therefore delineate their functions within LAR tumours. How CAFs can modulate plasma cell differentiation has notably been neglected, despite their prevalence to secrete chemokines including CXCL12 that are heavily implicated in plasma cell migration.

Initial studies by Lehmann and Harano *et al.,* have attributed levels of immune infiltration to TNBC classifications, demonstrating an enrichment in immune modulatory signatures within BL1 but a depletion in the BL2, LAR and M TNBC subtypes. AR has been shown to be expressed on multiple subsets of the lymphocytic lineage during development (Ben-Batalla et al., 2020), and as aforementioned in chapter 3, androgen signalling within the LAR subtype has been linked to CD8+ T cell exhaustion and limiting immune checkpoint blockade efficiency. Furthermore, androgens have been shown to augment the immunosuppressive function of regulatory T cells (Tregs) within mouse models of allergic airway inflammation (Gandhi et al., 2022). In contrast, few studies have investigated the role for these hormones and associated signalling pathways on terminally differentiated B cell subsets, particularly within the context of breast and other cancers. There has been a small number of studies attributing the role of androgen signalling on B cell maturation, and in this setting, mice with depleted AR expression exhibited intrinsic deficiencies in B cell tolerance, with an elevated level of autoreactive antibodies and susceptibility to developing autoimmune diseases (Altuwaijri et al., 2009). This, therefore, points to a potential role for AR and its subsequent downstream signalling in influencing antibody secreting cell (ASC) development.

Antibodies are secreted by terminally differentiated plasma cells which can arise from two pathways, namely the extrafollicular pathways or the GC response. There is debate surrounding the original paradigm that the extrafollicular pathway results in only short-lived proliferating plasmablasts whereas the GC will generate long-lived quiescent plasma cells (Kallies et al., 2004). It is now known that the lifespan and proliferation status of plasma cells can operate independently, resulting in short-lived plasmablasts and plasma cells that do not proliferate and highly proliferative long-lived plasma cells that never become quiescent (Nutt et al., 2015). These differentiation pathways further present as a continuum where canonical B cell marker expression (B220, CD19, MHC II) is gradually lost and plasma cell markers including BLIMP-1, IRF4 and CD138 are upregulated, which presents with challenges when

defining the distinction between short-lived and longer-lived plasma cells (Kallies et al., 2004). Notably, extrafollicular derived plasma cells are known to express high levels of CXCR4 at the T/B border within secondary lymphoid organs, which implicates the CXCR4/CXCL12 axis in their migration outside of a GC response. This further may imply that plasma cell infiltration within lThP tumours is recruited from an extrafollicular response.

The role of the extrafollicular and GC pathway is also related to the nature of the antigenic stimuli. Antigen can activate B cells in both a T-independent or T-dependent manner, during which T-independent responses do not require cognate T cell help, and therefore plasma cell differentiation can occur in the absence of GC formation. Within this T-independent (TI) manner, TI-1 antigens can trigger B cell activation through engagement of Toll-like receptors (TLR), including bacterial polysaccharide LPS, and TI-2 antigens that will facilitate crosslinking of the BCR, namely polymeric protein antigens or repeated structural motifs. Antigen affinity is therefore important within the TI-2 response, as competition for antigen will enhance this activation and subsequent expansion of high-affinity antibody secreting cells (Jeurissen et al., 2004; Shih et al., 2002). Whilst these pathways are considered to be a predominantly extrafollicular response, it has been shown that TI-2 and on occasion TI-1 antigens can initiate a transient GC (Lentz and Manser, 2001). Further, it has been proposed that the characteristic of the antigen is therefore not the leading determinant of the response, and instead driven primarily the B cell subsets and ancillary cells involved (Vinuesa and Chang, 2013).

In contrast, T-dependent responses will be more likely to facilitate the formation of GC, predominantly dominated by follicular B cells. Within the GC, factors including affinity will contribute towards which cells will differentiate into plasma cells, and higher affinity GC B cells will largely follow this path in comparison to those destined for a memory B cell fate. Whilst light zone (LZ) B cells will become memory B cells early in the GC reaction, plasma cells are formed later. Within the GC, cytokines, TLRs and transcription factors will further contribute to decision pathways that facilitate plasma cell production (Shinnakasu et al.,

2016). T follicular helper (Tfh) derived IL-21 is the most potent cytokine that subsequently favours plasma cell differentiation within the GCs, and is further responsible for memory B to plasma cell differentiation within the periphery (Zotos et al., 2010). BACH2, a pivotal transcription factor involved in selection within the LZ, is required for memory B cell differentiation and in conjunction with ABF-1 will prevent plasma cells from being formed (Chiu et al., 2014). In contrast, Blimp-1, XPB1 and IRF4 upregulation create a feed-forward loop that suppresses B cell signalling factors by downregulation of Pax5. XBP1 specifically will promote an unfolded protein response required to produce high levels of immunoglobulin necessary for plasma cell function (Reimold et al., 2001). Whilst plasma cell differentiation is predominantly initiated within the LZ, cells will subsequently migrate to the DZ and proliferating plasmablasts will transit out of the GC at distinct locations from extrafollicular plasma cells (Meyer-Hermann et al., 2012).

Within the context of the extrafollicular response, there is currently limited understanding as to how AR signalling may contribute to or impede the differentiation of plasma cells. However, nuclear receptors including AR have been shown to modulate responses and influence cell migration within the GC. Particularly within the T-cell compartment, they regulate T cell receptor sensitivity, cell-fate potential, metabolism, and migratory behaviour. Although acting in a diverse manner, they typically facilitate mechanisms of action by binding to DNA hormone response elements (HREs) or recruiting corepressors including nuclear corepressor (NCoR) and silencing mediator of retinoic and thyroid receptors (SMRTs). Alternatively, they are involved in recruiting co-activators such as members of the steroid receptor co-activator family (SRC). Due to the myriad of functions that can be modulated by nuclear receptors, they are often implicated in disease, ranging from autoimmunity, cancer, and type 2 diabetes (Evans and Mangelsdorf, 2014). Whilst there is substantial evidence to suggest these receptors can influence immune functions, there are few studies investigating their role in modulating GC B cells, Tfh or supporting cells including follicular dendritic cells (FDCs). Those that have been performed have implicated estrogren receptor (ER),

progesterone receptor (PR), glucocorticoid receptor (GR), mineralocorticoid receptor (MR), and crucially AR in regulating the function of these subsets and their subsequent contribution to autoimmune diseases (Olson et al., 2020). AR, in particular, has been attributed to the regulation of class switching mechanisms, ICOSL-ICOS mediated interactions between B cells and Tfh, and plasma cell responses within the GC. Furthermore, studies have suggested B cell positioning and migration within the GC to be altered in a sex-biased fashion. B cells within female mice can more efficiently position within the GCs compared to those within male, which is influenced by the binding of CCL21 to GPR174 on B cells. Supplementing female mice with testosterone subsequently mimicked male B cell migration patterns, which indicates androgen mediated mechanisms can regulate B cell positioning within the GC (Zhao et al., 2020). However, how this may influence plasma cell responses at the primary breast carcinoma is currently unknown.

Aims and objectives:

In this chapter, I explored the transcriptional profiles of lThP tumours to determine whether certain pathways and effector molecules are associated with AR signalling, and if this indirectly influences tumour progression, plasma cell differentiation and GC responses within the adjacent LNs. To confirm the expression analyses, identified features were tested in both *in vitro* and *in vivo* breast cancer models. The ultimate objective was to identify deregulated pathways that may promote plasma cell presence at the primary tumour lesion and modulate GC responses in the tumour adjacent LNs.

This enabled the:

- Characterisation of transcriptomic profiles within lThP tumours that may be associated with an inferior disease trajectory and plasma cell infiltration

- Assessment of how these genes may implicate tumour growth, plasma cell differentiation and GC formation *in vitro* and *in vivo*

The objectives were to investigate following hypothesis:

1. Do lThP tumours display deregulated pathways based on gene expression profiles that are associated with plasma cell infiltration and migration?
2. Do these genes influence plasma cell differentiation, maintenance, or immunoglobulin subtype?
3. Can these genes impact tumour growth, plasma cell differentiation and GC formation in the LNs in *in vitro* and *in vivo* breast cancer models?

5.1 lThP tumours upregulate growth factor signalling, innate immune pathways and plasma cell recruitment

First, I performed differential gene expression analyses, comparing lThP tumours with all the other groups (lTlP, hThP and hTlP combined), to provide a detailed molecularly characterisation of the lThP tumours. Genes associated with fatty acid metabolism (*HMGCS2*), lipid metabolism (*APOD*), androgen signalling *(AR, PIP*) and growth factors *IGF1*, *HGF* and *EGF* were statistically significantly increased in lThP cancer (Figure 71A-B). This was in concordance with data from chapter 3, which identified lThP patients as being predominantly of the LAR subtype. When apocrine cells are stimulated by androgens, they secrete growth factors including EGF, which subsequently promotes cell proliferation though activation of EGFR (Kolyvas et al., 2022). Further, pathway analysis using hallmark and reactome pathways demonstrated upregulation of androgen response pathways, fatty acid pathways, metabolism of lipids and downregulation of those associated with cell cycle, which is in agreement with published data profiling LAR tumours (Thompson et al., 2022). IGF1, in particular, has a role in potentiating androgen signalling through inactivation of FOXO1, an AR suppressor that directly interacts with the C-terminus in a ligand-dependent manner (Yanase and Fan, 2009). Other notable differences indicated an upregulation of genes

associated with KRAS signalling (Figure 72A). EGF and IGF1 are involved in signalling through the Ras pathway, which induces oligomerization of the EGF or IGF1 receptors and allows activation and transphosphorylation of catalytic domains. This leads to upregulation of cell growth, division, and differentiation, frequently implicated in many cancers including breast (Voudouri et al., 2015).

GSEA analysis identified immune related pathways, predominantly those associated with the innate immune system were significantly upregulated in the IThP tumours (Figure 72B). Genes included *C7*, *TLR7*, *TLR10*, *FCER1A*, *CD36*, *S100A7* and *SL100A8*. CD36 is a signalling receptor and fatty acid transporter that is expressed on many non-immune and immune cells, and can be upregulated on B cells in response to TLR signalling and fatty acid uptake (Chen et al., 2022). TLR7 in particular, is associated with the activation of autoreactive B cells, subsequent autoantibody production and has been implicated in SLE (Fillatreau et al., 2021). This is also in concordance with S100A8, another protein expressed on B cells that is associated with SLE and released in response to environmental triggers and cellular damage (Gao, 2021). Although the functional role for TLR10 is less well understood, it is highly expressed in human B cell populations (Zhang et al., 2019). FCER1A bindings to the Fc region of immunoglobulin epsilon, and has been implicated in initiating the allergic response, which may suggest IgE expression within these tumours (Froidure et al., 2016).

S100A7, also known as psoriasin, is among the most highly expressed genes in preinvasive breast cancer and a marker of poor survival when expressed in invasive disease. It has been implicated in MMTV mouse models as having a role in upregulating proliferation, tissue remodelling and recruitment of macrophages (Nasser et al. 2012). Furthermore, when analysing immune related gene sets in the previously described tonsil scRNA sequencing dataset (H. King et al., 2021) (chapter 3, section 3.14), the only significantly upregulated immune subset was macrophages (Normalized enrichment score = 1.80, adjusted $p < 0.01$). Genes implicated within this pathway included *KYNU, S100A8, S100A7, SLC40A1,*

IQGAP2, PAPSS2, and IGF1. AR has been shown to be expressed in intratumoral macrophages within breast carcinomas, which contribute to an aggressive phenotype particularly within a high androgen environment (Yamaguchi et al., 2021). Moreover, TAMs and CAFs are thought to be the major source of IGF1 within the TME, and IGF1R activation is positively correlated with advanced breast tumour stage (Ireland et al., 2018).

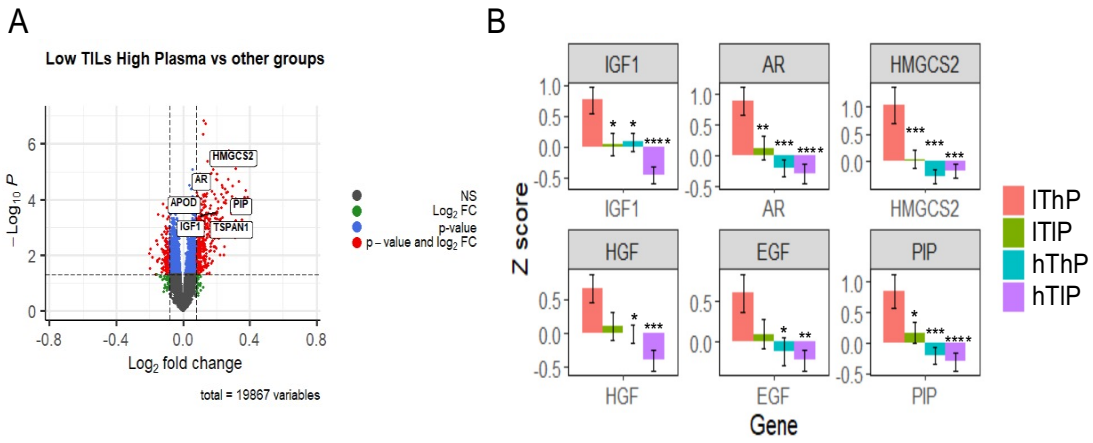

Figure 71: IThP tumours upregulate androgen receptor and growth factor gene expression. (A) Volcano plot of differentially expressed genes between IThP tumours and ITIP, hThP, hTIP combined. Grey indicates genes that are not significantly altered (NS), green indicates genes above the log2-fold change threshold, blue indicates genes above the p-value threshold and red shows genes that were above both the log2-fold change cut-off and the p-value cut-off. Genes of interest are highlighted on the plot. (B) Normalised gene expression of growth factor genes and those related to the androgen signalling pathway across IThP tumours, ITIP, hThP and hTIP tumours. Paired T tests comparing IThP to each group, * = $p < 0.05$, ** = $p < 0.01$, *** = $p < 0.001$, **** = $p < 0.0001$.

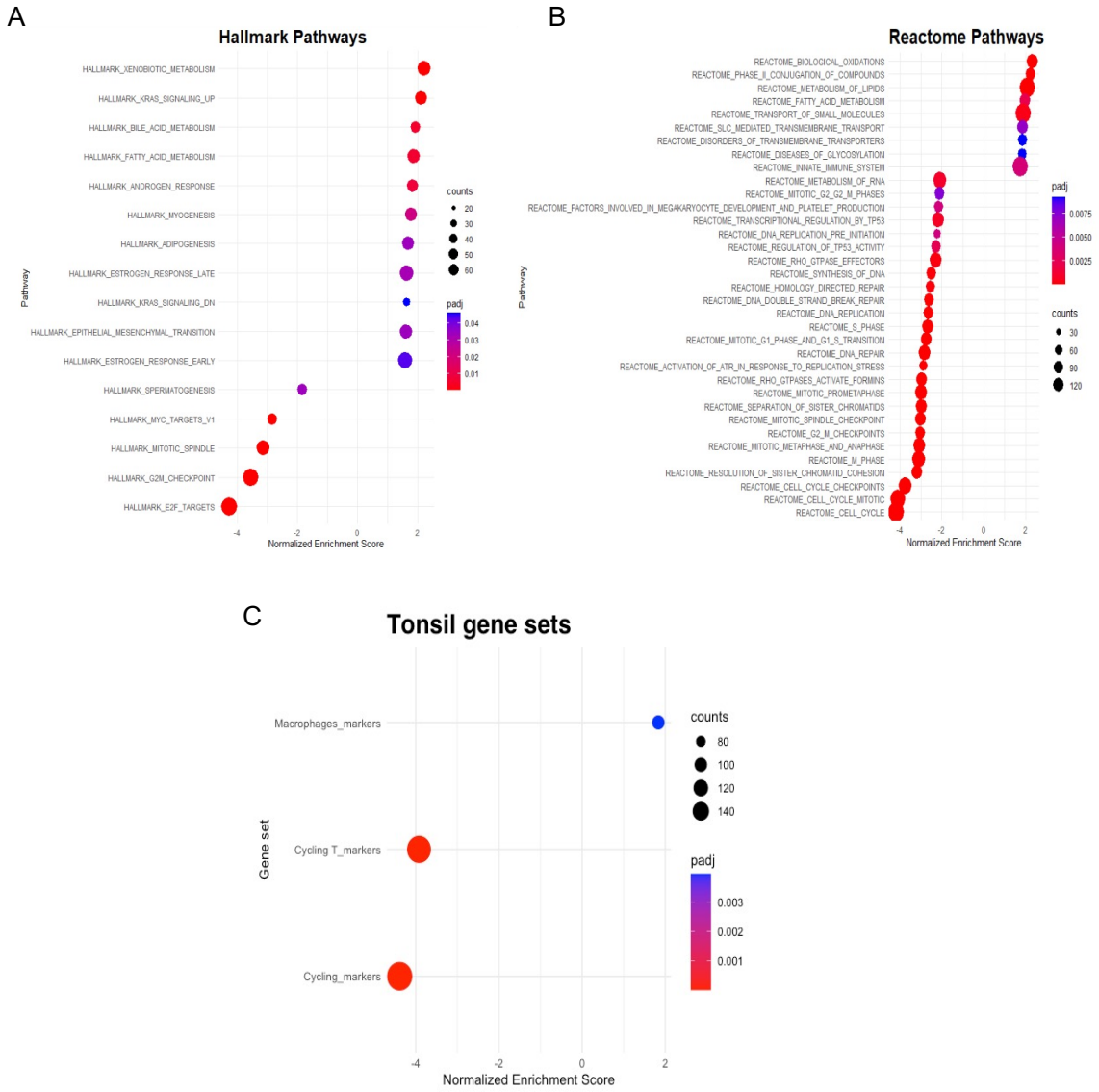

Figure 72: IThP tumours upregulate pathways associated with androgen signalling, fatty acid metabolism and innate immune signalling. Pathway enrichment analyses of differentially expressed genes (adjusted p value of < 0.05) upregulated in the IThP group, when looking at (A) hallmark pathways and (B) reactome pathways, as normalised enrichment score. The size of the circle indicates the number of genes that contribute to each pathway, coloured by the adjusted p value. (C) Gene set enrichment analysis of differentially expressed genes upregulated in IThP associated with immune cells within the tonsil dataset (H. King et al., 2021).

Within the context of plasma cell recruitment, IGF1 was further of interest due to its role in the migration of malignant myeloma cells, where it has been shown to synergise with CXCL12 and HGF *in vitro* to facilitate adhesion and movement (Rø et al., 2013). Within the IThP patients, there was a positive correlation between IGF1 and both HGF and CXCL12 ($R = 0.80$, $p < 0.001$, $R = 0.67$, $p < 0.01$ respectively) (Figure 73). This may suggest that within these tumours, there are chemokine mediated niches that could facilitate plasma cell infiltration, and innate immune upregulation that may contribute to autoantibody production and inflammation mediated signalling through IGF1.

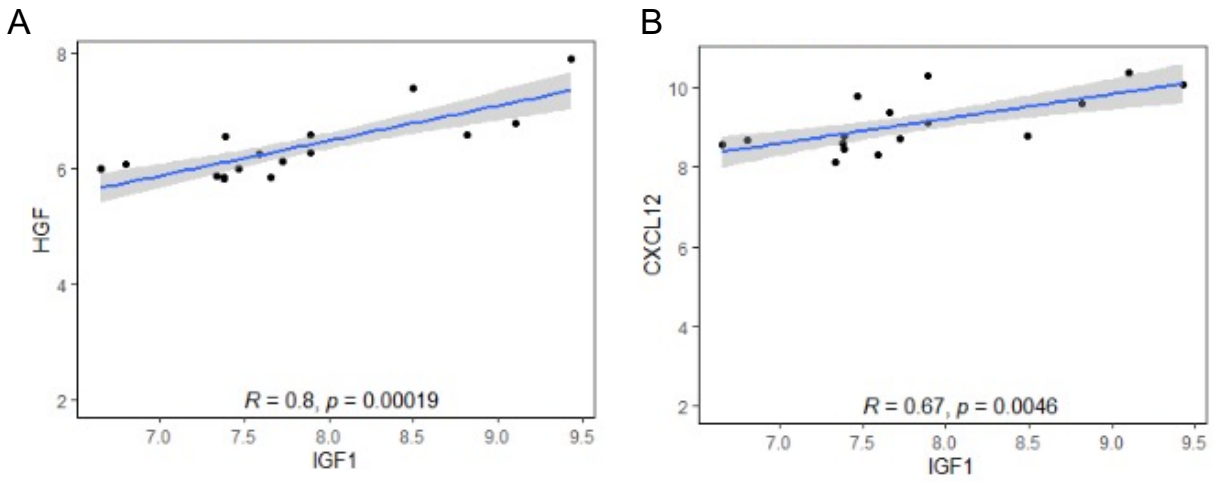

Figure 73: IGF1 expression correlates with plasma cell migration markers in IThP cancers. Spearman's rank correlation coefficient for correlations between gene expression of IGF1 with HGF expression (A) and CXCL12 expression (B).

5.2 Correlation of gene expression in iThP cancers with GC formation in adjacent lymph nodes

Next, I asked whether the expression of the differentially expressed genes upregulated in iThP cancers was correlated with histologically assessed immune responses in the patient matched LNs. Data acquired previously using a deep learning framework (Gregory Verghese and Mengyuan Li) to histologically capture and quantify GCs and sinuses within LNs was applied (Figure 74A). The mean expression of the differentially expressed genes within the lThP tumours compared to all other groups was calculated and correlated to the number of GCs within the adjacent LNs. There was a strong negative correlation between the mean expression of these genes within the tumours, and the average number of GCs within their axillary LNs (R = -0.83, p = 0.01) (Figure 74B). This is suggestive of mechanisms within the tumour microenvironment that may be repressive of GC formation within the axillary LNs.

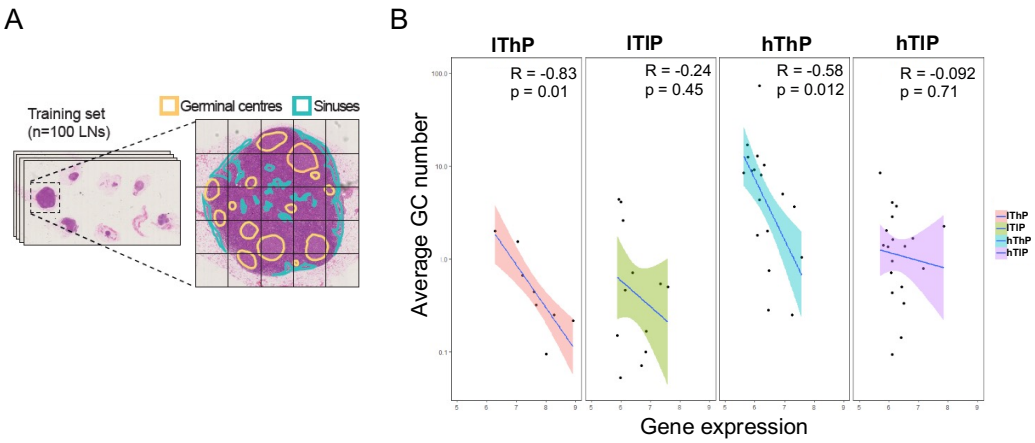

Figure 74: Genes upregulated in lThP patients negatively correlate with GC formation in the lymph nodes. (A) Schematic of deep learning methods applied to detect and quantify germinal centres(GC) and sinuses withing histological sections of lymph nodes. (B) Spearman's rank correlation coefficient for correlations between average expression of differentially expressed genes with average numbers of GCs across lThP, lTlP, hThP and hTlP tumours.

5.2.1 AR and IGF1 expression associated with a high immune-stromal-histological risk score in TNBC tumours

Our group has recently published a method for stratifying outcome within LN-positive TNBC patients based on histological features within cancer-free LNs and primary tumour. Here, features including TIL scores, lymphocytic lobulitis, and size and location of GCs within cancer-free LNs was used to develop an immune-stromal-histological (ISH) risk score (Grigoriadis et al., 2018). This revealed that patients with a low quartile ISH score had a 10-year distant metastasis free survival of 87% compared with 18% for those with an upper quartile ISH score. ISH score data was available for 49/124 TNBC patients. Assessment of IGF1 and AR expression within these patients revealed that those with a high ISH score had significantly higher expression of IGF1 (Figure 75A) (Wilcoxon rank signed test, p = 0.038 and AR (Wilcoxon rank signed test, p = 0.042) (Figure 75B) within their primary tumours compared to those with a low ISH score. This indicates that increased levels of both IGF1 and AR are associated with a cold TME and diminished LN-reactivity.

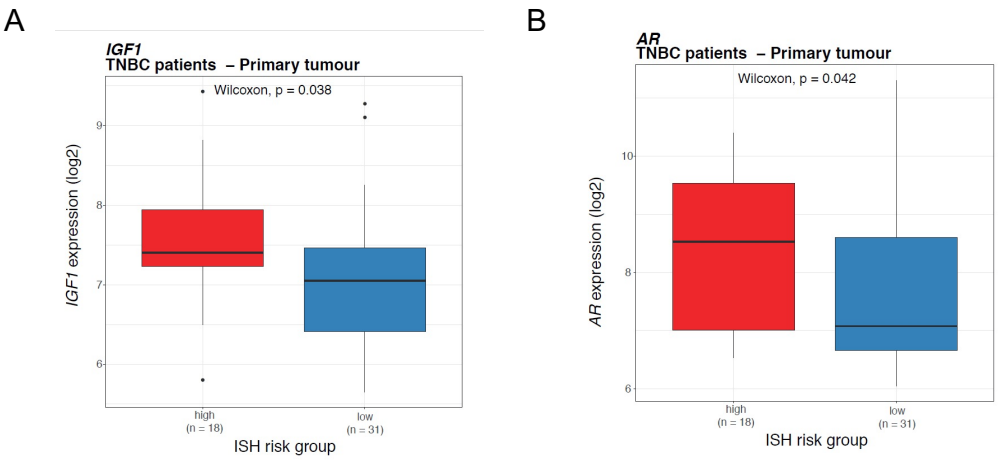

Figure 75: IGF1 and AR associated with a high-risk score in TNBC patients. Log2 expression of IGF1 (A) and AR (B) within TNBC primary tumours comparing those with a low immune-stromal-histological (ISH) score and those with a high ISH score.

5.3 Cells within the tumour microenvironment of TNBC mouse models secrete IGF1

As aforementioned, CAFs can increase tumour growth and promote breast cancer migration by secreting chemokines and pro-tumour factors including CXCL12 and IGF1 (Fernández-Nogueira et al., 2021). To examine the levels of IGF1 secreted by non-metastatic tumours vs metastatic, tumour slices from the mouse models established in chapter 3 were acquired using a vibratome. After being cultured *in vitro* for 48 hours, the supernatant was extracted for analysis via ELISA. This was compared with supernatant taken from the culture of cell lines and revealed that although the cell lines alone did not secrete IGF1. There was evidence that it was present within the secretome of the metastatic 4T1 and 4T1.2 tumours (76A-B). In contrast, IGF1 was not present within the secretome of the non-metastatic 67NR tumour slices, which may further indicate a role for IGF1 in potentiating metastasis. As there was no evidence of IGF1 within the supernatant taken from the cell lines, it was hypothesised it had been secreted by the stroma.

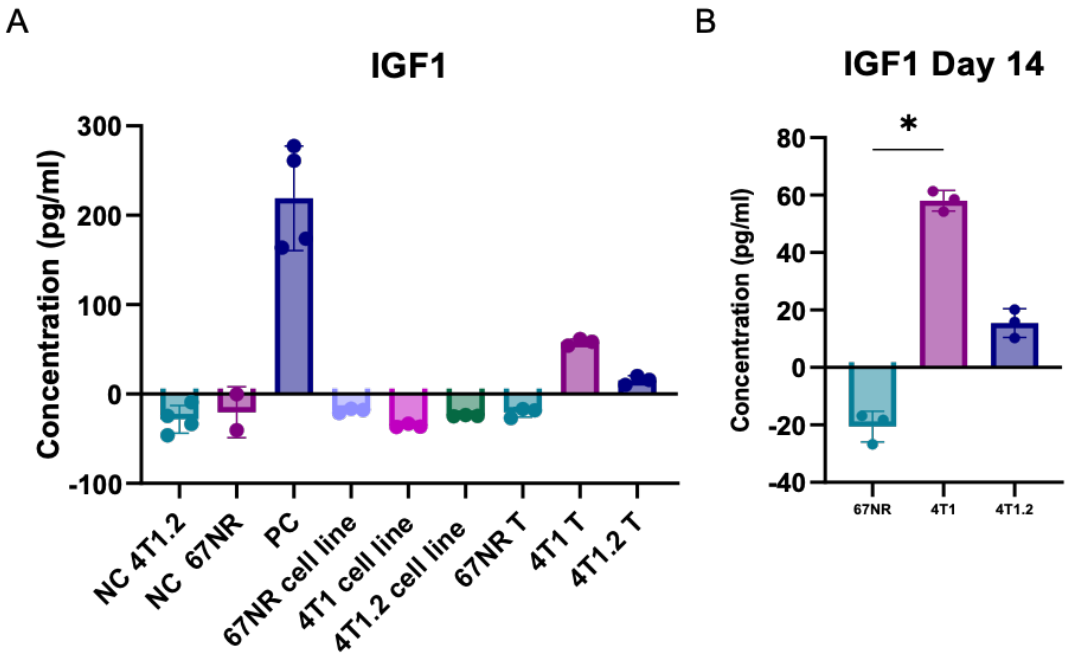

Figure 76: 4T1 and 4T1.2 tumours secrete IGF1 *in vitro*. (A) Concentration of IGF1 in secretome of 67NR, 4T1.2 (day 14) and 4T1 (day 14 & day 20). NC = negative control, PC = positive control. (B) Concentration of IGF1 in secretome of 67NR, 4T1 and 67NR at day 14. Kruskal-Wallis test, * = $p < 0.05$).

5.3.1 Overexpression of IGF1 in CAF cell lines

To validate this, a CAF cell line derived from a 4T1 tumour was kindly gifted from a collaborating group in Italy (Avalle et al. 2022). Analysis of the supernatant when the CAF cell line was cultured *in vitro* showed no evidence of IGF1 production (Figure 77A), which indicated that it is induced only within the TME. A vector construct containing the *IGF1* gene with a GFP-reporter was subsequently used to transfect the CAF cell line, and cells sorted based on GFP expression to obtain clones with the highest transfection efficiency. Further, the supernatant of the CAF cell lines was tested for IGF1, which showed those with highest GFP expression secreted the highest amount of IGF1 (Figure 77A, B).

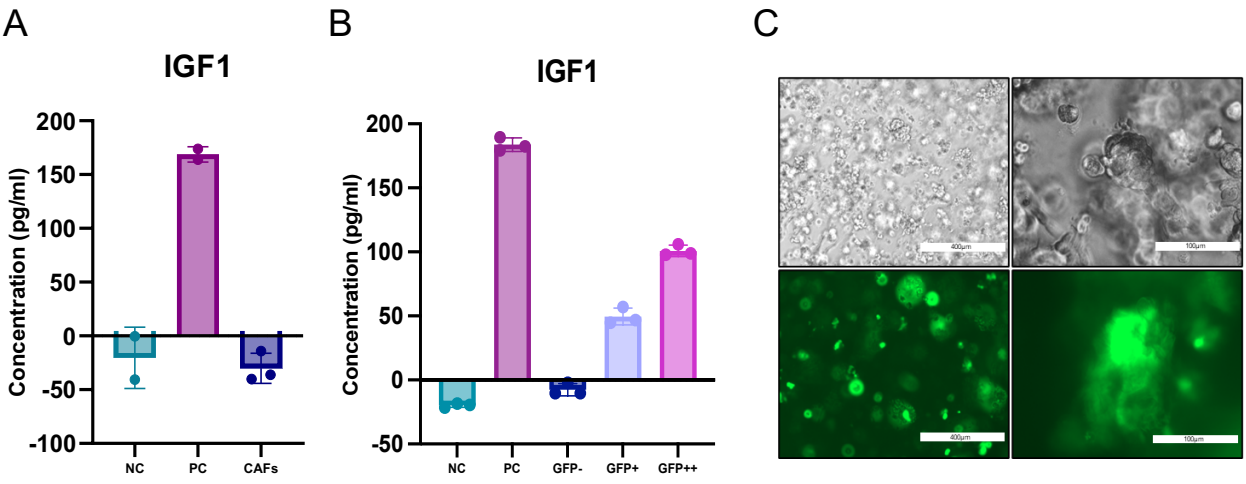

Figure 77: 4T1 and 4T1.2 tumours secrete IGF1 *in vitro*. (A) Concentration of IGF1 in secretome of CAF cell lines. NC = negative control, PC = positive control. (B) Concentration of IGF1 in the secrometome of CAF cell lines after transfection with igf1_GFP+ plasmid. NC = negative control, PC = positive control. (C) Representative EVOS images of the 4T1.2 cell line alone, cultured with an immortalised CAF cell line and when cultured with an CAF cell line transfected with IGF1 expressing GFP.

5.3.2 CAF secreted IGF1 increases tumour spheroid growth *in vitro*

To test the effect of overexpression of IGF1 *in vitro*, 4T1.2 spheroids were generated in Matrigel gels, and co-cultured with CAFs upregulating IGF1. Fluorescence imaging revealed 3D structures comprised of GFP- and GFP+ positive cells, which indicated CAF incorporation in the 4T1.2 spheroids (Figure 77C). 4T1.2 spheroids co-cultured with CAFs enhanced their growth (Kruskal-Wallis, $p < 0.01$), which was even more evident in those co-cultured with CAFs overexpressing IGF1 (Kruskal-Wallis, $p < 0.0001$) (Figure 78A-B). This implied that overexpression of IGF1 could increase both stromal and tumour growth *in vitro.*

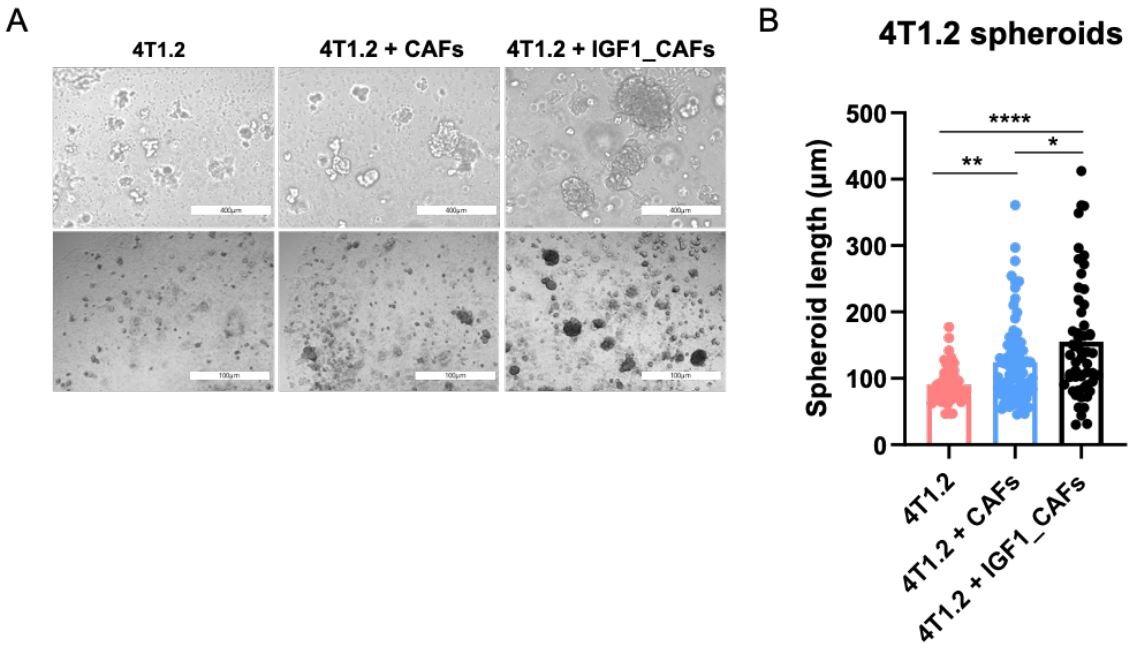

Figure 78: IGF1 increases 4T1.2 spheroid growth in vitro. (A) Representative images of 4T1.2 spheroids at day 7, when cultured alone, with immortalised cancer associated fibroblast (CAF) cells, or with CAF cells transfected with IGF1. (B) Spheroid length of 4T1.2 after 7 days in culture, when cultured alone, with CAF cells or with CAF cells transfected with IGF1.

5.4 IGF1 receptor expression within involved lymph nodes associated with distant metastasis development

To examine what role IGF1 may have on plasma cell differentiation and maturation, primary tumours and LNs from the Barts TNBC cohort were examined for expression of the IGF1 receptor (IGF1R) on plasma cells, comparing patients that developed distant metastasis and those that did not. There is conflicting literature surrounding whether IGF1R is present on normal plasma cells, but it has routinely been implicated in multiple myeloma, with high expression contributing to their proliferation, treatment resistance and a poor prognosis (Kuhn et al., 2012). There was a trend towards increased density of IGF1R+CD138+ cells within the primary tumours of patients who developed distant metastasis (Mann-Whitney U test, $p = 0.1429$) and a significant increase within the involved LNs (Mann-Whitney U test, p

< 0.05) (Figure 79A). Furthermore, IGF1R expression was evident on a small population of plasma cells present within the tumour draining LNs of 4T1.2 mice (Figure 79B).

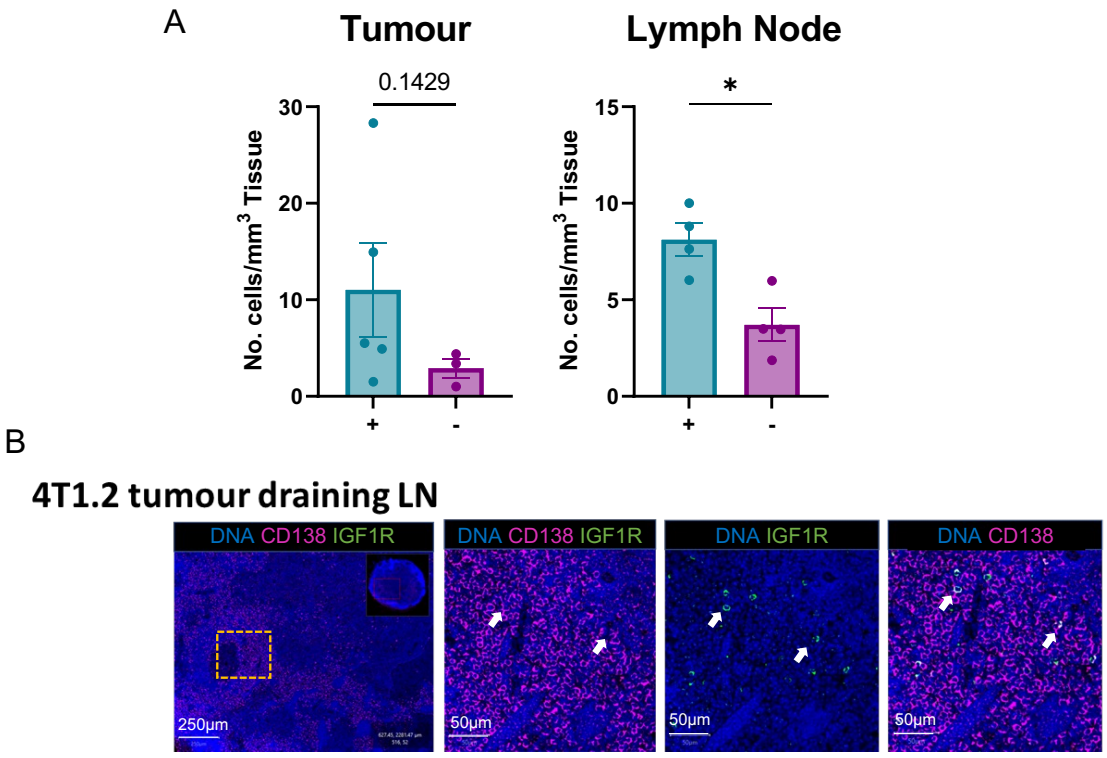

Figure 79: IGF1R+ plasma cells in involved lymph nodes associated with distance metastasis development in TNBC. (A) Number of IGF1R+CD138+ plasma cells per mm^2 tissue in human primary tumours and lymph nodes in patients who developed distant metastasis (+) and those who did not (-). Each dot represents a patient. (B) Histological staining of IGF1R (green) and CD138 (magenta) within 4T1.2 tumour draining lymph node (LN) at day 21 post implantation. White arrows indicate IGF1R+CD138+ plasma cells.

5.5 IGF1 does not increase plasma cell numbers when B cells are stimulated through Toll-like receptors

To determine if IGF1 plays a role in B cell differentiation towards a plasma cell phenotype, LN cells were extracted from wildtype BALB/c mice, the B cells isolated and incubated with, LPS, IGF1 and a combination of LPS and IGF1. LPS is a potent stimulant of B cells and will induce proliferation and differentiation into antibody secreting cells via TLR (Toll-like receptor) signalling (Venkataraman et al., 1999). After 5 days in culture, the cells were harvested for flow cytometry analysis (Figure 80A). Whilst LPS stimulation resulted in a significant increase in plasma cells as a percentage of live cells (Kruskal-Wallis, $p < 0.01$), IGF1 stimulation did not further increase the percentage of plasma cells within the B cell population compared to untreated B cells. This was also observed when B cells were stimulated with LPS and IGF1; IGF1 did not promote an additive effect to LPS (Figure 80B). This may be in part due to either the capacity of LPS to act as a potent stimulator on B cells, which may mask any responses that were due to the addition of IGF1, naïve B cells within this context do not express IGF1R, or the type of stimulation is not synergistic with IGF1 signalling.

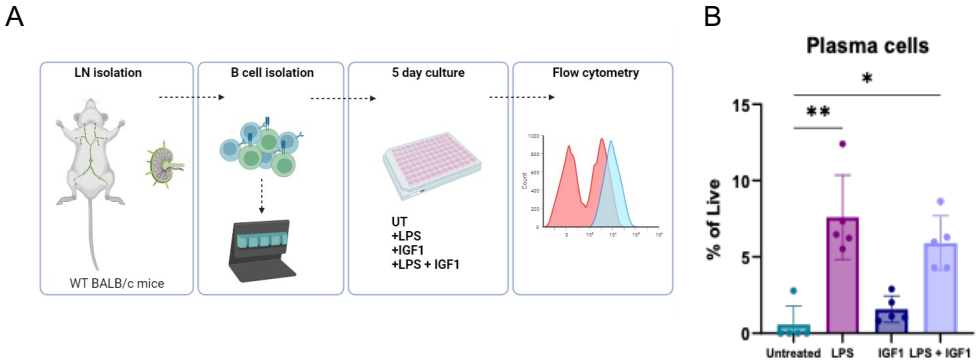

Figure 80: IGF1 does not induce B cell differentiation to plasma cells with LPS stimulation. (A) Schematic illustration of the experimental design; B cells isolated from lymph nodes (LNs) of WT BALB/c mice and treated with LPS, IGF1 or combination of both for 5 days, before analysis using flow cytometry. (B) Barplots showing CD138+B220- plasma cells as a percentage of live cells within untreated, LPS treated, IGF1 or LPS and IGF1. n = 5, Kruskal-Wallis test, * = $p < 0.05$, ** = $p < 0.01$.

5.5.1 IGF1 promotes IgM+ plasma cell differentiation after IgD crosslinking

Previous studies have suggested a role for IGF1 in T cell independent responses, and the addition of IGF1 to splenic B cells isolated from wildtype mice generated a potent IgM antibody response within the supernatant in combination with polyvalent membrane-IgD cross-linking and IL-5 (Baudler et al., 2005). This utilised IgD-dextran, which is an efficient and potent polyclonal B cell activator. The authors suggested that IGF1 was able to mimic the actions of IL-4 to promote IgM secretion *in vitro.* To test if this was due to enhanced IgM+ plasma cell differentiation, splenic B cells were isolated from wild type BALB/c mice and cultured alone, with (i) IgD-Dextran, IL-5, IGF1, individually, (ii) IgD-Dextran + IL-5, (iii) IgD-Dextran + IGF1, IL-5 + IGF1, IL-5 + IGF1, and (iv) IgD-Dextran + IL-5 + IGF1. After 4 days in culture, cells were harvested to investigate plasma cell levels, IGF1R and immunoglobulin expression (Figure 81).

B cells stimulated with IgD-Dextran, IL-5 and IGF1 exhibited a modest yet significantly higher amount of plasma cells as a percentage of live cells than IgD-Dextran and IL-5 (Figure 82A) (Kruskal-Wallis, $p < 0.05$). There was also a significant increase in the percentage of plasma cells expressing IgM (Kruskal-Wallis, $p < 0.05$) (Figure 82B-C), and an increase in IgM MFI (Kruskal-Wallis, $p < 0.05$) (Figure 80D-E). A small proportion of the plasma cells in the IgD-Dextran + IL-5 + IGF1 group expressed the IGF1R (4%), which was higher than that of those generated from IgD-Dextran + IL-5 alone (0.65%) (Kruskal-Wallis, $p < 0.05$) (Figure 83A-B). Notably, the majority of the IGF1R+ plasma cells were IgM+ (90%) (Figure 83C). Taken together, this is suggestive of IGF1 to influence plasma cell production when stimulated through IgD-crosslinking and facilitate an IgM+ phenotype. Within the context of the lThP TNBC patients, this may be indicative of an environment that favours IgM+ immunoglobulin production over other isotypes and potentially resulting in an inferior disease progression.

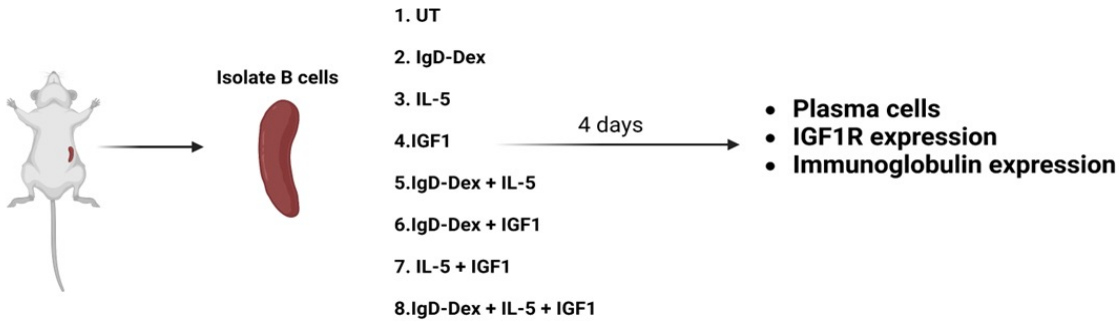

Figure 81: Schematic illustration of IgD-dextran stimulation on splenic B cells. B cells were isolated from the spleens of wild type BALB/c mice and then treated with IgD-dextran and combinations of IGF1 and IL-5. Cells were cultured for 4 days and then analysed for plasma cell production, IGF1R expression and immunoglobulin isotype.

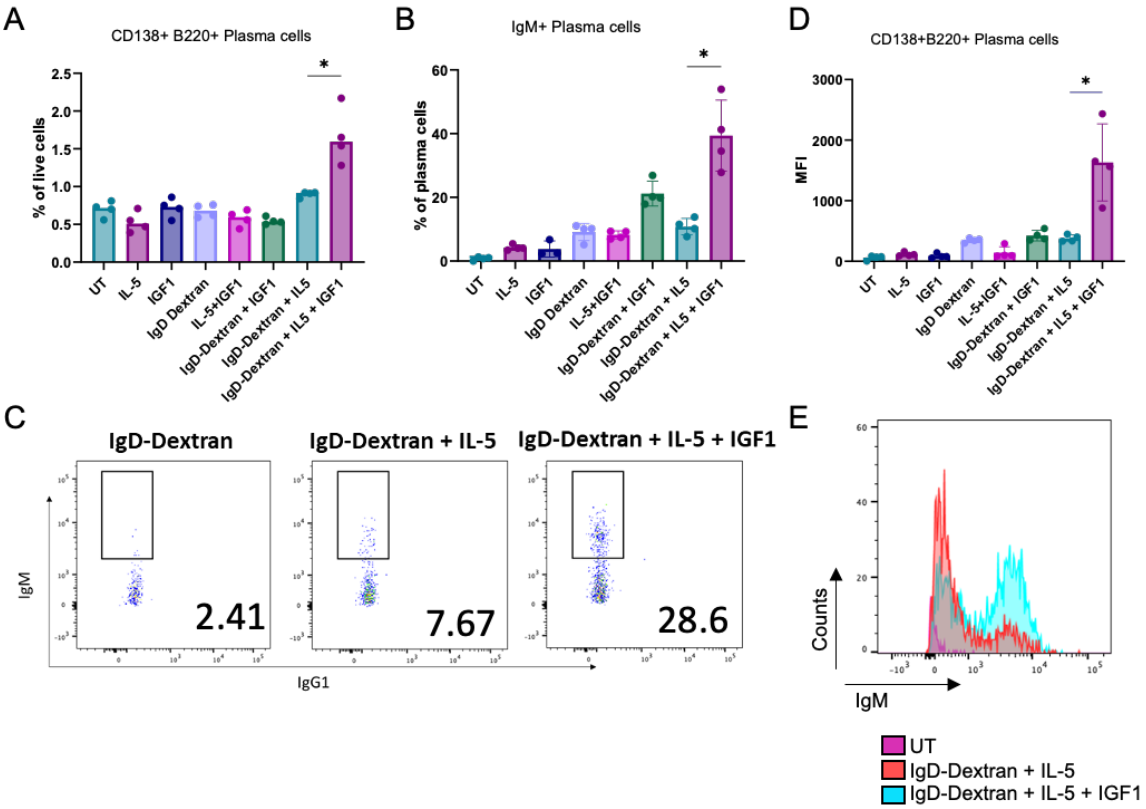

Figure 82: IGF1 and IgD crosslinking in combination induces IgM+B220+ plasma cells *in vitro*. (A) B220+ plasma cells as a percentage of live cells within each treatment condition. (B) The percentage of IgM+ plasma cells as a percentage of plasma cells within each treatment condition. (C) Median fluorescence intensity (MFI) of IgM on B220+CD138+ cells within each treatment condition. (D) Representative flow cytometry plots of IgD-Dextran treated, IgD-Dextran + IL-5 and IgD-Dextran + IL-5 + IGF1 IgM+ plasma cells 4 days post stimulation. Always add the number of samples, and which test you used for analyses (E) Representative median fluorescence intensity of IgM on B220+CD138+ plasma cells within untreated cells (UT) (purple), those treated with IgD-Dextran + IL-5 (red), and those treated with IgD-Dextran, IL-5 and IGF1 (blue).

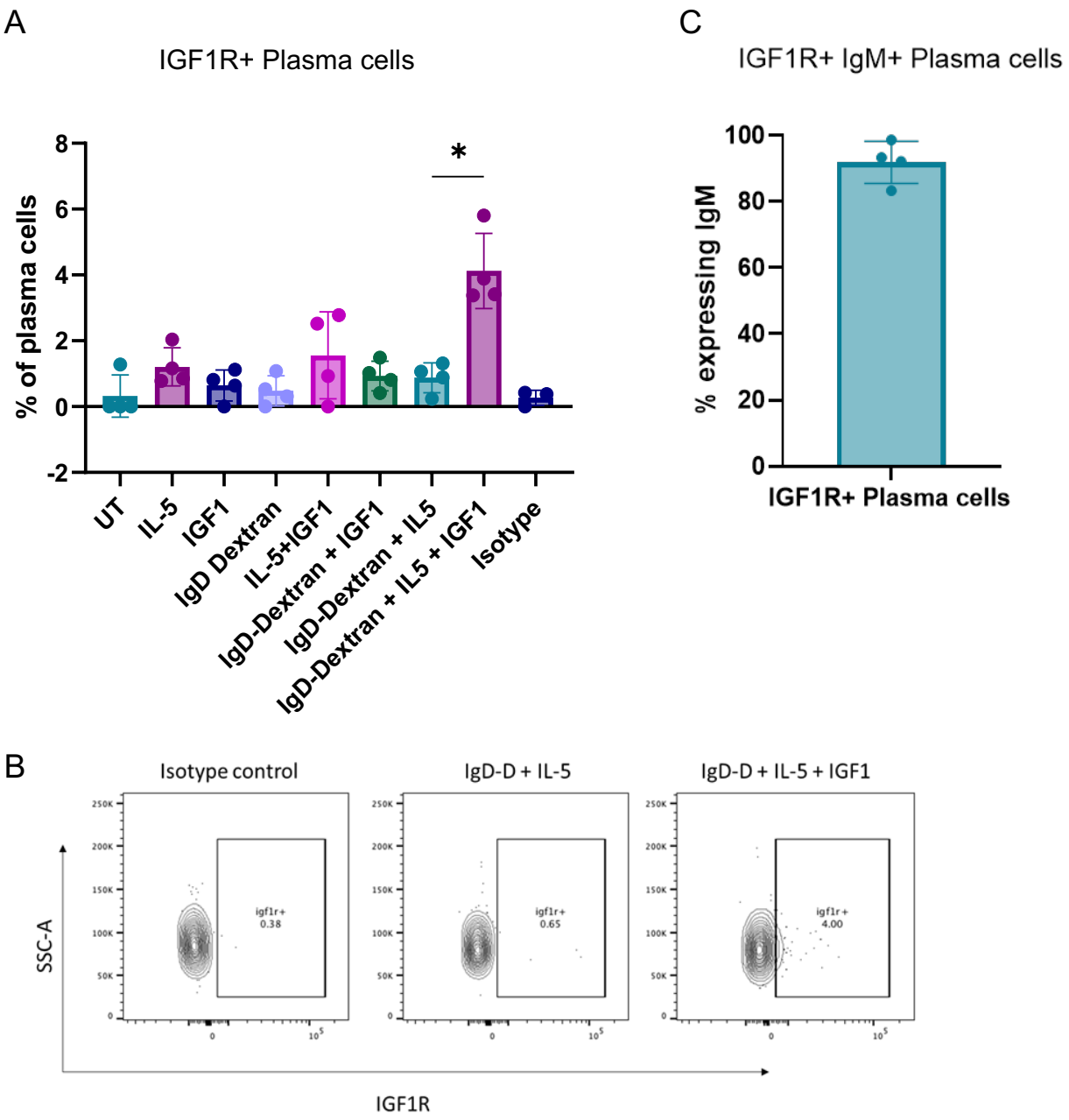

Figure 83: IGF1 treated IgM+ plasma cells upregulate IGF1R. (A) IGF1R+ plasma cells as a percentage of total plasma cells within all conditions. (B) Representative flow cytometry plots of IGF1R expression within plasma cells stained with an isotype control, treated with IgD-Dextran + IL-5, and treated with IgD-Dextran, IL-5 and IGF1. (C) The percentage of IGF1R+ plasma cells expressing IgM after treatment with IgD-Dextran, IL-5, and IGF1.

5.5.2 IGF1 and IL-5 stimulate IGF1 production by B cells *in vitro*

Whilst most of the current literature implicates epithelial and stromal cell populations as the primary contenders for IGF1 production in both a healthy and diseased setting(Laron, 2001; Sprynski et al., 2009). Somasundaram *et al.*, described mechanisms of acquired therapy resistance in the tumour microenvironment mediated by tumour-associated B cells. They showed that constitutive secretion of FGF-2 by melanoma cells stimulated tumour infiltrating B cells to produce IGF1 (Somasundaram et al., 2017). Whilst FGF-2 was not added in these experiments, analysis of the supernatant the B cells treated with combinations of IgD-dextran, IL-4, IL-5 and IGF1 by ELISA (Figure 84A) revealed that the addition of IL-5 and IGF1 to naïve B cells increased the IGF1 production *in vitro* (Figure 84B). This suggests that IGF1 may act in an autocrine fashion on B cells in the same way that is has been shown to do so on stromal and tumour cells. Thus, it may act as a contributor within IThP tumours to modulate B cell and plasma cell responses.

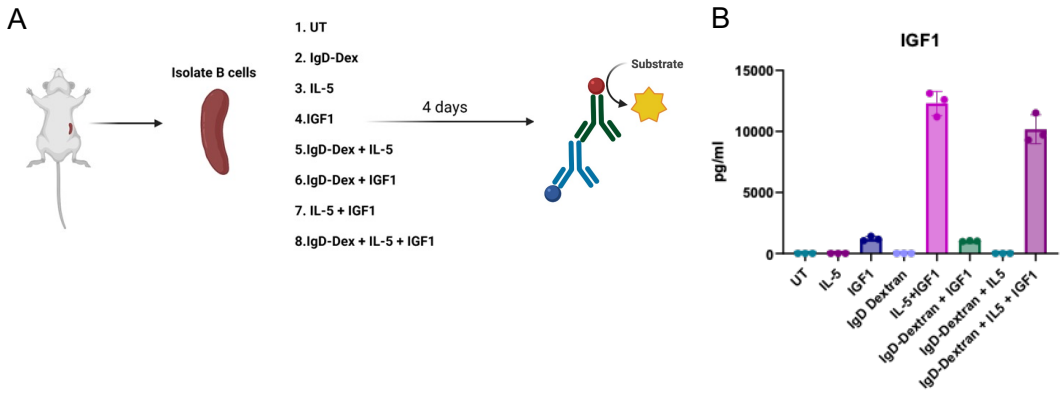

Figure 84: IL-5 and IGF1 induce B cell production of IGF1 *in vitro.* (A) Schematic illustration of stimulation of splenic B cells isolated from wild type BALB/c mice and then treated with IgD-dextran and combinations of IGF1 and IL-5. Cells were cultured for 4 days and then the supernatant analysed by ELISA. (B) The concentration of IGF1 within the supernatant of cells treated with media alone, IL-5, IGF1, IgD-Dextran, IL-5+ IGF1, IgD-Dextran + IGF1, IgD-Dextran + IL-5 and IgD-Dextran + IL-5 + IGF1.

5.6 IGF1 treatment increases tumour growth in 67NR mice

Finally, to assess the impact of IGF1 *in vivo*, the 67NR model was utilised due to its slow tumour growth and lack of plasma cell presence. I hypothesised that IGF1 could accelerate tumour growth, suppress GC formation in LNs, and enhance IgM+ plasma cell populations at the primary tumour site. Mice were inoculated with 67NR cell lines, before daily administration of 10ug/ml of IGF1 or PBS control subcutaneously to the mammary fat pad. Due to an unexpected inflammatory response at the injection site, this was reduced to every other day for the next 5 days until day 10. Tumours were then allowed to grow until harvesting of non-draining LNs (nd-LNs) and tumour draining LNs (td-LNs) at day 21 for flow cytometry analyses (Figure 85). IGF1 treated mice exhibited weight loss that was significant at day 8 (Mann-Whitney U test, $p < 0.05$) but stabilised by day 10 (Figure 86A). IGF1 treated tumours exhibited an initial increased in tumour growth compared to control tumours at day 17 (Mann-Whitney U test, $p < 0.05$), but when harvested at day 21, there were no differences between IGF1, and control treated tumours (Figure 86B).

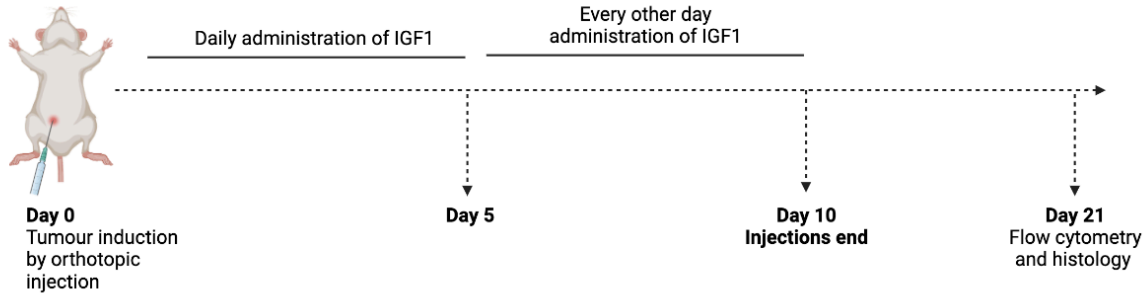

Figure 85: Experimental design of IGF1 treatment *in vivo*. Wild type BALB/c mice were implanted with the 67NR cell line, before daily subcutaneous administration of IGF1 for 5 days, following by dosages every other day until day 10. Tumours were allowed to grow till day 21 and lymph nodes isolated for analysis by flow cytometry and histology.

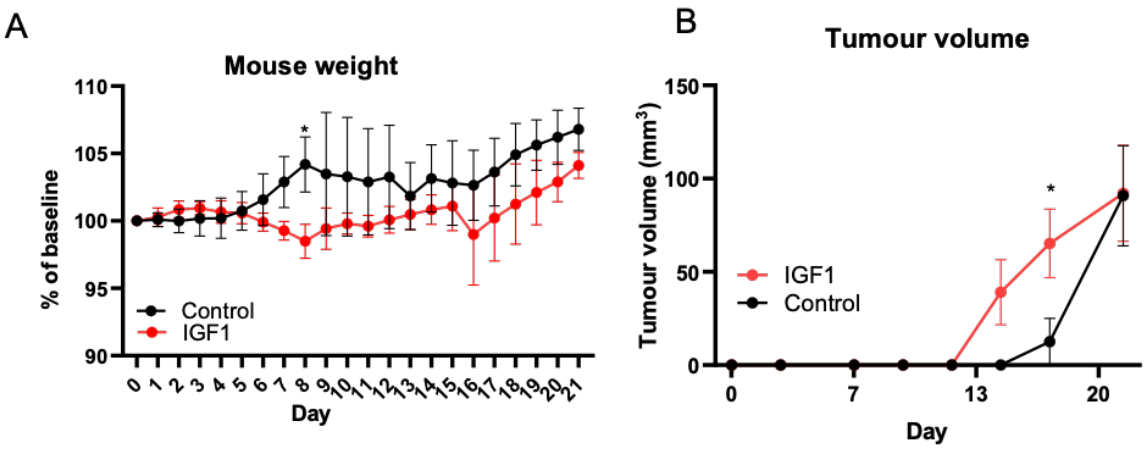

Figure 86: IGF1 treatment induces early weight loss and increased tumour growth. (A) The weight of each mouse as a percentage of baseline weight from day 0 to day 21, control group shown in black and those treated with IGF1 shown in red. (B) Tumour volume in control mice (black) compared with those treated with IGF1 (red).

5.6.1 IGF1 treatment depletes GC B cells without affecting plasma cells percentage in td-LNs of 67NR mice

To determine if IGF1 treatment impacted immune GC B cells and plasma cells within the adjacent LNs nd-LNs and td-LNs were extracted at day 21 before processing and analysis via flow cytometry. GC B cells (defined as $CD38^{low}$ $CD95/Fas^{high}$) as a percentage of B cells were significantly depleted in the td-LNs of IGF1 treated mice compared to control mice (Kruskal-Wallis, $p < 0.05$). (Figure 87A, C). Plasma cells, as a percentage of live cells were unchanged between control and IGF1 treated mice, and there was no difference in the percentage of plasma cells expressing IgM or IgG1 (Figure 88A-D). This suggests that IGF1 may have a role in suppressing the antigenic stimulation required to initiate a GC response or is in part responsible for GC collapse. Since there was no significant increase in plasma cells, IGF1 alone may not induce directly a plasma cell response. As seen in chapter 3, several dysfunctional mechanisms can occur within GC and within LNs that prevent the production of plasma cells.

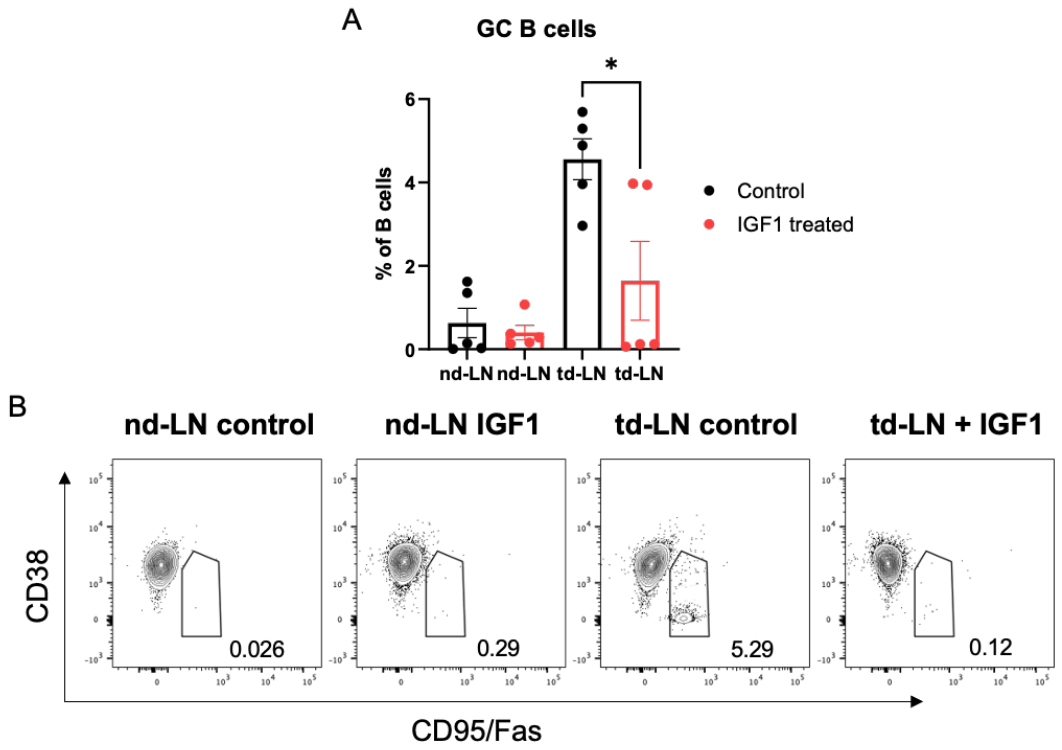

Figure 87: IGF1 treatment reduces GC B cell formation in td-LNs of 67NR mice. (A) GC B cells as a percentage of B cells within non-draining LNs (nd-LN) and tumour draining lymph nodes (td-LN) of control 67NR mice (black) and 67NR mice treated with IGF1(red). Kruskal-Wallis test. * = $p < 0.05$). (B) Representative flow cytometry plots of $CD38^{low}CD95/Fas^{high}$ GC B cells from nd-LNs and td-LNs from control 67NR and 67NR mice treated with IGF1.

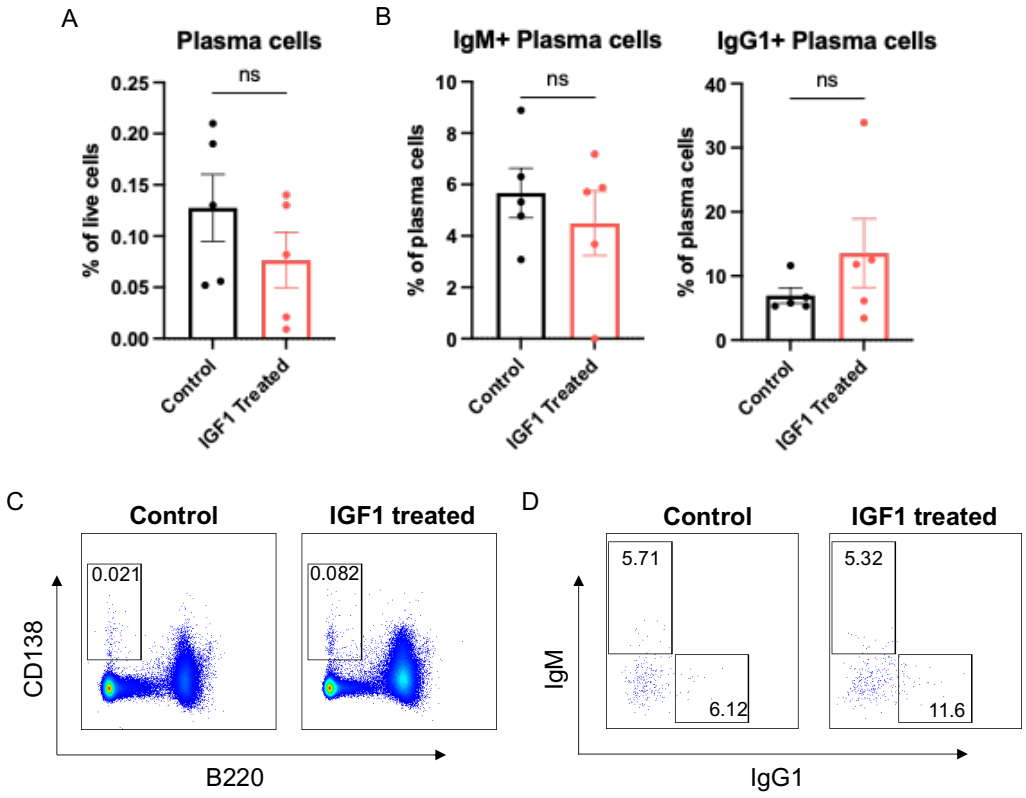

Figure 88: IGF1 administration does not affect plasma cell production in 67NR model. (A) Plasma cells as a percentage of live cells within 67NR control mice and 67NR mice treated with IGF1. (B) IgM+ plasma cells as a percentage of plasma cells within 67NR control mice and 67NR mice treated with IGF1 (Mann-Whitney U tests used for statistical testing between control and IGF1 treated results). (C) Representative flow cytometry plots of plasma cells in 67NR control mice and mice treated with IGF1. (D) Representative flow cytometry plots of IgM+ and IgG1+ plasma cells in 67NR control mice and 67NR mice treated with IGF1.

5.7 Discussion

In this chapter, gene expression analyses were performed on lThP TNBC tumours to delineate differentially expressed genes and upregulated pathways that may be associated with a low sTILs and high plasma cell infiltration phenotype. Further, expression of these genes and associated pathways were correlated with the numbers of GCs within adjacent LNs to investigate if there may be a potential relationship between the upregulated genes within the tumours of this subgroup of patients and GC response within the LNs.

Genes of interest, namely IGF1, due to its previous association with plasma cell development (Sprynski et al., 2009), was investigated further to delineate how it may contribute towards B cell differentiation towards a plasma cell phenotype, and if plasma cells may express the receptor which would imply ability to respond to IGF1.

Finally, the impact of IGF1 was tested *in vivo* to determine the impact of IGF1 on tumour growth and plasma cell secretion within the td-LNs of mice inoculated with the 67NR mice. The hypothesis was that IGF1 may hold immunosuppressive properties, and its increased present within the tumour can prevent or suppress sufficient GC derived B cell responses within the adjacent LNs.

Differential gene expression was performed on lThP TNBC tumours from the Guy's cohort compared to all the others combined (lTlP, hThP, hTlP). This revealed an upregulation in genes associated with androgen signalling, fatty acid metabolism and growth factors; IGF1, HGF and EGF. This was reflective of the previous data in chapter 3, section 3.10.3 showing that lThP patients were predominantly of the LAR subtype compared to other TNBC classifications, and the impact that androgens have on breast cancer progression and plasma cell infiltration has been discussed previously. Other notable enriched pathways within lThP patients included that of KRAS signalling, adipogenesis, epithelial mesenchymal transition (EMT) and estrogen responses. Within breast cancer, induction of CYP1 enzymes in human mammary epithelial cells can increase the metabolic activation of potential breast

carcinogenic factors and facilitate tumour growth (Williams and Phillips, 2000). Xenobiotic metabolism has further been implicated within colorectal cancer and shown to promote T cell mediated exhaustion and apoptosis within the TME, resulting in these cells upregulating checkpoint markers PD-1 and LAG-3 (Wen and Han, 2021). Whilst this link has not been extensively discussed within breast cancer, it is likely that this is a mechanism that promotes an environment within LAR tumours that supports minimal sTIL infiltration and/or immune cell death.

The upregulation of KRAS signalling is more prominently observed in cancers that exhibit high KRAS mutations, including pancreatic and non-small cell lung cancer (NSCLC) (Xie et al., 2021), however than 2% of all breast cancers have KRAS mutations, and activation is typically associated with a mesenchymal phenotype and potent regulator of metastatic behaviour (Kim et al., 2015).

Supporting an increase in LN involvement within these patients, lThP tumours upregulated pathways associated with EMT, which is implicated frequently in TNBC and other cancers, enhancing mobility, invasion, and resistance to apoptosis. TGF-β, a cytokine secreted also by CAFs, is frequently reported to be upregulated in LAR tumours and a potent stimulator of EMT. TGF-β induced EMT can acquire properties that allow dissemination throughout that lymphatic system in a targeted fashion similar to activated dendritic cells (Karlsson et al., 2017). Whilst the ways in which tumour secreted factors may modulate B cell and plasma cell infiltration are yet to be concretely defined, Khadri *et al.,* demonstrated a strong association between tumour infiltrating plasma cells and EMT related markers, such as EpCAM and Vimentin, within the TME of breast cancer patients (Khadri et al., 2021). Further, studies have implicated miR-210, shown to orchestrate metastasis and tumour cell renewal (Tang et al., 2018) in the regulation of B and plasma cells, with tumour infiltrating plasma cells in TNBC expressing high levels of miR-210 compared to those in non-tumoral tissues. A hypoxic environment often present within tumours and may regulate the ability of plasma cells to secrete antibody efficiently within the TME (Laron, 2001). Within lThP TNBC,

this is perhaps a factor that needs to be considered to delineate further the functionality of plasma cells within low sTILs patients (Bar et al., 2020). LAR samples amongst the lThP TNBC also exhibited a downregulation of genes involved in cell cycle pathways (G2M_Checkpoint and E2F_Targets). Downregulation of these pathways is associated with a reduced response rate to neoadjuvant chemotherapy (Thompson et al., 2022).

The upregulation of innate immune related genes within lThP tumours, namely TLR7 suggests a potential pathway of plasma cell differentiation. DN 2 B cells originate from the extrafollicular areas within secondary lymphoid organs and may be associated with B cell exhaustion and dysfunction. Upon stimulation with TLR7, IL-21, IFN-γ, DN B cells rapidly differentiate into plasma cells in the absence of a GC response (Fillatreau et al., 2021). This in turn further strengthens my hypothesise that plasma cell infiltration could originate from an extrafollicular or exhausted pathway. Subsequently, these plasma cells are a bystander of an active immune response and secrete insufficiently class switched antibodies against tumour-associated antigens.

My research focused on the upregulation of growth factors prevalent within lThP tumours, explicitly IGF1. IGF1 was of interest due to its modulation of plasma cell responses in multiple myeloma and modulation activity of the AR signalling pathway (Sprynski et al., 2009). IGF1, also known as somatomedin C, is a hormone that is molecularly akin to insulin and plays a major role in early growth and anabolism in adults (Laron, 2001). It is primarily produced by the liver, stimulated by growth hormone (GH) and is the most potent natural activator of the AKT signalling pathway (Zheng and Quirion, 2006). As a major growth factor, it is responsible for stimulating growth of all cell types and has, therefore, emerged as a player in cancer development. In addition to direct contribution of malignant transformation, tumour growth, local invasion, and distant metastasis, it can indirectly interact with oncogenes, tumour suppressors and hormones (Larsson et al., 2005). Within breast cancer, *IGF1R* is overexpressed in malignant cells compared to normal breast, and IGF1 synergizes with ER to promote tumour progression (Voudouri et al., 2015). As aforementioned, IGF1

can prevent FOXO1 mediated inhibition of AR through direct competition, and induce signalling of androgens and other sex hormones (Yanase and Fan, 2009).

Within the B cell field, IGF1 has primarily been implicated at the primary B cell lymphopoieses stage, secreted by bone marrow stromal cells to regulate the B pro-cell stage (Landreth et al., 1992). However, recent studies have identified *IGF1* mRNA within macrophages and follicular dendritic cells of secondary lymphoid organs, where it can exert paracrine effects on B cells (Oberlin et al., 2009). This suggests a role for IGF1 in the modulation of B cells within the GC reactions, as follicular dendritic cells play a key part in antigen presentation within the LZ of the GC. Furthermore, the expression of upregulated genes within IThP tumours exhibited a strong negative correlation with the average number of GCs within the adjacent LNs and both IGF1 and AR expression were associated with a high ISH risk score. IGF1 has been shown to promote immunosuppression via the STAT3 pathway, and is further implicated in cellular senescence, chronic inflammation, and accelerated aging (Bartke et al., 2003). It can subsequently enhance IL-10 secretion in monocytes, stimulate the expansion of Tregs, and polarise macrophages from an M1 to M2 phenotype (Salminen et al., 2021). Taken together, this is perhaps reflective of a TME that is unable to deliver adequate antigen presentation, and immune cell stimulation required to generate a GC response within the adjacent LNs. With regards to plasma cell regulation, IGF1 may synergise with HGF and CXCL12 to induce their migration (Kuhn et al., 2012). Although these studies have primarily investigated the impact of IGF1 on malignant plasma cells, the correlation between these factors may be recapitulating a similar IGF1-high environment within the tumour that promotes plasma cell infiltration through the CXCL12/CXCR4 axis. As there are indications that the TME within IThP tumours is highly immunosuppressive, this points to either the plasma cell infiltration as dysfunctional and either acting as a bystander, or in some way contributing to a pro-tumour environment.

In concordance with levels of IGF1 being associated with more aggressive characteristics, the metastatic 4T1 and 4T1.2 tumour slices secreted IGF1 *ex vivo*, but not the non-

metastatic 67NR. Although it was surprising that a higher level was observed in the 4T1 supernatant compared to the 4T1.2, as the 4T1.2 exerts the most aggressive features (Figure 54). This may be since only one tumour slice was examined and may not be reflective of the whole secretome. It was, therefore, possible to recapitulate this data *in vitro*, whereby the addition of IGF1 secreting CAFs significantly increased the size of 4T1.2 spheroids compared to those not secreting IGF1. Whilst it is possible the IGF1 is exhibiting both paracrine and autocrine effects on the tumour cells and stromal cells respectively, *in vivo* studies further confirmed that the addition of IGF1 could temporarily enhance tumour growth. The lack of difference in tumour mass at the end of the study could possibly be attributed that IGF1 administration was stopped at day 10 of the experiment and was no longer exerting the same pro-tumoral growth affects by day 21 when organs were harvested.

IGF1R was also found to be expressed on a fraction of plasma cells within the tumour and involved LNs of breast cancer patients, and within the tumour draining LNs of the 4T1.2 mode. Although current data has not analysed the expression of IGF1R within this context, studies have suggested that plasma cells do not express IGF1R, however it is aberrantly expressed by 31%-50% of malignant myeloma cells (Sprynski et al., 2009). IGF1R in peripheral blood leukocytes of rheumatoid arthritis patients is directly correlated to higher disease activity, and the IGF1/IGF1R axis has been implicated in tolerance mechanisms within the spleens of mBSA-immunised mice (Erlandsson et al., 2022). Whilst no significant differences were found within the tumours, there was a suggestion that an increased prevalence of IGF1R+ plasma cells within the involved LNs of breast cancer patients was associated with distant metastasis development. Despite lack of functional studies, it may indicate that the plasma cell formation within these patients is improperly directed against tumour antigen and signalling through IGF1 may affect the clearance of tumour cells within the LNs, leading to distant metastasis development.

This may also be attributed to an increased production of IgM+ plasma cells compared to other immunoglobulin subtypes. IGF1 can upregulate overall antibody production in mice, but can also modulate class switching (Robbins et al., 1994). Yang *et al.,* have suggested that inhibiting IGF1R resulted in reduced IgM production, which would suggest that increased IGF1 would stimulate the production of IgM+ plasma cells. In concordance with this, the most notable effect seen on plasma cells *in vitro* after addition of IGF1 was a significant increase in IgM+ plasma cells and an upregulate in surface IgM, which encompassed 90% of IGF1R+ plasma cells. These differences were only observed with the addition of IL-5, and is in concordance with findings from Baudler *et al,* who speculated that IGF1 can mimic IL-4 and synergise with IL-5 to enhance a IgD-dextran stimulated IgM production in purified B cells (Baudler et al., 2005). IL-5 is a T-helper 2 cytokine that has been implicated in the pathogenesis of many allergic inflammatory responses, however its role in tumour biology has only more recently been investigated. Breast carcinomas exhibiting higher levels of IL-5 has been linked to metalloprotease-11 (MMP-11) expression, and an increased prevalence of distant metastasis development (Eiró et al., 2012). Furthermore, IL-5 can facilitate a favourable environment for lung colonization by tumour cells by recruiting sentinel inflammatory cells from the microenvironment of the distal lung (Zaynagetdinov et al., 2015), which may suggest this is a mechanism by which IL-5 and IGF1 can promote distant metastasis. Unexpectedly, the addition of IGF1 and IL-5 also stimulated the production of IGF1 from purified B cells. Although this has not been recognised within breast tumours, Somasundaram *et al.,* have implicated B cell derived IGF1 in resistance of melanomas to BRAF and MEK inhibitors. Here, they showed that tumour derived FGF-2 induced tumour infiltrated B cells to secrete IGF1. This subsequently induced a heterogenous tumour subpopulation with cancer stem-cell like characteristics and conferred therapy resistance (Somasundaram et al., 2017). Moreover, loss of *FGFR2* in prostate epithelial cells can inhibit response to androgens and FGFR2 may be therefore upregulated within LAR tumours. Taken together, this may suggest that a IGF1 within the tumour microenvironment of lThP tumours may synergise with IL-5 to favour the expansion

of IgM+ plasma cells over other immunoglobulin isotypes, including IgG, which is not conducive to an anti-tumour response. Further, the crosstalk between IGF1, IL-5 and other possible factors including FGF2 may promote a paracrine secretion of IGF1 by tumour infiltrating B cells, which in turn promote plasma cell production and modulates the characteristics of malignant epithelial cells.

Baudler *et al.,* also showed that IGF1 was an important regulator of functional T-independent B cell responses, which would therefore suggest that the IGF1/IGF1R axis predominantly promotes antibody responses in extrafollicular regions of secondary lymphoid organs. Whilst here there were no changes seen to the percentage of plasma cells produced within the td-LNs of the 67NR model, there was significant reduction in the percentage of GC B cells. This may suggest that the B cell development within IGF1 treated 67NR mice is being suppressed or diverted towards a T independent response and no longer supports the formation of a GC. As aforementioned, the lack of plasma cell production in control mice and IGF1 mice, may be indicative of other immunosuppressive mechanisms that prevent plasma cell development that cannot be overcome solely by the addition of IGF1. This therefore suggests that the addition of IGF1 *in vivo* is reflective of the observation of reduced numbers of GCs within the adjacent LNs of lThP patients and requires further investigation to delineate the mechanisms behind which this suppression is facilitated.

In summary, data within this chapter has highlighted the potential drivers within LAR tumours, including upregulation of growth factors and innate immune subsets that may be attributed to heightened plasma cell infiltration and impacting the formation of GCs within adjacent LNs. In particular this data attributed growth factor IGF1 as being correlated to several genes that are involved in plasma cell migration and has been previously implicated in multiple myeloma. Subsequent data revealed that the expression of the IGF1R on plasma cells within involved LNs was associated with distant metastasis development. Preliminary data implicated IGF1 in promoting an IgM plasma cell phenotype, although this was not recapitulated *in vivo.* Furthermore, IGF1 was secreted by metastatic tumours 4T1 and 4T1.2

but the not non-metastatic 67NR, and upregulation promoted tumour growth *in vitro* and *in vivo.*

5.8 Limitations and future work

One of the main limitations of this work was the fact that further tissue samples from tumours that were taken for gene expression data were not available. This would allow further profiling of the LAR tumours for IGF1R+ plasma cell prevalence using more high throughput analysis including IMC, flow cytometry of single cell RNA sequencing, and therefore would identify if there were clonally related cells within the primary tumour and adjacent LNs. This would also identify the levels of somatic hypermutation and gene expression profiles that may indicate whether these plasma cells originated from an extrafollicular or GC response.

Another limitation is that the chemotactic effect of IGF1 was not tested. It is perhaps that the plasma cell infiltration is simply a bystander due to the elevated levels of chemokines including CXCL12 that are implicated in the migration of plasma cells. Therefore, it would be important to delineate whether IGF1 can induce plasma cell infiltration towards a heightened androgen environment and subsequently LAR tumours.

Despite evidence that IGF1 secretion was evident within 4T1 and 4T1.2 tumours, it would be important to determine from which cell type it originated from. Culturing of tumour and stromal cell populations separately would therefore identify which cell type was more likely to secrete IGF1 within this setting. This would pave the way for *in vivo* experiments, where IGF1 was knocked down or knocked out, to test how this affected plasma cell production and metastasis development.

Within the *in vivo* models presented here, there was a preliminary effect on tumour growth which was no longer sustained by the time of tissue harvest. This in part may be due to the nature of the subcutaneous injections, which were within the mammary gland but not directly at the tumour site. Future experiments should utilise a stromal or tumour cell like that

overexpress IGF1, so it is localised to the tumour similarly to what was identified within the human LAR TNBC tumours.

Finally, although there was evidence that IGF1 could promote an IgM+ phenotype in plasma cells, this was difficult to measure due to the mediocre increase in plasma cell production. Testing the effect of IGF1 within a setting that stimulates a substantial plasma cell response would determine if it had a role in promoting IgM over other immunoglobulin phenotypes. These cells could then be tested for their functional role in immunosuppression and tumour progression.

Chapter 6

Discussion

6.1 Summary

This thesis profiled the immunophenotype of the GC and immune subsets within the LNs of patients with opposing disease trajectories. This highlighted a decrease in PD1+ T cell subsets within the GCs of patients with an inferior outcome. In parallel there was an expansion of immunosuppressive subsets, namely Tregs, and a propensity for these cells to colocalize with macrophages and DN B cell in metastatic areas of the LN. Subsequent integration of gene expression data and immunofluorescence images indicated that increased plasma cell infiltration within immunologically cold tumours and paired in-LNs was associated with an increased risk of distant metastasis development. Critically, this subgroup of low sTIL TNBC patients presented with features of the LAR subtype, low numbers of GCs within the sentinel LNs and high incidence of nodal involvement. Studying the temporal changes of the GC response within the td-LNs of TNBC mouse models additionally highlighted deviations in the GC, memory B and plasma cells kinetics between models with a range of metastatic characteristics. Harnessing these mouse models and *in vitro* studies further demonstrated that the IGF1 pathway was capable of modulating plasma cells, B cells, and potentially suppressing the GC response. Therefore, I hypothesise that upregulation of androgen and IGF signalling within low sTIL tumours could influence migration of plasma cells and influence their anti-tumour responses. I furthermore postulate that these pathways could contribute to an immune cold TME, which may impact the ability to form GCs in the tumour-adjacent LNs, and influence disease trajectory in these high-risk TNBC patients.

6.2 The immunophenotype of the LNs of TNBC patients

Most current analyses within the LNs of breast cancer patients has primarily focussed on T cell responses, revealing distinct transcriptional profiles within the sentinel LNs. T cell subsets upregulating genes associated with immune cell homing and antigen processing would suggest an active humoral anti-tumour response within which the LN acts as the first site of initial interaction between tumour and immune cells (Liao et al., 2023). In contrast, those associated with immune exhaustion would indicate there is a pool of T cells no longer able to respond to TAA exposure. Vahidi *et al.,* observed a correlation between the depletion of CD8+ T cells, in particular the naive subsets, and tumour dissemination from primary tumour to the td-LNs, however it is not clear how this might affect tumour progression to distant sites (Vahidi et al., 2020). I have shown that a global reduction in CD8+ T cells within the LNs was associated with an inferior disease trajectory and low sTIL infiltration at the primary tumour lesion. This was in parallel to an increase in CD4+ T cells, which in turn suggested a decreased CD8+/CD4+ T cell ratio could contribute to distant metastasis development. This is in concordance with data suggesting that a diminished CD8+/CD4+ T cell ratio within the primary tumour can facilitate LN metastasis but is currently not known if this applies within the context of the LN itself. This could also be in part associated with the CD8+/Treg ratio, which is shown to be significantly lower in the in-LNs compared to adjacent normal (Chen et al., 2021). In agreement, I observed a decrease in CD8+ T cells and increased Treg prevalence in in-LN of the TNBC patient that developed distant metastasis. Further, work on CD4+ T cells in gastric cancer has indicated CD4+ effector memory subsets are depleted within in-LNs compared to cf-LNs, notably exhibiting a lower Th1/Th2 ratio (Okita et al., 2015). I hypothesise this is due to tumour migration into the LNs, leading to exhaustion and subsequent inadequate signalling from antigen-presenting cells to induce differentiation of naïve CD4+ T cells into an effector memory phenotype.

To the best of my knowledge, I am the first to study in depth GC reactions in the LNs of breast cancer patients and their mouse models. This has alluded to the importance of CD4+ and CD8+ T cells within the td- LN GC reactions and the role they play in modulating the selection and maturation of B cells. However, it specifically highlights how there was a significant reduction in PD-1+CD4+ and PD1+CD8+ T cells within the LN of the patient that developed distant metastasis, with a notable absence of PD-1+CD4+ T cells within the GCs. This would suggest that these cells are Tfh cells, compared to Tfr, by virtue of FoxP3 negativity. This is in alignment with work by Piersiala *et al.,* who showed that an increased percentage of CD3+PD-1+ cells within td-LNs of oral squamous cell carcinoma patients had significantly lower disease-free and overall survival rates (Piersiala et al., 2021). Furthermore, although not characterised using PD-1 expression, single cell RNA-sequencing has revealed that CD4+CXCL13+ cells within td-LNs of breast cancer patients can be reprogrammed to an exhausted state, expressing lower levels of pro-inflammatory cytokines including *IFNG* (Liu et al., 2022). This gene expression profile suggests these cells are of a Tfh-like phenotype, as Tfh within the GC will secrete CXCL13 to recruit CXCR5+ T and B cells towards the B cell zone (Cosgrove et al., 2020). Taken together, this indicates an immune environment within the in-LNs of patients that develop distant metastasis will present with low levels of Tfh cells, which are required for selection mechanisms within the GC and subsequent differentiation of memory B and plasma cells. This emphasises how the impact of T cell activation within the LNs of these patients may be implicating B cell development within the GC.

Moreover, an accumulation of macrophages within stromal ROIs and spatial co-localisation with tumour cells and Tregs was present in patients who developed distant metastasis. This is in concordance with data that implicates TAMs in promoting tumorigenesis, angiogenesis, and metastasis from the primary tumour in many solid cancers (Yibing Chen et al., 2019). Furthermore, secretion of cytokines, namely CCL20 and CCL22 can recruit Tregs to the TME, which subsequently impairs cancer antigen presentation.

This, in alignment with work from Liu *et al.*, who showed a downregulation of antigen presentation pathways by metastatic tumour cells within in-LNs, which implies this is one way in which the initiation of a GC response may be impaired (Liu et al., 2022). This lack of functionality of the GC may perhaps be further corroborated by a significant reduction in the plasma cell output and propensity for IgG+ plasma cells to localise within GCs in the LN of the patient that developed distant metastasis. This reflects a possible immunosuppressive environment that may be impeding an effective GC response.

Collectively, this emphasises the importance of assessing the prevalence but also spatial composition of immune cells within the tumour adjacent LNs of TNBC patients. Whilst overall abundance of immune populations may contribute to or impede disease progression, their colocalization or spatial propensities may indicate communication that requires further investigation. This is in part similar to the spatial analysis of TILs within the primary tumour, which has recently been shown prognostic for overall survival in TNBC. Hammerl *et al.,* described how distinct spatial immunophenotypes predicted response to immune checkpoint therapy (Hammerl et al., 2021). Therefore, the spatial distribution of immune populations within both the primary tumour and tumour adjacent LN may be predictive of response to therapy and disease trajectory.

6.3 Defining immunologically cold TNBC tumours

The assessment of sTILs within TNBC has been frequently shown greater propensity over traditional TNM staging to predict response to outcome, chemotherapy and immunotherapy (Loi et al., 2019; Salgado et al., 2015). Therefore, the quantification of TILs within stromal tissue before and after chemotherapy has revealed a TIL density of >30% can predict both response to therapy and overall survival(Luen et al., 2019). Despite this, only one third of TNBCs present with a high sTIL density and low levels of TILs does not equate to disease progression (Salgado et al., 2015). Additionally, the nature of the TIL scoring within TNBC

does not define populations present within the tumour, and subsequently the ratio of lymphocyte to other immune subsets, including plasma cells.

This thesis describes how a heightened plasma cell response within primary tumours and in-LNs of TNBC patients is associated with reduced distant disease-free survival time, specifically within tumours with low histological sTIL scores. As this phenotype is only apparent within immunologically cold tumours, this implicates this plasma cell infiltration as a response or result of stimuli within an immune-suppressed tumour. Despite advancements and recommendations by the International TILS Working group, sTIL scores are not routinely applied within clinical practice (Salgado et al., 2015). With the advent of immunotherapies approved for early stage and advanced TNBC(Schmid et al., 2020), it is important to consider immune populations that are present within low sTIL tumours and if they might be responsive to these treatments.

Further these data suggest that an immunologically cold TNBC tumour with high levels of plasma cell infiltration is indicative of those classified as a LAR phenotype and high incidence of LN metastasis. Studies targeting AR, namely selective AR modulators (SARMs), such as enobosarm, have been applied in preclinical models and indicated favourable results concerning migration and invasion. *In vivo* studies indicated that SARMs could reduce tumour weight by 90%, and this is has been investigated in a phase II clinical trial for patients with metastatic of locally advanced ER+ and AR+ breast cancer (Narayanan et al., 2014). Bicalutamide, a first-generation AR antagonist, showed promising results in a phase II clinical trial of AR+ER-PR- advanced breast cancers, with a clinical benefit rate (the percentage of patients that achieve complete response, partial response or at least 6 months of stable disease as a result of therapy)(Delgado and Guddati, 2021) of 19% at 6 months and a median progress-free survival duration of 12 weeks, and is currently being trialled in metastatic TNBC (Gucalp et al., 2013). Other AR antagonists including enzalutamide demonstrated a clinical benefit in AR+ TNBC patients of 33% at 16 weeks, 28% at 24 weeks and a median overall survival of 16.5 months (Traina et al., 2018).

Additionally, there is evidence that AR activity may have a role in regulating the DNA damage response (DDR). Using a prostatic adenocarcinoma model, Goodwin *et al.,* described how AR signalling can allow for resolution of DNA double-stranded breaks independently of cell-cycling effects and act as a transcriptional regulator of DNA-PKcs, a kinase critical in non-homologous end joining (NHEJ) that implements DNA repair following DNA damage (Goodwin et al., 2013). Further, the AR inhibition can enhance the antitumour effect of PARP inhibitors, due to the accumulation of DNA damage from the inactivation of DDR molecules including ATM and chk2 (Luo et al., 2016; Min et al., 2018). The relationship between AR and DDR subsequently implicates androgen signalling as an interesting target for combination treatment with radiotherapy. Work by Yard *et al.,* showed that AR mRNA levels were correlated with relative radiotherapy resistance within a subgroup of breast cancer cell lines (Yard et al., 2016), and other studies have demonstrated that targeting AR may be a method of radio sensitising TNBC, in part by impairing dsDNA break repair (Speers et al., 2017; Spratt et al., 2015).

Despite many current anti-androgen therapies acting with tolerable side effects, there is an unmet need to develop alternative therapeutics that improve these response rates. This may in part be due to the selection process used to evaluate patients who will respond to these types of therapies. Although the LAR subtype is defined through overexpression of AR, and this has been reported previously as a diagnostic marker, the prevalence and accuracy of AR expression in TNBC is heterogenous (Micello et al., 2010). A range of AR expression can be detected by immunohistochemical methods in up to 77% of all invasive breast cancers (Kumar et al., 2017), therefore new biomarkers are needed to stratify patients that will benefit most from these treatments.

Although studies have investigated how AR within the LAR subtype can interact with the stromal and epithelial populations of the TME, previous work has not characteristed in depth the effect of AR signalling on immune populations. Androgens can modulate the CXCL12/CXCR4 axes, which induces the motility of prostate and breast cancer cell lines *in*

vitro (Azariadis et al., 2017). As the CXCL12/CXCR4 axis is crucial for the migration of plasma cells from secondary lymphoid organs to the bone marrow (Biajoux et al., 2016), this may indicate that the increased level of androgens within these tumours can induce plasma cell infiltration. Despite more work being required to fully elucidate the functional capacity and immunoglobulin isotype of these plasma cells, their association with the LAR phenotype may provide a novel biomarker to define this subgroup within immune-cold tumours.

6.4 Crosstalk between LN and primary tumour in TNBC patients

Despite extensive analyses of immune infiltration within TNBCs, the relationship between TIL-B and B cells within adjacent LNs has not been fully investigated. High throughput B cell receptor (BCR) sequencing by McDaniel *et al.,* has revealed evidence of B cell affinity maturation and IgG antibody production against cancer-testis antigens within sentinel LNs and the periphery. This is indicative of a systemic immune response that may originate from tumour adjacent LNs (McDaniel et al., 2018). Although studies have been performed to assess immune cell populations within the LNs, studies in the tumour and patient-matched tumour adjacent LNs in parallel are limited.

This thesis showed that immunohistochemical methods to detect plasma cells subsequently indicated that the B cell environment within the TME was phenotypically similar to that of the in-LN, but not the cf-LN. Explicitly, there was a reduction in memory B cell infiltration and an increase in plasma cell infiltration, which in low sTIL tumours was prevalent in patients who had a shorter distant disease-free survival time. These similarities between the TME at the primary tumour and the in-LN suggests a microenvironment in both areas that is functionally distinct to cf-LNs. Previous work has primarily investigated T cell clones present within the draining LNs and those within the primary tumour. Okamura and colleagues showed that the TCRs of PD-1+ CD8+ T cells isolated from the tumour-adjacent LNs of patients with colorectal cancer were commonly shared with those from the primary tumour and could be

induced from cells isolated from cf-LNs by coculturing with autologous cancer cells (Okamura et al., 2022). Further, Jiao *et al.,* described that all expanded T cell clones from sentinel LNs of breast cancer patients were found within the primary tumour(Jiao et al., 2022). Whilst this has not been investigated in depth within the B cells, this emphasises a crucial role of the LN for anti-tumour responses that should be considered within a clinical setting. The standard treatment of care for TNBC patients with clinically and radiologically negative nodes before surgery is surgical resection of the sentinel LNs, although how this may impact local immune responses has not been considered. However, with the implementation of modern techniques to more precisely define LN staging, including targeted axillary dissection, targeted LN biopsy and sentinel LN biopsies, there is effort to deescalate full axillary LN removal (Banys-Paluchowski and de Boniface, 2023). In addition, how NACT, targeted treatments, and immunotherapeutic treatments may impact the B cell responses within the adjacent LNs has not been examined. Given the highly proliferative nature of the GC response and necessity of the PD-1/PD-L1 and CTLA-4/B7 axes in GC B cell affinity maturation, this requires further investigation(De Silva and Klein, 2015; Good-Jacobson et al., 2010; Hams et al., 2011).

6.5 Novel insights into breast cancer induced GC responses within tumour draining lymph nodes

GCs are transient entities within secondary lymphoid organs including the LN and the spleen that occur as a site of B cell maturation. After T-cell help and BCR binding to cognate antigen, B cells migrate in a cyclical fashion between polarised areas within the GC (the DZ and LZ), where they undergo SHM and antigen presentation from Tfh, modulated by CD40L-CD40 interactions and production of the cytokines IL-12 and IL-4 (Calado et al., 2012; Dominguez-Sola et al., 2012; Nakagawa et al., 2021). After rigorous rounds of selection, affinity matured memory B cells and plasma cells will exit the GC tailored of the nature of the antigen (Nakagawa et al., 2021).

To the best of my knowledge, this is the first study to demonstrate that multiple TNBC *in vivo* mouse models can induce a GC B cell response specifically within the td-LNs. These studies showed that the induction of a tumour can directly potentiate a B cell response and generate heterogenous B cell populations depending on the nature of the tumour. In concordance with this, studies by Louie *et al.,* using the E0771 model described evidence of TAAs within the FDCs of GCs in td-LNs, however further research is required to determine the characteristics of these antigens and how they elicit a GC response (Louie et al., 2022). Within breast cancer patients, this would elucidate novel markers eligible for targeted therapy, which may induce a GC response within the td-LNs and potentially contribute to an improved disease trajectory.

In addition, differences between the mouse models utilised in this thesis, namely the highly metastatic 4T1.2 and non-metastatic 67NR, suggested that tumour cell entry into the LN may also interfere with the GC reactions. It is well documented that CD8 T cells will develop an exhausted phenotype, upregulating inhibitory molecules such as PD-1, LAG3, and CTLA-4 in response to constitutive activation within cancer and other chronic diseases (Carter et al., 1989). Although the understanding of CD4 T cell exhaustion is somewhat lacking, Tfh cells from late-stage patients with hepatitis B virus (HBV)-related hepatocellular carcinoma (HCC) demonstrate impaired abilities to induce naïve B cells towards antibody secreting plasma cells, which is correlated with the intensity of PD-L1 expression in the resected tumours (Zhou et al., 2016). This may suggest that impaired T cell function within the td-LNs is in part responsible for the decline of the GCs and may be impacted in patients unable to retain or initiate a GC response. These data are perhaps corroborated further by results from chapter 3 that suggested a decrease in PD1+ T cells within the in-LN of the patient that developed distant metastasis.

To fully elucidate the type of GC reactions being induced by tumour cells, it is important to compare the nature of these responses with traditional immunisation and infection models. Studying B cell responses to immunisation or infection is broadly categorised into canonical

responses that will generate a GC reaction and non-canonical responses that lack GCs and present with extrafollicular plasma cell production. Canonical GC responses often are preceded by a short window of extrafollicular proliferation and differentiation, while non-canonical pathways exhibit a sustained phase of response at extrafollicular sites (MacLennan et al., 1991). Whilst the type of B cell response to a specific immunisation or pathogen can be documented within animal models, in human infection and vaccination this remains relatively unclear. Pathogens including *Salmonella enterica* and *Ehrlichia muris* will typically generate an extrafollicular response, GC suppression and disruption architecture in secondary lymphoid organs (Elsner and Shlomchik, 2020; Popescu et al., 2019). Within *Salmonella enterica* infections, contributing mechanisms that prevent Tfh and GC induction have been shown to be regulated by IL-12, LPS and TLR4 (Elsner and Shlomchik, 2020). Others including influenza virus and vesicular stomatitis virus will generate long lasting GC responses, with minimal effects on the architecture of the LN and spleen (De Giovanni et al., 2020; Elsner et al., 2012). Within vesicular stomatitis, this has been attributed to an increased level of IL-6, which promotes an early GC response by upregulating Tfh and blocking Th1 responses (De Giovanni et al., 2020). Harnessing similarities between the nature of these systems and those within the td-LNs of TNBC models will provide insight into mechanisms that contribute to the longevity of the GC response and potentially an improved overall survival in TNBC patients.

6.6 Stromal induced factors and the modulation of plasma cells and GC B cell responses

Finally, I elucidated the possible mechanisms through which androgen signalling within IThP tumours may contribute to plasma cell modulation and GC suppression. This primarily focussed on IGF1, identifying it as a novel target within these tumours that was highly upregulated and potentially has a role in contributing to an immunosuppressive microenvironment. As a major growth factor, it is responsible for stimulating growth of all cell types and has, therefore, emerged as a player in cancer development. In addition to direct contribution of malignant transformation, tumour growth, local invasion, and distant metastasis, it can indirectly interact with oncogenes, tumour suppressors and hormones (Larsson et al., 2005). Due to the expression of the IGF1-R on breast tumours, it has become a target for inhibition in multiple subtypes of breast cancers (Ekyalongo and Yee, 2017). Different therapeutic strategies have been evaluation to inhibit the IGF1R signalling pathway, namely monoclonal anti-IGF1R antibodies, small molecule tyrosine kinase inhibitors (TKIs) and IGF ligand antibodies. Preclinical studies have indicated that these classes of drug demonstrate different profiles of selectivity, efficacy and toxicity that may implicate their use in clinical practice (Burtrum et al., 2003; Maloney et al., 2003). This includes MEDI-573, a humanised antibody that can inhibit IGF1 *in vitro* and *in vivo*, however was discontinued after the completion of a phase 2 study in metastatic breast cancer (Gao et al., 2011). Xentuzumub, an IGF1/2 targeting monoclonal antibody was evaluated in a phase Ib/II trial in combination with exemestane and everolimus in HR+, HER2- locally advanced breast cancer, however this did not improve progression free survival and led to early discontinuation of the trial. Despite these results, a preclinical study combining BMS-754807, a small molecule inhibitor of IGF1R, and chemotherapy showed complete regression *in vivo* using the MC1 tumour-graft model of TNBC, compared to any agent alone (Adam et al., 2012). Whilst many of these studies aim to directly target the tumour cells, there has not

been an investigation to understand how these therapeutics may modulate the immune microenvironment at the primary tumour and adjacent LNs.

To investigate this in relation to plasma cell development, I have further described how IGF1R is present on a fraction of plasma cells within the primary tumour and in-LNs of TNBC patients and may be associated with a shorter distant disease survival time. These data additionally suggested that IGF1 could potentiate a predominantly IgM+ plasma cell response *in vitro* and perhaps influence the development of the GC response within td-LNs. Although current data has not analysed the expression of IGF1R within this context in solid tumours, studies have suggested that plasma cells do not express IGF1R, however it is aberrantly expressed by 31%-50% of malignant myeloma cells (Sprynski et al., 2009). Due to the current data describing the synergy between androgens, the CXCL12/CXCR4 axis, and the IGF1 signalling pathway (Azariadis et al., 2017; W et al., 2007), this may indicate a TME that leads to the generation of IGF1R+ plasma cells. More work is needed to fully elucidate the functional role of these cells, and if they can be harnessed as a biomarker of LAR TNBC and their disease trajectory.

In conclusion, I hypothesise that stromal and macrophage derived IGF1 and upregulated AR signalling within immunologically cold primary TNBCs act synergistically to promote an immunosuppressive environment. Furthermore, these two pathways potentiate the CXCL12/CXCR4 axis which can lead to plasma cell recruitment within these tumours. These immune-cold tumours subsequently exhibit low levels of antigen presentation, anti-tumour T cell priming and GC formation within the adjacent LN. The upregulation of these factors and lack of ani-tumour response consequently promotes local metastasis to the adjacent LN and metastasis to distant organs (Figure 89).

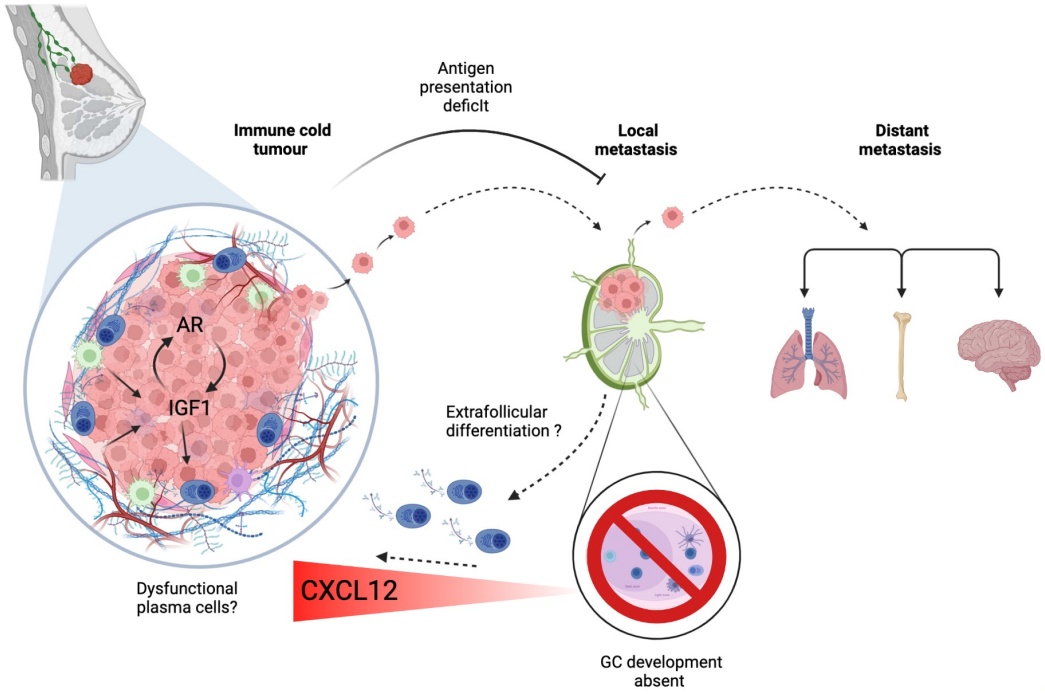

Figure 89: Overview of potential mechanism of plasma infiltration and GC suppression in IThP TNBC. IGF1 and AR signalling promoted by stromal cells and macrophages within the tumour microenvironment act in synergy to potentiate the CXCL12/CXCR4 axis and an immunosuppressive environment. This leads to a lack of antigen presentation and a favourable niche for tumour cells to proliferate and metastasise to both local and distant organs. This lack of immune cell activation prevents adequate GC formation within the adjacent LN and may indicate that plasma cells are generated from an extrafollicular pathway. The heightened CXCL12 gradient within the primary tumour subsequently can recruit plasma cells towards the tumour microenvironment where they may be unable to facilitate an anti-tumour response.

6.7 Limitations and future work

One major limitation of these studies was the lack of concordant paired human samples for gene expression, IMC analyses and IF analyses to confirm the presence of plasma cells, their spatial distribution and how this may be related to disease trajectory. Therefore, although the plasma cell gene signature could be attributed to distant metastasis development and reduced GC response within the adjacent LNs of low sTILs patients, infiltration of plasma cells and other B cell subsets could not be investigated histologically within the same samples. This meant that an independent cohort was used, and therefore it

was not possible to ascertain if the tumours within this cohort with a high plasma cell and low memory B cell phenotype were of the LAR subtype. To overcome these limitations, low sTIL tumours exhibiting the LAR phenotype should be profiled with the IMC panel, alongside paired in-LNs, histological quantification of GC numbers and clinical outcome data including distant disease-survival and overall survival. This would delineate the plasma cell phenotype, spatial interactions with other immune subsets, and immunoglobulin phenotypes within this subset of patients in both the tumour and paired LNs that may be attributed to distant metastasis development and poor disease trajectory. Harnessing the IMC panel in depth would also determine the immunophenotype and spatial arrangement of immune subsets identified using the pilot study with the Bart's TNBC cohort. This would enable confirmation of changes observed, were consistent with those developing distant metastasis and further provide a better understanding as to the immune composition of the LNs within those with an inferior disease trajectory. Furthermore, isolation of IGF1R+ plasma cells for scRNA sequencing would determine if they exhibited a distinct transcriptional profile to canonical plasma cells, and if this could contribute to disease pathology in TNBC.

Other limitations within the mouse models included characterising GC B cell populations over an acute timeframe, as samples were analysed at most 28 days post inoculation. This is not representative of analyses performed on human samples taken after tumour and LN resection. Establishing a chronic model of TNBC to study the longevity of GC and GC derived populations, including hallmarks of exhaustion would be more illustrative of the mechanisms that facilitate both local and distant metastasis. Other key future experiments would further investigate *in vivo* other populations present within the GC reactions for analyses, including that of Tfh, dendritic cells and regulatory subsets. Characterising these cells would better our understanding of tumour derived moieties which can directly impact the formation and maintenance of the GC.

To examine the features of LAR tumours in more depth, experiments overexpress features associated with this subtype in the mouse tumour cell lines should be performed, namely

AR, IGF1, HGF and probing the effect on tumour growth, GC B cell and plasma cells responses within the td-LN and primary tumour. This would overcome limitations from the human studies that prevented paired histological and gene expression data to determine the associated between IGF1R+ plasma cells and the LAR phenotype. High throughput analyses including single cell RNA sequencing, BCR sequencing and spatial transcriptomics would identify the immunoglobulin isotype of these cells, and the clonality between primary tumour and td-LN. Further, the chemotactic effect of IGF1 was not tested. It is perhaps that the plasma cell infiltration is a bystander due to the elevated levels of chemokines including CXCL12 that are implicated in the migration of plasma cells. Therefore, it would be important to delineate whether IGF1 can induce plasma cell infiltration towards a heightened androgen environment and subsequently LAR tumours.

Within the *in vivo* models presented here, there was a preliminary effect on tumour growth which was no longer sustained by the time of tissue harvest. This in part may be due to the nature of the subcutaneous injections, which were within the mammary gland but not directly at the tumour site. Future experiments should also utilise a stromal or tumour cell like that overexpress IGF1, so it is localised to the tumour similarly to what was identified within the human LAR TNBC tumours. Finally, although there was evidence that IGF1 could promote an IgM+ phenotype in plasma cells, this was difficult to measure due to the mediocre increase in plasma cell production. Testing the effect of IGF1 within a setting that stimulates a substantial plasma cell response would determine if it had a role in promoting IgM over other immunoglobulin phenotypes. These cells could then be tested for their functional role in immunosuppression and tumour progression.

References

Abdelhafez, A.H., Musall, B.C., Adrada, B.E., Hess, KennethR., Son, J.B., Hwang, K.-P., Candelaria, R.P., Santiago, L., Whitman, G.J., Le-Petross, H.T., Moseley, T.W., Arribas, E., Lane, D.L., Scoggins, M.E., Leung, J.W.T., Mahmoud, H.S., White, J.B., Ravenberg, E.E., Litton, J.K., Valero, V., Wei, P., Thompson, A.M., Moulder, S.L., Pagel, M.D., Ma, J., Yang, W.T., Rauch, G.M., 2021. Tumor necrosis by pretreatment breast MRI: association with neoadjuvant systemic therapy (NAST) response in triple-negative breast cancer (TNBC). Breast Cancer Res Treat 185, 1–12. https://doi.org/10.1007/s10549-020-05917-7

Achour, A., Simon, Q., Mohr, A., Séité, J.-F., Youinou, P., Bendaoud, B., Ghedira, I., Pers, J.-O., Jamin, C., 2017. Human regulatory B cells control the TFH cell response. Journal of Allergy and Clinical Immunology 140, 215–222. https://doi.org/10.1016/j.jaci.2016.09.042

Adam, P.J., Friedbichler, K., Hofmann, M.H., Bogenrieder, T., Borges, E., Adolf, G.R., 2012. BI 836845, a fully human IGF ligand neutralizing antibody, to improve the efficacy of rapamycin by blocking rapamycin-induced AKT activation. JCO 30, 3092–3092. https://doi.org/10.1200/jco.2012.30.15_suppl.3092

Adwan, H., Bäuerle, T.J., Berger, M.R., 2004. Downregulation of osteopontin and bone sialoprotein II is related to reduced colony formation and metastasis formation of MDA-MB-231 human breast cancer cells. Cancer Gene Ther 11, 109–120. https://doi.org/10.1038/sj.cgt.7700659

Ahn, S.G., Kim, S.J., Kim, C., Jeong, J., 2016. Molecular Classification of Triple-Negative Breast Cancer. J Breast Cancer 19, 223–230. https://doi.org/10.4048/jbc.2016.19.3.223

Alberts, E., Wall, I., Calado, D.P., Grigoriadis, A., 2021. Immune Crosstalk Between Lymph Nodes and Breast Carcinomas, With a Focus on B Cells. Front Mol Biosci 8, 673051. https://doi.org/10.3389/fmolb.2021.673051

Ali, H.R., Provenzano, E., Dawson, S.-J., Blows, F.M., Liu, B., Shah, M., Earl, H.M., Poole, C.J., Hiller, L., Dunn, J.A., Bowden, S.J., Twelves, C., Bartlett, J.M.S., Mahmoud, S.M.A., Rakha, E., Ellis, I.O., Liu, S., Gao, D., Nielsen, T.O., Pharoah, P.D.P., Caldas, C., 2014. Association between CD8+ T-cell infiltration and breast cancer survival in 12,439 patients. Ann Oncol 25, 1536–1543. https://doi.org/10.1093/annonc/mdu191

Al-Mahmood, S., Sapiezynski, J., Garbuzenko, O.B., Minko, T., 2018. Metastatic and triple-negative breast cancer: challenges and treatment options. Drug Deliv Transl Res 8, 1483–1507. https://doi.org/10.1007/s13346-018-0551-3

Altuwaijri, S., Chuang, K.-H., Lai, K.-P., Lai, J.-J., Lin, H.-Y., Young, F.M., Bottaro, A., Tsai, M.-Y., Zeng, W.-P., Chang, H.-C., Yeh, S., Chang, C., 2009. Susceptibility to Autoimmunity and B Cell Resistance to Apoptosis in Mice Lacking Androgen Receptor in B Cells. Mol Endocrinol 23, 444–453. https://doi.org/10.1210/me.2008-0106

Ansel, K.M., McHeyzer-Williams, L.J., Ngo, V.N., McHeyzer-Williams, M.G., Cyster, J.G., 1999. In vivo-activated CD4 T cells upregulate CXC chemokine receptor 5 and reprogram their response to lymphoid chemokines. J Exp Med 190, 1123–1134. https://doi.org/10.1084/jem.190.8.1123

Apavaloaei, A., Hardy, M.-P., Thibault, P., Perreault, C., 2020. The Origin and Immune Recognition of Tumor-Specific Antigens. Cancers (Basel) 12, 2607. https://doi.org/10.3390/cancers12092607

Appelgren, D., Eriksson, P., Ernerudh, J., Segelmark, M., 2018. Marginal-Zone B-Cells Are Main Producers of IgM in Humans, and Are Reduced in Patients With Autoimmune Vasculitis. Frontiers in Immunology 9.

Arias-Pulido, H., Cimino-Mathews, A., Chaher, N., Qualls, C., Joste, N., Colpaert, C., Marotti, J.D., Foisey, M., Prossnitz, E.R., Emens, L.A., Fiering, S., 2018. The combined presence of CD20+ B cells and PD-L1+ tumor infiltrating lymphocytes in inflammatory breast cancer is prognostic of improved patient outcome. Breast Cancer Res Treat 171, 273–282. https://doi.org/10.1007/s10549-018-4834-7

Arroyo-Crespo, J.J., Armiñán, A., Charbonnier, D., Deladriere, C., Palomino-Schätzlein, M., Lamas-Domingo, R., Forteza, J., Pineda-Lucena, A., Vicent, M.J., 2019. Characterization of triple-negative breast cancer preclinical models provides functional evidence of metastatic progression. International Journal of Cancer 145, 2267–2281. https://doi.org/10.1002/ijc.32270

Arulraj, T., Binder, S.C., Robert, P.A., Meyer-Hermann, M., 2019. Synchronous Germinal Center Onset Impacts the Efficiency of Antibody Responses. Front Immunol 10, 2116. https://doi.org/10.3389/fimmu.2019.02116

Aslakson, C.J., McEachern, D., Conaway, D.H., Miller, F.R., 1991. Inhibition of lung colonization at two different steps in the metastatic sequence. Clin Exp Metastasis 9, 139–150. https://doi.org/10.1007/BF01756385

Aslakson, C.J., Miller, F.R., 1992. Selective events in the metastatic process defined by analysis of the sequential dissemination of subpopulations of a mouse mammary tumor. Cancer Res 52, 1399–1405.

Attalla, S., Taifour, T., Bui, T., Muller, W., 2021. Insights from transgenic mouse models of PyMT-induced breast cancer: recapitulating human breast cancer progression in vivo. Oncogene 40, 475–491. https://doi.org/10.1038/s41388-020-01560-0

Avalle, L., Raggi, L., Monteleone, E., Savino, A., Viavattene, D., Statello, L., Camperi, A., Stabile, S.A., Salemme, V., De Marzo, N., Marino, F., Guglielmi, C., Lobascio, A., Zanini, C., Forni, M., Incarnato, D., Defilippi, P., Oliviero, S., Poli, V., 2022. STAT3 induces breast cancer growth via ANGPTL4, MMP13 and STC1 secretion by cancer associated fibroblasts. Oncogene 41, 1456–1467. https://doi.org/10.1038/s41388-021-02172-y

Azamjah, N., Soltan-Zadeh, Y., Zayeri, F., 2019. Global Trend of Breast Cancer Mortality Rate: A 25-Year Study. Asian Pac J Cancer Prev 20, 2015–2020. https://doi.org/10.31557/APJCP.2019.20.7.2015

Azariadis, K., Kiagiadaki, F., Pelekanou, V., Bempi, V., Alexakis, K., Kampa, M., Tsapis, A., Castanas, E., Notas, G., 2017. Androgen Triggers the Pro-Migratory CXCL12/CXCR4 Axis in AR-Positive Breast Cancer Cell Lines: Underlying Mechanism and Possible Implications for the Use of Aromatase Inhibitors in Breast Cancer. Cell Physiol Biochem 44, 66–84. https://doi.org/10.1159/000484584

B, D., Y, Z., A, K., Wh, W., Kg, B., Mj, S., R, S., 2010. Single round of antigen receptor signaling programs naive B cells to receive T cell help. Immunity 32. https://doi.org/10.1016/j.immuni.2010.02.013

Bankhead, P., Loughrey, M.B., Fernández, J.A., Dombrowski, Y., McArt, D.G., Dunne, P.D., McQuaid, S., Gray, R.T., Murray, L.J., Coleman, H.G., James, J.A., Salto-Tellez, M., Hamilton, P.W., 2017. QuPath: Open source software for digital pathology image analysis. Sci Rep 7, 16878. https://doi.org/10.1038/s41598-017-17204-5

Bannard, O., Horton, R.M., Allen, C.D.C., An, J., Nagasawa, T., Cyster, J.G., 2013. Germinal Center Centroblasts Transition to a Centrocyte Phenotype According to a Timed Program and Depend on the Dark Zone for Effective Selection. Immunity 39, 912–924. https://doi.org/10.1016/j.immuni.2013.08.038

Banys-Paluchowski, M., de Boniface, J., 2023. Axillary staging in node-positive breast cancer converting to node negativity through neoadjuvant chemotherapy: Current evidence and perspectives. Scand J Surg 14574969221145892. https://doi.org/10.1177/14574969221145892

Bar, I., Theate, I., Haussy, S., Beniuga, G., Carrasco, J., Canon, J.-L., Delrée, P., Merhi, A., 2020. MiR-210 Is Overexpressed in Tumor-infiltrating Plasma Cells in Triple-negative Breast Cancer. J Histochem Cytochem 68, 25–32. https://doi.org/10.1369/0022155419892965

Barrett, T., Bowden, D.J., Greenberg, D.C., Brown, C.H., Wishart, G.C., Britton, P.D., 2009. Radiological staging in breast cancer: which asymptomatic patients to image and how. Br J Cancer 101, 1522–1528. https://doi.org/10.1038/sj.bjc.6605323

Bartke, A., Chandrashekar, V., Dominici, F., Turyn, D., Kinney, B., Steger, R., Kopchick, J.J., 2003. Insulin-like growth factor 1 (IGF-1) and aging: controversies and new insights. Biogerontology 4, 1–8. https://doi.org/10.1023/a:1022448532248

Basso, K., Dalla-Favera, R., 2010. BCL6: master regulator of the germinal center reaction and key oncogene in B cell lymphomagenesis. Adv Immunol 105, 193–210. https://doi.org/10.1016/S0065-2776(10)05007-8

Basso, K., Saito, M., Sumazin, P., Margolin, A.A., Wang, K., Lim, W.-K., Kitagawa, Y., Schneider, C., Alvarez, M.J., Califano, A., Dalla-Favera, R., 2010. Integrated biochemical and computational approach identifies BCL6 direct target genes controlling multiple pathways in normal germinal center B cells. Blood 115, 975–984. https://doi.org/10.1182/blood-2009-06-227017

Batista, F.D., Harwood, N.E., 2009. The who, how and where of antigen presentation to B cells. Nat Rev Immunol 9, 15–27. https://doi.org/10.1038/nri2454

Baudler, S., Baumgartl, J., Hampel, B., Buch, T., Waisman, A., Snapper, C.M., Krone, W., Brüning, J.C., 2005. Insulin-like growth factor-1 controls type 2 T cell-independent B cell response. J Immunol 174, 5516–5525. https://doi.org/10.4049/jimmunol.174.9.5516

Baumjohann, D., Okada, T., Ansel, K.M., 2011. Cutting Edge: Distinct waves of BCL6 expression during T follicular helper cell development. J Immunol 187, 2089–2092. https://doi.org/10.4049/jimmunol.1101393

Ben-Batalla, I., Vargas-Delgado, M.E., von Amsberg, G., Janning, M., Loges, S., 2020. Influence of Androgens on Immunity to Self and Foreign: Effects on Immunity and Cancer. Frontiers in Immunology 11.

Berg, S., Kutra, D., Kroeger, T., Straehle, C.N., Kausler, B.X., Haubold, C., Schiegg, M., Ales, J., Beier, T., Rudy, M., Eren, K., Cervantes, J.I., Xu, B., Beuttenmueller, F., Wolny, A., Zhang, C., Koethe, U., Hamprecht, F.A., Kreshuk, A., 2019. ilastik: interactive machine learning for (bio)image analysis. Nat Methods 16, 1226–1232. https://doi.org/10.1038/s41592-019-0582-9

Bergström, J.J.E., Heyman, B., 2017. Mice Immunized with IgG Anti-Sheep Red Blood Cells (SRBC) Together With SRBC Have a Suppressed Anti-SRBC Antibody Response but Generate Germinal Centers and Anti-IgG Antibodies in Response to the Passively Administered IgG. Front Immunol 8, 911. https://doi.org/10.3389/fimmu.2017.00911

Bhate, S.S., Barlow, G.L., Schürch, C.M., Nolan, G.P., 2022. Tissue schematics map the specialization of immune tissue motifs and their appropriation by tumors. Cell Systems 13, 109-130.e6. https://doi.org/10.1016/j.cels.2021.09.012

Biajoux, V., Natt, J., Freitas, C., Alouche, N., Sacquin, A., Hemon, P., Gaudin, F., Fazilleau, N., Espéli, M., Balabanian, K., 2016. Efficient Plasma Cell Differentiation and Trafficking Require Cxcr4 Desensitization. Cell Reports 17, 193–205. https://doi.org/10.1016/j.celrep.2016.08.068

Bohannon, C., Powers, R., Satyabhama, L., Cui, A., Tipton, C., Michaeli, M., Skountzou, I., Mittler, R.S., Kleinstein, S.H., Mehr, R., Lee, F.E.-Y., Sanz, I., Jacob, J., 2016. Long-lived antigen-induced IgM plasma cells demonstrate somatic mutations and contribute to long-term protection. Nat Commun 7, 11826. https://doi.org/10.1038/ncomms11826

Bortnick, A., Allman, D., 2013. What Is and What Should Always Have Been: Long-lived Plasma cells Induced by T-cell Independent Antigens. Journal of immunology (Baltimore, Md. : 1950) 190, 5913. https://doi.org/10.4049/jimmunol.1300161

Bos, P.D., Nguyen, D.X., Massagué, J., 2010. Modeling metastasis in the mouse. Curr Opin Pharmacol 10, 571–577. https://doi.org/10.1016/j.coph.2010.06.003

Bosisio, F.M., Wilmott, J.S., Volders, N., Mercier, M., Wouters, J., Stas, M., Blokx, W.A., Massi, D., Thompson, J.F., Scolyer, R.A., van Baren, N., van den Oord, J.J., 2016. Plasma cells in primary melanoma. Prognostic significance and possible role of IgA. Mod Pathol 29, 347–358. https://doi.org/10.1038/modpathol.2016.28

Brasó-Maristany, F., Filosto, S., Catchpole, S., Marlow, R., Quist, J., Francesch-Domenech, E., Plumb, D.A., Zakka, L., Gazinska, P., Liccardi, G., Meier, P., Gris-Oliver, A., Cheang, M.C.U., Perdrix-Rosell, A., Shafat, M., Noël, E., Patel, N., McEachern, K., Scaltriti, M., Castel, P., Noor, F.,

Buus, R., Mathew, S., Watkins, J., Serra, V., Marra, P., Grigoriadis, A., Tutt, A.N., 2016. PIM1 kinase regulates cell death, tumor growth and chemotherapy response in triple-negative breast cancer. Nat Med 22, 1303–1313. https://doi.org/10.1038/nm.4198

Brown, A.S., Hunt, K.K., Shen, J., Huo, L., Babiera, G.V., Ross, M.I., Meric-Bernstam, F., Feig, B.W., Kuerer, H.M., Boughey, J.C., Ching, C.D., Gilcrease, M.Z., 2010. Histologic Changes Associated With False-Negative Sentinel Lymph Nodes After Preoperative Chemotherapy in Patients With Confirmed Lymph Node-Positive Breast Cancer Before Treatment. Cancer 116, 2878–2883. https://doi.org/10.1002/cncr.25066

Brumec, M., Sobočan, M., Takač, I., Arko, D., 2021. Clinical Implications of Androgen-Positive Triple-Negative Breast Cancer. Cancers (Basel) 13, 1642. https://doi.org/10.3390/cancers13071642

Brynjolfsson, S.F., Persson Berg, L., Olsen Ekerhult, T., Rimkute, I., Wick, M.-J., Mårtensson, I.-L., Grimsholm, O., 2018. Long-Lived Plasma Cells in Mice and Men. Front. Immunol. 9. https://doi.org/10.3389/fimmu.2018.02673

Buisseret, L., Garaud, S., de Wind, A., Van den Eynden, G., Boisson, A., Solinas, C., Gu-Trantien, C., Naveaux, C., Lodewyckx, J.-N., Duvillier, H., Craciun, L., Veys, I., Larsimont, D., Piccart-Gebhart, M., Stagg, J., Sotiriou, C., Willard-Gallo, K., 2017. Tumor-infiltrating lymphocyte composition, organization and PD-1/ PD-L1 expression are linked in breast cancer. Oncoimmunology 6, e1257452. https://doi.org/10.1080/2162402X.2016.1257452

Burstein, M.D., Tsimelzon, A., Poage, G.M., Covington, K.R., Contreras, A., Fuqua, S.A.W., Savage, M.I., Osborne, C.K., Hilsenbeck, S.G., Chang, J.C., Mills, G.B., Lau, C.C., Brown, P.H., 2015. Comprehensive genomic analysis identifies novel subtypes and targets of triple-negative breast cancer. Clin Cancer Res 21, 1688–1698. https://doi.org/10.1158/1078-0432.CCR-14-0432

Burtrum, D., Zhu, Z., Lu, D., Anderson, D.M., Prewett, M., Pereira, D.S., Bassi, R., Abdullah, R., Hooper, A.T., Koo, H., Jimenez, X., Johnson, D., Apblett, R., Kussie, P., Bohlen, P., Witte, L., Hicklin, D.J., Ludwig, D.L., 2003. A fully human monoclonal antibody to the insulin-like growth factor I receptor blocks ligand-dependent signaling and inhibits human tumor growth in vivo. Cancer Res 63, 8912–8921.

Calado, D.P., Sasaki, Y., Godinho, S.A., Pellerin, A., Köchert, K., Sleckman, B.P., de Alborán, I.M., Janz, M., Rodig, S., Rajewsky, K., 2012a. MYC is essential for the formation and maintenance of germinal centers. Nat Immunol 13, 1092–1100. https://doi.org/10.1038/ni.2418

Calado, D.P., Sasaki, Y., Godinho, S.A., Pellerin, A., Köchert, K., Sleckman, B.P., de Alborán, I.M., Janz, M., Rodig, S., Rajewsky, K., 2012b. The cell-cycle regulator c-Myc is essential for the formation and maintenance of germinal centers. Nat Immunol 13, 1092–1100. https://doi.org/10.1038/ni.2418

Cancer Statistics Review, 1975-2015 - Previous Version - SEER Cancer Statistics Review [WWW Document], n.d. . SEER. URL https://seer.cancer.gov/archive/csr/1975_2015/index.html (accessed 9.11.22).

Cardiff, R.D., Anver, M.R., Gusterson, B.A., Hennighausen, L., Jensen, R.A., Merino, M.J., Rehm, S., Russo, J., Tavassoli, F.A., Wakefield, L.M., Ward, J.M., Green, J.E., 2000. The mammary pathology of genetically engineered mice: the consensus report and recommendations from the Annapolis meeting. Oncogene 19, 968–988. https://doi.org/10.1038/sj.onc.1203277

Carey, L.A., Barry, W.T., Pitcher, B., Hoadley, K.A., Cheang, M.C.U., Anders, C.K., Henry, N.L., Tolaney, S.M., Dang, C.T., Krop, I.E., Harris, L., Berry, D.A., Perou, C.M., Winer, E.P., Hudis, C.A., 2014. Gene expression signatures in pre- and post-therapy (Rx) specimens from CALGB 40601 (Alliance), a neoadjuvant phase III trial of weekly paclitaxel and trastuzumab with or without lapatinib for HER2-positive breast cancer (BrCa). JCO 32, 506–506. https://doi.org/10.1200/jco.2014.32.15_suppl.506

Carpenter, E., Alaguthurai, T., Hossain, F., Graham, R., Kakkassery, H., Keane, S., Irshad, S., 2022. 972 Enrichment of atypical memory double negative (CD27— IgD—) tumour infiltrating B cells

following neoadjuvant chemotherapy for early-stage breast cancer. J Immunother Cancer 10. https://doi.org/10.1136/jitc-2022-SITC2022.0972
Casey, A.E., Laster, W.R., Ross, G.L., 1951. Sustained enhanced growth of carcinoma EO771 in C57 black mice. Proc Soc Exp Biol Med 77, 358–362. https://doi.org/10.3181/00379727-77-18779
Castro, C.D., Flajnik, M.F., 2014. Putting J-chain back on the map: how might its expression define plasma cell development? J Immunol 193, 3248–3255. https://doi.org/10.4049/jimmunol.1400531
Centuori, S.M., Gomes, C.J., Kim, S.S., Putnam, C.W., Larsen, B.T., Garland, L.L., Mount, D.W., Martinez, J.D., 2018. Double-negative (CD27-IgD-) B cells are expanded in NSCLC and inversely correlate with affinity-matured B cell populations. J Transl Med 16, 30. https://doi.org/10.1186/s12967-018-1404-z
Cervenak, L., Magyar, A., Boja, R., László, G., 2001. Differential expression of GL7 activation antigen on bone marrow B cell subpopulations and peripheral B cells. Immunol Lett 78, 89–96. https://doi.org/10.1016/s0165-2478(01)00239-5
Chandler, C., Liu, T., Buckanovich, R., Coffman, L., 2019. The double edge sword of fibrosis in cancer. Transl Res 209, 55–67. https://doi.org/10.1016/j.trsl.2019.02.006
Chaplin, D.D., 2010. Overview of the Immune Response. J Allergy Clin Immunol 125, S3-23. https://doi.org/10.1016/j.jaci.2009.12.980
Chen, B., Zhang, G., Lai, J., Xiao, W., Li, X., Li, C., Mok, H., Li, K., Wang, Y., Cao, L., Jia, M., Ren, C., Wen, L., Wei, G., Lin, J., Li, Y., Zhang, Y., Chen, X., Wu, X., Zhang, H., Li, M., Liu, J., Balch, C.M., Liao, N., 2021. Genetic and immune characteristics of sentinel lymph node metastases and multiple lymph node metastases compared to their matched primary breast tumours. eBioMedicine 71, 103542. https://doi.org/10.1016/j.ebiom.2021.103542
Chen, Yibing, Song, Y., Du, W., Gong, L., Chang, H., Zou, Z., 2019. Tumor-associated macrophages: an accomplice in solid tumor progression. Journal of Biomedical Science 26. https://doi.org/10.1186/s12929-019-0568-z
Chen, Yuhong, Yu, M., Zheng, Y., Fu, G., Xin, G., Zhu, W., Luo, L., Burns, R., Li, Q.-Z., Dent, A.L., Zhu, N., Cui, W., Malherbe, L., Wen, R., Wang, D., 2019. CXCR5+PD-1+ follicular helper CD8 T cells control B cell tolerance. Nat Commun 10, 4415. https://doi.org/10.1038/s41467-019-12446-5
Chen, Y., Zhang, J., Cui, W., Silverstein, R.L., 2022. CD36, a signaling receptor and fatty acid transporter that regulates immune cell metabolism and fate. Journal of Experimental Medicine 219, e20211314. https://doi.org/10.1084/jem.20211314
Cheng, Q., Khodadadi, L., Taddeo, A., Klotsche, J., F. Hoyer, B., Radbruch, A., Hiepe, F., 2018. CXCR4–CXCL12 interaction is important for plasma cell homing and survival in NZB/W mice. European Journal of Immunology 48, 1020–1029. https://doi.org/10.1002/eji.201747023
Chiaruttini, G., Mele, S., Opzoomer, J., Crescioli, S., Ilieva, K.M., Lacy, K.E., Karagiannis, S.N., 2017. B cells and the humoral response in melanoma: The overlooked players of the tumor microenvironment. Oncoimmunology 6, e1294296. https://doi.org/10.1080/2162402X.2017.1294296
Chiu, Y.-K., Lin, I.-Y., Su, S.-T., Wang, K.-H., Yang, S.-Y., Tsai, D.-Y., Hsieh, Y.-T., Lin, K.-I., 2014. Transcription Factor ABF-1 Suppresses Plasma Cell Differentiation but Facilitates Memory B Cell Formation. The Journal of Immunology 193, 2207–2217. https://doi.org/10.4049/jimmunol.1400411
Choi, Y.S., Kageyama, R., Eto, D., Escobar, T.C., Johnston, R.J., Monticelli, L., Lao, C., Crotty, S., 2011. ICOS receptor instructs T follicular helper cell versus effector cell differentiation via induction of the transcriptional repressor Bcl6. Immunity 34, 932–946. https://doi.org/10.1016/j.immuni.2011.03.023
Chumsri, S., Carter, J.M., Ma, Y., Hinerfeld, D., Brauer, H.A., Warren, S., Nielsen, T.O., Asleh, K., Joensuu, H., Perez, E.A., Leon-Ferre, R.A., Hillman, D.W., Boughey, J.C., Liu, M.C., Ingle, J.N.,

Kalari, K.R., Couch, F., Knutson, K.L., Goetz, M.P., Thompson, E.A., 2020. Role of intratumoral NK cells in triple-negative breast cancer in the FinXX trial and Mayo Clinic cohort. JCO 38, 510–510. https://doi.org/10.1200/JCO.2020.38.15_suppl.510

Chung, W., Eum, H.H., Lee, H.-O., Lee, K.-M., Lee, H.-B., Kim, K.-T., Ryu, H.S., Kim, S., Lee, J.E., Park, Y.H., Kan, Z., Han, W., Park, W.-Y., 2017. Single-cell RNA-seq enables comprehensive tumour and immune cell profiling in primary breast cancer. Nature Communications 8, 15081. https://doi.org/10.1038/ncomms15081

Ciocca, D.R., 1980. Immunomorphologic lymph node changes in rats bearing experimental breast tumors. Am J Pathol 99, 193–206.

Clocchiatti, A., Cora, E., Zhang, Y., Dotto, G.P., 2016. Sexual dimorphism in cancer. Nat Rev Cancer 16, 330–339. https://doi.org/10.1038/nrc.2016.30

Cortes, J., Cescon, D.W., Rugo, H.S., Nowecki, Z., Im, S.-A., Yusof, M.M., Gallardo, C., Lipatov, O., Barrios, C.H., Holgado, E., Iwata, H., Masuda, N., Otero, M.T., Gokmen, E., Loi, S., Guo, Z., Zhao, J., Aktan, G., Karantza, V., Schmid, P., Luis, F., Gonzalo, G.A., Diego, K., Ruben, K., Matias, M., Mirta, V., Sally, B.-H., Stephen, B., Philip, C., Sherene, L., Dhanusha, S., Andrea, G., Donatienne, T., Carlos, B., Leandro, B., Fabiano, C., Ruffo, de F.J., Roberto, H., Carvalho, L.D., Toniazzi, L.F.C., Odebrecht, R.R., Orlando, S.N.A., Felipe, S., David, C., Danielle, C., Cristiano, F., Xinni, S., Joanne, Y., Alejandro, A., Carlos, G., Claudio, S., Cesar, S., Eduardo, Y., Alvaro, G.D., Jesus, S., Petra, H., Zdenek, K., Bohuslav, M., Katarina, P., Jana, P., Vesna, G., Erik, J., Jeanette, J., Soren, L., Tamas, L., Herve, B., Isabelle, D., Anthony, G., Anne-Claire, H.-B., Luis, T., Jens-Uwe, B., Peter, F., Dirk, F., Nadia, H., Jens, H., Anna, K.F. de S., Christian, K., Sibylle, L., Diana, L., Tjoung-Won, P.-S., Von, S.R., Pauline, W., Louis, C., Ava, K., Roger, N.K.C., Peter, A., Tibor, C., Zsuzsanna, K., Laszlo, L., Karoly, M., Gabor, R., John, C., Catherine, K., Seamus, O., Saverio, C., Antonietta, Da., Enrico, R., Tomoyuki, A., Takaaki, F., Kenichi, I., Takashi, I., Yoshinori, I., Tsutomu, I., Hiroji, I., Yoshimasa, K., Koji, M., Yasuo, M., Hirofumi, M., Seigo, N., Naoki, N., Shoichiro, O., Akihiko, O., Yasuaki, S., Eiji, S., Masato, T., Yuko, T., Kenji, T., Koichiro, T., Junichiro, W., Naohito, Y., Yutaka, Y., Teruo, Y., Anita, B., Mastura, M.Y., Angel, G.V., Alejandro, J.R., Jorge, M.R., Flavia, M.-V., Jessica, R.C., Karin, B., Vivianne, T.-H., David, P., Ewa, C., Ewa, N.-Z., Zbigniew, N., Barbara, R., Joanna, S., Cezary, S., Rafal, T., Bogdan, Z., Alexander, A., Natalia, F., Oleg, L., Andrey, M., Vladimir, M., Guzel, M., Hee, A.J., Seock-Ah, I., Seok, L.K., Hwa, P.K., Hee, P.Y., Begona, B. de las H., Javier, C., Josefina, C.J., Luis, de la C.M., Jose, G.S., Maria, G., Esther, H., Esther, Z.A., Chien-Ting, L., Mei-Ching, L., Chiun-Sheng, H., Chao-Jung, T., Ling-Ming, T., Cagatay, A., Gul, B., Irfan, C., Erhan, G., Seyda, G., Nil, M.M., Mustafa, O., Ozgur, O., Sinan, Y., Steve, C., Janine, G., Iain, M., Peter, S., Nicholas, T., Mark, T., Christopher, T., Duncan, W., Hryhoriy, A., Oleksandr, B., Igor, B., Oleksii, K., Olena, K., Hanna, K., Anna, K., Iurii, L., Alla, N., Natalya, O., Olga, P., Andrii, R., Sergii, S., Yaroslav, S., Dmytro, T., Grygorii, U., Ihor, V., Sibel, B., Madhu, C., Michael, C., Patrick, C., Scott, C., Jennifer, D., Keerthi, G., Jeffrey, H., Kent, H., William, I., Randa, L., Janice, L., Raul, M., Susan, M., Rita, N., Ira, O., Coral, O., Timothy, P., Amit, P., Brian, P., Hope, R., Irina, R., Michael, Schleider, Robert, S., Michael, Simon, Laura, S., Bradley, S., Michaela, T., Frances, V.-A., 2020. Pembrolizumab plus chemotherapy versus placebo plus chemotherapy for previously untreated locally recurrent inoperable or metastatic triple-negative breast cancer (KEYNOTE-355): a randomised, placebo-controlled, double-blind, phase 3 clinical trial. The Lancet 396, 1817–1828. https://doi.org/10.1016/S0140-6736(20)32531-9

Cosgrove, J., Novkovic, M., Albrecht, S., Pikor, N.B., Zhou, Z., Onder, L., Mörbe, U., Cupovic, J., Miller, H., Alden, K., Thuery, A., O'Toole, P., Pinter, R., Jarrett, S., Taylor, E., Venetz, D., Heller, M., Uguccioni, M., Legler, D.F., Lacey, C.J., Coatesworth, A., Polak, W.G., Cupedo, T., Manoury, B., Thelen, M., Stein, J.V., Wolf, M., Leake, M.C., Timmis, J., Ludewig, B., Coles, M.C., 2020. B cell zone reticular cell microenvironments shape CXCL13 gradient formation. Nat Commun 11, 3677. https://doi.org/10.1038/s41467-020-17135-2

Cui, M., Huang, J., Zhang, S., Liu, Q., Liao, Q., Qiu, X., 2021. Immunoglobulin Expression in Cancer Cells and Its Critical Roles in Tumorigenesis. Front Immunol 12, 613530. https://doi.org/10.3389/fimmu.2021.613530

Cyster, J.G., Ansel, K.M., Reif, K., Ekland, E.H., Hyman, P.L., Tang, H.L., Luther, S.A., Ngo, V.N., 2000. Follicular stromal cells and lymphocyte homing to follicles. Immunol Rev 176, 181–193. https://doi.org/10.1034/j.1600-065x.2000.00618.x

Dai, X., Cheng, H., Bai, Z., Li, J., 2017. Breast Cancer Cell Line Classification and Its Relevance with Breast Tumor Subtyping. J Cancer 8, 3131–3141. https://doi.org/10.7150/jca.18457

Davey, R.A., Grossmann, M., 2016. Androgen Receptor Structure, Function and Biology: From Bench to Bedside. Clin Biochem Rev 37, 3–15.

Dawson, S.-J., Rueda, O.M., Aparicio, S., Caldas, C., 2013. A new genome-driven integrated classification of breast cancer and its implications. EMBO J 32, 617–628. https://doi.org/10.1038/emboj.2013.19

De Giovanni, M., Cutillo, V., Giladi, A., Sala, E., Maganuco, C.G., Medaglia, C., Di Lucia, P., Bono, E., Cristofani, C., Consolo, E., Giustini, L., Fiore, A., Eickhoff, S., Kastenmüller, W., Amit, I., Kuka, M., Iannacone, M., 2020. Spatiotemporal regulation of type I interferon expression determines the antiviral polarization of CD4+ T cells. Nat Immunol 21, 321–330. https://doi.org/10.1038/s41590-020-0596-6

De Silva, N.S., Klein, U., 2015a. Dynamics of B cells in germinal centres. Nature Reviews Immunology 15, 137–148. https://doi.org/10.1038/nri3804

De Silva, N.S., Klein, U., 2015b. Dynamics of B cells in germinal centres. Nat Rev Immunol 15, 137–148. https://doi.org/10.1038/nri3804

Delgado, A., Guddati, A.K., 2021. Clinical endpoints in oncology - a primer. Am J Cancer Res 11, 1121–1131.

Dexter, D.L., Kowalski, H.M., Blazar, B.A., Fligiel, Z., Vogel, R., Heppner, G.H., 1978. Heterogeneity of tumor cells from a single mouse mammary tumor. Cancer Res 38, 3174–3181.

Díaz-Zaragoza, M., Hernández-Ávila, R., Viedma-Rodríguez, R., Arenas-Aranda, D., Ostoa-Saloma, P., 2015. Natural and adaptive IgM antibodies in the recognition of tumor-associated antigens of breast cancer (Review). Oncol Rep 34, 1106–1114. https://doi.org/10.3892/or.2015.4095

Dickinson and Company, Becton, 2023. FlowJo™ Software.

Dimcić, M., Stevanović, O., Jakovljević, B., 1997. [Metastasis in axillary lymph nodes in breast carcinoma--possibilities of mammographic diagnosis]. Srp Arh Celok Lek 125, 124–126.

Dominguez-Sola, D., Victora, G.D., Ying, C.Y., Phan, R.T., Saito, M., Nussenzweig, M.C., Dalla-Favera, R., 2012. The proto-oncogene MYC is required for selection in the germinal center and cyclic reentry. Nature Immunology 13, 1083–1091. https://doi.org/10.1038/ni.2428

duPre', S.A., Hunter, K.W., 2007. Murine mammary carcinoma 4T1 induces a leukemoid reaction with splenomegaly: Association with tumor-derived growth factors. Experimental and Molecular Pathology 82, 12–24. https://doi.org/10.1016/j.yexmp.2006.06.007

Eiger, D., Agostinetto, E., Saúde-Conde, R., de Azambuja, E., 2021. The Exciting New Field of HER2-Low Breast Cancer Treatment. Cancers (Basel) 13, 1015. https://doi.org/10.3390/cancers13051015

Eiró, N., González, L., González, L.O., Fernandez-Garcia, B., Lamelas, M.L., Marín, L., González-Reyes, S., del Casar, J.M., Vizoso, F.J., 2012. Relationship between the Inflammatory Molecular Profile of Breast Carcinomas and Distant Metastasis Development. PLoS One 7, e49047. https://doi.org/10.1371/journal.pone.0049047

Ekyalongo, R.C., Yee, D., 2017. Revisiting the IGF-1R as a breast cancer target. NPJ Precision Oncology 1. https://doi.org/10.1038/s41698-017-0017-y

Eling, N., Damond, N., Hoch, T., Bodenmiller, B., 2020. cytomapper: an R/Bioconductor package for visualization of highly multiplexed imaging data. Bioinformatics 36, 5706–5708. https://doi.org/10.1093/bioinformatics/btaa1061

Elsner, R.A., Ernst, D.N., Baumgarth, N., 2012. Single and coexpression of CXCR4 and CXCR5 identifies CD4 T helper cells in distinct lymph node niches during influenza virus infection. Journal of Virology 86, 7146–7157. https://doi.org/10.1128/JVI.06904-11

Elsner, R.A., Shlomchik, M.J., 2020a. Germinal Center and Extrafollicular B Cell Responses in vaccination, immunity and autoimmunity. Immunity 53, 1136–1150. https://doi.org/10.1016/j.immuni.2020.11.006

Elsner, R.A., Shlomchik, M.J., 2020b. Germinal Center and Extrafollicular B Cell Responses in Vaccination, Immunity, and Autoimmunity. Immunity 53, 1136–1150. https://doi.org/10.1016/j.immuni.2020.11.006

Erlandsson, M.C., Erdogan, S., Wasén, C., Andersson, K.M.E., Silfverswärd, S.T., Pullerits, R., Bemark, M., Bokarewa, M.I., 2022. IGF1R signalling is a guardian of self-tolerance restricting autoantibody production. Frontiers in Immunology 13.

Ersching, J., Efeyan, A., Mesin, L., Jacobsen, J.T., Pasqual, G., Grabiner, B.C., Dominguez-Sola, D., Sabatini, D.M., Victora, G.D., 2017. Germinal Center Selection and Affinity Maturation Require Dynamic Regulation of mTORC1 Kinase. Immunity 46, 1045-1058.e6. https://doi.org/10.1016/j.immuni.2017.06.005

Evans, R.M., Mangelsdorf, D.J., 2014. Nuclear Receptors, RXR, and the Big Bang. Cell 157, 255–266. https://doi.org/10.1016/j.cell.2014.03.012

Feng, T., Elson, C.O., Cong, Y., 2011. Treg cell-IgA axis in maintenance of host immune homeostasis with microbiota. Int Immunopharmacol 11, 589–592. https://doi.org/10.1016/j.intimp.2010.11.016

Fernández-Nogueira, P., Fuster, G., Gutierrez-Uzquiza, Á., Gascón, P., Carbó, N., Bragado, P., 2021. Cancer-Associated Fibroblasts in Breast Cancer Treatment Response and Metastasis. Cancers 13, 3146. https://doi.org/10.3390/cancers13133146

Figenschau, S.L., Fismen, S., Fenton, K.A., Fenton, C., Mortensen, E.S., 2015. Tertiary lymphoid structures are associated with higher tumor grade in primary operable breast cancer patients. BMC Cancer 15, 101. https://doi.org/10.1186/s12885-015-1116-1

Fillatreau, S., Manfroi, B., Dörner, T., 2021. Toll-like receptor signalling in B cells during systemic lupus erythematosus. Nat Rev Rheumatol 17, 98–108. https://doi.org/10.1038/s41584-020-00544-4

Finke, D., Baribaud, F., Diggelmann, H., Acha-Orbea, H., 2001. Extrafollicular Plasmablast B Cells Play a Key Role in Carrying Retroviral Infection to Peripheral Organs. The Journal of Immunology 166, 6266–6275. https://doi.org/10.4049/jimmunol.166.10.6266

Finkin, S., Hartweger, H., Oliveira, T.Y., Kara, E.E., Nussenzweig, M.C., 2019. Protein Amounts of the MYC Transcription Factor Determine Germinal Center B Cell Division Capacity. Immunity 51, 324-336.e5. https://doi.org/10.1016/j.immuni.2019.06.013

Firmino, N.S., Cederberg, R.A., Lee, C.-M., Shi, R., Wadsworth, B.J., Franks, S.E., Thomas, K.N., Decotret, L.R., Bennewith, K.L., n.d. Germinal center hypoxia in tumor-draining lymph nodes negatively regulates tumor-induced humoral immune responses in mouse models of breast cancer. Oncoimmunology 10, 1959978. https://doi.org/10.1080/2162402X.2021.1959978

Folcarelli, R., van Staveren, S., Tinnevelt, G., Cadot, E., Vrisekoop, N., Buydens, L., Koenderman, L., Jansen, J., van den Brink, O.F., 2022. Transformation of multicolour flow cytometry data with OTflow prevents misleading multivariate analysis results and incorrect immunological conclusions. Cytometry A 101, 72–85. https://doi.org/10.1002/cyto.a.24491

Forsell, M.N.E., Kvastad, L., Sedimbi, S.K., Andersson, J., Karlsson, M.C.I., 2017. Regulation of Subunit-Specific Germinal Center B Cell Responses to the HIV-1 Envelope Glycoproteins by Antibody-Mediated Feedback. Front Immunol 8, 738. https://doi.org/10.3389/fimmu.2017.00738

Foulkes, W.D., Smith, I.E., Reis-Filho, J.S., 2010. Triple-negative breast cancer. N Engl J Med 363, 1938–1948. https://doi.org/10.1056/NEJMra1001389

Froidure, A., Mouthuy, J., Durham, S.R., Chanez, P., Sibille, Y., Pilette, C., 2016. Asthma phenotypes and IgE responses. European Respiratory Journal 47, 304–319. https://doi.org/10.1183/13993003.01824-2014

Gandhi, V.D., Cephus, J.-Y., Norlander, A.E., Chowdhury, N.U., Zhang, J., Ceneviva, Z.J., Tannous, E., Polosukhin, V.V., Putz, N.D., Wickersham, N., Singh, A., Ware, L.B., Bastarache, J.A., Shaver, C.M., Chu, H.W., Peebles, R.S., Newcomb, D.C., n.d. Androgen receptor signaling promotes Treg suppressive function during allergic airway inflammation. J Clin Invest 132, e153397. https://doi.org/10.1172/JCI153397

Gao, B., 2021. Identification of Feature Autophagy-Related Genes and DNA Methylation Profiles in Systemic Lupus Erythematosus Patients. Med Sci Monit 27, e933425-1-e933425-27. https://doi.org/10.12659/MSM.933425

Gao, J., Chesebrough, J.W., Cartlidge, S.A., Ricketts, S.-A., Incognito, L., Veldman-Jones, M., Blakey, D.C., Tabrizi, M., Jallal, B., Trail, P.A., Coats, S., Bosslet, K., Chang, Y.S., 2011. Dual IGF-I/II-neutralizing antibody MEDI-573 potently inhibits IGF signaling and tumor growth. Cancer Res 71, 1029–1040. https://doi.org/10.1158/0008-5472.CAN-10-2274

Garaud, S., Buisseret, L., Solinas, C., Gu-Trantien, C., de Wind, A., Van den Eynden, G., Naveaux, C., Lodewyckx, J.-N., Boisson, A., Duvillier, H., Craciun, L., Ameye, L., Veys, I., Paesmans, M., Larsimont, D., Piccart-Gebhart, M., Willard-Gallo, K., 2019. Tumor infiltrating B-cells signal functional humoral immune responses in breast cancer. JCI Insight 5. https://doi.org/10.1172/jci.insight.129641

Garaud, S., Zayakin, P., Buisseret, L., Rulle, U., Silina, K., de Wind, A., Van den Eyden, G., Larsimont, D., Willard-Gallo, K., Line, A., 2018. Antigen Specificity and Clinical Significance of IgG and IgA Autoantibodies Produced in situ by Tumor-Infiltrating B Cells in Breast Cancer. Front Immunol 9, 2660. https://doi.org/10.3389/fimmu.2018.02660

Genestier, L., Taillardet, M., Mondiere, P., Gheit, H., Bella, C., Defrance, T., 2007. TLR Agonists Selectively Promote Terminal Plasma Cell Differentiation of B Cell Subsets Specialized in Thymus-Independent Responses. The Journal of Immunology 178, 7779–7786. https://doi.org/10.4049/jimmunol.178.12.7779

Germain, C., Gnjatic, S., Dieu-Nosjean, M.-C., 2015. Tertiary Lymphoid Structure-Associated B Cells are Key Players in Anti-Tumor Immunity. Front. Immunol. 6. https://doi.org/10.3389/fimmu.2015.00067

Goddard, E.T., Fischer, J., Schedin, P., 2016. A Portal Vein Injection Model to Study Liver Metastasis of Breast Cancer. J Vis Exp 54903. https://doi.org/10.3791/54903

Good-Jacobson, K.L., Szumilas, C.G., Chen, L., Sharpe, A.H., Tomayko, M.M., Shlomchik, M.J., 2010a. PD-1 regulates germinal center B cell survival and the formation and affinity of long-lived plasma cells. Nat Immunol 11, 535–542. https://doi.org/10.1038/ni.1877

Good-Jacobson, K.L., Szumilas, C.G., Chen, L., Sharpe, A.H., Tomayko, M.M., Shlomchik, M.J., 2010b. PD-1 regulates germinal center B cell survival and the formation and affinity of long-lived plasma cells. Nature Immunology 11, 535–542. https://doi.org/10.1038/ni.1877

Goodwin, J.F., Schiewer, M.J., Dean, J.L., Schrecengost, R.S., de Leeuw, R., Han, S., Ma, T., Den, R.B., Dicker, A.P., Feng, F.Y., Knudsen, K.E., 2013. A hormone-DNA repair circuit governs the response to genotoxic insult. Cancer Discov 3, 1254–1271. https://doi.org/10.1158/2159-8290.CD-13-0108

Gravekamp, C., Sypniewska, R., Gauntt, S., Tarango, M., Price, P., Reddick, R., 2004. Behavior of metastatic and nonmetastatic breast tumors in old mice. Exp Biol Med (Maywood) 229, 665–675. https://doi.org/10.1177/153537020422900711

Grigoriadis, A., Gazinska, P., Pai, T., Irhsad, S., Wu, Y., Millis, R., Naidoo, K., Owen, J., Gillett, C.E., Tutt, A., Coolen, A.C., Pinder, S.E., 2018a. Histological scoring of immune and stromal features in breast and axillary lymph nodes is prognostic for distant metastasis in lymph node-positive breast cancers. The Journal of Pathology: Clinical Research 4, 39–54. https://doi.org/10.1002/cjp2.87

Grigoriadis, A., Gazinska, P., Pai, T., Irhsad, S., Wu, Y., Millis, R., Naidoo, K., Owen, J., Gillett, C.E., Tutt, A., Coolen, A.C., Pinder, S.E., 2018b. Histological scoring of immune and stromal features in breast and axillary lymph nodes is prognostic for distant metastasis in lymph node-positive breast cancers. The Journal of Pathology: Clinical Research 4, 39–54. https://doi.org/10.1002/cjp2.87

Gu, Y., Liu, Y., Fu, L., Zhai, L., Zhu, J., Han, Y., Jiang, Y., Zhang, Y., Zhang, P., Jiang, Z., Zhang, X., Cao, X., 2019a. Tumor-educated B cells selectively promote breast cancer lymph node metastasis by. Nat Med 25, 312–322. https://doi.org/10.1038/s41591-018-0309-y

Gu, Y., Liu, Y., Fu, L., Zhai, L., Zhu, J., Han, Y., Jiang, Y., Zhang, Y., Zhang, P., Jiang, Z., Zhang, X., Cao, X., 2019b. Tumor-educated B cells selectively promote breast cancer lymph node metastasis by. Nat Med 25, 312–322. https://doi.org/10.1038/s41591-018-0309-y

Guan, H., Wan, Y., Lan, J., Wang, Q., Wang, Zhangyu, Li, Y., Zheng, J., Zhang, X., Wang, Zemin, Shen, Y., Xie, F., 2016. PD-L1 is a critical mediator of regulatory B cells and T cells in invasive breast cancer. Sci Rep 6, 35651. https://doi.org/10.1038/srep35651

Gucalp, A., Tolaney, S., Isakoff, S.J., Ingle, J.N., Liu, M.C., Carey, L.A., Blackwell, K., Rugo, H., Nabell, L., Forero, A., Stearns, V., Doane, A.S., Danso, M., Moynahan, M.E., Momen, L.F., Gonzalez, J.M., Akhtar, A., Giri, D.D., Patil, S., Feigin, K.N., Hudis, C.A., Traina, T.A., Translational Breast Cancer Research Consortium (TBCRC 011), 2013. Phase II trial of bicalutamide in patients with androgen receptor-positive, estrogen receptor-negative metastatic Breast Cancer. Clin Cancer Res 19, 5505–5512. https://doi.org/10.1158/1078-0432.CCR-12-3327

Guo, F., Wang, Y., Liu, J., Mok, S.C., Xue, F., Zhang, W., 2016. CXCL12/CXCR4: a symbiotic bridge linking cancer cells and their stromal neighbors in oncogenic communication networks. Oncogene 35, 816–826. https://doi.org/10.1038/onc.2015.139

Hammerl, D., Martens, J.W.M., Timmermans, M., Smid, M., Trapman-Jansen, A.M., Foekens, R., Isaeva, O.I., Voorwerk, L., Balcioglu, H.E., Wijers, R., Nederlof, I., Salgado, R., Horlings, H., Kok, M., Debets, R., 2021a. Spatial immunophenotypes predict response to anti-PD1 treatment and capture distinct paths of T cell evasion in triple negative breast cancer. Nat Commun 12, 5668. https://doi.org/10.1038/s41467-021-25962-0

Hammerl, D., Martens, J.W.M., Timmermans, M., Smid, M., Trapman-Jansen, A.M., Foekens, R., Isaeva, O.I., Voorwerk, L., Balcioglu, H.E., Wijers, R., Nederlof, I., Salgado, R., Horlings, H., Kok, M., Debets, R., 2021b. Spatial immunophenotypes predict response to anti-PD1 treatment and capture distinct paths of T cell evasion in triple negative breast cancer. Nat Commun 12, 5668. https://doi.org/10.1038/s41467-021-25962-0

Hams, E., McCarron, M.J., Amu, S., Yagita, H., Azuma, M., Chen, L., Fallon, P.G., 2011. Blockade of B7-H1 (Programmed Death Ligand 1) Enhances Humoral Immunity by Positively Regulating the Generation of T Follicular Helper Cells. The Journal of Immunology 186, 5648–5655. https://doi.org/10.4049/jimmunol.1003161

Han, S., Hathcock, K., Zheng, B., Kepler, T.B., Hodes, R., Kelsoe, G., 1995. Cellular interaction in germinal centers. Roles of CD40 ligand and B7-2 in established germinal centers. J Immunol 155, 556–567.

Handelsman, D.J., Hirschberg, A.L., Bermon, S., 2018. Circulating Testosterone as the Hormonal Basis of Sex Differences in Athletic Performance. Endocr Rev 39, 803–829. https://doi.org/10.1210/er.2018-00020

Hardiman, T., 2022. Deciphering the molecular and cellular alterations in the premetastatic lymph node niche in breast cancer.

Harris, R.J., Cheung, A., Ng, J.C.F., Laddach, R., Chenoweth, A.M., Crescioli, S., Fittall, M., Dominguez-Rodriguez, D., Roberts, J., Levi, D., Liu, F., Alberts, E., Quist, J., Santaolalla, A., Pinder, S.E., Gillett, C., Hammar, N., Irshad, S., Van Hemelrijck, M., Dunn-Walters, D.K., Fraternali, F., Spicer, J.F., Lacy, K.E., Tsoka, S., Grigoriadis, A., Tutt, A.N.J., Karagiannis, S.N., 2021. Tumor-Infiltrating B Lymphocyte Profiling Identifies IgG-Biased, Clonally Expanded Prognostic

Phenotypes in Triple-Negative Breast Cancer. Cancer Res 81, 4290–4304. https://doi.org/10.1158/0008-5472.CAN-20-3773
Heise, N., De Silva, N.S., Silva, K., Carette, A., Simonetti, G., Pasparakis, M., Klein, U., 2014. Germinal center B cell maintenance and differentiation are controlled by distinct NF-κB transcription factor subunits. J Exp Med 211, 2103–2118. https://doi.org/10.1084/jem.20132613
Hiraga, T., Ninomiya, T., 2019. Establishment and characterization of a C57BL/6 mouse model of bone metastasis of breast cancer. J Bone Miner Metab 37, 235–242. https://doi.org/10.1007/s00774-018-0927-y
Hoch, T., Schulz, D., Eling, N., Gómez, J.M., Levesque, M.P., Bodenmiller, B., 2022. Multiplexed imaging mass cytometry of the chemokine milieus in melanoma characterizes features of the response to immunotherapy. Science Immunology 7, eabk1692. https://doi.org/10.1126/sciimmunol.abk1692
Hollern, D.P., Xu, N., Thennavan, A., Glodowski, C., Garcia-Recio, S., Mott, K.R., He, X., Garay, J.P., Carey-Ewend, K., Marron, D., Ford, J., Liu, S., Vick, S.C., Martin, M., Parker, J.S., Vincent, B.G., Serody, J.S., Perou, C.M., 2019. B Cells and T Follicular Helper Cells Mediate Response to Checkpoint Inhibitors in High Mutation Burden Mouse Models of Breast Cancer. Cell 179, 1191-1206.e21. https://doi.org/10.1016/j.cell.2019.10.028
Holmes, A.B., Corinaldesi, C., Shen, Q., Kumar, R., Compagno, N., Wang, Z., Nitzan, M., Grunstein, E., Pasqualucci, L., Dalla-Favera, R., Basso, K., 2020. Single-cell analysis of germinal-center B cells informs on lymphoma cell of origin and outcome. J Exp Med 217. https://doi.org/10.1084/jem.20200483
Hu, Q., Hong, Y., Qi, P., Lu, G., Mai, X., Xu, S., He, X., Guo, Y., Gao, L., Jing, Z., Wang, J., Cai, T., Zhang, Y., 2021. Atlas of breast cancer infiltrated B-lymphocytes revealed by paired single-cell RNA-sequencing and antigen receptor profiling. Nat Commun 12, 2186. https://doi.org/10.1038/s41467-021-22300-2
Hurst, J., Maniar, N., Tombarkiewicz, J., Lucas, F., Roberson, C., Steplewski, Z., James, W., Perras, J., 1993. A novel model of a metastatic human breast tumour xenograft line. Br J Cancer 68, 274–276. https://doi.org/10.1038/bjc.1993.327
Iglesia, M.D., Vincent, B.G., Parker, J.S., Hoadley, K., Carey, L.A., Perou, C.M., Serody, J.S., 2014. Prognostic B-Cell Signatures using mRNA-Seq in Patients with Subtype-Specific Breast and Ovarian Cancer. Clin Cancer Res 20, 3818–3829. https://doi.org/10.1158/1078-0432.CCR-13-3368
Ignatiadis, M., Van den Eynden, G., Roberto, S., Fornili, M., Bareche, Y., Desmedt, C., Rothé, F., Maetens, M., Venet, D., Holgado, E., McNally, V., Kiermaier, A., Savage, H.M., Wilson, T.R., Cortes, J., Schneeweiss, A., Willard-Gallo, K., Biganzoli, E., Sotiriou, C., 2019. Tumor-Infiltrating Lymphocytes in Patients Receiving Trastuzumab/Pertuzumab-Based Chemotherapy: A TRYPHAENA Substudy. J Natl Cancer Inst 111, 69–77. https://doi.org/10.1093/jnci/djy076
Ireland, L., Santos, A., Campbell, F., Figueiredo, C., Hammond, D., Ellies, L.G., Weyer-Czernilofsky, U., Bogenrieder, T., Schmid, M., Mielgo, A., 2018. Blockade of insulin-like growth factors increases efficacy of paclitaxel in metastatic breast cancer. Oncogene 37, 2022–2036. https://doi.org/10.1038/s41388-017-0115-x
Ishigami, E., Sakakibara, M., Sakakibara, J., Masuda, T., Fujimoto, H., Hayama, S., Nagashima, T., Sangai, T., Nakagawa, A., Nakatani, Y., Otsuka, M., 2019. Coexistence of regulatory B cells and regulatory T cells in tumor-infiltrating lymphocyte aggregates is a prognostic factor in patients with breast cancer. Breast Cancer 26, 180–189. https://doi.org/10.1007/s12282-018-0910-4
Jenkins, D.E., Hornig, Y.S., Oei, Y., Dusich, J., Purchio, T., 2005. Bioluminescent human breast cancer cell lines that permit rapid and sensitive in vivodetection of mammary tumors and multiple metastases in immune deficient mice. Breast Cancer Research 7, R444. https://doi.org/10.1186/bcr1026

Jenks, S.A., Cashman, K.S., Zumaquero, E., Marigorta, U.M., Patel, A.V., Wang, X., Tomar, D., Woodruff, M.C., Simon, Z., Bugrovsky, R., Blalock, E.L., Scharer, C.D., Tipton, C.M., Wei, C., Lim, S.S., Petri, M., Niewold, T.B., Anolik, J.H., Gibson, G., Lee, F.E.-H., Boss, J.M., Lund, F.E., Sanz, I., 2018. Distinct Effector B Cells Induced by Unregulated Toll-like Receptor 7 Contribute to Pathogenic Responses in Systemic Lupus Erythematosus. Immunity 49, 725-739.e6. https://doi.org/10.1016/j.immuni.2018.08.015

Jeurissen, A., Ceuppens, J.L., Bossuyt, X., 2004. T lymphocyte dependence of the antibody response to 'T lymphocyte independent type 2' antigens. Immunology 111, 1–7. https://doi.org/10.1111/j.1365-2567.2004.01775.x

Ji, R.-C., 2016. Lymph Nodes and Cancer Metastasis: New Perspectives on the Role of Intranodal Lymphatic Sinuses. Int J Mol Sci 18. https://doi.org/10.3390/ijms18010051

Jiao, S., Xiong, Q., Yan, M., Zhan, X., Yang, Z., Peng, C., Sun, B., Pang, D., Liu, T., 2022. Intratumor expanded T cell clones can be non-sentinel lymph node derived in breast cancer revealed by single-cell immune profiling. J Immunother Cancer 10, e003325. https://doi.org/10.1136/jitc-2021-003325

Jin, Y.W., Hu, P., 2020. Tumor-Infiltrating CD8 T Cells Predict Clinical Breast Cancer Outcomes in Young Women. Cancers (Basel) 12, 1076. https://doi.org/10.3390/cancers12051076

Johnstone, C.N., Smith, Y.E., Cao, Y., Burrows, A.D., Cross, R.S.N., Ling, X., Redvers, R.P., Doherty, J.P., Eckhardt, B.L., Natoli, A.L., Restall, C.M., Lucas, E., Pearson, H.B., Deb, S., Britt, K.L., Rizzitelli, A., Li, J., Harmey, J.H., Pouliot, N., Anderson, R.L., 2015. Functional and molecular characterisation of EO771.LMB tumours, a new C57BL/6-mouse-derived model of spontaneously metastatic mammary cancer. Dis Model Mech 8, 237–251. https://doi.org/10.1242/dmm.017830

Joseph, R., Soundararajan, R., Vasaikar, S., Yang, F., Allton, K.L., Tian, L., den Hollander, P., Isgandarova, S., Haemmerle, M., Mino, B., Zhou, T., Shin, C., Martinez-Paniagua, M., Sahin, A.A., Rodriguez-Canales, J., Gelovani, J., Chang, J.T., Acharya, G., Sood, A.K., Wistuba, I.I., Gibbons, D.L., Solis, L.M., Barton, M.C., Varadarajan, N., Rosen, J.M., Zhang, X.H., Mani, S.A., 2021. CD8+ T cells inhibit metastasis and CXCL4 regulates its function. Br J Cancer 125, 176–189. https://doi.org/10.1038/s41416-021-01338-5

Kallies, A., Hasbold, J., Tarlinton, D.M., Dietrich, W., Corcoran, L.M., Hodgkin, P.D., Nutt, S.L., 2004. Plasma Cell Ontogeny Defined by Quantitative Changes in Blimp-1 Expression. Journal of Experimental Medicine 200, 967–977. https://doi.org/10.1084/jem.20040973

Kang, Y., Siegel, P.M., Shu, W., Drobnjak, M., Kakonen, S.M., Cordón-Cardo, C., Guise, T.A., Massagué, J., 2003. A multigenic program mediating breast cancer metastasis to bone. Cancer Cell 3, 537–549. https://doi.org/10.1016/s1535-6108(03)00132-6

Karlsson, M.C., Gonzalez, S.F., Welin, J., Fuxe, J., 2017. Epithelial-mesenchymal transition in cancer metastasis through the lymphatic system. Mol Oncol 11, 781–791. https://doi.org/10.1002/1878-0261.12092

Kassambara et al., 2022. rstatix: Pipe-Friendly Framework for Basic Statistical Tests_. R package version 0.7.1.

Kennedy, D.E., Okoreeh, M.K., Maienschein-Cline, M., Ai, J., Veselits, M., McLean, K.C., Dhungana, Y., Wang, H., Peng, J., Chi, H., Mandal, M., Clark, M.R., 2020. Novel specialized cell state and spatial compartments within the germinal center. Nature Immunology 21, 660–670. https://doi.org/10.1038/s41590-020-0660-2

Keren, L., Bosse, M., Marquez, D., Angoshtari, R., Jain, S., Varma, S., Yang, S.-R., Kurian, A., Van Valen, D., West, R., Bendall, S.C., Angelo, M., 2018. A Structured Tumor-Immune Microenvironment in Triple Negative Breast Cancer Revealed by Multiplexed Ion Beam Imaging. Cell 174, 1373-1387.e19. https://doi.org/10.1016/j.cell.2018.08.039

Kerfoot, S.M., Yaari, G., Patel, J.R., Johnson, K.L., Gonzalez, D.G., Kleinstein, S.H., Haberman, A.M., 2011. Germinal center B cell and T follicular helper cell development initiates in the interfollicular zone. Immunity 34, 947–960. https://doi.org/10.1016/j.immuni.2011.03.024

Khadri, F.-Z., Issac, M.S.M., Gaboury, L.A., 2021. Impact of Epithelial–Mesenchymal Transition on the Immune Landscape in Breast Cancer. Cancers 13, 5099. https://doi.org/10.3390/cancers13205099
Kim, J.B., O'Hare, M.J., Stein, R., 2004. Models of breast cancer: is merging human and animal models the future? Breast Cancer Res 6, 22–30. https://doi.org/10.1186/bcr645
Kim, R.-K., Suh, Y., Yoo, K.-C., Cui, Y.-H., Kim, H., Kim, M.-J., Gyu Kim, I., Lee, S.-J., 2015. Activation of KRAS promotes the mesenchymal features of basal-type breast cancer. Exp Mol Med 47, e137–e137. https://doi.org/10.1038/emm.2014.99
King, H., Orban, N., Riches, J., Clear, A., Warnes, G., Teichmann, S., James, L., 2021. Single-cell analysis of human B cell maturation predicts how antibody class switching shapes selection dynamics. Science Immunology 6, eabe6291. https://doi.org/10.1126/sciimmunol.abe6291
King, H.W., Orban, N., Riches, J.C., Clear, A.J., Warnes, G., Teichmann, S.A., James, L.K., 2021. Single-cell analysis of human B cell maturation predicts how antibody class switching shapes selection dynamics. Sci Immunol 6, eabe6291. https://doi.org/10.1126/sciimmunol.abe6291
Kishi, Y., Aiba, Y., Higuchi, T., Furukawa, K., Tokuhisa, T., Takemori, T., Tsubata, T., 2010. Augmented antibody response with premature germinal center regression in CD40L transgenic mice. J Immunol 185, 211–219. https://doi.org/10.4049/jimmunol.0901694
Klein, L., Kyewski, B., Allen, P.M., Hogquist, K.A., 2014. Positive and negative selection of the T cell repertoire: what thymocytes see and don't see. Nat Rev Immunol 14, 377–391. https://doi.org/10.1038/nri3667
Kohrt, H.E., Nouri, N., Nowels, K., Johnson, D., Holmes, S., Lee, P.P., 2005a. Profile of Immune Cells in Axillary Lymph Nodes Predicts Disease-Free Survival in Breast Cancer. PLOS Medicine 2, e284. https://doi.org/10.1371/journal.pmed.0020284
Kohrt, H.E., Nouri, N., Nowels, K., Johnson, D., Holmes, S., Lee, P.P., 2005b. Profile of immune cells in axillary lymph nodes predicts disease-free survival in breast cancer. PLoS Med 2, e284. https://doi.org/10.1371/journal.pmed.0020284
Kolyvas, E.A., Caldas, C., Kelly, K., Ahmad, S.S., 2022. Androgen receptor function and targeted therapeutics across breast cancer subtypes. Breast Cancer Research 24, 79. https://doi.org/10.1186/s13058-022-01574-4
Koncz, G., Hueber, A.-O., 2012. The Fas/CD95 Receptor Regulates the Death of Autoreactive B Cells and the Selection of Antigen-Specific B Cells. Front Immunol 3, 207. https://doi.org/10.3389/fimmu.2012.00207
Korotkevich, G., Sukhov, V., Budin, N., Shpak, B., Artyomov, M.N., Sergushichev, A., 2021. Fast gene set enrichment analysis. https://doi.org/10.1101/060012
Kozai, M., Kubo, Y., Katakai, T., Kondo, H., Kiyonari, H., Schaeuble, K., Luther, S.A., Ishimaru, N., Ohigashi, I., Takahama, Y., 2017. Essential role of CCL21 in establishment of central self-tolerance in T cells. Journal of Experimental Medicine 214, 1925–1935. https://doi.org/10.1084/jem.20161864
Kuhn, D.J., Berkova, Z., Jones, R.J., Woessner, R., Bjorklund, C.C., Ma, W., Davis, R.E., Lin, P., Wang, H., Madden, T.L., Wei, C., Baladandayuthapani, V., Wang, M., Thomas, S.K., Shah, J.J., Weber, D.M., Orlowski, R.Z., 2012. Targeting the insulin-like growth factor-1 receptor to overcome bortezomib resistance in preclinical models of multiple myeloma. Blood 120, 3260–3270. https://doi.org/10.1182/blood-2011-10-386789
Kumar, V., Yu, J., Phan, V., Tudor, I.C., Peterson, A., Uppal, H., 2017. Androgen Receptor Immunohistochemistry as a Companion Diagnostic Approach to Predict Clinical Response to Enzalutamide in Triple-Negative Breast Cancer. JCO Precision Oncology 1–19. https://doi.org/10.1200/PO.17.00075
Kuperwasser, C., Dessain, S., Bierbaum, B.E., Garnet, D., Sperandio, K., Gauvin, G.P., Naber, S.P., Weinberg, R.A., Rosenblatt, M., 2005. A mouse model of human breast cancer metastasis to human bone. Cancer Res 65, 6130–6138. https://doi.org/10.1158/0008-5472.CAN-04-1408

Kuraoka, M., Liao, D., Yang, K., Allgood, S.D., Levesque, M.C., Kelsoe, G., Ueda, Y., 2009. Activation-Induced Cytidine Deaminase Expression and Activity in the Absence of Germinal Centers: Insights into Hyper-IgM Syndrome. J Immunol 183, 3237–3248. https://doi.org/10.4049/jimmunol.0901548

Kwon, H., Schafer, J.M., Song, N.-J., Kaneko, S., Li, A., Xiao, T., Ma, A., Allen, C., Das, K., Zhou, L., Riesenberg, B., Chang, Y., Weltge, P., Velegraki, M., Oh, D.Y., Fong, L., Ma, Q., Sundi, D., Chung, D., Li, X., Li, Z., 2022. Androgen Conspires with the CD8+ T Cell Exhaustion Program and Contributes to Sex Bias in Cancer. Sci Immunol 7, eabq2630. https://doi.org/10.1126/sciimmunol.abq2630

Kwon, H., Thierry-Mieg, D., Thierry-Mieg, J., Kim, H.-P., Oh, J., Tunyaplin, C., Carotta, S., Donovan, C.E., Goldman, M.L., Tailor, P., Ozato, K., Levy, D.E., Nutt, S.L., Calame, K., Leonard, W.J., 2009. Analysis of interleukin-21-induced Prdm1 gene regulation reveals functional cooperation of STAT3 and IRF4 transcription factors. Immunity 31, 941–952. https://doi.org/10.1016/j.immuni.2009.10.008

Laidlaw, B.J., Cyster, J.G., 2020. Transcriptional regulation of memory B cell differentiation. Nat Rev Immunol. https://doi.org/10.1038/s41577-020-00446-2

Laidlaw, B.J., Duan, L., Xu, Y., Vazquez, S.E., Cyster, J.G., 2020. The transcription factor Hhex cooperates with the corepressor Tle3 to promote memory B cell development. Nat Immunol 21, 1082–1093. https://doi.org/10.1038/s41590-020-0713-6

Landreth, K.S., Narayanan, R., Dorshkind, K., 1992. Insulin-like growth factor-I regulates pro-B cell differentiation. Blood 80, 1207–1212.

Larionova, I., Tuguzbaeva, G., Ponomaryova, A., Stakheyeva, M., Cherdyntseva, N., Pavlov, V., Choinzonov, E., Kzhyshkowska, J., 2020. Tumor-Associated Macrophages in Human Breast, Colorectal, Lung, Ovarian and Prostate Cancers. Frontiers in Oncology 10.

Laron, Z., 2001. Insulin-like growth factor 1 (IGF-1): a growth hormone. Mol Pathol 54, 311–316.

Larsson, O., Girnita, A., Girnita, L., 2005. Role of insulin-like growth factor 1 receptor signalling in cancer. Br J Cancer 92, 2097–2101. https://doi.org/10.1038/sj.bjc.6602627

Le Naour, A., Koffi, Y., Diab, M., Le Guennec, D., Rougé, S., Aldekwer, S., Goncalves-Mendes, N., Talvas, J., Farges, M.-C., Caldefie-Chezet, F., Vasson, M.-P., Rossary, A., 2020a. EO771, the first luminal B mammary cancer cell line from C57BL/6 mice. Cancer Cell International 20, 328. https://doi.org/10.1186/s12935-020-01418-1

Le Naour, A., Rossary, A., Vasson, M., 2020b. EO771, is it a well-characterized cell line for mouse mammary cancer model? Limit and uncertainty. Cancer Med 9, 8074–8085. https://doi.org/10.1002/cam4.3295

Lee, H.J., Park, I.A., Song, I.H., Shin, S.-J., Kim, J.Y., Yu, J.H., Gong, G., 2016. Tertiary lymphoid structures: prognostic significance and relationship with tumour-infiltrating lymphocytes in triple-negative breast cancer. J. Clin. Pathol. 69, 422–430. https://doi.org/10.1136/jclinpath-2015-203089

Lehmann, B.D., Bauer, J.A., Chen, X., Sanders, M.E., Chakravarthy, A.B., Shyr, Y., Pietenpol, J.A., 2011. Identification of human triple-negative breast cancer subtypes and preclinical models for selection of targeted therapies. J Clin Invest 121, 2750–2767. https://doi.org/10.1172/JCI45014

Lentz, V.M., Manser, T., 2001. Cutting Edge: Germinal Centers Can Be Induced in the Absence of T Cells1. The Journal of Immunology 167, 15–20. https://doi.org/10.4049/jimmunol.167.1.15

Li, M., He, L., Zhu, J., Zhang, P., Liang, S., 2022. Targeting tumor-associated macrophages for cancer treatment. Cell Biosci 12, 85. https://doi.org/10.1186/s13578-022-00823-5

Li, Q., Lao, X., Pan, Q., Ning, N., Yet, J., Xu, Y., Li, S., Chang, A.E., 2011. Adoptive transfer of tumor reactive B cells confers host T-cell immunity and tumor regression. Clin Cancer Res 17, 4987–4995. https://doi.org/10.1158/1078-0432.CCR-11-0207

Li Q., Xia Y., 2015. Antitumor effector B cells directly kill tumor cells involving the CXCL12/CXCR4 pathway and their therapeutic efficacy is enhanced by IL-2. J. Immunother. Cancer, 30th

Annual Scientific Meeting of the Society for Immunotherapy of Cancer, SITC 2015. National Harbor, MD United States. 3.
Li, X., Gadzinsky, A., Gong, L., Tong, H., Calderon, V., Li, Y., Kitamura, D., Klein, U., Langdon, W.Y., Hou, F., Zou, Y.-R., Gu, H., 2018. Cbl Ubiquitin Ligases Control B Cell Exit from the Germinal-Center Reaction. Immunity 48, 530-541.e6. https://doi.org/10.1016/j.immuni.2018.03.006
Li, Y., Li, Z., Hu, F., 2021. Double-negative (DN) B cells: an under-recognized effector memory B cell subset in autoimmunity. Clinical & Experimental Immunology 205, 119–127. https://doi.org/10.1111/cei.13615
Liao, N., Li, C., Cao, L., Chen, Y., Ren, C., Chen, X., Mok, H., Wen, L., Li, K., Wang, Y., Zhang, Y., Li, Y., Lv, J., Cao, F., Luo, Y., Li, H., Wu, W., Balch, C.M., Giuliano, A.E., 2023. Single-cell profile of tumor and immune cells in primary breast cancer, sentinel lymph node, and metastatic lymph node. Breast Cancer 30, 77–87. https://doi.org/10.1007/s12282-022-01400-x
Lin, E.Y., Jones, J.G., Li, P., Zhu, L., Whitney, K.D., Muller, W.J., Pollard, J.W., 2003. Progression to malignancy in the polyoma middle T oncoprotein mouse breast cancer model provides a reliable model for human diseases. Am J Pathol 163, 2113–2126. https://doi.org/10.1016/S0002-9440(10)63568-7
Linterman, M.A., Pierson, W., Lee, S.K., Kallies, A., Kawamoto, S., Rayner, T.F., Srivastava, M., Divekar, D.P., Beaton, L., Hogan, J.J., Fagarasan, S., Liston, A., Smith, K.G.C., Vinuesa, C.G., 2011. Foxp3+ follicular regulatory T cells control the germinal center response. Nat Med 17, 975–982. https://doi.org/10.1038/nm.2425
Liu, F., Hardiman, T., Wu, K., Quist, J., Gazinska, P., Ng, T., Purushotham, A., Salgado, R., Guo, X., Pinder, S.E., Grigoriadis, A., 2021. Systemic immune reaction in axillary lymph nodes adds to tumor-infiltrating lymphocytes in triple-negative breast cancer prognostication. npj Breast Cancer 7, 1–10. https://doi.org/10.1038/s41523-021-00292-y
Liu, R., Lu, Z., Gu, J., Liu, J., Huang, E., Liu, X., Wang, L., Yang, J., Deng, Y., Qian, Jiawen, Luo, F., Wang, Z., Zhang, H., Jiang, X., Zhang, D., Qian, Jing, Liu, G., Zhu, H., Qian, Y., Liu, Z., Chu, Y., 2018. MicroRNAs 15A and 16-1 Activate Signaling Pathways That Mediate Chemotaxis of Immune Regulatory B cells to Colorectal Tumors. Gastroenterology 154, 637-651.e7. https://doi.org/10.1053/j.gastro.2017.09.045
Liu, T., Liu, C., Yan, M., Zhang, L., Zhang, J., Xiao, M., Li, Z., Wei, X., Zhang, H., 2022. Single cell profiling of primary and paired metastatic lymph node tumors in breast cancer patients. Nat Commun 13, 6823. https://doi.org/10.1038/s41467-022-34581-2
Liu, Y., Cheng, L.-S., Wu, S., Wang, S.-Q., Li, L., She, W.-M., Li, J., Wang, J.-Y., Jiang, W., 2016. IL-10-producing regulatory B-cells suppressed effector T-cells but enhanced regulatory T-cells in chronic HBV infection. Clin. Sci. 130, 907–919. https://doi.org/10.1042/CS20160069
Loder, F., Mutschler, B., Ray, R.J., Paige, C.J., Sideras, P., Torres, R., Lamers, M.C., Carsetti, R., 1999. B cell development in the spleen takes place in discrete steps and is determined by the quality of B cell receptor-derived signals. J Exp Med 190, 75–89. https://doi.org/10.1084/jem.190.1.75
Loi, S., Drubay, D., Adams, S., Pruneri, G., Francis, P.A., Lacroix-Triki, M., Joensuu, H., Dieci, M.V., Badve, S., Demaria, S., Gray, R., Munzone, E., Lemonnier, J., Sotiriou, C., Piccart, M.J., Kellokumpu-Lehtinen, P.-L., Vingiani, A., Gray, K., Andre, F., Denkert, C., Salgado, R., Michiels, S., 2019a. Tumor-Infiltrating Lymphocytes and Prognosis: A Pooled Individual Patient Analysis of Early-Stage Triple-Negative Breast Cancers. J Clin Oncol 37, 559–569. https://doi.org/10.1200/JCO.18.01010
Loi, S., Drubay, D., Adams, S., Pruneri, G., Francis, P.A., Lacroix-Triki, M., Joensuu, H., Dieci, M.V., Badve, S., Demaria, S., Gray, R., Munzone, E., Lemonnier, J., Sotiriou, C., Piccart, M.J., Kellokumpu-Lehtinen, P.-L., Vingiani, A., Gray, K., Andre, F., Denkert, C., Salgado, R., Michiels, S., 2019b. Tumor-Infiltrating Lymphocytes and Prognosis: A Pooled Individual Patient Analysis of Early-Stage Triple-Negative Breast Cancers. J Clin Oncol 37, 559–569. https://doi.org/10.1200/JCO.18.01010

Loi, S., Winer, E., Lipatov, O., Im, S.-A., Goncalves, A., Cortes, J., Lee, K.S., Schmid, P., Testa, L., Witzel, I., Ohtani, S., Turner, N., Zambelli, S., Harbeck, N., Andre, F., Dent, R., Huang, L., Mejia, J., Karantza, V., Salgado, R., 2020. Abstract PD5-03: Relationship between tumor-infiltrating lymphocytes (TILs) and outcomes in the KEYNOTE-119 study of pembrolizumab vs chemotherapy for previously treated metastatic triple-negative breast cancer (mTNBC). Cancer Res 80, PD5-03-PD5-03. https://doi.org/10.1158/1538-7445.SABCS19-PD5-03

Lores, B., Garcia-Estevez, J.M., Arias, C., 1998. Lymph nodes and human tumors (review). Int J Mol Med 1, 729–733. https://doi.org/10.3892/ijmm.1.4.729

Louie, D.A.P., Oo, D., Leung, G., Lin, Y., Stephens, M., Alrashed, O., Tso, M., Liao, S., 2022. Tumor-Draining Lymph Node Reconstruction Promotes B Cell Activation During E0771 Mouse Breast Cancer Growth. Front Pharmacol 13, 825287. https://doi.org/10.3389/fphar.2022.825287

Luen, S.J., Salgado, R., Dieci, M.V., Vingiani, A., Curigliano, G., Gould, R.E., Castaneda, C., D'Alfonso, T., Sanchez, J., Cheng, E., Andreopoulou, E., Castillo, M., Adams, S., Demaria, S., Symmans, W.F., Michiels, S., Loi, S., 2019. Prognostic implications of residual disease tumor-infiltrating lymphocytes and residual cancer burden in triple-negative breast cancer patients after neoadjuvant chemotherapy. Ann Oncol 30, 236–242. https://doi.org/10.1093/annonc/mdy547

Lund, F.E., Randall, T.D., 2010. Effector and regulatory B cells: modulators of CD4+ T cell immunity. Nat Rev Immunol 10, 236–247. https://doi.org/10.1038/nri2729

Luo, J., Jin, J., Yang, F., Sun, Z., Zhang, W., Shi, Y., Xu, J., Guan, X., 2016. The Correlation Between PARP1 and BRCA1 in AR Positive Triple-negative Breast Cancer. Int J Biol Sci 12, 1500–1510. https://doi.org/10.7150/ijbs.16176

MacLennan, I.C.M., Johnson, G.D., Liu, Y.-J., Gordon, J., 1991. The heterogeneity of follicular reactions. Research in Immunology 142, 253–257. https://doi.org/10.1016/0923-2494(91)90070-Y

MacLennan, I.C.M., Toellner, K.-M., Cunningham, A.F., Serre, K., Sze, D.M.-Y., Zúñiga, E., Cook, M.C., Vinuesa, C.G., 2003. Extrafollicular antibody responses. Immunological Reviews 194, 8–18. https://doi.org/10.1034/j.1600-065X.2003.00058.x

Maglione, J.E., Moghanaki, D., Young, L.J., Manner, C.K., Ellies, L.G., Joseph, S.O., Nicholson, B., Cardiff, R.D., MacLeod, C.L., 2001. Transgenic Polyoma middle-T mice model premalignant mammary disease. Cancer Res 61, 8298–8305.

Mahfoudh, W., Bettaieb, I., Ghedira, R., Snoussi, K., Bouzid, N., Klayech, Z., Gabbouj, S., Remadi, Y., Hassen, E., Bouaouina, N., Zakhama, A., 2019. Contribution of BRCA1 5382insC mutation in triple negative breast cancer in Tunisia. J Transl Med 17, 123. https://doi.org/10.1186/s12967-019-1873-8

Maloney, E.K., McLaughlin, J.L., Dagdigian, N.E., Garrett, L.M., Connors, K.M., Zhou, X.-M., Blättler, W.A., Chittenden, T., Singh, R., 2003. An anti-insulin-like growth factor I receptor antibody that is a potent inhibitor of cancer cell proliferation. Cancer Res 63, 5073–5083.

Mayer, C.T., Gazumyan, A., Kara, E.E., Gitlin, A.D., Golijanin, J., Viant, C., Pai, J., Oliveira, T.Y., Wang, Q., Escolano, A., Medina-Ramirez, M., Sanders, R.W., Nussenzweig, M.C., 2017. The microanatomic segregation of selection by apoptosis in the germinal center. Science 358, eaao2602. https://doi.org/10.1126/science.aao2602

McAllister, E.J., Apgar, J.R., Leung, C.R., Rickert, R.C., Jellusova, J., 2017. New methods to analyze B cell immune responses to the thymus dependent antigen sheep red blood cells. J Immunol 199, 2998–3003. https://doi.org/10.4049/jimmunol.1700454

McCarron, M.J., Park, P.W., Fooksman, D.R., 2017. CD138 mediates selection of mature plasma cells by regulating their survival. Blood 129, 2749–2759. https://doi.org/10.1182/blood-2017-01-761643

McDaniel, J.R., Pero, S.C., Voss, W.N., Shukla, G.S., Sun, Y., Schaetzle, S., Lee, C.-H., Horton, A.P., Harlow, S., Gollihar, J., Ellefson, J.W., Krag, C.C., Tanno, Y., Sidiropoulos, N., Georgiou, G., Ippolito, G.C., Krag, D.N., 2018. Identification of tumor-reactive B cells and systemic IgG in

breast cancer based on clonal frequency in the sentinel lymph node. Cancer Immunol Immunother 67, 729–738. https://doi.org/10.1007/s00262-018-2123-2
McHeyzer-Williams, L.J., Milpied, P.J., Okitsu, S.L., McHeyzer-Williams, M.G., 2015. Class-switched memory B cells remodel BCRs within secondary germinal centers. Nat Immunol 16, 296–305. https://doi.org/10.1038/ni.3095
Mehdipour, F., Razmkhah, M., Hosseini, A., Bagheri, M., Safaei, A., Talei, A.-R., Ghaderi, A., 2016a. Increased B Regulatory Phenotype in Non-Metastatic Lymph Nodes of Node-Positive Breast Cancer Patients. Scand J Immunol 83, 195–202. https://doi.org/10.1111/sji.12407
Mehdipour, F., Razmkhah, M., Hosseini, A., Bagheri, M., Safaei, A., Talei, A.-R., Ghaderi, A., 2016b. Increased B Regulatory Phenotype in Non-Metastatic Lymph Nodes of Node-Positive Breast Cancer Patients. Scand J Immunol 83, 195–202. https://doi.org/10.1111/sji.12407
Meyer-Hermann, M., Mohr, E., Pelletier, N., Zhang, Y., Victora, G.D., Toellner, K.-M., 2012. A Theory of Germinal Center B Cell Selection, Division, and Exit. Cell Reports 2, 162–174. https://doi.org/10.1016/j.celrep.2012.05.010
Micello, D., Marando, A., Sahnane, N., Riva, C., Capella, C., Sessa, F., 2010. Androgen receptor is frequently expressed in HER2-positive, ER/PR-negative breast cancers. Virchows Arch 457, 467–476. https://doi.org/10.1007/s00428-010-0964-y
Miles, B., Connick, E., 2018. Control of the Germinal Center by Follicular Regulatory T Cells During Infection. Front Immunol 9. https://doi.org/10.3389/fimmu.2018.02704
Miles, D., Gligorov, J., André, F., Cameron, D., Schneeweiss, A., Barrios, C., Xu, B., Wardley, A., Kaen, D., Andrade, L., Semiglazov, V., Reinisch, M., Patel, S., Patre, M., Morales, L., Patel, S.L., Kaul, M., Barata, T., O'Shaughnessy, J., IMpassion131 investigators, 2021. Primary results from IMpassion131, a double-blind, placebo-controlled, randomised phase III trial of first-line paclitaxel with or without atezolizumab for unresectable locally advanced/metastatic triple-negative breast cancer. Ann Oncol 32, 994–1004. https://doi.org/10.1016/j.annonc.2021.05.801
Miller, F.R., 1983. Tumor subpopulation interactions in metastasis. Invasion Metastasis 3, 234–242.
Min, A., Jang, H., Kim, S., Lee, K.-H., Kim, D.K., Suh, K.J., Yang, Y., Elvin, P., O'Connor, M.J., Im, S.-A., 2018. Androgen Receptor Inhibitor Enhances the Antitumor Effect of PARP Inhibitor in Breast Cancer Cells by Modulating DNA Damage Response. Mol Cancer Ther 17, 2507–2518. https://doi.org/10.1158/1535-7163.MCT-18-0234
Minn, A.J., Gupta, G.P., Siegel, P.M., Bos, P.D., Shu, W., Giri, D.D., Viale, A., Olshen, A.B., Gerald, W.L., Massagué, J., 2005. Genes that mediate breast cancer metastasis to lung. Nature 436, 518–524. https://doi.org/10.1038/nature03799
Mittendorf, E.A., Philips, A.V., Meric-Bernstam, F., Qiao, N., Wu, Y., Harrington, S., Su, X., Wang, Y., Gonzalez-Angulo, A.M., Akcakanat, A., Chawla, A., Curran, M., Hwu, P., Sharma, P., Litton, J.K., Molldrem, J.J., Alatrash, G., 2014. PD-L1 Expression in Triple-Negative Breast Cancer. Cancer Immunology Research 2, 361–370. https://doi.org/10.1158/2326-6066.CIR-13-0127
Monteran, L., Ershaid, N., Sabah, I., Fahoum, I., Zait, Y., Shani, O., Cohen, N., Eldar-Boock, A., Satchi-Fainaro, R., Erez, N., 2020. Bone metastasis is associated with acquisition of mesenchymal phenotype and immune suppression in a model of spontaneous breast cancer metastasis. Sci Rep 10, 13838. https://doi.org/10.1038/s41598-020-70788-3
Muramatsu, M., Kinoshita, K., Fagarasan, S., Yamada, S., Shinkai, Y., Honjo, T., 2000. Class switch recombination and hypermutation require activation-induced cytidine deaminase (AID), a potential RNA editing enzyme. Cell 102, 553–563. https://doi.org/10.1016/s0092-8674(00)00078-7
Nakagawa, R., Toboso-Navasa, A., Schips, M., Young, G., Bhaw-Rosun, L., Llorian-Sopena, M., Chakravarty, P., Sesay, A.K., Kassiotis, G., Meyer-Hermann, M., Calado, D.P., 2021a. Permissive selection followed by affinity-based proliferation of GC light zone B cells dictates cell fate and ensures clonal breadth. PNAS 118. https://doi.org/10.1073/pnas.2016425118

Nakagawa, R., Toboso-Navasa, A., Schips, M., Young, G., Bhaw-Rosun, L., Llorian-Sopena, M., Chakravarty, P., Sesay, A.K., Kassiotis, G., Meyer-Hermann, M., Calado, D.P., 2021b. Permissive selection followed by affinity-based proliferation of GC light zone B cells dictates cell fate and ensures clonal breadth. PNAS 118. https://doi.org/10.1073/pnas.2016425118

Narayanan, R., Ahn, S., Cheney, M.D., Yepuru, M., Miller, D.D., Steiner, M.S., Dalton, J.T., 2014. Selective androgen receptor modulators (SARMs) negatively regulate triple-negative breast cancer growth and epithelial:mesenchymal stem cell signaling. PLoS One 9, e103202. https://doi.org/10.1371/journal.pone.0103202

Nasser, M.W., Qamri, Z., Deol, Y.S., Ravi, J., Powell, C.A., Trikha, P., Schwendener, R.A., Bai, X.-F., Shilo, K., Zou, X., Leone, G., Wolf, R., Yuspa, S.H., Ganju, R.K., 2012. S100A7 Enhances Mammary Tumorigenesis through Upregulation of Inflammatory Pathways. Cancer Research 72, 604–615. https://doi.org/10.1158/0008-5472.CAN-11-0669

Nedeljković, M., Damjanović, A., 2019. Mechanisms of Chemotherapy Resistance in Triple-Negative Breast Cancer—How We Can Rise to the Challenge. Cells 8, 957. https://doi.org/10.3390/cells8090957

Nederlof, I., Horlings, H.M., Curtis, C., Kok, M., 2021. A High-Dimensional Window into the Micro-Environment of Triple Negative Breast Cancer. Cancers (Basel) 13, 316. https://doi.org/10.3390/cancers13020316

Nelson, H.D., Cantor, A., Humphrey, L., Fu, R., Pappas, M., Daeges, M., Griffin, J., 2016. Table 1, Breast Cancer Staging System* [WWW Document]. URL https://www.ncbi.nlm.nih.gov/books/NBK343820/table/ch1.t1/ (accessed 9.11.22).

Nounou, M.I., ElAmrawy, F., Ahmed, N., Abdelraouf, K., Goda, S., Syed-Sha-Qhattal, H., 2015. Breast Cancer: Conventional Diagnosis and Treatment Modalities and Recent Patents and Technologies. Breast Cancer (Auckl) 9, 17–34. https://doi.org/10.4137/BCBCR.S29420

Novinger, L.J., Ashikaga, T., Krag, D.N., 2015. Identification of tumor-binding scFv derived from clonally related B cells in tumor and lymph node of a patient with breast cancer. Cancer Immunol Immunother 64, 29–39. https://doi.org/10.1007/s00262-014-1612-1

Núñez, N.G., Tosello Boari, J., Ramos, R.N., Richer, W., Cagnard, N., Anderfuhren, C.D., Niborski, L.L., Bigot, J., Meseure, D., De La Rochere, P., Milder, M., Viel, S., Loirat, D., Pérol, L., Vincent-Salomon, A., Sastre-Garau, X., Burkhard, B., Sedlik, C., Lantz, O., Amigorena, S., Piaggio, E., 2020. Tumor invasion in draining lymph nodes is associated with Treg accumulation in breast cancer patients. Nature Communications 11, 3272. https://doi.org/10.1038/s41467-020-17046-2

Nutt, S.L., Hodgkin, P.D., Tarlinton, D.M., Corcoran, L.M., 2015a. The generation of antibody-secreting plasma cells. Nature Reviews Immunology 15, 160–171. https://doi.org/10.1038/nri3795

Nutt, S.L., Hodgkin, P.D., Tarlinton, D.M., Corcoran, L.M., 2015b. The generation of antibody-secreting plasma cells. Nat Rev Immunol 15, 160–171. https://doi.org/10.1038/nri3795

Nutt, S.L., Taubenheim, N., Hasbold, J., Corcoran, L.M., Hodgkin, P.D., 2011. The genetic network controlling plasma cell differentiation. Seminars in Immunology, Parsing Gene Networks Underpinning Immune System Development 23, 341–349. https://doi.org/10.1016/j.smim.2011.08.010

Nzula, S., Going, J.J., Stott, D.I., 2003. Antigen-driven clonal proliferation, somatic hypermutation, and selection of B lymphocytes infiltrating human ductal breast carcinomas. Cancer Res 63, 3275–3280.

Oberlin, D., Fellbaum, C., Eppler, E., 2009. Insulin-like growth factor I messenger RNA and protein are expressed in the human lymph node and distinctly confined to subtypes of macrophages, antigen-presenting cells, lymphocytes and endothelial cells. Immunology 128, 342–350. https://doi.org/10.1111/j.1365-2567.2009.03136.x

Ochiai, K., Maienschein-Cline, M., Simonetti, G., Chen, J., Rosenthal, R., Brink, R., Chong, A.S., Klein, U., Dinner, A.R., Singh, H., Sciammas, R., 2013. Transcriptional regulation of germinal center

B and plasma cell fates by dynamical control of IRF4. Immunity 38, 918–929. https://doi.org/10.1016/j.immuni.2013.04.009
Okamura, K., Nagayama, S., Tate, T., Chan, H.T., Kiyotani, K., Nakamura, Y., 2022. Lymphocytes in tumor-draining lymph nodes co-cultured with autologous tumor cells for adoptive cell therapy. Journal of Translational Medicine 20, 241. https://doi.org/10.1186/s12967-022-03444-1
Okita, Y., Ohira, M., Tanaka, H., Tokumoto, M., Go, Y., Sakurai, K., Toyokawa, T., Kubo, N., Muguruma, K., Sawada, T., Maeda, K., Hirakawa, K., 2015. Alteration of CD4 T cell subsets in metastatic lymph nodes of human gastric cancer. Oncology Reports 34, 639–647. https://doi.org/10.3892/or.2015.4064
Oliver, A.M., Martin, F., Kearney, J.F., 1997. Mouse CD38 is down-regulated on germinal center B cells and mature plasma cells. J Immunol 158, 1108–1115.
Olson, W.J., Jakic, B., Hermann-Kleiter, N., 2020. Regulation of the germinal center response by nuclear receptors and implications for autoimmune diseases. FEBS J 287, 2866–2890. https://doi.org/10.1111/febs.15312
Onitilo, A.A., Engel, J.M., Greenlee, R.T., Mukesh, B.N., 2009. Breast cancer subtypes based on ER/PR and Her2 expression: comparison of clinicopathologic features and survival. Clin Med Res 7, 4–13. https://doi.org/10.3121/cmr.2009.825
Orimo, A., Gupta, P.B., Sgroi, D.C., Arenzana-Seisdedos, F., Delaunay, T., Naeem, R., Carey, V.J., Richardson, A.L., Weinberg, R.A., 2005. Stromal fibroblasts present in invasive human breast carcinomas promote tumor growth and angiogenesis through elevated SDF-1/CXCL12 secretion. Cell 121, 335–348. https://doi.org/10.1016/j.cell.2005.02.034
Oshi, M., Asaoka, M., Tokumaru, Y., Yan, L., Matsuyama, R., Ishikawa, T., Endo, I., Takabe, K., 2020. CD8 T Cell Score as a Prognostic Biomarker for Triple Negative Breast Cancer. Int J Mol Sci 21, 6968. https://doi.org/10.3390/ijms21186968
Parker, J.S., Mullins, M., Cheang, M.C.U., Leung, S., Voduc, D., Vickery, T., Davies, S., Fauron, C., He, X., Hu, Z., Quackenbush, J.F., Stijleman, I.J., Palazzo, J., Marron, J.S., Nobel, A.B., Mardis, E., Nielsen, T.O., Ellis, M.J., Perou, C.M., Bernard, P.S., 2009. Supervised Risk Predictor of Breast Cancer Based on Intrinsic Subtypes. J Clin Oncol 27, 1160–1167. https://doi.org/10.1200/JCO.2008.18.1370
Paus, D., Phan, T.G., Chan, T.D., Gardam, S., Basten, A., Brink, R., 2006. Antigen recognition strength regulates the choice between extrafollicular plasma cell and germinal center B cell differentiation. J Exp Med 203, 1081–1091. https://doi.org/10.1084/jem.20060087
Peng, M., Mo, Y., Wang, Y., Wu, P., Zhang, Y., Xiong, F., Guo, C., Wu, X., Li, Y., Li, X., Li, G., Xiong, W., Zeng, Z., 2019. Neoantigen vaccine: an emerging tumor immunotherapy. Molecular Cancer 18, 128. https://doi.org/10.1186/s12943-019-1055-6
Perou, C.M., Jeffrey, S.S., van de Rijn, M., Rees, C.A., Eisen, M.B., Ross, D.T., Pergamenschikov, A., Williams, C.F., Zhu, S.X., Lee, J.C.F., Lashkari, D., Shalon, D., Brown, P.O., Botstein, D., 1999. Distinctive gene expression patterns in human mammary epithelial cells and breast cancers. Proc Natl Acad Sci U S A 96, 9212–9217.
Perou, C.M., Sørlie, T., Eisen, M.B., van de Rijn, M., Jeffrey, S.S., Rees, C.A., Pollack, J.R., Ross, D.T., Johnsen, H., Akslen, L.A., Fluge, O., Pergamenschikov, A., Williams, C., Zhu, S.X., Lønning, P.E., Børresen-Dale, A.L., Brown, P.O., Botstein, D., 2000. Molecular portraits of human breast tumours. Nature 406, 747–752. https://doi.org/10.1038/35021093
Piersiala, K., Silva, P.F.N. da, Hjalmarsson, E., Kolev, A., Kågedal, Å., Starkhammar, M., Elliot, A., Marklund, L., Margolin, G., Munck-Wikland, E., Georén, S.K., Cardell, L.-O., 2021. CD4+ and CD8+ T cells in sentinel nodes exhibit distinct pattern of PD-1, CD69, and HLA-DR expression compared to tumor tissue in oral squamous cell carcinoma. Cancer Science 112, 1048. https://doi.org/10.1111/cas.14816
Popescu, M., Cabrera-Martinez, B., Winslow, G.M., 2019. TNF-α Contributes to Lymphoid Tissue Disorganization and Germinal Center B Cell Suppression during Intracellular Bacterial

Infection. The Journal of Immunology 203, 2415–2424. https://doi.org/10.4049/jimmunol.1900484
Popi, A.F., Longo-Maugéri, I.M., Mariano, M., 2016. An Overview of B-1 Cells as Antigen-Presenting Cells. Frontiers in Immunology 7.
Pu, S., Wang, K., Liu, Y., Liao, X., Chen, H., He, J., Zhang, J., 2020. Nomogram-derived prediction of pathologic complete response (pCR) in breast cancer patients treated with neoadjuvant chemotherapy (NCT). BMC Cancer 20, 1120. https://doi.org/10.1186/s12885-020-07621-7
Quist, J., Mirza, H., Cheang, M.C.U., Telli, M.L., O'Shaughnessy, J.A., Lord, C.J., Tutt, A.N.J., Grigoriadis, A., 2019. A Four-gene Decision Tree Signature Classification of Triple-negative Breast Cancer: Implications for Targeted Therapeutics. Mol Cancer Ther 18, 204–212. https://doi.org/10.1158/1535-7163.MCT-18-0243
Rabinovich, A., Medina, L., Piura, B., Huleihel, M., 2010. Expression of IL-10 in human normal and cancerous ovarian tissues and cells. Eur Cytokine Netw 21, 122–128. https://doi.org/10.1684/ecn.2010.0188
Rakha, E.A., Reis-Filho, J.S., Baehner, F., Dabbs, D.J., Decker, T., Eusebi, V., Fox, S.B., Ichihara, S., Jacquemier, J., Lakhani, S.R., Palacios, J., Richardson, A.L., Schnitt, S.J., Schmitt, F.C., Tan, P.-H., Tse, G.M., Badve, S., Ellis, I.O., 2010. Breast cancer prognostic classification in the molecular era: the role of histological grade. Breast Cancer Res 12, 207. https://doi.org/10.1186/bcr2607
Rao, C., Shetty, J., Prasad, K.H., 2013. Immunohistochemical Profile and Morphology in Triple – Negative Breast Cancers. J Clin Diagn Res 7, 1361–1365. https://doi.org/10.7860/JCDR/2013/5823.3129
Redig, A.J., McAllister, S.S., 2013. Breast cancer as a systemic disease: a view of metastasis. J Intern Med 274, 113–126. https://doi.org/10.1111/joim.12084
Reimold, A.M., Iwakoshi, N.N., Manis, J., Vallabhajosyula, P., Szomolanyi-Tsuda, E., Gravallese, E.M., Friend, D., Grusby, M.J., Alt, F., Glimcher, L.H., 2001. Plasma cell differentiation requires the transcription factor XBP-1. Nature 412, 300–307. https://doi.org/10.1038/35085509
Revy, P., Muto, T., Levy, Y., Geissmann, F., Plebani, A., Sanal, O., Catalan, N., Forveille, M., Dufourcq-Lagelouse, R., Gennery, A., Tezcan, I., Ersoy, F., Kayserili, H., Ugazio, A.G., Brousse, N., Muramatsu, M., Notarangelo, L.D., Kinoshita, K., Honjo, T., Fischer, A., Durandy, A., 2000. Activation-Induced Cytidine Deaminase (AID) Deficiency Causes the Autosomal Recessive Form of the Hyper-IgM Syndrome (HIGM2). Cell 102, 565–575. https://doi.org/10.1016/S0092-8674(00)00079-9
Richert, M.M., Phadke, P.A., Matters, G., DiGirolamo, D.J., Washington, S., Demers, L.M., Bond, J.S., Manni, A., Welch, D.R., 2005. Metastasis of hormone-independent breast cancer to lung and bone is decreased by α-difluoromethylornithine treatment. Breast Cancer Research 7, R819. https://doi.org/10.1186/bcr1292
Riedel, R., Addo, R., Ferreira-Gomes, M., Heinz, G.A., Heinrich, F., Kummer, J., Greiff, V., Schulz, D., Klaeden, C., Cornelis, R., Menzel, U., Kröger, S., Stervbo, U., Köhler, R., Haftmann, C., Kühnel, S., Lehmann, K., Maschmeyer, P., McGrath, M., Naundorf, S., Hahne, S., Sercan-Alp, Ö., Siracusa, F., Stefanowski, J., Weber, M., Westendorf, K., Zimmermann, J., Hauser, A.E., Reddy, S.T., Durek, P., Chang, H.-D., Mashreghi, M.-F., Radbruch, A., 2020. Discrete populations of isotype-switched memory B lymphocytes are maintained in murine spleen and bone marrow. Nat Commun 11, 2570. https://doi.org/10.1038/s41467-020-16464-6
Ritchie, M.E., Phipson, B., Wu, D., Hu, Y., Law, C.W., Shi, W., Smyth, G.K., 2015. limma powers differential expression analyses for RNA-sequencing and microarray studies. Nucleic Acids Res 43, e47. https://doi.org/10.1093/nar/gkv007
Rø, T.B., Holien, T., Fagerli, U.-M., Hov, H., Misund, K., Waage, A., Sundan, A., Holt, R.U., Børset, M., 2013. HGF and IGF-1 synergize with SDF-1α in promoting migration of myeloma cells by cooperative activation of p21-activated kinase. Exp Hematol 41, 646–655. https://doi.org/10.1016/j.exphem.2013.03.002

Robbins, K., McCabe, S., Scheiner, T., Strasser, J., Clark, R., Jardieu, P., 1994. Immunological effects of insulin-like growth factor-I--enhancement of immunoglobulin synthesis. Clin Exp Immunol 95, 337–342.

Roco, J.A., Mesin, L., Binder, S.C., Nefzger, C., Gonzalez-Figueroa, P., Canete, P.F., Ellyard, J., Shen, Q., Robert, P.A., Cappello, J., Vohra, H., Zhang, Y., Nowosad, C.R., Schiepers, A., Corcoran, L.M., Toellner, K.-M., Polo, J., Meyer-Hermann, M., Victora, G., Vinuesa, C.G., 2019. Class Switch Recombination Occurs Infrequently in Germinal Centers. Immunity 51, 337-350.e7. https://doi.org/10.1016/j.immuni.2019.07.001

Rodriguez, A., Peske, J.D., Woods, A.N., Leick, K.M., Mauldin, I.S., Young, S.J., Lindsay, R.S., Melssen, M.M., Cyranowski, S., Parriott, G., Meneveau, M.O., Conaway, M.R., Fu, Y.-X., Slingluff Jr, C.L., Engelhard, V.H., 2020. Immune Mechanisms Orchestrate Tertiary Lymphoid Structures in Tumors Via Cancer-Associated Fibroblasts. https://doi.org/10.2139/ssrn.3575119

Rosales, C., Uribe-Querol, E., 2017. Phagocytosis: A Fundamental Process in Immunity. Biomed Res Int 2017, 9042851. https://doi.org/10.1155/2017/9042851

RStudio Team, 2020. Rstudio.

Rumfelt, L.L., Zhou, Y., Rowley, B.M., Shinton, S.A., Hardy, R.R., 2006. Lineage specification and plasticity in CD19− early B cell precursors. J Exp Med 203, 675–687. https://doi.org/10.1084/jem.20052444

Rye, I.H., Huse, K., Josefsson, S.E., Kildal, W., Danielsen, H.E., Schlichting, E., Garred, Ø., Riis, M.L., OSBREAC, Lingjærde, O.C., Myklebust, J.H., Russnes, H.G., 2022. Breast cancer metastasis: immune profiling of lymph nodes reveals exhaustion of effector T cells and immunosuppression. Mol Oncol 16, 88–103. https://doi.org/10.1002/1878-0261.13047

Sage, P.T., Paterson, A.M., Lovitch, S.B., Sharpe, A.H., 2014. The coinhibitory receptor CTLA-4 controls B cell responses by modulating T follicular helper, T follicular regulatory, and T regulatory cells. Immunity 41, 1026–1039. https://doi.org/10.1016/j.immuni.2014.12.005

Sahai, E., Astsaturov, I., Cukierman, E., DeNardo, D.G., Egeblad, M., Evans, R.M., Fearon, D., Greten, F.R., Hingorani, S.R., Hunter, T., Hynes, R.O., Jain, R.K., Janowitz, T., Jorgensen, C., Kimmelman, A.C., Kolonin, M.G., Maki, R.G., Powers, R.S., Puré, E., Ramirez, D.C., Scherz-Shouval, R., Sherman, M.H., Stewart, S., Tlsty, T.D., Tuveson, D.A., Watt, F.M., Weaver, V., Weeraratna, A.T., Werb, Z., 2020. A framework for advancing our understanding of cancer-associated fibroblasts. Nat Rev Cancer 20, 174–186. https://doi.org/10.1038/s41568-019-0238-1

Salgado, R., Denkert, C., Demaria, S., Sirtaine, N., Klauschen, F., Pruneri, G., Wienert, S., Van den Eynden, G., Baehner, F.L., Penault-Llorca, F., Perez, E.A., Thompson, E.A., Symmans, W.F., Richardson, A.L., Brock, J., Criscitiello, C., Bailey, H., Ignatiadis, M., Floris, G., Sparano, J., Kos, Z., Nielsen, T., Rimm, D.L., Allison, K.H., Reis-Filho, J.S., Loibl, S., Sotiriou, C., Viale, G., Badve, S., Adams, S., Willard-Gallo, K., Loi, S., International TILs Working Group 2014, 2015a. The evaluation of tumor-infiltrating lymphocytes (TILs) in breast cancer: recommendations by an International TILs Working Group 2014. Ann Oncol 26, 259–271. https://doi.org/10.1093/annonc/mdu450

Salgado, R., Denkert, C., Demaria, S., Sirtaine, N., Klauschen, F., Pruneri, G., Wienert, S., Van den Eynden, G., Baehner, F.L., Penault-Llorca, F., Perez, E.A., Thompson, E.A., Symmans, W.F., Richardson, A.L., Brock, J., Criscitiello, C., Bailey, H., Ignatiadis, M., Floris, G., Sparano, J., Kos, Z., Nielsen, T., Rimm, D.L., Allison, K.H., Reis-Filho, J.S., Loibl, S., Sotiriou, C., Viale, G., Badve, S., Adams, S., Willard-Gallo, K., Loi, S., International TILs Working Group 2014, 2015b. The evaluation of tumor-infiltrating lymphocytes (TILs) in breast cancer: recommendations by an International TILs Working Group 2014. Ann Oncol 26, 259–271. https://doi.org/10.1093/annonc/mdu450

Salgado, R., Denkert, C., Demaria, S., Sirtaine, N., Klauschen, F., Pruneri, G., Wienert, S., Van den Eynden, G., Baehner, F.L., Penault-Llorca, F., Perez, E.A., Thompson, E.A., Symmans, W.F., Richardson, A.L., Brock, J., Criscitiello, C., Bailey, H., Ignatiadis, M., Floris, G., Sparano, J., Kos,

Z., Nielsen, T., Rimm, D.L., Allison, K.H., Reis-Filho, J.S., Loibl, S., Sotiriou, C., Viale, G., Badve, S., Adams, S., Willard-Gallo, K., Loi, S., International TILs Working Group 2014, 2015c. The evaluation of tumor-infiltrating lymphocytes (TILs) in breast cancer: recommendations by an International TILs Working Group 2014. Ann Oncol 26, 259–271. https://doi.org/10.1093/annonc/mdu450

Salminen, A., Kaarniranta, K., Kauppinen, A., 2021. Insulin/IGF-1 signaling promotes immunosuppression via the STAT3 pathway: impact on the aging process and age-related diseases. Inflamm Res 70, 1043–1061. https://doi.org/10.1007/s00011-021-01498-3

Sautès-Fridman, C., Petitprez, F., Calderaro, J., Fridman, W.H., 2019. Tertiary lymphoid structures in the era of cancer immunotherapy. Nat. Rev. Cancer 19, 307–325. https://doi.org/10.1038/s41568-019-0144-6

Schettini, F., Paré, L., Marín-Aguilera, M., Puig, S., Mezquita, L., Baste, N., Pascual, T., Saez, O.M., Conte, B., Jares, P., Puig-Butillé, J.A., Torres, E.S., González-Farre, B., Villagrasa, P., Conte, P.F., Perou, C., Parker, J.S., Maristany, F.B., Prat, A., 2022. 14-gene immunoglobulin (IGG) and proliferation signatures and association with overall survival across cancer-types. Journal of Clinical Oncology. https://doi.org/10.1200/JCO.2022.40.16_suppl.2636

Schmid, P., Adams, S., Rugo, H.S., Schneeweiss, A., Barrios, C.H., Iwata, H., Diéras, V., Hegg, R., Im, S.-A., Shaw Wright, G., Henschel, V., Molinero, L., Chui, S.Y., Funke, R., Husain, A., Winer, E.P., Loi, S., Emens, L.A., 2018. Atezolizumab and Nab-Paclitaxel in Advanced Triple-Negative Breast Cancer. N Engl J Med 379, 2108–2121. https://doi.org/10.1056/NEJMoa1809615

Schmid, P., Cortes, J., Pusztai, L., McArthur, H., Kümmel, S., Bergh, J., Denkert, C., Park, Y.H., Hui, R., Harbeck, N., Takahashi, M., Foukakis, T., Fasching, P.A., Cardoso, F., Untch, M., Jia, L., Karantza, V., Zhao, J., Aktan, G., Dent, R., O'Shaughnessy, J., 2020. Pembrolizumab for Early Triple-Negative Breast Cancer. New England Journal of Medicine 382, 810–821. https://doi.org/10.1056/NEJMoa1910549

Schmidt, M., Edlund, K., Hengstler, J.G., Heimes, A.-S., Almstedt, K., Lebrecht, A., Krajnak, S., Battista, M.J., Brenner, W., Hasenburg, A., Rahnenführer, J., Gehrmann, M., Kellokumpu-Lehtinen, P.-L., Wirtz, R.M., Joensuu, H., 2021. Prognostic Impact of Immunoglobulin Kappa C (IGKC) in Early Breast Cancer. Cancers (Basel) 13, 3626. https://doi.org/10.3390/cancers13143626

Schrörs, B., Boegel, S., Albrecht, C., Bukur, T., Bukur, V., Holtsträter, C., Ritzel, C., Manninen, K., Tadmor, A.D., Vormehr, M., Sahin, U., Löwer, M., 2020. Multi-Omics Characterization of the 4T1 Murine Mammary Gland Tumor Model. Frontiers in Oncology 10.

Seow, D.Y.B., Yeong, J.P.S., Lim, J.X., Chia, N., Lim, J.C.T., Ong, C.C.H., Tan, P.H., Iqbal, J., 2020. Tertiary lymphoid structures and associated plasma cells play an important role in the biology of triple-negative breast cancers. Breast Cancer Res Treat. https://doi.org/10.1007/s10549-020-05548-y

Shah, S.P., Roth, A., Goya, R., Oloumi, A., Ha, G., Zhao, Y., Turashvili, G., Ding, J., Tse, K., Haffari, G., Bashashati, A., Prentice, L.M., Khattra, J., Burleigh, A., Yap, D., Bernard, V., McPherson, A., Shumansky, K., Crisan, A., Giuliany, R., Heravi-Moussavi, A., Rosner, J., Lai, D., Birol, I., Varhol, R., Tam, A., Dhalla, N., Zeng, T., Ma, K., Chan, S.K., Griffith, M., Moradian, A., Cheng, S.-W.G., Morin, G.B., Watson, P., Gelmon, K., Chia, S., Chin, S.-F., Curtis, C., Rueda, O.M., Pharoah, P.D., Damaraju, S., Mackey, J., Hoon, K., Harkins, T., Tadigotla, V., Sigaroudinia, M., Gascard, P., Tlsty, T., Costello, J.F., Meyer, I.M., Eaves, C.J., Wasserman, W.W., Jones, S., Huntsman, D., Hirst, M., Caldas, C., Marra, M.A., Aparicio, S., 2012. The clonal and mutational evolution spectrum of primary triple-negative breast cancers. Nature 486, 395–399. https://doi.org/10.1038/nature10933

Shahaf, G., Zisman-Rozen, S., Benhamou, D., Melamed, D., Mehr, R., 2016. B Cell Development in the Bone Marrow Is Regulated by Homeostatic Feedback Exerted by Mature B Cells. Frontiers in Immunology 7.

Shankwitz, K., Pallikkuth, S., Sirupangi, T., Kirk Kvistad, D., Russel, K.B., Pahwa, R., Gama, L., Koup, R.A., Pan, L., Villinger, F., Pahwa, S., Petrovas, C., 2020. Compromised steady-state germinal

center activity with age in nonhuman primates. Aging Cell 19, e13087. https://doi.org/10.1111/acel.13087
Shen, M., Wang, J., Ren, X., 2018. New Insights into Tumor-Infiltrating B Lymphocytes in Breast Cancer: Clinical Impacts and Regulatory Mechanisms. Front Immunol 9. https://doi.org/10.3389/fimmu.2018.00470
Shen, S., Sun, Q., Liang, Z., Cui, X., Ren, X., Chen, H., Zhang, X., Zhou, Y., 2014. A Prognostic Model of Triple-Negative Breast Cancer Based on miR-27b-3p and Node Status. PLOS ONE 9, e100664. https://doi.org/10.1371/journal.pone.0100664
Shi, J., Hou, S., Fang, Q., Liu, Xin, Liu, Xiaolong, Qi, H., 2018. PD-1 Controls Follicular T Helper Cell Positioning and Function. Immunity 49, 264-274.e4. https://doi.org/10.1016/j.immuni.2018.06.012
Shih, T.-A.Y., Roederer, M., Nussenzweig, M.C., 2002. Role of antigen receptor affinity in T cell–independent antibody responses in vivo. Nat Immunol 3, 399–406. https://doi.org/10.1038/ni776
Shinkura, R., Matsuda, F., Sakiyama, T., Tsubata, T., Hiai, H., Paumen, M., Miyawaki, S., Honjo, T., 1996. Defects of somatic hypermutation and class switching in alymphoplasia (aly) mutant mice. Int Immunol 8, 1067–1075. https://doi.org/10.1093/intimm/8.7.1067
Shinnakasu, R., Inoue, T., Kometani, K., Moriyama, S., Adachi, Y., Nakayama, M., Takahashi, Y., Fukuyama, H., Okada, T., Kurosaki, T., 2016. Regulated selection of germinal-center cells into the memory B cell compartment. Nat Immunol 17, 861–869. https://doi.org/10.1038/ni.3460
Sidwell, T., Kallies, A., 2016. Bach2 is required for B cell and T cell memory differentiation. Nature Immunology 17, 744–745. https://doi.org/10.1038/ni.3493
Singh, D.D., Parveen, A., Yadav, D.K., 2021. Role of PARP in TNBC: Mechanism of Inhibition, Clinical Applications, and Resistance. Biomedicines 9, 1512. https://doi.org/10.3390/biomedicines9111512
Smith, K.G., Nossal, G.J., Tarlinton, D.M., 1995. FAS is highly expressed in the germinal center but is not required for regulation of the B-cell response to antigen. Proc Natl Acad Sci U S A 92, 11628–11632.
Solinas, C., Garaud, S., De Silva, P., Boisson, A., Van den Eynden, G., de Wind, A., Risso, P., Rodrigues Vitoria, J., Richard, F., Migliori, E., Noel, G., Duvillier, H., Craciun, L., Veys, I., Awada, A., Detours, V., Larsimont, D., Piccart-Gebhart, M., Willard-Gallo, K., 2017. Immune Checkpoint Molecules on Tumor-Infiltrating Lymphocytes and Their Association with Tertiary Lymphoid Structures in Human Breast Cancer. Front Immunol 8, 1412. https://doi.org/10.3389/fimmu.2017.01412
Somasundaram, R., Zhang, G., Fukunaga-Kalabis, M., Perego, M., Krepler, C., Xu, X., Wagner, C., Hristova, D., Zhang, J., Tian, T., Wei, Z., Liu, Q., Garg, K., Griss, J., Hards, R., Maurer, M., Hafner, C., Mayerhöfer, M., Karanikas, G., Jalili, A., Bauer-Pohl, V., Weihsengruber, F., Rappersberger, K., Koller, J., Lang, R., Hudgens, C., Chen, G., Tetzlaff, M., Wu, L., Frederick, D.T., Scolyer, R.A., Long, G.V., Damle, M., Ellingsworth, C., Grinman, L., Choi, H., Gavin, B.J., Dunagin, M., Raj, A., Scholler, N., Gross, L., Beqiri, M., Bennett, K., Watson, I., Schaider, H., Davies, M.A., Wargo, J., Czerniecki, B.J., Schuchter, L., Herlyn, D., Flaherty, K., Herlyn, M., Wagner, S.N., 2017. Tumor-associated B-cells induce tumor heterogeneity and therapy resistance. Nat Commun 8, 607. https://doi.org/10.1038/s41467-017-00452-4
Song, H., Liu, A., Liu, G., Wu, F., Li, Z., 2019. T follicular regulatory cells suppress Tfh-mediated B cell help and synergistically increase IL-10-producing B cells in breast carcinoma. Immunol Res 67, 416–423. https://doi.org/10.1007/s12026-019-09090-y
Speers, C., Zhao, S.G., Chandler, B., Liu, M., Wilder-Romans, K., Olsen, E., Nyati, S., Ritter, C., Alluri, P.G., Kothari, V., Hayes, D.F., Lawrence, T.S., Spratt, D.E., Wahl, D.R., Pierce, L.J., Feng, F.Y., 2017. Androgen receptor as a mediator and biomarker of radioresistance in triple-negative breast cancer. npj Breast Cancer 3, 1–10. https://doi.org/10.1038/s41523-017-0038-2

Spratt, D.E., Evans, M.J., Davis, B.J., Doran, M.G., Lee, M.X., Shah, N., Wongvipat, J., Carnazza, K.E., Klee, G.G., Polkinghorn, W., Tindall, D.J., Lewis, J.S., Sawyers, C.L., 2015. Androgen Receptor Upregulation Mediates Radioresistance after Ionizing Radiation. Cancer Res 75, 4688–4696. https://doi.org/10.1158/0008-5472.CAN-15-0892

Sprynski, A.C., Hose, D., Caillot, L., Rème, T., Shaughnessy, J.D., Barlogie, B., Seckinger, A., Moreaux, J., Hundemer, M., Jourdan, M., Meissner, T., Jauch, A., Mahtouk, K., Kassambara, A., Bertsch, U., Rossi, J.-F., Goldschmidt, H., Klein, B., 2009. The role of IGF-1 as a major growth factor for myeloma cell lines and the prognostic relevance of the expression of its receptor. Blood 113, 4614–4626. https://doi.org/10.1182/blood-2008-07-170464

Stacker, S.A., Williams, S.P., Karnezis, T., Shayan, R., Fox, S.B., Achen, M.G., 2014. Lymphangiogenesis and lymphatic vessel remodelling in cancer. Nat Rev Cancer 14, 159–172. https://doi.org/10.1038/nrc3677

Starr, T.K., Jameson, S.C., Hogquist, K.A., 2003. Positive and negative selection of T cells. Annu Rev Immunol 21, 139–176. https://doi.org/10.1146/annurev.immunol.21.120601.141107

Sterlin, D., Mathian, A., Miyara, M., Mohr, A., Anna, F., Claër, L., Quentric, P., Fadlallah, J., Devilliers, H., Ghillani, P., Gunn, C., Hockett, R., Mudumba, S., Guihot, A., Luyt, C.-E., Mayaux, J., Beurton, A., Fourati, S., Bruel, T., Schwartz, O., Lacorte, J.-M., Yssel, H., Parizot, C., Dorgham, K., Charneau, P., Amoura, Z., Gorochov, G., 2021. IgA dominates the early neutralizing antibody response to SARS-CoV-2. Science Translational Medicine 13, eabd2223. https://doi.org/10.1126/scitranslmed.abd2223

Stirling, D.R., Swain-Bowden, M.J., Lucas, A.M., Carpenter, A.E., Cimini, B.A., Goodman, A., 2021. CellProfiler 4: improvements in speed, utility and usability. BMC Bioinformatics 22, 433. https://doi.org/10.1186/s12859-021-04344-9

Su, S., Liu, Q., Chen, Jingqi, Chen, Jianing, Chen, F., He, C., Huang, D., Wu, W., Lin, L., Huang, W., Zhang, J., Cui, X., Zheng, F., Li, H., Yao, H., Su, F., Song, E., 2014. A positive feedback loop between mesenchymal-like cancer cells and macrophages is essential to breast cancer metastasis. Cancer Cell 25, 605–620. https://doi.org/10.1016/j.ccr.2014.03.021

Subramanian, A., Tamayo, P., Mootha, V.K., Mukherjee, S., Ebert, B.L., Gillette, M.A., Paulovich, A., Pomeroy, S.L., Golub, T.R., Lander, E.S., Mesirov, J.P., 2005. Gene set enrichment analysis: a knowledge-based approach for interpreting genome-wide expression profiles. Proc Natl Acad Sci U S A 102, 15545–15550. https://doi.org/10.1073/pnas.0506580102

Sun, X., Zhang, T., Li, M., Yin, L., Xue, J., 2019. Immunosuppressive B cells expressing PD-1/PD-L1 in solid tumors: A mini review. QJM. https://doi.org/10.1093/qjmed/hcz162

Sundling, C., Lau, A.W.Y., Bourne, K., Young, C., Laurianto, C., Hermes, J.R., Menzies, R.J., Butt, D., Kräutler, N.J., Zahra, D., Suan, D., Brink, R., 2021. Positive selection of IgG+ over IgM+ B cells in the germinal center reaction. Immunity 54, 988-1001.e5. https://doi.org/10.1016/j.immuni.2021.03.013

Tadmor, T., Zhang, Y., Cho, H.-M., Podack, E.R., Rosenblatt, J.D., 2011. The absence of B lymphocytes reduces the number and function of T-regulatory cells and enhances the anti-tumor response in a murine tumor model. Cancer Immunol Immunother 60, 609–619. https://doi.org/10.1007/s00262-011-0972-z

Tang, T., Yang, Z., Zhu, Q., Wu, Y., Sun, K., Alahdal, M., Zhang, Y., Xing, Y., Shen, Y., Xia, T., Xi, T., Pan, Y., Jin, L., 2018. Up-regulation of miR-210 induced by a hypoxic microenvironment promotes breast cancer stem cells metastasis, proliferation, and self-renewal by targeting E-cadherin. FASEB J fj201801013R. https://doi.org/10.1096/fj.201801013R

Tao H., Lu L., Egenti M., Chang A.E., Li Q., 2013. Effector B cells in cancer adoptive immunotherapy. Cancer Res., 104th Annual Meeting of the American Association for Cancer Research, AACR 2013. Washington, DC United States. 73. https://doi.org/10.1158/1538-7445.AM2013-487

Tao, H., Lu, L., Xia, Y., Dai, F., Wang, Y., Bao, Y., Lundy, S.K., Ito, F., Pan, Q., Zhang, X., Zheng, F., Shu, G., Fang, B., Jiang, J., Xia, J., Huang, S., Li, Q., Chang, A.E., 2015. Antitumor effector B cells

directly kill tumor cells via the Fas/FasL pathway and are regulated by IL-10. Eur J Immunol 45, 999–1009. https://doi.org/10.1002/eji.201444625
Tao, K., Fang, M., Alroy, J., Sahagian, G.G., 2008. Imagable 4T1 model for the study of late stage breast cancer. BMC Cancer 8, 228. https://doi.org/10.1186/1471-2407-8-228
Tashiro, Y., Murakami, A., Hara, Y., Shimizu, T., Kubo, M., Goitsuka, R., Kishimoto, H., Azuma, T., 2018. High-affinity IgM+ memory B cells are defective in differentiation into IgM antibody-secreting cells by re-stimulation with a T cell-dependent antigen. Sci Rep 8, 14559. https://doi.org/10.1038/s41598-018-32926-w
Templeton, A.J., McNamara, M.G., Šeruga, B., Vera-Badillo, F.E., Aneja, P., Ocaña, A., Leibowitz-Amit, R., Sonpavde, G., Knox, J.J., Tran, B., Tannock, I.F., Amir, E., 2014. Prognostic Role of Neutrophil-to-Lymphocyte Ratio in Solid Tumors: A Systematic Review and Meta-Analysis. JNCI: Journal of the National Cancer Institute 106, dju124. https://doi.org/10.1093/jnci/dju124
Thompson, K.J., Leon-Ferre, R.A., Sinnwell, J.P., Zahrieh, D.M., Suman, V.J., Metzger, F.O., Asad, S., Stover, D.G., Carey, L., Sikov, W.M., Ingle, J.N., Liu, M.C., Carter, J.M., Klee, E.W., Weinshilboum, R.M., Boughey, J.C., Wang, L., Couch, F.J., Goetz, M.P., Kalari, K.R., 2022. Luminal androgen receptor breast cancer subtype and investigation of the microenvironment and neoadjuvant chemotherapy response. NAR Cancer 4, zcac018. https://doi.org/10.1093/narcan/zcac018
Toboso-Navasa, A., Gunawan, A., Morlino, G., Nakagawa, R., Taddei, A., Damry, D., Patel, Y., Chakravarty, P., Janz, M., Kassiotis, G., Brink, R., Eilers, M., Calado, D.P., 2020. Restriction of memory B cell differentiation at the germinal center B cell positive selection stage. J Exp Med 217. https://doi.org/10.1084/jem.20191933
Traina, T.A., Miller, K., Yardley, D.A., Eakle, J., Schwartzberg, L.S., O'Shaughnessy, J., Gradishar, W., Schmid, P., Winer, E., Kelly, C., Nanda, R., Gucalp, A., Awada, A., Garcia-Estevez, L., Trudeau, M.E., Steinberg, J., Uppal, H., Tudor, I.C., Peterson, A., Cortes, J., 2018. Enzalutamide for the Treatment of Androgen Receptor-Expressing Triple-Negative Breast Cancer. J Clin Oncol 36, 884–890. https://doi.org/10.1200/JCO.2016.71.3495
Ullah, T.R., 2019. The role of CXCR4 in multiple myeloma: Cells' journey from bone marrow to beyond. J Bone Oncol 17, 100253. https://doi.org/10.1016/j.jbo.2019.100253
Vahidi, Y., Bagheri, M., Ghaderi, A., Faghih, Z., 2020. CD8-positive memory T cells in tumor-draining lymph nodes of patients with breast cancer. BMC Cancer 20. https://doi.org/10.1186/s12885-020-6714-x
Venkataraman, C., Shankar, G., Sen, G., Bondada, S., 1999. Bacterial lipopolysaccharide induced B cell activation is mediated via a phosphatidylinositol 3-kinase dependent signaling pathway. Immunol Lett 69, 233–238. https://doi.org/10.1016/s0165-2478(99)00068-1
Victora, G.D., Nussenzweig, M.C., 2012. Germinal Centers. Annual Review of Immunology 30, 429–457. https://doi.org/10.1146/annurev-immunol-020711-075032
Victora, G.D., Schwickert, T.A., Fooksman, D.R., Kamphorst, A.O., Meyer-Hermann, M., Dustin, M.L., Nussenzweig, M.C., 2010. Germinal Center Dynamics Revealed by Multiphoton Microscopy with a Photoactivatable Fluorescent Reporter. Cell 143, 592–605. https://doi.org/10.1016/j.cell.2010.10.032
Vidula, N., Yau, C., Wolf, D., Rugo, H.S., 2019. Androgen receptor gene expression in primary breast cancer. NPJ Breast Cancer 5, 47. https://doi.org/10.1038/s41523-019-0142-6
Vinuesa, C.G., Chang, P.-P., 2013. Innate B cell helpers reveal novel types of antibody responses. Nat Immunol 14, 119–126. https://doi.org/10.1038/ni.2511
Vivier, E., Tomasello, E., Baratin, M., Walzer, T., Ugolini, S., 2008. Functions of natural killer cells. Nat Immunol 9, 503–510. https://doi.org/10.1038/ni1582
Vos, Q., Lees, A., Wu, Z.Q., Snapper, C.M., Mond, J.J., 2000. B-cell activation by T-cell-independent type 2 antigens as an integral part of the humoral immune response to pathogenic

microorganisms. Immunol Rev 176, 154–170. https://doi.org/10.1034/j.1600-065x.2000.00607.x
Voudouri, K., Berdiaki, A., Tzardi, M., Tzanakakis, G.N., Nikitovic, D., 2015. Insulin-Like Growth Factor and Epidermal Growth Factor Signaling in Breast Cancer Cell Growth: Focus on Endocrine Resistant Disease. Anal Cell Pathol (Amst) 2015, 975495. https://doi.org/10.1155/2015/975495
W, F., T, Y., H, M., T, O., M, N., H, D., A, F., S, K., R, T., H, N., 2007. Insulin-like growth factor 1/insulin signaling activates androgen signaling through direct interactions of Foxo1 with androgen receptor. The Journal of biological chemistry 282. https://doi.org/10.1074/jbc.M610447200
Wang, K., Shen, T., Siegal, G.P., Wei, S., 2017. The CD4/CD8 ratio of tumor-infiltrating lymphocytes at the tumor-host interface has prognostic value in triple-negative breast cancer. Hum Pathol 69, 110–117. https://doi.org/10.1016/j.humpath.2017.09.012
Wen, L., Han, Z., 2021. Identification and validation of xenobiotic metabolism-associated prognostic signature based on five genes to evaluate immune microenvironment in colon cancer. J Gastrointest Oncol 12, 2788–2802. https://doi.org/10.21037/jgo-21-655
Wherry, E.J., Kurachi, M., 2015. Molecular and cellular insights into T cell exhaustion. Nat Rev Immunol 15, 486–499. https://doi.org/10.1038/nri3862
Wickham et al., 2016. ggplot2: Elegant Graphics for Data Analysis. New York: Springer-Verlag; 2016. ISBN 978-3-319-24277-4.
Willard-Mack, C.L., 2006. Normal Structure, Function, and Histology of Lymph Nodes. Toxicol Pathol 34, 409–424. https://doi.org/10.1080/01926230600867727
Williams, J.A., Phillips, D.H., 2000. Mammary Expression of Xenobiotic Metabolizing Enzymes and Their Potential Role in Breast Cancer1. Cancer Research 60, 4667–4677.
Windhager, J., Bodenmiller, B., Eling, N., 2021. An end-to-end workflow for multiplexed image processing and analysis. https://doi.org/10.1101/2021.11.12.468357
Wing, J.B., Ise, W., Kurosaki, T., Sakaguchi, S., 2014. Regulatory T cells control antigen-specific expansion of Tfh cell number and humoral immune responses via the coreceptor CTLA-4. Immunity 41, 1013–1025. https://doi.org/10.1016/j.immuni.2014.12.006
Winkelmann, R., Sandrock, L., Porstner, M., Roth, E., Mathews, M., Hobeika, E., Reth, M., Kahn, M.L., Schuh, W., Jäck, H.-M., 2011. B cell homeostasis and plasma cell homing controlled by Krüppel-like factor 2. Proceedings of the National Academy of Sciences 108, 710–715. https://doi.org/10.1073/pnas.1012858108
Wortman, J.C., He, T.-F., Solomon, S., Zhang, R.Z., Rosario, A., Wang, R., Tu, T.Y., Schmolze, D., Yuan, Y., Yost, S.E., Li, X., Levine, H., Atwal, G., Lee, P.P., Yu, C.C., 2021. Spatial distribution of B cells and lymphocyte clusters as a predictor of triple-negative breast cancer outcome. NPJ Breast Cancer 7, 84. https://doi.org/10.1038/s41523-021-00291-z
Wu, L., Zhang, X.H.-F., 2020. Tumor-Associated Neutrophils and Macrophages—Heterogenous but Not Chaotic. Front Immunol 11, 553967. https://doi.org/10.3389/fimmu.2020.553967
Wynn, T.A., Barron, L., 2010. Macrophages: Master Regulators of Inflammation and Fibrosis. Semin Liver Dis 30, 245–257. https://doi.org/10.1055/s-0030-1255354
Xie, M., Xu, X., Fan, Y., 2021. KRAS-Mutant Non-Small Cell Lung Cancer: An Emerging Promisingly Treatable Subgroup. Frontiers in Oncology 11.
Xing, F., Saidou, J., Watabe, K., 2010. Cancer associated fibroblasts (CAFs) in tumor microenvironment. Front Biosci 15, 166–179.
Yamaguchi, M., Takagi, K., Sato, M., Sato, A., Miki, Y., Onodera, Y., Miyashita, M., Sasano, H., Suzuki, T., 2021. Androgens enhance the ability of intratumoral macrophages to promote breast cancer progression. Oncology Reports 46, 1–11. https://doi.org/10.3892/or.2021.8139
Yanase, T., Fan, W., 2009. Modification of androgen receptor function by IGF-1 signaling implications in the mechanism of refractory prostate carcinoma. Vitam Horm 80, 649–666. https://doi.org/10.1016/S0083-6729(08)00623-7

Yang, C., Jin, J., Yang, Y., Sun, H., Wu, L., Shen, M., Hong, X., Li, W., Lu, L., Cao, D., Wang, X., Sun, J., Ye, Y., Su, B., Deng, L., 2022. Androgen receptor-mediated CD8+ T cell stemness programs drive sex differences in antitumor immunity. Immunity 55, 1268-1283.e9. https://doi.org/10.1016/j.immuni.2022.05.012

Yang, Y., Jiang, G., Zhang, P., Fan, J., 2015. Programmed cell death and its role in inflammation. Military Medical Research 2, 12. https://doi.org/10.1186/s40779-015-0039-0

Yard, B.D., Adams, D.J., Chie, E.K., Tamayo, P., Battaglia, J.S., Gopal, P., Rogacki, K., Pearson, B.E., Phillips, J., Raymond, D.P., Pennell, N.A., Almeida, F., Cheah, J.H., Clemons, P.A., Shamji, A., Peacock, C.D., Schreiber, S.L., Hammerman, P.S., Abazeed, M.E., 2016. A genetic basis for the variation in the vulnerability of cancer to DNA damage. Nat Commun 7, 11428. https://doi.org/10.1038/ncomms11428

Ye, B.H., Cattoretti, G., Shen, Q., Zhang, J., Hawe, N., Waard, R. de, Leung, C., Nouri-Shirazi, M., Orazi, A., Chaganti, R.S.K., Rothman, P., Stall, A.M., Pandolfi, P.-P., Dalla-Favera, R., 1997. The BCL-6 proto-oncogene controls germinal-centre formation and Th2-type inflammation. Nat Genet 16, 161–170. https://doi.org/10.1038/ng0697-161

Yin, L., Duan, J.-J., Bian, X.-W., Yu, S., 2020. Triple-negative breast cancer molecular subtyping and treatment progress. Breast Cancer Research 22, 61. https://doi.org/10.1186/s13058-020-01296-5

Yoshida, K., Cologne, J.B., Cordova, K., Misumi, M., Yamaoka, M., Kyoizumi, S., Hayashi, T., Robins, H., Kusunoki, Y., 2017. Aging-related changes in human T-cell repertoire over 20years delineated by deep sequencing of peripheral T-cell receptors. Exp Gerontol 96, 29–37. https://doi.org/10.1016/j.exger.2017.05.015

Zaha, D.C., 2014. Significance of immunohistochemistry in breast cancer. World J Clin Oncol 5, 382–392. https://doi.org/10.5306/wjco.v5.i3.382

Zaynagetdinov, R., Sherrill, T.P., Gleaves, L.A., McLoed, A.G., Saxon, J.A., Habermann, A.C., Connelly, L., Dulek, D., Peebles, R.S., Fingleton, B., Yull, F.E., Stathopoulos, G.T., Blackwell, T.S., 2015. Interleukin-5 Facilitates Lung Metastasis by Modulating the Immune Microenvironment. Cancer Res 75, 1624–1634. https://doi.org/10.1158/0008-5472.CAN-14-2379

Zhang, H., Katerji, H., Turner, B.M., Hicks, D.G., 2022. HER2-Low Breast Cancers. Am J Clin Pathol 157, 328–336. https://doi.org/10.1093/ajcp/aqab117

Zhang, Y., Cao, R., Ying, H., Du, J., Chen, S., Wang, N., Shen, B., 2019. Erratum to “Increased Expression of TLR10 in B Cell Subsets Correlates with Disease Activity in Rheumatoid Arthritis.” Mediators of Inflammation 2019, e8419439. https://doi.org/10.1155/2019/8419439

Zhang, Yang, Meyer-Hermann, M., George, L.A., Figge, M.T., Khan, M., Goodall, M., Young, S.P., Reynolds, A., Falciani, F., Waisman, A., Notley, C.A., Ehrenstein, M.R., Kosco-Vilbois, M., Toellner, K.-M., 2013. Germinal center B cells govern their own fate via antibody feedback. J Exp Med 210, 457–464. https://doi.org/10.1084/jem.20120150

Zhang, Yu, Morgan, R., Podack, E.R., Rosenblatt, J., 2013. B cell regulation of anti-tumor immune response. Immunol Res 57, 115–124. https://doi.org/10.1007/s12026-013-8472-1

Zhao, R., Chen, X., Ma, W., Zhang, J., Guo, J., Zhong, X., Yao, J., Sun, J., Rubinfien, J., Zhou, X., Wang, J., Qi, H., 2020. A GPR174–CCL21 module imparts sexual dimorphism to humoral immunity. Nature 577, 416–420. https://doi.org/10.1038/s41586-019-1873-0

Zheng F., Pan Q., Egenti M., Chang A.E., Li Q., 2012. Blockade of IL-10 production in effector B cells significantly increases their therapeutic efficacy in cancer adoptive immunotherapy. Cancer Res., 103rd Annual Meeting of the American Association for Cancer Research, AACR 2012. Chicago, IL United States. 72. https://doi.org/10.1158/1538-7445.AM2012-4840

Zheng, W.-H., Quirion, R., 2006. Insulin-like growth factor-1 (IGF-1) induces the activation/phosphorylation of Akt kinase and cAMP response element-binding protein (CREB) by activating different signaling pathways in PC12 cells. BMC Neurosci 7, 51. https://doi.org/10.1186/1471-2202-7-51

Zhou, Z.-Q., Tong, D.-N., Guan, J., Tan, H.-W., Zhao, L.-D., Zhu, Y., Yao, J., Yang, J., Zhang, Z.-Y., 2016. Follicular helper T cell exhaustion induced by PD-L1 expression in hepatocellular carcinoma results in impaired cytokine expression and B cell help, and is associated with advanced tumor stages. Am J Transl Res 8, 2926–2936.

Zotos, D., Coquet, J.M., Zhang, Y., Light, A., D'Costa, K., Kallies, A., Corcoran, L.M., Godfrey, D.I., Toellner, K.-M., Smyth, M.J., Nutt, S.L., Tarlinton, D.M., 2010. IL-21 regulates germinal center B cell differentiation and proliferation through a B cell–intrinsic mechanism. Journal of Experimental Medicine 207, 365–378. https://doi.org/10.1084/jem.20091777

Zou, Z., Bellenger, S., Massey, K.A., Nicolaou, A., Geissler, A., Bidu, C., Bonnotte, B., Pierre, A.-S., Minville-Walz, M., Rialland, M., Seubert, J., Kang, J.X., Lagrost, L., Narce, M., Bellenger, J., 2013. Inhibition of the HER2 pathway by n-3 polyunsaturated fatty acids prevents breast cancer in fat-1 transgenic mice. J Lipid Res 54, 3453–3463. https://doi.org/10.1194/jlr.M042754

Zuccarino-Catania, G.V., Sadanand, S., Weisel, F.J., Tomayko, M.M., Meng, H., Kleinstein, S.H., Good-Jacobson, K.L., Shlomchik, M.J., 2014. CD80 and PD-L2 define functionally distinct memory B cell subsets that are independent of antibody isotype. Nature immunology 15, 631. https://doi.org/10.1038/ni.2914